TID-28939

SODIUM-SULFUR BATTERY DEVELOPMENT PROGRAM, PHASE II

Final Report, June 1976–October 31, 1977

By
A. Topouzian

Work Performed Under Contract No. EY-76-C-02-2566

Ford Motor Company
Scientific & Research Laboratory
Dearborn, Michigan

U. S. DEPARTMENT OF ENERGY

Division of Energy Storage Systems

TID-28939
Distribution Category UC-94c

SODIUM-SULFUR BATTERY DEVELOPMENT PROGRAM

Progress Report for Period June 1976 - October 31, 1977

Submitted by:

A. Topouzian
Research Staff
FORD MOTOR COMPANY
P. O. Box 2053
Dearborn, Michigan 48121

Prepared for:

Department of Energy
Division of Energy Storage Systems

Under Contract No. EY-76-C-02-2566

SODIUM-SULFUR BATTERY DEVELOPMENT PROGRAM

Period June 1976 - October 1977

ABSTRACT

This report was prepared in cooperation with staff members of Ford Motor Company, the University of Utah, and the Aeronutronic Division, FACC.

The Phase II sodium-sulfur battery development program was organized along five tasks:

1. Electric Vehicle Development and Demonstration
2. Load Leveling
3. Container and Seal Development
4. Development of Ceramic Electrolyte and Seal Technology
5. Fabrication and Testing

Electric Vehicle Battery Design

Much of the EV cell development effort was common to load leveling. LL hardware was utilized to evaluate EV cell characteristics.

Vehicle battery studies for the CVS cycle established a 44 KW Na/S battery need for powering an 1134 kg EV; equipped with manual transmission and employing regenerative braking.

Load Leveling Battery Design

A conceptual design of a 5 MWh battery was developed based upon consideration of system requirements, fault isolation and monitoring, thermal and charge control factors.

Container and Seal Development

Static corrosion tests were used to screen potential candidates for the sulfur container material system. The results indicated further evaluation of the following group of materials and coatings: high chromium content alloys; aluminum; molybdenum; chromium coating; carbon/graphite; glass/ceramic coatings; oxidized and chromated surfaces.

Extensive exploratory cell testing established the Mark I prototype cell sulfur container material system--silicate-bonded graphite coating (Tiodize CC-400) on low crack density chromium electroplated on E-Brite stainless steel.

Development of Ceramic Electrolyte and Seal Technology

A pre-pilot ceramic plant was established to produce quality ceramic electrolyte tubing at a rate of 200 tubes/month. The development process has been improved continuously. This plant will operate into Phase III.

The pilot plant for producing ceramic electrolyte has been planned, designed and constructed adjacent to the University of Utah campus. This facility consisting of approximately 9000 sq. ft. will have the capacity to ultimately produce 150 β"-alumina tubes per day. Most of the equipment has been specified and placed on order.

Fabricating and Testing

Fabrication and testing of exploratory cells has been accomplished at Ford (Dearborn) and Aeronutronic (Newport Beach).

Over 85 cells were assembled and evaluated. These cells were designed primarily to evaluate different candidate material systems for the sulfur container. The cells also provided a test bed for developing improved seal and assembly procedures, for evaluating intermediate size ceramic tubes (1.5 x 20 cm) and for characterizing electrical properties of sulfur electrodes in larger cells.

Twenty individual cell test stations with automatic test controls are in operation at Ford-Dearborn, while test facilities have been installed and successfully test operated at Aeronutronic, Newport Beach, California. An additional 20 cell stations will be operational by early 1978 at Aeronutronic.

TABLE OF CONTENTS

LIST OF FIGURES

LIST OF TABLES

SUMMARY

A comparison of program status at the beginning of Phase II (June 1976) with the present status (October 1977) indicates that major accomplishments have been obtained in the areas of: Prototype cell design and performance; ceramic electrolyte development; materials development; installation of production and test facilities; and system design.

The main areas toward which future efforts will have to be directed fall into two categories; the areas affecting cell performance and life, and the modification of cell design to optimize the total weight and volume of the cells.

To improve cell life and decrease the rate of deterioration of cell performance with time, better protective coatings of the sulfur container have to be obtained. Cell impedances can be lowered by achieving better contact of the felt electrodes to the sulfur container and by lowering the resistance of the β"-alumina electrolyte. Further work is needed in the area of sulfur electrode design to achieve high utilization of reactants in the two-phase region.

Modification of the mechanical design of the cell is needed to simplify assembly, decrease cost and reduce weight and volume of the cell. Main efforts in this area will be to redesign the seal between the sodium and sulfur containers with the ceramic insulator. The present seal is excessively heavy and expensive, and requires close tolerances of cell components and careful polishing of the ceramic surfaces.

The major accomplishments are discussed below.

Prototype Cells

At the beginning of the year, only two prototype cells (EV high power design) and over 100 laboratory cells had been evaluated. These cells were small (<25 Wh) but useful in developing an understanding of cell operation.

During Phase II, ten series of prototype cells, constituting over 85 cells, were assembled and evaluated. The cells incorporated the largest ceramic tubes, the preferred materials and best designs available at the time of construction. These tests provided experience in fabrication of large cells and allowed in-situ evaluation of candidate materials systems.

Significant progress in cell operation was obtained. For the preferred container material, degradation of cell capacity of less than 10% was obtained during 8 months of operation. In some cells employing the same material system, energy densities of 160 Wh/Kg and capacity utilization of 85% were obtained at the C/14 rate. Other similar cells did not perform as well.

Still larger prototype cells (Mark I), with 280 Wh (theoretical) capacity, have been assembled and placed on test.

Compression seals based on deformation of aluminum gaskets have been developed for the prototype cells and provide adequate seal quality. This seal approach has eliminated the additional high temperature cycles associated with the glaze and braze seals previously used. Additional seal developments are required, however, to reduce overall volume and to permit looser tolerance for other cell components.

Ceramic Developments

Ceramic improvements have resulted both from process refinements and from production facility development.

In addition to the increase in ceramic size from 1.0 x 15 to 3.3 x 25 cm (OD x L), reductions in tube wall thickness and improvements in dimensional control, chemical homogeniety and physical characteristics have been obtained. Ceramic components having conductivities exceeding 0.2 $(\text{ohm-cm})^{-1}$, strengths exceeding 25 Kpsi and microstructures with few grains larger than 50 μm are now routinely obtained. Production improvements include: development of high rate operations for powder preparation, green forming and sintering; evaluation of non-destructive test quality control methods; and development of fixtures and procedures for sealing large ceramic components.

Process developments now allow substitution of 2-5 $/lb alumina powders in place of 10-15 $/lb powders previously used without adversely affecting ceramic properties. The electrolyte tubes have been platinum encapsulated for the sintering process in Phase II.

Materials

A sulfur container material system has been developed which provides improved durability. In over 8 months of cell operation, the container suffered minor deterioration, based on the <10% degradation of cell capacity observed during the test.

Other alternate material systems, offering potential cost benefits, have been identified through static corrosion testing, and will be further evaluated in the coming year.

Facilities

Operation of a pre-pilot plant for ceramic production at UU has been successful, and production rates of 200 per month have been obtained. Construction of the pilot plant for production of larger tubes has begun, and operation by June '78 is projected for the Ceramatec facility.

Facilities for pre-pilot cell assembly, including sodium and sulfur filling stations have been installed and are undergoing development modifications to improve the yield and uniformity of assembled cells.

Test facilities for automatically controlling and acquiring data from 35 individual cells have been installed and successfully test operated at Aeronutronic Division, FACC. An additional 20-cell quality assurance test facility has been built and is expected to be operational within a month. Twenty individual cell test stations with automatic test control, but manual data reduction are in operation at Ford-Dearborn.

System Design

A conceptual design of a Na/S battery was created that would satisfy the requirements for load leveling application. Several preliminary designs of the requisite thermal control system were developed. Possible configurations for modules and cell interconnections were proposed.

Cost studies were initiated to evaluate the production feasibility of the present prototype cell vs a potential advanced cell; extrusion vs isostatic processing of ceramic. Eventually the battery system will be cost analyzed.

INTRODUCTION

As a result of Ford Motor Company research on the sodium-sulfur battery, which began in 1960, the National Science Foundation (NSF) - Research For Applied National Needs (RANN) awarded contract NSF-C 805 to Ford, for the period July, 1973 to June, 1977. The program objective was to demonstrate the technical feasibility of the sodium-sulfur battery.

On November 11, 1974 the Atomic Energy Administration issued Request for Proposal No. AT (11-1)-P-74-007 soliciting proposals for a planned five-year sodium-sulfur battery development program which was to result at the onset in a CPFF contract for Phase I (the first program year) of the multi-year procurement. The objectives, to be attained by the end of the fifth year, were the construction of two systems - a 1MW battery for utility load leveling and a 35 kW battery for an electric vehicle.

Ford Motor Company submitted a proposal in response to that solicitation on December 9, 1974 and, based on that proposal, and successes of the NSF-RANN contract, Ford and the Energy Research and Development Administration (ERDA) the successor agency to AEC for energy research, entered into Contract No. E(11-1)-2566 covering Phase I of the program. As contemplated by that proposal Ford awarded appropriate subcontracts to Ford Aerospace and Communications Corporation, Aeronutronic Division and the University of Utah.

The present Ford/ERDA program is geared to develop batteries for two major applications, electric utility load leveling and automotive propulsion. In future phases, attention will also be given to identifying solar missions suitable for Na/S battery storage. For load leveling, the battery must have long cycle life, and relatively low power output. The automotive battery must achieve high utilization of reactants to minimize battery weight and volume and higher power output levels. Cost and electrical efficiency are important factors in both applications. The performance goals and technical approaches employed for the development of the stationary and mobile batteries have become more distinguishable, although most of the research and some of the testing are common to both.

Some electric vehicle studies were performed and reported under an associated NSF-RANN contract. Results from these NSF studies have been used to establish tentative goals for the battery and cells required for EV applications. However, further studies are required to select the vehicle type and mission, and to finalize the battery specifications.

In Phase II, development of Na/S cells and batteries emphasized the transition from laboratory design to prototype hardware. The work was concentrated on a materials development program and involved the evaluation of many prototype cells. Much of the work for EV cell development was in common with the cell development efforts for the load leveling application (Task II). Only those results specific to EV applications will be reported in this section. Some highlights of the NSF system studies will also be included in this section to indicate our development approach and to place test results in perspective.

I.1 Battery Specifications

The power and energy requirements for an EV battery depend strongly on the vehicle type and mission. Data presented in Table I.1 were derived for a compact vehicle, equipped with manual transmission and employing regenerative braking.

Table I.1

DRIVE CYCLES

	Max. Speed (MPH)	Ave. Speed (MPH)	Max. Power (Kw)	Ave. Power (Kw)	Specific "Fuel" Consumption (KWh/Mile)
CVS	56.7	19.5	37.0	5.6	0.287
HWY.	59.9	48.3	31.0	13.8	0.286
SAE (J227)	45.0	24.1	26.8	6.5	0.270
TAXI	33.5	6.9	32.4	2.5	0.362
UPS	32.6	3.5	24.0	1.1	0.314
	1134 Kg Test Wt.				

The power and energy requirements of the battery have been refined to consider the short duration power demands experienced with the 1134 kg electric vehicle under a combination of driving conditions. These are summarized below:

Energy	33.0 kWh
Power - Max Instantaneous	37.0 kW
5 sec.	34.2 kW
20 sec.	30.0 kW
1 min.	15.3 kW
Average (CVS)	5.6 kW

The instantaneous 5 second and average power requirements are based upon the Federal Urban Driving Cycle (CVS); the 20 sec. power rating is derived from vehicle performance (WOT) requirements; the one-minute requirement is for hill climbing and is based upon a 30% grade. The energy rating gives a vehicle driving range (on the CVS cycle) of approximately 161 km with regenerative braking. To account for the decrease in power as the battery becomes discharged or aged, a higher power rating for a new fully charged battery is specified (44.5 kW).

Other features of battery design that were investigated include preliminary consideration of: (1) heat generation and thermal control; (2) packaging; and (3) sizing and strategy for cell interconnection straps. For further details, the reader is referred to NSF-C 805 final report.

1.2 Hybrid Battery

The possible advantages of using a hybrid high energy-high power battery are being evaluated from a system study approach, and will be validated by prototype cell design and evaluation. Substantial overall weight savings are projected for a combined battery, as shown in Table I.2.

Table I.2

HYBRID BATTERY

NaS*	- WT. (Kg)	466	314	208
	- Kw	44.5	26.5	13.5
	- Kwh	33	33	33
NiCd	- WT. (Kg)	0	41	70
	- Kw	0	18	31
TOTAL WT. (Kg)		466	355	278

*Load Leveling Cell, Design B of Table I.3

1.3 Cell Developments

In addition to the main effort on materials development, two other aspects of cell development were addressed -- cell design and prototype evaluation.

1.4 Cell Design

Because EV cell designs are required to provide a high power to energy ratio, the dimensions of the ceramic electrolyte strongly influence the projected cell and battery characteristics. Designs based on small ceramic tubes provide better electrical characteristics and improved packaging capabilities, as shown in Table I.3. Offsetting these benefits are the increased number of cells required.

Table I.3

CELL DESIGNS

	Design A	Design B
Ceramic		
OD x Length (cm)	1.5 x 20	3.35 x 25
Cell		
OD x Length (cm)	2.2 x 22	4.0 x 28
Weight (gm)	245	784
Specific Power (W/kg)	175	109
Specific Energy (Wh/kg)	130	81
Battery		
Number of Cells	1040	520
Weight (kg)	300	466
Volume (m3)	.227	.356
Specific Power (W/kg)	150	95
Specific Energy (Wh/kg)	111	71

Design improvements relating to more efficient use of sodium reservoir volume, safety features, and reduced seal volume are being developed. These efforts overlap and will be discussed in the following section (Task II). Alternate cell designs, such as horizontal cells and sulfur-core cells, are discussed in Tasks II and III as part of the materials development program, although these designs are expected to have larger impact for EV applications than for load leveling uses.

1.5 Prototype Cell Evaluation

Two series of prototype cells, A40 (5 cells) and A130 (2 cells) employed sulfur electrodes that were designed for power/energy ratios representative of EV requirements. The theoretical ampere-hour capacity of each series was 46 and 35 Ah based on conversion of total sulfur to Na_2S_3. The projected maximum energy densities available from these cells based on their actual non-optimized weights are 82 and 107 Wh/kg (trickle discharge).

At a 5 hour discharge rate, the average of the A40 series attained values of 65% of the ampere hour and 59% of the theoretical watt hour capacity. Of particular interest is the excellent pulse response of cell A40-3 to pulse loads of 5, 20 and 60 seconds duration. Power densities approaching 1 watt per square centimeter of ceramic area were attained for 5 second periods, varying with cell temperature and state of charge. These pulse power levels are up to double those predicted from internal cell losses under steady conditions at lower current levels. Large weight reductions of EV batteries could be possible if such pulse response can satisfy peak requirements (e.g., peaks of CVS driving cycle) allowing the battery to be designed for more average loads. Additional pulse data for cell A40-3 are presented in Figure I.1.

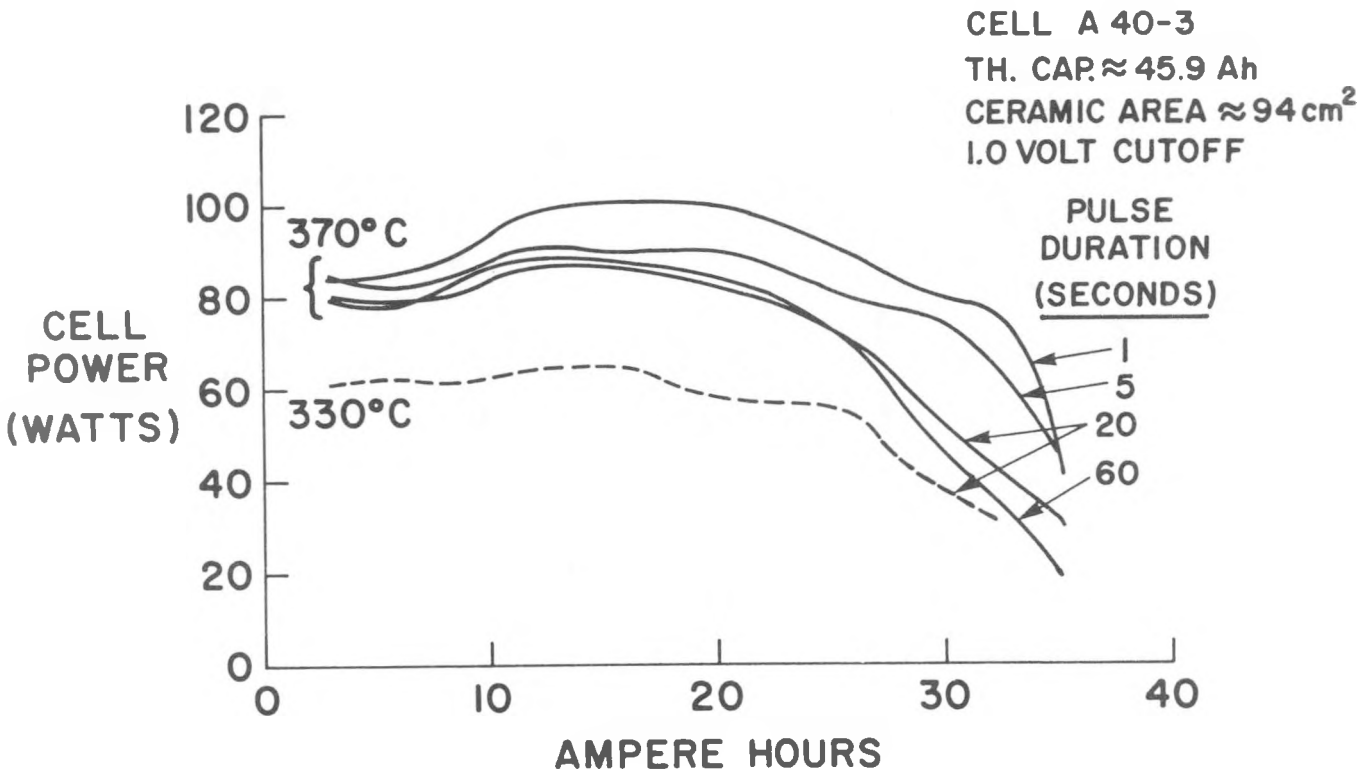

FIGURE I.1 - Pulse Load Response - Maximum Delivered Power for Loads of Short Duration

2.1 BATTERY REQUIREMENTS

The tentative requirements for the Ford Na-S load leveling battery have been altered somewhat in response to additional analysis of utility applications[1]. The addition of the physical constraints (e.g., truckable, weatherproof unit, footprint) and the sizing of the battery for shorter duration discharge times are included in the new tentative goals.

Table II.1

Tentative Goals
BEST Load Leveling Battery

Energy Delivered	5 MWH	Life - Cycle	2500
		Years*	10*
Power - Peak	1.5 MW		
Sustained	1.0 MW	Footprint	> 8 kWH/ft^2
Storage Efficiency	70%	Weatherproof Truckable Unit	
Discharge/Charge Time	5/7 (Hours)		

*Projected from one year module test.

The influence of these battery requirements on cell design has been evaluated for both sodium-core and sulfur-core cells.

Projections for sodium-core cells indicate that the energy delivered per cell is controlled by cell resistance, whereas for sulfur-core cells, the delivered energy can be limited by reactant volume. In sodium-core cells, the discharge current, hence Ah and Wh, is limited by internal cell resistance. The projected energy and discharge current as function of cell efficiency is shown in Figure II.1. Incomplete reactant utilization has only minor effect on the energy delivered per cell because overall cell diameter and sulfur loadings can be increased as necessary to accommodate the fractional usage. Although cell size and weight are increased by poor utilization, the number of cells/MWh would be unchanged except for the small effect associated with the relation between

[1] The BEST Facility - Workshop II, New Orleans, La., Feb. 8-10, 1977.

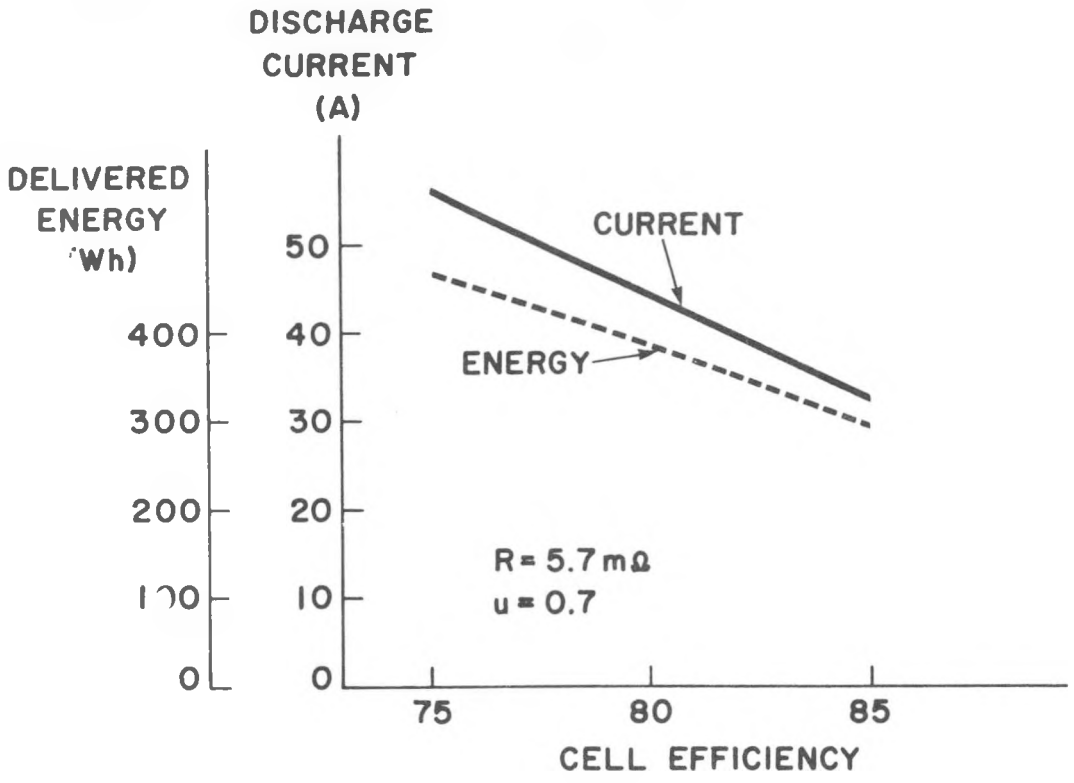

FIGURE II.1 - Projected Cell Characteristics. Discharge Current and Energy vs. Energy Storage Efficiency

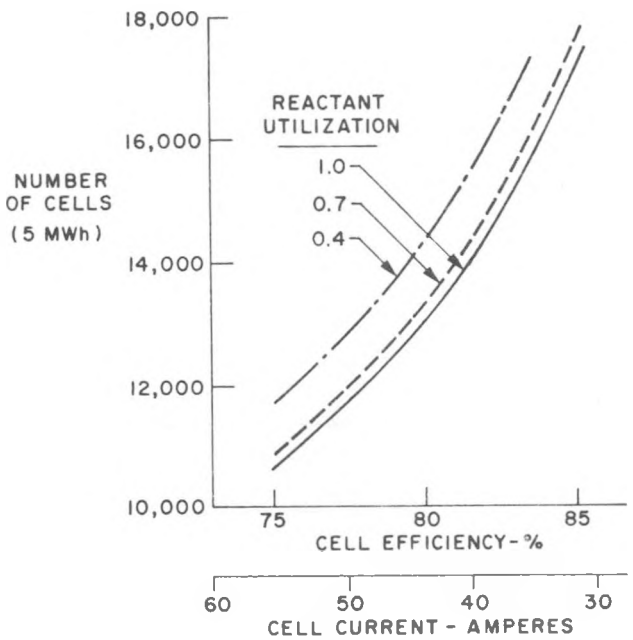

FIGURE II.2 - Number of Cells Projected for 5 MWh Battery

average cell voltage and utilization. Experience indicates that low utilization ($U \leq 0.4$) generally corresponds to one phase operation $OCV_{avg} \sim 1.93$ V, whereas for complete utilization $OCV_{avg} \sim 2.0$ V. The number of sodium-core cells required for the 5 MWH battery is shown in Figure II.2.

In contrast, sulfur-core cell designs based on presently envisioned ceramic electrolyte diameters (3.3 cm OD) are energy storage limited because of insufficient interior volume. The energy per cell becomes severely restricted if reactant utilization is not complete. A comparison of requisite number of cells for sodium and sulfur-core designs is presented in Figure II.3. For a ceramic diameter of 5 cm or larger, either sodium-core or sulfur-core designs predict similar cell requirements for discharge times up to 5 hours.

Improvements in cell resistance for either configuration could result in major cost and performance improvements for the battery. For designs based on sodium-core cells or on large sulfur-core cells not energy storage limited, the battery cost and number of cells are predicted to decrease nearly in proportion to the resistance. The projections are based on the possible higher current, Ah and Wh ratings for the lower resistance cells, and assume that cell life and control system complexity would not be adversely affected by the more vigorous operating conditions. For sulfur-core cells that were initially energy limited, benefits from improved resistance would be minor.

2.2 BATTERY CONCEPTS

A conceptual design of a 5 MWh load leveling battery is being developed based on consideration of the following factors:

System Requirements	BEST Requirements
Fault Isolation & Monitoring	Charge Control
Thermal Control	

A preliminary version of the Mark I concept is presented in Figure II.4 and reflects the present evaluation of the most favorable tradeoff of system factors.

Electrical Design. Particular emphasis has been placed on examining cell interconnection requirements and on selecting the cell interconnection strategy. The

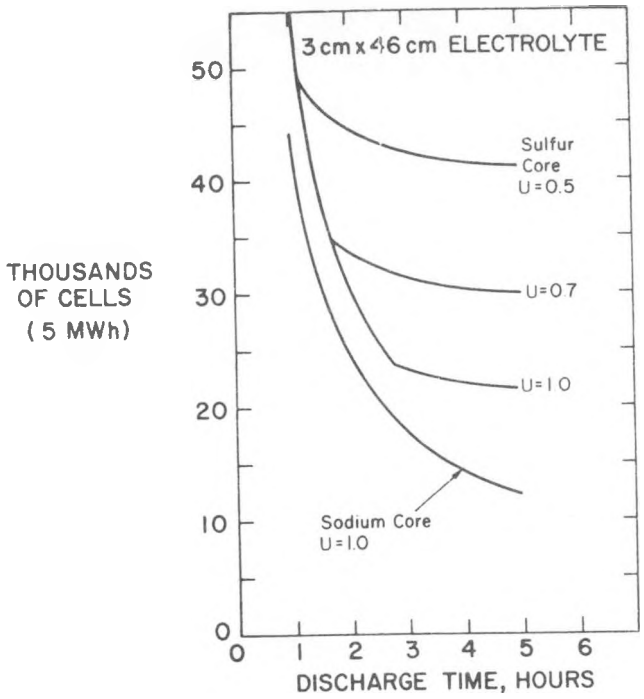

FIGURE II.3 - Comparison of Sulfur-Core vs. Sodium-Core Cells Required for 5 MWh Battery

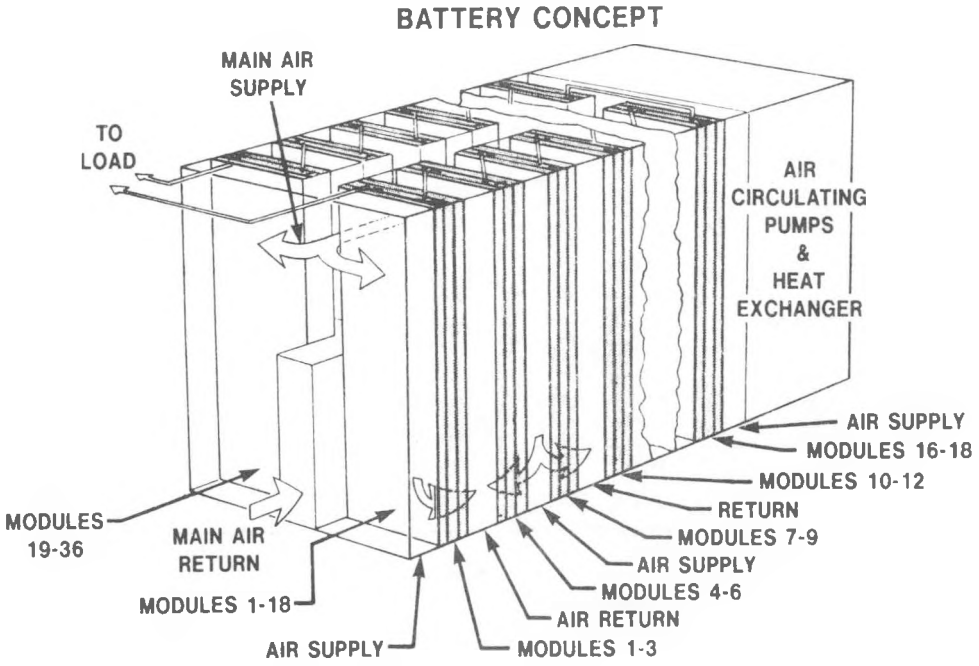

FIGURE II.4 - Concept Design - 5 MWh Battery

importance of failure mode for individual cells and the availability of fault isolation procedures indicate advantages in favor of maximizing the number of cells in parallel (a unit defined as a submodule). Several submodules would be packaged into a module for simplification of handling and installation. Concept designs for the submodule and module are given in Figures II.5 and II.6.

The battery would be electrically connected as a single series string of (C.A. 300) submodules to provide a voltage level in the range recommended for testing in the BEST facility. Monitoring and charge control circuits would be required to maintain balance within the battery. The housing is designed to provide simple removal and replacement of defective modules. Space would be provided to maintain an extra module at temperature to permit quick restoration of full battery power by simple electrical connection.

Thermal Design. The thermal control system for the concept battery is based on forced convection in which hot air is recirculated to maintain uniform temperature within the battery and to prevent thermal-electrical instability of cells connected in parallel. Heat removal from the battery is provided by partial exhaust of hot gases and intake of ambient makeup air. Temperature variations within the battery are constrained to remain below the corrosion limit and above the minimum operating temperature, both while the battery is operating and during periods of idle. It is estimated that a 15 hp fan operating 16 hours per week would maintain cell temperatures between 300 and 350°C. A projected daily cycle is shown in Figure II.7.

The method of cooling has not been finalized. Alternate control system designs, including some based on radiative cooling, are continuing to be evaluated. Radiative cooling to cold pipes does not appear to offer good control over cell temperature, but lends itself to use of inert gas as the coolant more so than does forced convection. The relative advantages and disadvantages of convection and radiation must be weighed.

2.3 THERMAL CONTROL SYSTEM REQUIREMENTS

The results reported in this section are based on preliminary studies and should be treated accordingly.

Limits. Limits on cell temperatures and temperature differences within the battery are set by corrosion rates, electrical characteristics and the uniformity of operation. Corrosion data for many candidate container materials indicate a rapid increase in the rate of corrosion above 350°C. An upper temperature limit T_{max} in the range of 350-375°C is proposed, subject to further material developments. The temperature dependence of cell capacity and efficiency are functions of cell design. For present prototype designs, cell performance decreases rapidly below 300°C. Minimum cell operating temperature is set at 300°C, although a slow startup bootstrap operation (self heating) may be possible from somewhat lower temperatures (275°C). Requirements for temperature uniformity, especially for cells in parallel, are to be determined next year.

Rates. On discharge, heat is generated within the cells as a result of combined entropy and Joule heating, whereas on charge, a small net cooling rate is expected. The calculated heating rates and resultant temperature change during charge and discharge cycles are shown in Figure II.8. Heat removal during discharge is required to prevent cell over-temperatures. Radiative as well as convective cooling of cells is possible for the levels of heat exchange required in this application (less than 50 mW/cm^2 of cell surface).

Energy Conservation. Methods to conserve energy required for thermal control have been explored. Two primary approaches are: (1) storage of thermal energy during discharge as specific heat of cells and structures to provide the required entropy and system conduction losses during charge and idle periods; and (2) utilization of the rejected heat.

Because of the limited temperature cycle range and the substantial entropy cooling, it appears necessary to greatly increase the heat capacity of the system, possibly through installation of phase-change materials (e.g., lead) within the battery or recirculating plenums. Increasing fan power to narrow the temperature

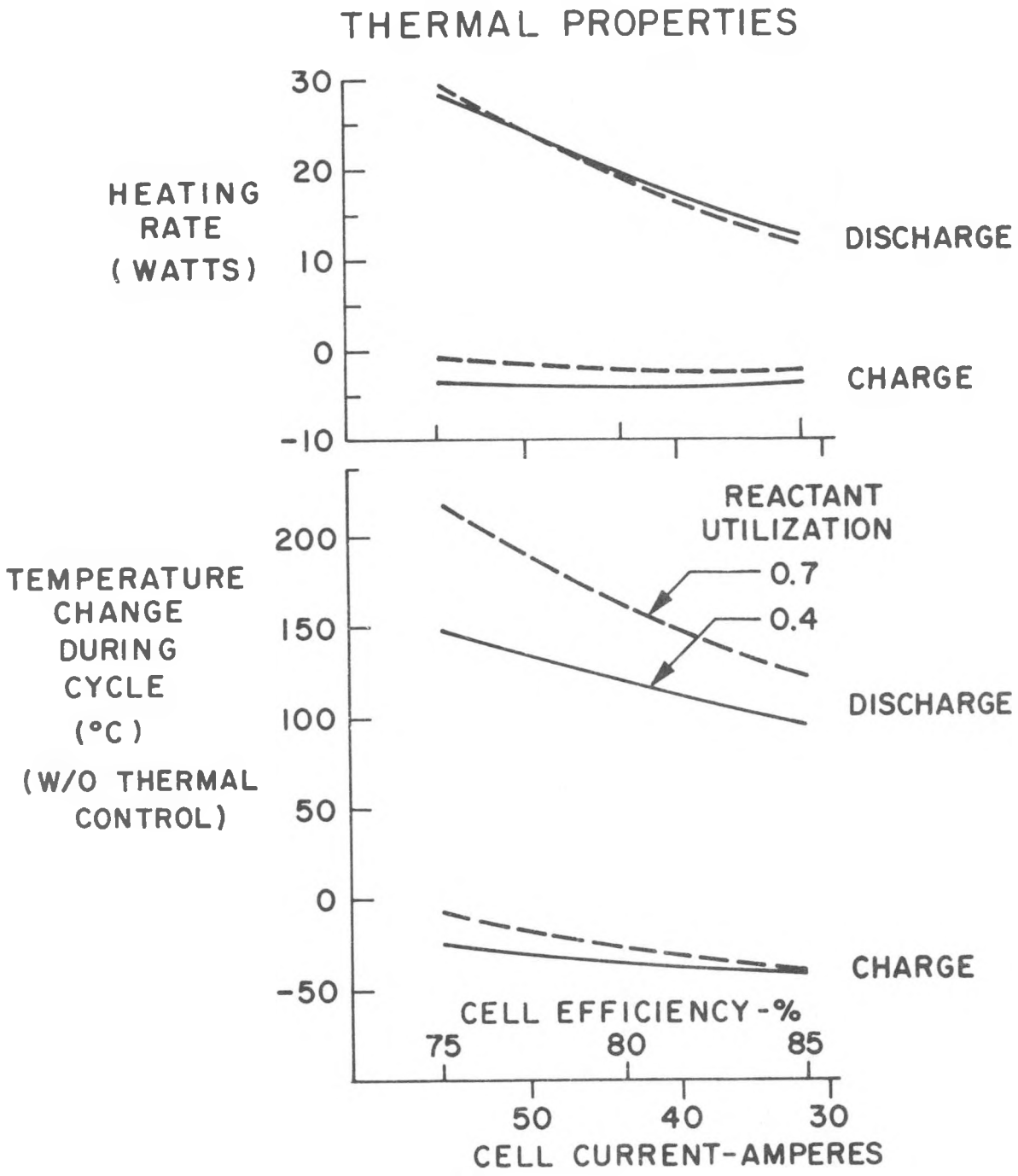
THERMAL PROPERTIES
HEATING RATE (WATTS)
30
20
10
0
-10
DISCHARGE
CHARGE
TEMPERATURE CHANGE DURING CYCLE (°C) (W/O THERMAL CONTROL)
200
150
100
50
0
-50
REACTANT UTILIZATION
0.7
0.4
DISCHARGE
CHARGE
CELL EFFICIENCY-%
75
80
85
50
40
30
CELL CURRENT-AMPERES

FIGURE II.8

differences would allow an increased average cell temperature so that more specific heat could be stored. Such tradeoffs are being evaluated. However, it may prove more effective to recharge at higher rates with lower efficiency.

Although utilization of waste heat is of less importance than system reliability for the BEST 5 MWh battery, such energy recovery would impact the system efficiency of large utility storage systems. Designs which provide high grade heat rejection are being considered.

2.4 CELL DESIGN AND ANALYSIS

Exploratory Prototype Cells

The exploratory cells were designed to serve several functions. The primary function was to evaluate different candidate material systems for the sulfur container. Secondly, the cells provided a test bed for developing improved seal and assembly techniques, for evaluating the intermediate sized ceramic tubes (1.5 x 20 cm), and for characterizing electrical properties of sulfur electrodes in larger cells. The results of the materials testing effort are presented in Task III, and the results of safety and electrical testing in Task V.

A parametric analysis defining relative cell dimensions and resultant cell characteristics was performed[1]. Relationships for component dimensions, cell capacity and resistance were developed to gain insight into the probable range of cell dimensions which anticipated design changes might impose. An extensive tabulation of selected physical properties was formed.

An analysis of cell-burst conditions considered the effects of confined gases during cell assembly, overfilling with sulfur and/or sodium, and cell temperatures[2]. Analysis indicates that close control of cell filling is necessary, but that a properly assembled cell should withstand temperatures over 750°C arising, for example, from failure of an adjacent cell.

---

[1] Appendices A & B.

[2] Ibid, Appendix C

Considerable effort was expended on calculating residual stresses in seals between the alpha- and beta"-alumina components. Finite element models were generated and response stresses computed for several seal joint geometries. Thermal stresses induced from cool down are greatest in the vicinity of the glass seal. A summary of the analytical results for the 1.5 cm OD beta"-alumina tube seal is presented in Table II.2 for several seal geometries[3].

Table II.2

SUMMARY OF STRESS RESPONSE DUE TO COOL DOWN FROM 824°C TO 70°C[3]

Configuration	Critical Stresses in Joint Region, kpsi				
	σ_R	σ_Z	σ_H	σ_{max}	τ_{max}
1. Curved Alpha-Alumina Element (Figure D-3)	5.6	5.0	3.7	6.5	4.5
2. Straight Seal (Figure D-4)	5.5	3.4	7.5	6.1	3.8
3. Straight Seal (Figure D-5)	4.0	4.7	4.2	4.7	4.4
4. Straight Seal (Figure D-6)	5.1	6.3	6.4	6.7	5.4

The cantilever stresses resulting from misalignment defects were calculated. Potentially large stress levels, resulting from the forced centering of the electrolyte during cell assembly, can result from slight misalignment of the alpha- and beta"-alumina bodies during glass sealing operations. Tighter jig tolerances will likely be required.

Thermal analysis for cells was made, based on the design of an exploratory prototype cell[4]. Test data was used to estimate cell losses, and literature values for entropic heat and thermal conductivities were used. Internal temperature variations of less than 3°C were predicted for a 100 mA/cm^2 discharge current density. Heat exchange at the outer cell surface can be effectively accomplished by either forced air convection or by radiation. Flow rates, heatup times and energy inputs were calculated in this study.

[3] Ibid. Appendix D.

[4] Ibid. Appendix E.

Mark I Prototype Cell

The development and demonstration of a corrosion-resistant metallic sulfur container coincided with the development of large (3.3 x 25 cm) beta"-alumina electrolyte tubes by the University of Utah Research Institute. The two developments were incorporated into the Mark I load-leveling cell, a prototype intended for beginning multi-cell testing, for production experience, and as a design base for subsequent improvements. Design and analysis began late in January 1977, safety tests were conducted in June, and the first electrical tests commenced in July at the Aeronutronic test facility.

The design of the Mark I cell is basically an enlarged version of the successful exploratory cell. It is a "sodium-core cell" in which the sodium is contained inside a beta"-alumina tube that in turn is surrounded by the sulfur electrode, a sulfur-impregnated graphite felt. Additional sodium is stored in a metallic container located above the beta"-alumina tube and from which sodium flows (by gravity) through holes in a stainless steel "safety" tube into the beta"-alumina tube.

The sodium reservoir and the sulfur container form separate hermetic seals to the flat disk of alpha-alumina. Compression of aluminum gasket material is provided by a set of flanges mechanically secured by bolts and nuts. The alpha-alumina disk is glass sealed to the beta"-alumina tube. As designed, the cell will provide a 150 Ah (300 Wh) theoretical capacity and weight approximately 1.85 kg. The design for Mark I is shown in Figure II-9.

MARK I CELL

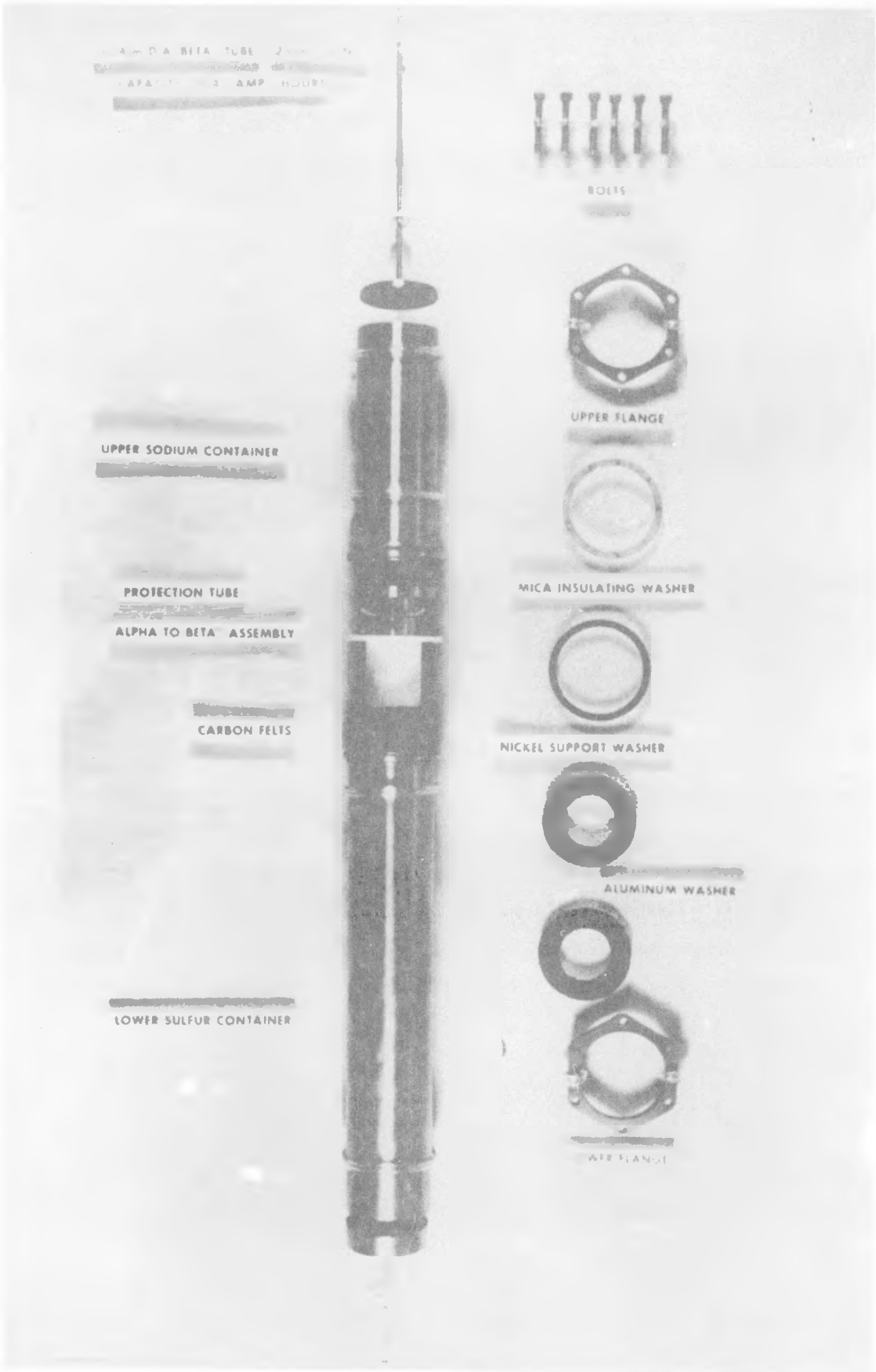

FIGURE II.9 - Mark I Prototype Cell Design

TASK III - CONTAINER AND SEAL DEVELOPMENT

The primary effort of this task was to develop an electrically conductive sulfur container, resistant to sodium polysulfide corrosion. It was performed by the Aeronutronic Division, Ford Aerospace and Communications Corporation and the Ford Motor Company.

Previous development work at Ford Motor Company Research Laboratory and Aeronutronic indicated that most metallic materials were highly reactive with sodium polysulfide. Molybdenum, chrominum and alloys with a high chromium content had improved corrosion resistance while metal oxides and carbon appeared to be stable.

In continuation of this development effort, a variety of materials and coating systems for various substrates were selected for the static corrosion tests*. A 30-day screening test was utilized for the preliminary evaluation of untried material systems. Materials and coating systems that showed promise were tested for longer durations. The most promising systems were fabricated into cell containers and dynamically tested as fully operational cells at the Ford Motor Company Research Laboratory.

3.1 Surface Treated and Coated Alloys

Table III-1 lists the results of the screening tests on surface-treated alloys, metallic coatings and non-metallic coatings. The durability of protective coatings depends a great deal on the corrosion behavior of the substrate. Defects such as pin holes, cracks, etc., occur in all thin coatings. The more corrosion resistant substrates such as the chrome-bearing alloys, will form reaction products that tend to plug the defect, thus remaining stable. The highly corrodable substrates such as iron and nickel will form loose, non-protective reaction products resulting in the undercutting and eventual shedding of the coating. This occurs even if the coating is truly inert.

Metallic coatings of chromium and molybdenum showed low corrosion rates. Some chromium coatings were highly cracked, resulting in eventual substrate corrosion. Chromizing (a diffused chromium-rich coating and chromium electroplating) characterized by low crack density, offered good protection against sodium polysulfide corrosion.

A silicate-bonded graphite coating (Tiodize CC-400) showed good corrosion resistance. This coating was evaluated on a variety of substrates and in duplex coatings of Tiodize on chromium coatings.

Glass and ceramic coatings also offered good corrosion protection, but they were not electrically conductive. Thus these coatings cannot be used in cell designs where the metal sulfur container is also used as the current collector.

Additional corrosion tests were performed on Tiodize CC-400/chromized Type 446 stainless steel. The results are shown in Table III-2.

*Ibid, Appendix F

TABLE III-1. INITIAL SCREENING TESTS ON SURFACE-TREATED AND COATED ALLOYS EXPOSED TO Na_2S_4 AT 400°C FOR 30 DAYS

Sample	Corrosion Behavior	Stability
SURFACE-TREATED ALLOYS		
Oxidized Chromium	No reaction	I
Oxidized Chromized Type-446 Stainless Steel	Scattered pitting	S
Oxidized Chromized Fe-42Ni	No reaction	I
Anodized Aluminum	No reaction	I
Chem-Treated 6061 Aluminum	3-mil corrosion depth	U
Anodized Titanium	10-mil corrosion depth	U
Anodized Columbium	20-mil corrosion depth	U
Anodized Tantalum	15-mil corrosion depth	U
METALLIC COATINGS		
CVD Molybdenum on Armco Iron	High substrate corrosion; some areas protected	U
Plasma Sprayed (PS) Molybdenum on Type-446 Stainless Steel	Slight surface corrosion	S
PS Molybdenum on 3003 AL	Coating disintegrated	U
PS Chromium on Type-446 Stainless Steel	2-mil surface corrosion	S
Electroplated Chromium on Type 446 Stainless Steel	<0.5-mil surface corrosion	S
Electroplated Chromium on Fe-42Ni	<0.5-mil surface corrosion	S
Electrolyze on Type-446 Stainless Steel	<0.5-mil surface corrosion	S
Chromize on Armco Iron	Complete substrate corrosion	U
Chromize on Type-446 Stainless Steel	0.1-mil surface corrosion	S
Chromize on Fe-42 Ni	Complete substrate corrosion	U
Chromize on Inconel 601	2-mil surface corrosion	S

I = Inert, no measurable reaction

S = Stable, some surface corrosion or pitting

U = Unstable, massive corrosion or shedding of coating

TABLE III-1 INITIAL SCREENING TESTS ON SURFACE-TREATED AND COATED ALLOYS EXPOSED TO Na_2S_4 AT 400°C FOR 30 DAYS (Continued)

Sample	Corrosion Behavior	Stability
Aluminide on Armco Iron	Complete substrate corrosion	U
Aluminide on Fe-42Ni	Complete substrate corrosion	U
Aluminide on Type-446 Stainless Steel	Complete substrate corrosion	U
NONMETALLIC COATINGS		
PS Al_2O_3 on Type-446 Stainless Steel	Complete substrate corrosion	U
Solar S-5210-27 (ceramic coating) on Type-446 Stainless Steel	No reaction	I
Solar GN-19X (ceramic coating) on Type-446 Stainless Steel	No reaction	S
EF 2396 on Type-446 Stainless Steel (Silicate-bonded carbon)	Slight substrate corrosion	S
EF 1000 on Type-446 Stainless Steel (Ceramic-bonded carbon)	Coating disintegrated	U
EF 2006 on Type-446 Stainless Steel ((Silicone-bonded carbon)	Coating degraded	U
EF 4006A on Type-446 Stainless Steel (Phenolic-bonded carbon)	Coating disintegrated	U
EF 2006 on 3003 Aluminum	4-mil substrate corrosion	U
Tiodize CC-250 on Armco Iron (Inorganic-Based bonded carbon)	Complete substrate corrosion	U
Tiodize CC-250 on Type-446 Stainless Steel	Complete substrate corrosion	U
Tiodize CC-400 on Armco Iron (Silicate-based bonded carbon)	Complete substrate corrosion	U

I = Inert, no measurable reaction

S = Stable, some surface corrosion or pitting

U = Unstable, massive corrosion or shedding of coating

TABLE III-1. INITIAL SCREENING TESTS ON SURFACE-TREATED AND COATED ALLOYS EXPOSED TO Na_2S_4 AT 400°C FOR 30 DAYS (Continued)

Sample	Corrosion Behavior	Stability
Tiodize CC-400 on Type-446 Stainless Steel	Very slight substrate corrosion	S
Tiodize CC-400 on Fe-42Ni	Complete substrate corrosion	U
Tiodize CS-250 on Armco Iron (Inorganic-Based bonded carbon)	Complete substrate corrosion	U
Tiodize CS-250 on Type-446 Stainless Steel	Complete substrate corrosion	U
Clay-Graphite	No reaction	I
Pencil Lead	Surface Corrosion	U
CVD Carbon, Low Temperature, on Nickel on Type -304 Stainless Steel	Complete substrate corrosion	U
CVD Carbon, High Temperature, on Nickel on Type-304 Stainless Steel	Complete substrate corrosion	U
CVD Carbon, Low Temperature, on Ceramic on Type-304 Stainless Steel	Complete substrate corrosion	U
CVD Carbon, High Temperature, on Ceramic on Type-304 Stainless Steel	Complete substrate corrosion	U
PVD Carbon on Type-304 Stainless Steel	Complete substrate corrosion	U
Tiodize CC-500 on Al_2O_3 (Polyphenylene Based)	Coating spalled below melt	U
Tiodize CC-500 on Type-446 Stainless Steel	Complete substrate corrosion	U
Tiodize CC-500 on Type-304 Stainless Steel	Coating spalled beneath melt; heavy corrosion of substrate edges	U
Tiodize CC-500 on 3003 Aluminum	Coating spalled, some substrate corrosion	U

I = Inert, no measurable reaction

S = Stable, some surface corrosion or pitting

U = Unstable, massive corrosion or shedding of coating

TABLE III-1 INITIAL SCREENING TESTS ON SURFACE-TREATED AND COATED ALLOYS EXPOSED TO Na_2S_4 AT 400°C FOR 30 DAYS (Continued)

Sample	Corrosion Behavior	Stability
Polyphenylene Sulfide on 3003 Aluminum, (Heated 14 days at 400°C in vacuum)	Coating "crazed", substrate corrosion in cracks	U
Polyphenylene sulfide on 3003 Aluminum	Complete substrate corrosion	U
Tiodize CC-250 on Al_2O_3 (Inorganic Based, Graphite-Filled)	Coating disintegrated	U
Tiodize CC-250 on Anodized 3003 Aluminum	Coating disintegrated	U
Tiodize CS-250 on Al_2O_3 (Inorganic Based)	Coating disintegrated	U
Tiodize CS-250 on Anodized 3003 Aluminum	Coating disintegrated	U
Tiodize CC-400 on Al_2O_3	No corrosion	I
Tiodize CC-400 on Molybdenum	Coating spalled off	U
Tiodize CC-400 on Molybdenum (120 days)	Coating spalled off	U
Tiodize CC-400 on Type 304 Stainless Steel	Coating spalled, edge pits	U
Tiodize CC-400 on Chromized Fe-42Ni	Coating spalled below melt, fine pyrite crystals above	U
Tiodize CC-400 on 3003 Aluminum (with window)	No corrosion	I
Tiodize CC-400 on 3003 Aluminum	Coating spalled on edges, slight pitting	S
Tiodize CC-400 on Chromized Armco Iron	Complete substrate corrosion	U
Tiodize CC-400 on graphite joined to graphite felt with graphite/silicate cement	No reaction	I

I = Inert, no measureable reaction

S = Stable, some surface corrosion or pitting

U = Unstable, massive corrosion or shedding of coating

TABLE III-1. INITIAL SCREENING TESTS ON SURFACE-TREATED AND COATED ALLOYS EXPOSED TO Na_2S_4 AT 400°C FOR 30 DAYS (Continued)

Sample	Corrosion Behavior	Stability
Tiodize CC-400 on Graphite felt joined to graphite felt with Tiodize C-400 paste	No reaction	I
Solar S-5210-2C on Type 446 Stainless Steel (Ceramic Coating)	No reaction (150-day test)	I
Solar GNX-19 on Type 446 Stainless Steel (Ceramic Coating)	No reaction (150-day test)	I
Glass-Molybdenum	Surface darkened	S
Glass on Chromized Type-446 Stainless Steel (Heated 16 hrs at 800°C in wet H_2)	No reaction	I
Glass/Molybdenum on Type 446 Stainless Steel	Surface darkened (18-day test)	S

I = Inert, no measureable reaction

S = Stable, some surface corrosion or pitting

U = Unstable, massive corrosion or shedding of coating

TABLE III-2 CORROSION TEST RESULTS FOR SILICATE-BONDED GRAPHITE (TIODIZE CC-400) ON CHROMIZED TYPE-446 STAINLESS STEEL EXPOSED TO Na_2S_4 AT 400°C

Time Days	Corrosion Behavior	Wt. Change (mg)
	TIODIZE CC-400 ON CHROMIZED GLASS-BEADED TYPE-446 STAINLESS STEEL (HEAVY COAT)	
30	Pyrite crystals above melt	-4
60	Pyrite crystals above melt	-3
120	Pyrite crystals above melt, shedding coating, black reaction product under coating	-17
	TIODIZE CC-400 ON CHROMIZED GLASS-BEADED TYPE-446 STAINLESS STEEL (STANDARD COAT)	
30	Fine pyrite crystals above melt	-2
60	Heavy pyrite crystals above melt, very fine crystals below, some shed coating	+2
120	Complete reaction with the melt, corrosion from one side	-1640
	TIODIZE CC-400 ON CHROMIZED TYPE-446 STAINLESS STEEL (STANDARD COAT)	
30	Fine pyrite crystals above melt	-2
120	Pitting corrosion (primarily below melt), pyrite crystals in pits	-72
120	Complete reaction from above melt, deep pitting	-1510
	TIODIZE CC-400 ON CHROMIZED TYPE-446 STAINLESS STEEL (THIN COAT)	
30	Very fine pyrite crystals above melt, fine pitting below	-1
60	Fine crystals, fine pitting, shed coating above melt, fine pitting below	-8
120	Heavy pitting above melt, some crystals fine pitting below	-280

3.2 Untreated Metals

A comparison of 60 day corrosion data for untreated metals is shown in Table III-2.

The untreated metals and alloys reacted to varying degrees during the exposure to sodium tetrasulfide. The iron, iron-nickel, and iron-nickel-cobalt alloys were most severely attacked, producing a low density solid reaction product of 10 to 20 times the volume of the metal which corroded.

Chromium metal and most alloys containing over 15 percent chromium were partially protected by a dense crystalline reaction layer. The volume of these reaction products was up to 10 times the volume of the displaced metals. These layers spalled on cool down and had little adhesion at room temperature.

Molybdenum was protected by a thin layer of molybdenum disulfide. This coating adhered well after cool down and cleaning.

Alloys of titanium, columbium and tantalum were heavily corroded. Zirconium exhibited reasonably good corrosion resistance.

The 3003 aluminum alloy in the as-received condition exhibited very good corrosion resistance initially; however, after a threshold period, it corroded at a significant rate.

Corrosion as a function of time was plotted for several metals in Figure III-1.

3.3 Other: Treated Aluminum

The 3003 aluminum alloy was further evaluated with a variety of surface treatments as shown in Table III-4. Anodizing and chromate coating (chemfilm) offered excellent corrosion protection. The chemfilm coating was electrically conductive, whereas anodizing was not.

Auger electron spectroscopic analysis of untreated 3003 aluminum alloy, chem-treated 3003 aluminum, and the chem-treated 3003 aluminum after 30 and 90 days immersion in Na_2S_4 at 400°C revealed the following features. The surface of the untreated 3003 aluminum is covered with an oxide layer. Other elements detected in the Auger spectra were: Si, C, F and Na. The spectra of the chem-treated 3003 aluminum show dominant and intense Cr-, Fe-, and O- peaks, indicating the presence of Cr-oxide and Fe-oxide surface layers. However, these layers were only about 50×10^{-10} m (Å) deep. After only 30 days immersion in molten Na_2S_4 the Auger spectrum of the sample shows the presence of O-peaks only, both the Cr- and Fe- peaks disappeared. However, even after 90 days immersion, the remaining Al-oxide layer extends to a depth of about 520×10^{-10} m (Å). Depth analysis was determined by sputtering at 5 kV at a rate of 65×10^{-10} m (Å) per minute.

TABLE III-3 CORROSION DATA FOR VARIOUS METALS EXPOSED TO Na_2S_4 AT 400°C FOR 60 DAYS

Sample	Density (g/cm^3)	Sample Area (cm^2)	Original Weight (g)	Weight Change (mg)	Corrosion Depth (microns)
Iron	7.86	10.4	5.0852	4162	625
Iron-42 Ni	8.12	7.4	3.1325	3133	575
Iron-29Ni-17Co	8.36	7.4	3.0033	3003	500
Type 446 S.S.	7.60	7.4			>500
Type 446 S.S.	7.60	7.4	2.8144	139	25
Inconel 600	8.45		4.6041	769	115
Inconel 601	8.1	7.6	4.4303	146	25
Inconel 671	7.9	9.0	9.3500	160	23
Hastelloy B	9.2	9.0	9.1922	2220	275
Hastelloy G	8.3	9.0	8.7861	228	30
Hastelloy C-278	8.9	9.0	11.3336	371	45
Kanthal					>500
Haynes 188	8.6	9.7	11.7652	69	8
Chromium	7.2	0.45	0.1719	3.3	10
Molybdenum	10.2	6.17	0.4642	12.2	1.9
TZM Molybdenum	10.2	2.1	8.5208	5	3
3003 Aluminum	2.7	7.6	0.8642	1	0
Titanium	4.5	7.4	1.9823	508	250
Zirconium	6.5	7.6	3.2223	117	25
Coumbium	8.6	8.8	3.8705	1910	625
Tantalum	16.6	10.1	6.9940	1965	375
Tungsten					>500
Type 304 S.S.	7.9	7.5	3.9223	276	46
Type 316 S.S.	7.9	7.6	3.8680	10	--

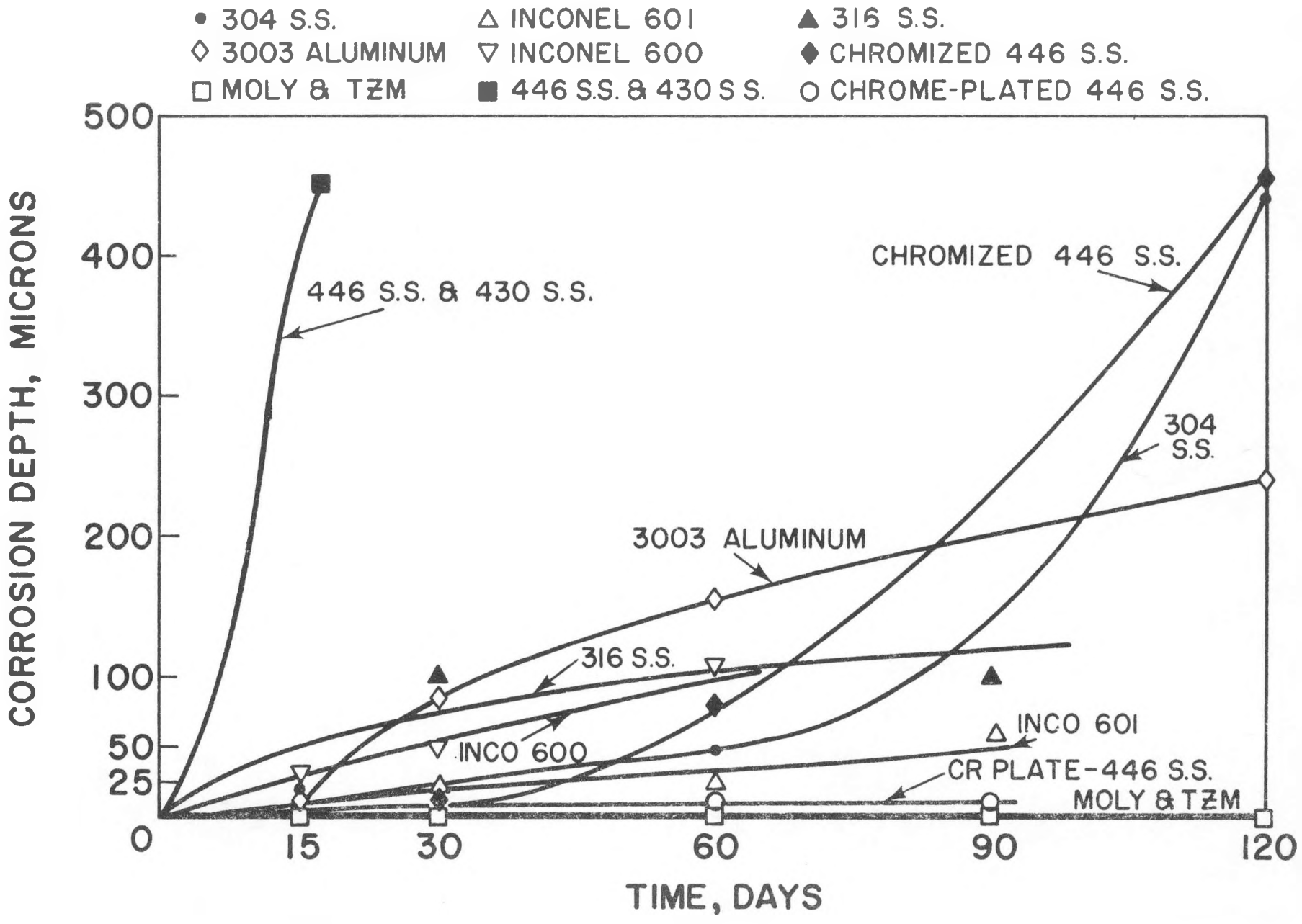

FIGURE III.1 - Corrosion Depth as a Function of Time for Selected Metals

TABLE III-4 CORROSION TESTS ON 3003 ALUMINUM WITH VARIOUS SURFACE TREATMENTS

Description	Time (Days)	Weight (g)	Weight Loss (mg)	Area (cm^2)	Corrosion Depth (Microns)
As Received	30	0.8642	0.5	7.6	0
As Received	30	1.9643	355	14.4	90
Grit Blasted	30	1.5482	1	11.3	0
Chem Deoxidized	30	1.9145	503	14.1	140
Anodized, 1 Minute	30	1.9060	15	14.0	4
Anodized, 2 Minutes	30	1.9170	6	14.1	1
Anodized, 30 Minutes	30	1.3089	0.4	9.6	0
Chem Treated (Chromate Conversion Coating)	30	1.5498	0.8	11.3	0
Type I Anodized-No Seal	30	1.2971	4	9.5	0
Type I Anodized-No Seal	60	1.3068	2	9.7	0
Type I Anodized-No Seal	120	1.3473	0	9.9	0
Chem Treated	30	1.5513	0	11.3	0
Chem Treated	60	1.5418	0	11.3	0
Chem Treated	90	1.5688	0	11.4	0
Type II Anodized-Chromate Seal	60	4.0681	13	29.7	2
Type II Anodized-Chromate Seal	120	4.1557	14	30.3	2

3.4 Test Results From Prototype Cell

The static corrosion tests had identified the following group of materials and coatings as candidates for use in prototype cell sulfur containers: high chromium content alloys; aluminum; molybdenum metal and coatings; chromium coatings; carbon/graphite; glass/ceramic coatings; oxidized and chromated surfaces.

The static corrosion testing of variations and combinations of these materials continued while some of these materials were fabricated into sulfur containers for prototype cell evaluation.

The A-30 series cells utilized a sulfur container fabricated from Type 446 stainless steel and coated with a silicate-bonded graphite, Tiodize CC-400. The graphite felt electrode was bonded to the continer with silicate/graphite cement. A press-in end cap made from the same materials system and having a one-degree taper fit was used. This design allowed the corrosion resistant coatings of the container and the end cap to overlap. Analysis of the container after testing indicated that some substrate corrosion had occurred through coating defects.

The A-40 series was of similar design; however, chromium electroplating with a low crack density was applied to the Type 446 stainless steel container before the Tiodize CC-400 coating. The graphite electrode was not bonded to the container. The end-cap assembly was Chromized before the Tiodize coating was applied. The inside of the sulfur container fill tube was not coated with the Tiodize CC-400. Some cells of this series lasted as long as ten months. Examination of cells removed from test showed that some corrosion occurred through coating defects, usually showing up as a crystal growth through the defects. The test results from the A-40 series cells were a significant factor in the selection of materials for the Mark I cells.

The A-90 series utilized a type 430 stainless steel sulfur container with a 3003 aluminum liner. A chromate conversion coating (Chemtreat) was applied to the aluminum. The Chemtreat coating is electrically conductive. The first test of a cell utilizing this materials system resulted in a fire. Further evaluations will be scheduled.

The A-100 series cells utilized a sulfur-container materials system similar to that of the A-40 series. Containers fabricated from E-Brite stainless steel (Fe-26 Cr-1 Mo) were first electroplated with chromium which has a low-crack density and then coated with Tiodize CC-400. The end caps were also Tiodize-coated, chromium-plated E-Brite stainless steel. However, the fill tubes were not coated on their internal surfaces, and the cells failed early due to corrosion of the fill tubes.

The A-120 series was similar to the A-100 series, except that chromizing was used instead of electroplated chromium. This series are currently on test.

3.5 Mark I Cell Sulfur Container

In order to continue the cell development program, it was important that a reasonably durable cell be established for the Mark I prototype design. The extensive static and dynamic tests performed allowed the selection of the Mark I sulfur container. It was E-Brite stainless steel with a .025 to .050 mm (.001 - .002 inch) thick layer of low crack density chromium electroplate. The chromium plating was then coated with Tiodize CC-400. The sulfur container end cap was E-Brite stainless steel with a coating of S5210-2C Solaramic.

TASK IV - DEVELOPMENT OF CERAMIC ELECTROLYTE AND SEAL TECHNOLOGY

The primary objective of this task was the production of quality ceramic electrolyte tubing in sufficient quantity to support the needs of the sodium-sulfur battery development program. The University of Utah was given the responsibility to set up a pre-pilot plant for limited electrolyte production, to develop the necessary production techniques to produce a cost effective-quality electrolyte. The University of Utah Research Institute was given the task of designing and constructing a pilot plant with the potential to produce efficently much larger quantities of ceramic electrolyte.

4.0 Pre-Pilot Electrolyte Development and Evaluation (University of Utah)

4.01 Production of Standard Tubing

The present pre-pilot batch plant shown in Figure IV-1, has the capability of producing approximately 200 β"-alumina electrolyte tubes per month.

Standard tubing (1.5 cm and 3.35 cm O.D. and up to 25 cm long) has been supplied unsealed, seald to α-alumina tubular headers (1.5 cm O.D.), or sealed at a rate consistent with the supply of machined α-alumina disk headers. During the period February 1976 - February 1978, 250 standard tubes of various sizes, sealed and unsealed have been shipped to Ford Motor Company and Aeronutronic, FACC.

Standard tubes were made with an α-alumina raw material costing under $2/lb using the so called "zeta-process". This process involves the following procedural steps: 1) The zeta lithia component is formulated in a 5.5:1 mole ratio of Al_2O_3 to Li_2O using α-alumina (Meller or Reynolds) and lithium oxalate. Prior to calcining, the raw materials are milled together, after which the mixture is calcined at 1260°C for 2 hours. The soda component is made in a similar manner using approximately a 5.2:1 mole ratio of Al_2O_3 to Na_2O using α-alumina (Meller or Reynolds) and Na_2CO_3 as the raw materials. Appropriate amounts of the lithia zeta component and the soda component are mixed together to yield a nominal composition of 8.85% Na_2O, 0.75% Li_2O, and 90.4% Al_2O_3 (by weight). One simplifying modification has been introduced in Phase II in the preparation of the standard "zeta-process" powder which eliminates the necessity of storing the soda component under vacuum dessication. This new procedure* involves mixing the zeta component (Li_2O:5 Al_2O_3) with reagent sodium carbonate and the appropriate amount of α-alumina. This mixture is calcined directly at 1260°C and thus eliminates the need for mixing and calcining separately the soda component. To date all tubes made with this modification in powder preparation have acceptable properties with the expected micro-structures.

After powder preparation, closed-end tubes are green formed by wet-bag isostatic pressing in special tooling designed specifically to give close dimensional tolerances. During Phase II studies have been made on the effect

* This procedure has been introduced for powder preparations involving only Meller alumina. It has not yet been incorporated into powder formulations using Reynolds aluminas.

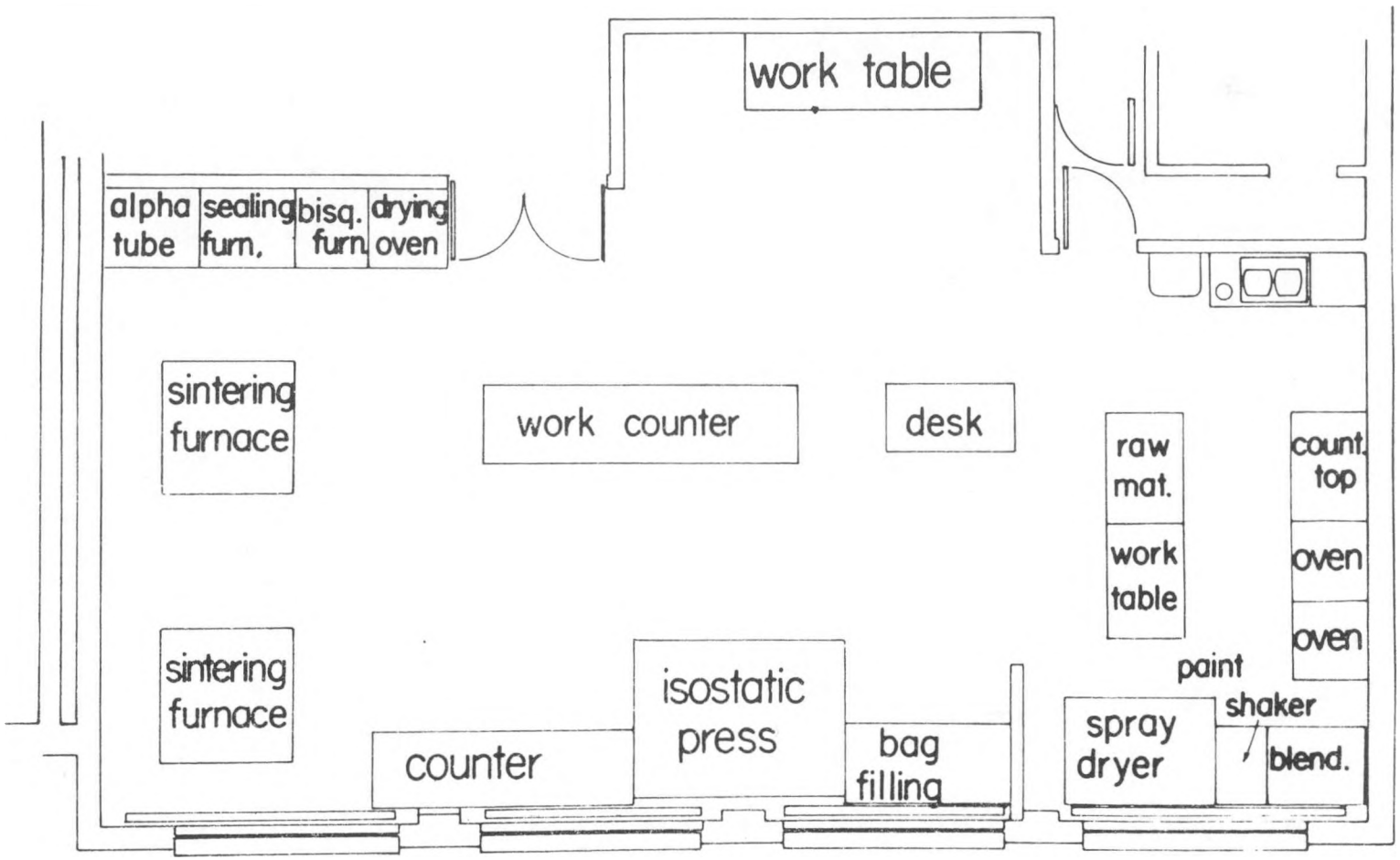

FIGURE IV.1 - Ceramic Pre-Pilot Plant (University of Utah)

of pressing pressure on the green and sintered densities. To date tubes fabricated with Reynolds RC-HP-DBM α-alumina have been pressed at pressures down to 5 kpsi and sintered to densities $\geq$ 3.18 g/cm^3. Tubes prepared from Meller α-alumina powder give identical results for pressing pressures down to 20 kpsi. Our ultimate objective in the pilot plant is to achieve comparable results with a fillable and flowable spray dried powder. Presently all standard tubing in the pre-pilot batch plant is isostatically pressed at 40 kpsi.

After green forming and bisque firing at 700-750°C (∿ 10 hours), the tubes are batch sintered by platinum encapsulation for 5-10 minutes at 1570-1590°C and annealed in the same furnace for one to three hours at 1475°C.

A complete description of the current standard process for fabricating standard β"-alumina tubing in the pre-pilot batch plant is given in Appendix G.

Standard tubing has been made in Phase II with basically three raw material sources of α-alumina: (1) Meller (∿ $16/lb.), (2) Reynolds RC-HP-DBM (∿ $5/lb.) and (3) recently Reynolds ERC-HPS-DBM (∿ $2/lb.). The ERC-HPS-DBM powder is a modification of the regular Reynolds RC-HP-DBM powder but contains an additional 0.12% Na_2O. Apart from economic considerations the transition from Meller to Reynolds α-alumina was advantageous in other aspects of the fabrication process. The Reynolds powder is much easier to process than the Meller raw material. It can be dry ball milled, which eliminates the hazard and expense of milling an acetone slurry. The powder has a higher compaction density than Meller alumina leading to a shorter time for bag filling in wet-bag isostatic pressing. After bisque firing, the green densities are high (∿ 60% of theoretical) leading to less shrinkage upon sintering (i.e., 16% linear shrinkage compared to 20% for Meller alumina).

In Table IV-1 typical properties of standard β"-alumina tubing are summarized with standard deviations indicated for density, sodium ion resistivity (300°C), and diametral strength. The data in Table IV-1 represent 15 mm OD tubing prepared from Meller α-alumina. Comparable data can be obtained with the Reynolds powders. Based on the data in Table IV-1 tentative specifications have been set for the physical properties of standard tubing fabricated in the pre-pilot batch plant. These are summarized in Table IV-2.

4.02 Fabrication of Tubing With a Nominal 3 cm OD

Large electrolyte tubes (3.35 cm OD, 25 cm long and 2.5 mm wall) have been developed with acceptable properties and dimensional tolerances significantly ahead of schedule.

In Table IV-3 a summary is given of the physical properties with standard deviations of large diameter β"-alumina tubing prepared by the zeta process using both Meller and Reynolds α-aluminas. As can be seen by comparison with the data in Table IV-1 the physical properties of the large diameter tubing are comparable to those of the smaller (1.5 cm) tubing.

TABLE IV-1

Physical Properties of "Zeta-Process" Production Tubing

(15 mm OD)

PRESSING PRESSURE (KPSI)	NUMBER OF TUBES	DENSITY (G/CM^3)	RESISTIVITY 300°C (OHM-CM)	DIAMETRAL STRENGTH (KPSI)
40	40	3.20 ± 0.01	4.12 ± 0.37	41.3 ± 7.0*
45	19	3.19 ± 0.01	4.02 ± 0.29	37.0*
50	13	3.20 ± 0.01	4.02 ± 0.16	32.4**
55	41	3.20 ± 0.01	4.10 ± 0.30	30.4*
30-55	17			38.5 ± 7.9

* Averages of 2 to 11 values ** Singular value

Range of Values

Density	3.18 - 3.23 g/cm^3
Resistivity	3.27 - 4.73 ohm-cm
Strength	27.7 - 54.9 kpsi

TABLE IV-2

Tentative Specifications on Physical Properties

Standard Production Tubing

PROPERTY	EXPECTED RANGE	EXPECTED MEAN $\pm$ STD. DEV.
Density	3.18 - 3.23	3.20 $\pm$ 0.01
Axial Resistivity (300°C in ohm-cm)	3.80 - 5.00	4.22 $\pm$ 0.30

SPECIFICATIONS ON PHYSICAL PROPERTIES

Density	$\geq$ 3.18 g/cm^3
Axial Resistivity (300°C)	$\leq$ 5 ohm-cm
Strength	$\geq$ 25,000 psi (four point bend)
Na-Na Cell Behavior	Capable of passing 1000 Ah/cm^2 of charge at a current density of 1.25 A/cm^2
Microstructure	Grains over 100 µm $\leq$ 0.01% in number Grains under 10 µm $\geq$ 99.00% in number
Helium Leak Rate	$\leq 10^{-10}$ cc/sec cm^2

TABLE IV-3

Physical Properties of Large Diameter β"-Alumina Tubing

"Zeta-Process"

40-55 Kpsi Pressing Pressure

BATCH	RAW MATERIAL	NUMBER OF TUBES	DENSITY (G/CM^3)	RESISTIVITY 300°C (OHM-CM)
A	Meller	15	3.20 ± 0.01	4.40 ± 0.28
B	Meller	17	3.21 ± 0.01	4.28 ± 0.27
C	Meller	25	3.21 ± 0.02	4.18 ± 0.40
D	Reynolds	10	3.22 ± 0.01	4.57 ± 0.61

4.03 Sealing

In Phase II three different types of sealing equipment have been designed and constructed in the pre-pilot batch plant: (1) a butt seal involving the joining of 15 mm OD β"-alumina tubing to α-alumina tube headers, (2) sealing 15 mm OD β"-alumina tubing to α-alumina plate (disk) headers (with a counterbore), (3) sealing 33.4 mm OD β"-alumina tubing to α-alumina plate headers (no counterbore). All of these seals involve the use of the sealing glass developed at Ford.

4.04 Thermal Expansion Measurements

In Phase II work was initiated on the measurement of the thermal expansion coefficient (α) of polycrystalline, lithia stabilized β"-alumina and commercial sources of polycrystalline alpha-alumina. Knowledge of the relative expansion coefficients of these two materials is essential from the point of view of seal design in Na-S cell construction. While some data exist on these materials from earlier work at Ford,[1] the thermal expansion coefficients of the current materials used in Na-S cell construction have not been measured. Secondly, no data are available on effects, if any, of texture or preferred orientation on the thermal expansion coefficient of β"-alumina. Consequently, thermal expansion measurements were performed on hot-pressed β"-alumina in directions perpendicular and parallel to the hot-pressing direction. These measurements were performed in addition to those on standard "zeta-processed" polycrystalline β"-alumina and two commercial sources of alpha-alumina.

The thermal expansion coefficients were measured on an Orton recording (X-Y) high temperature dilatometer. Specimens two inches in length were used in most cases. In special cases where two inch long specimens were not available, a few pieces were stacked together. This procedure was used to measure the thermal expansion coefficient in the direction parallel to hot-pressing (i.e., parallel to many of the "C" axes) in hot-pressed material. In Table IV-4 a summary is given for all the data taken to date in Phase II. For calibration purposes, the thermal expansion coefficient of nickel was measured with the apparatus and found to be in agreement with published values.

The data revealed that the thermal expansion coefficients of polycrystalline α-alumina (8.7 - 8.75 x 10^{-6}/°C) are somewhat higher than those for sintered polycrystalline β"-alumina (8.22 - 8.35 x 10^{-6}/°C). The coefficient of thermal expansion in hot-pressed β"-alumina is anisotropic. The expansion coefficient in the direction perpendicular to hot-pressing is approximately 10% higher than in the parallel direction. This result implies that the expansion coefficient is different along the "a" and "c" axis of β"-alumina. Thus in coarse-grained polycrystalline β"-alumina the formation of inter- or transgranular microcracks during processing should be possible because of this anisotropy in the coefficient of thermal expansion. Hence the fabrication of fine-grained materials in sintering is essential for maintaining a high degree of mechanical integrity in polycrystalline β"-alumina.

---

(1) J. A. Mangels, G. J. Tennenhouse and T. J. Whalen, Ford (Proprietary) Technical Memorandum, SRM 70-30, November 24, 1970.

TABLE IV-4

Coefficient of Thermal Expansion

Polycrystalline β" and α-Alumina

Material	Processing Method	Direction of Measurement	No. of Specimens Tested	Coefficient of Thermal Expansion ($°C^{-1}$) between 300°C and 800°C
α-alumina thermocouple tube (Coors AD-998)	As received	Along the length	One	8.70×10^{-6}
α-alumina tube (Lucalox)	As received	Along the length	Two	8.75×10^{-6}
β"-alumina	"Zeta-process" (10 min. sinter/ 1600°C)	Along the length of the bar	One	8.22×10^{-6}
β"-alumina	1000°C calcine 1 hr. sinter/1600°C	Along the length of the bar	Two	8.35×10^{-6}
β"-alumina	Zeta powder Hot pressed 1450°C-15 mins./ 4000 psi	Perpendicular to the hot-pressing direction	Eight	8.38×10^{-6}
β"-alumina	"Zeta-process" Hot pressed 15 mins./1450°C 4000 psi	Parallel to the hot-pressing direction	Four	7.6×10^{-6}

4.05 Elastic Modulus Measurements

In Phase II, Young's elastic modulus has been measured on polycrystalline β"-alumina samples which are similar to the "zeta-processed" material in the standard production with respect to microstructure and physical properties. Measurements have also been made on polycrystalline β"-alumina fabricated over a range of porosity levels (0.5 to 5.5%) and grain sizes (1-100 μm).

The measurement of elastic modulus involves the use of electromagnetic excitation and detection of the lowest order, longitudinal-mode mechanical resonance with the bar specimen (6.51 ± 0.01 cm long and about 0.4 cm^2 in cross section) pinned in the center. Experimentally, the ratio E/ρ is determined from the following expression

$$E/\rho = 4\ell^2 f^2$$

in which E is Young's elastic modulus, ρ is the density, ℓ is the length and f is the frequency for resonance of the first order of longitudinal mode.

In Table IV-5 a summary is given for the elastic modulus measurements on four bar specimens typical of the β"-alumina produced in the pre-pilot batch plant. The data in Table IV-5 yield an average for the elastic modulus of standard production β"-alumina equal to $1.96 \times 10^{11} N/m^2$ (28.4×10^6 psi).

Additional measurements of the elastic modulus over a wide range of grain sizes revealed no systematic dependence on grain size in the range between 1 and 100 μm. However, a strong dependence on porosity was noted by conducting measurements on 16 specimens over a range of porosities from 0.5 to 5.5%. The modulus data could be fit to an expression of the form

$$E = E_o \exp-(bP)$$

with $E_o = 30.4 \times 10^6$ psi and b = 0.052. Note E_o is the extrapolated value of the modulus of β"-alumina in the absence of porosity. P is the volume fraction porosity. The value of $E_o = 30.4 \times 10^6$ is reasonable in that E measured for 99% dense hot-pressed β"-alumina was 29.3×10^6 psi.

Finally the fact that the modulus was independent of grain size up to about 100 μm indicated the absence of any significant microcracks in this material. Microcracks might be expected to be present in material with larger grain sizes because of the anistropy in coefficient of thermal expansion which has been noted in β"-alumina.

4.06 Continuous Sintering and Sintering Without Platinum

Continuous sintering without the necessity of platinum encapsulation appears at this stage to be feasible. 15mm OD x 200 mm long β"-alumina tubes have been sintered continuously at rates up to 5 cm/min.

TABLE IV-5

Elastic Modulus of Polycrystalline, Lithia-Stabilized β"-Alumina

SPECIMEN	DENSITY (G/CM^3)	FREQUENCY (kHz)	ELASTIC MODULUS	
			(PSI)	N/m^2
1	3.22	60.17	29.7×10^6	1.98×10^{11}
2	3.22	59.78	28.3×10^6	1.95×10^{11}
3	3.21	59.76	28.3×10^6	1.95×10^{11}
4	3.21	59.89	28.4×10^6	1.96×10^{11}

4.07 NDT Electrical Quality Control Development

A non-destructive technique involving the use of removable band electrodes and resistivity measurements at 30 MHz has been developed which correlates (and is subject to calibration) within experimental scatter with low frequency QC measurements on standard (15 and 33.4 mm OD) electrolyte tubing. Further work remains in the scaling up of this technique to pilot scale operation.

4.1 Pilot Plant Production of Electrolyte Tubing (University of Utah Research Institute - (UURI)

UURI has devoted most of its effort in Phase II to (1) the design and lay-out of the pilot plant for the fabrication of β"-alumina tubing in large quantities (up to 150 per day) and (2) the negotiation of several major subcontracts related to (a) leasing 9135 sq. ft. of prime space on the Research Park for the pilot plant (b) the installation and/or construction of severable and non-severable improvements in the leased space which will house the pilot plant, and (c) the acquisition of a spray dryer, ball mill, and isostatic press (wet-bag).

4.11 Plant Lay-Out and Design

In Figure IV-2 an architectural drawing (to scale) is shown for the β"-alumina pilot plant. 9135 square feet of space have been leased at 580 Arapeen Drive which is on the Research Park adjacent to the University of Utah campus. The pilot plant consists of approximately 6000 square feet of plant area where all production operations will take place. Separate laboratories (∿ 1500 square feet) have been designed for quality control, mechanical and electrical testing (including a nine station sodium-sodium test facility for electrolyte tubing), chemical testing, and product storage. In the plant area, provisions have been made for two spray dryers, a ball mill, isostatic presses, four bisquing furnaces, four green storage ovens, a 50 foot long continuous sintering and annealing furnace, a continuous calcining furnace and 50 stations for sealing α-alumina disk headers to β"-alumina tubing.

The bulk of the severable improvements consist of (1) a special air handling system to dissipate heat and to provide for a clean dust (external) - free environment for tubing fabrication, and (2) special electric power (480 volt - 1400 amp system) to power all of the furnaces and plant equipment. Pilot plant production began on June 8, 1977.

4.12 Equipment Specification and Acquisition.

Except for the equipment to be constructed in-house, the second spray dryer, and several bisque furnaces, nearly all of the pilot plant equipment required for powder mixing, blending, screening, and milling; calcining; spray drying; isostatic pressing; and bisquing has been specified and placed on order. Major pieces of equipment which had to be treated as sub-contracts included the spray drayer, ball mill, and the wet-bag isostatic press.

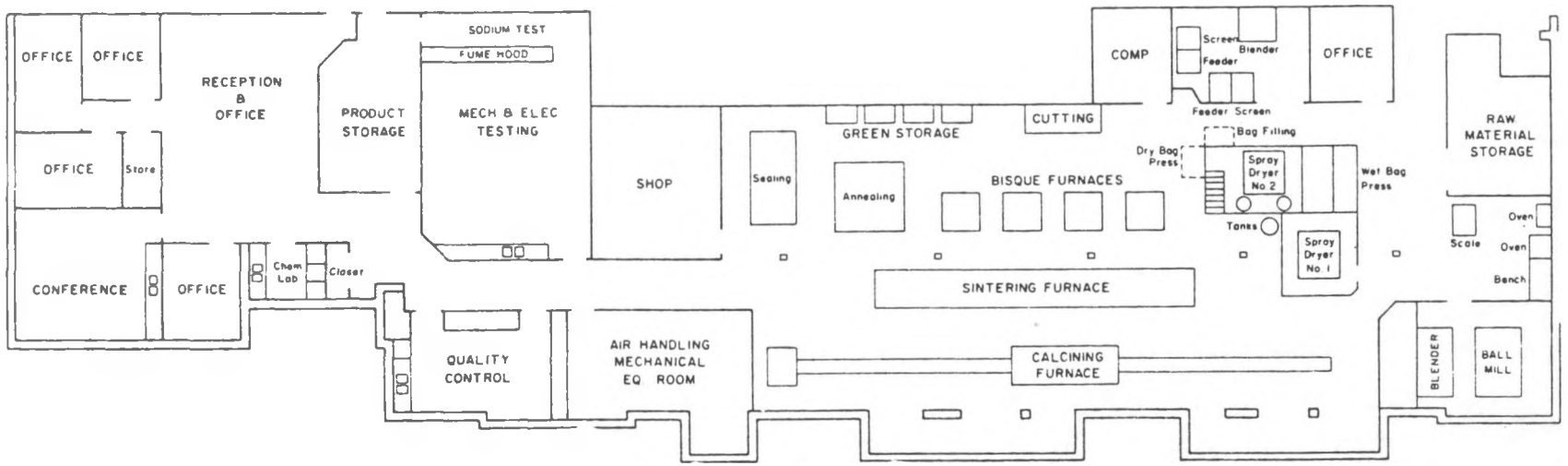

FIGURE IV.2 - CERAMIC PILOT PLANT (UNIVERSITY OF UTAH RESEARCH INSTITUTE)

TASK V - FABRICATION AND TESTING

Cell fabrication and prototype testing activities have been actively pursued at two locatings during Phase II - at Ford Research and at Aeronutronic Division, Ford Aerospace and Communications Corporation.

5.0 Fabrication

5.01 Facilities

A small facility for the assembly of a limited number of exploratory prototype cells was set up at the Ford Research Laboratory. The assembly operations were based on labor intensive practices in order to retain the flexibility needed to adapt to monthly changes in prototype cell designs and to accommodate the continual modifications of fabrication procedures. Cells were hand assembled, and components were machined to size almost on an individual basis. Production rates were limited to a maximum of 10 cells per month by labor limitations. Appropriate apparatus was developed for preparing and filling sodium and sulfur into these cells at a rate of one cell/day.

During Phase II, a prepilot assembly plant was installed at Aero. The facility, which became operational, is used for assembly, filling and inspection of Mark I prototype cells. The layout, shown in Figure V.1, is sized for production rates up to 100 cells per month. The sodium and sulfur filling stations are essentially identical except that sodium filling is performed inside a controlled atmosphere glove box. Figure V.2 shows the sulfur fill station apparatus.

Two methods of metering the amount of reactants into the cells are being developed in Phase II. Displaced volume, using a bellows-piston apparatus, has thus far provided better control than closure of valves based on monitored weight gain.

Sulfur is injected into the cell, but methods to produce precast assemblies are being explored. Sodium is precast into a cylindrical slug which is inserted into the cell at the time of cell assembly. Methods to precast directly into sodium

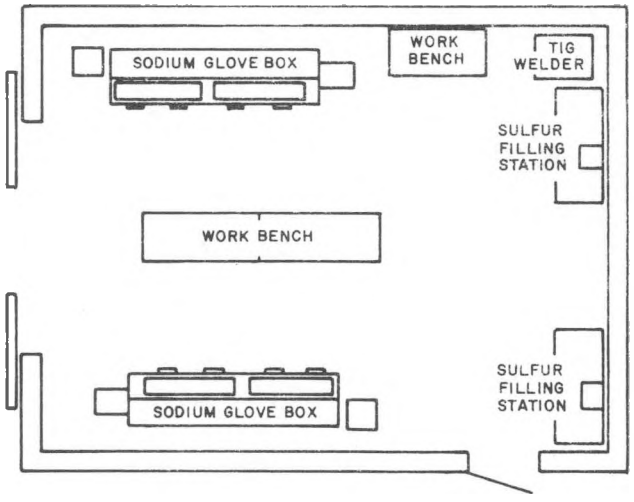

FIGURE V.1 - Pre-Pilot Plant

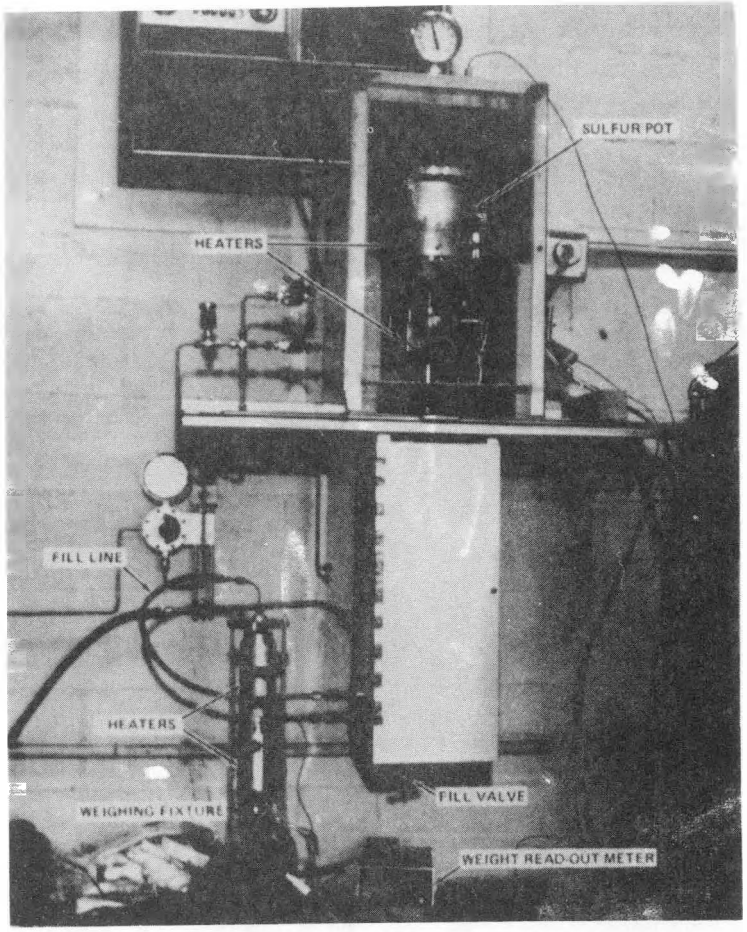

FIGURE V.2 - Sulfur Filling Station

container-safety tube are being examined. Filling procedures may be modified depending on results of these experiments.

5.02 Exploratory Cell Fabrication

Major emphasis was placed during Phase II on the evaluation of various sulfur container materials and coatings as actual hardware for exploratory prototype cells. To the extent possible, a standard cell design was employed, but design changes were introduced to permit interesting candidate materials to be tested using whatever sizes were available. Most components were fabricated in-house. Outside vendors were utilized to supply specialized processing and materials. A typical cell design is shown in Figure V.3. In addition to container material variations, these cells also incorporated variations in sulfur electrode (shape, surface treatment, additives) ceramic size, and seal design. The salient design features are summarized in Table V.1 for the various series of exploratory cells.

Mark I Fabrication

The design of the Mark I cell, shown in Figure V.4, involves many components and requires many sequential steps for its assembly, as indicated in Figure V.5. Successful production of cells has begun recently at Aeronutronic. As of October 17, 1977, 26 cells had been successfully assembled and delivered for electrical testing. Changes in assembly procedure and design are being developed to increase yield and production rates. To date, total cell production has been limited by the availability of quality components, as discussed below.

A major difficulty has been encountered with the initial cell production. The seals between the metal containers and the alpha alumina washer were frequently leaky. Higher compressive forces decreased the leak rate somewhat, but frequently lead to ceramic fracture. The problem was traced to warpage and inadequate surface preparation of the ceramic insulator washer and to minor defects on the container lip. Additional vendors have been contacted and their materials and polishing services are being evaluated to resolve the problem.

Difficulties with controlling reactant quantities were encountered with the first cells. Improvements in cell filling techniques have alleviated these problems.

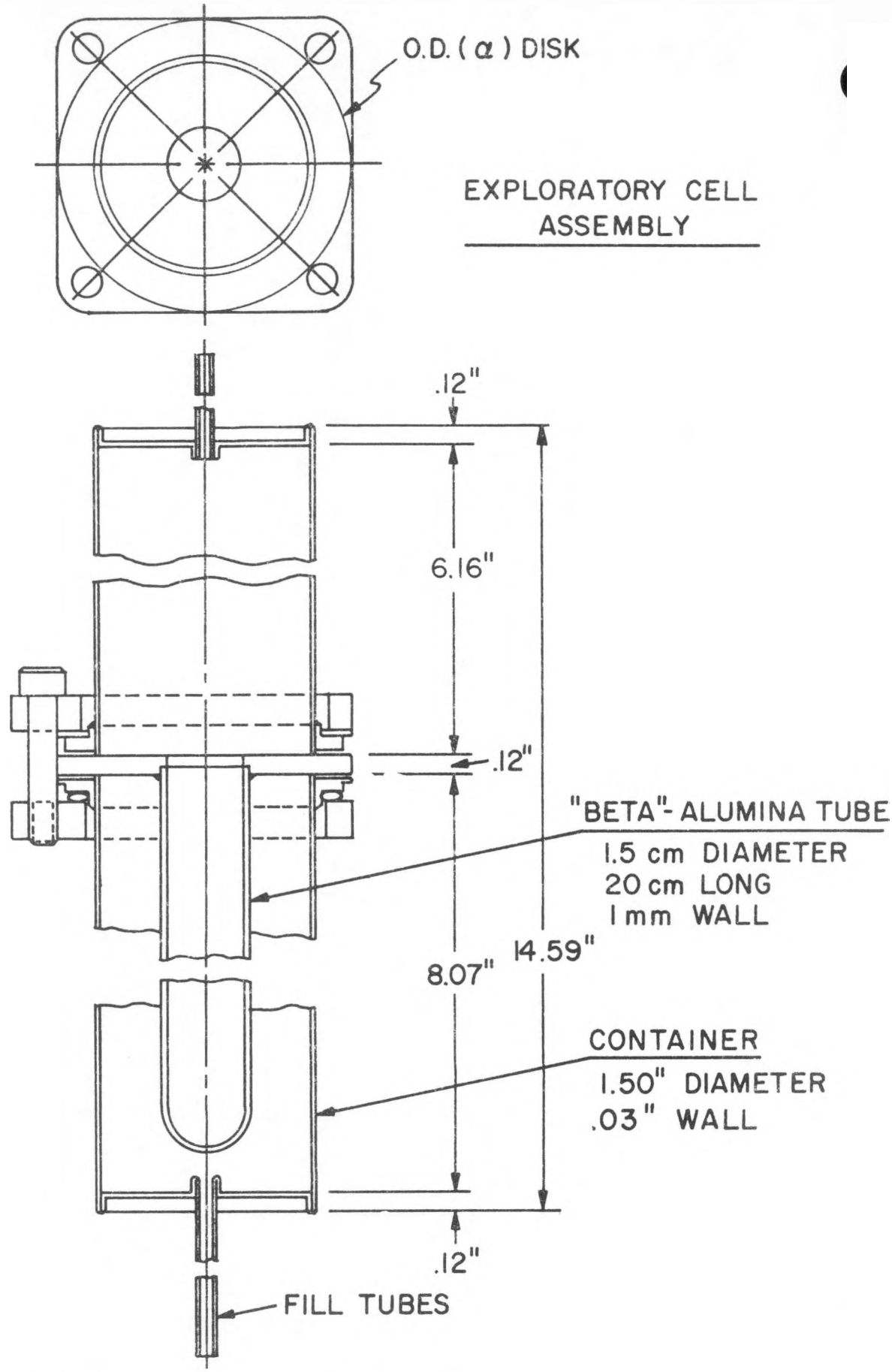

FIGURE V.3 - Exploratory Cell Assembly

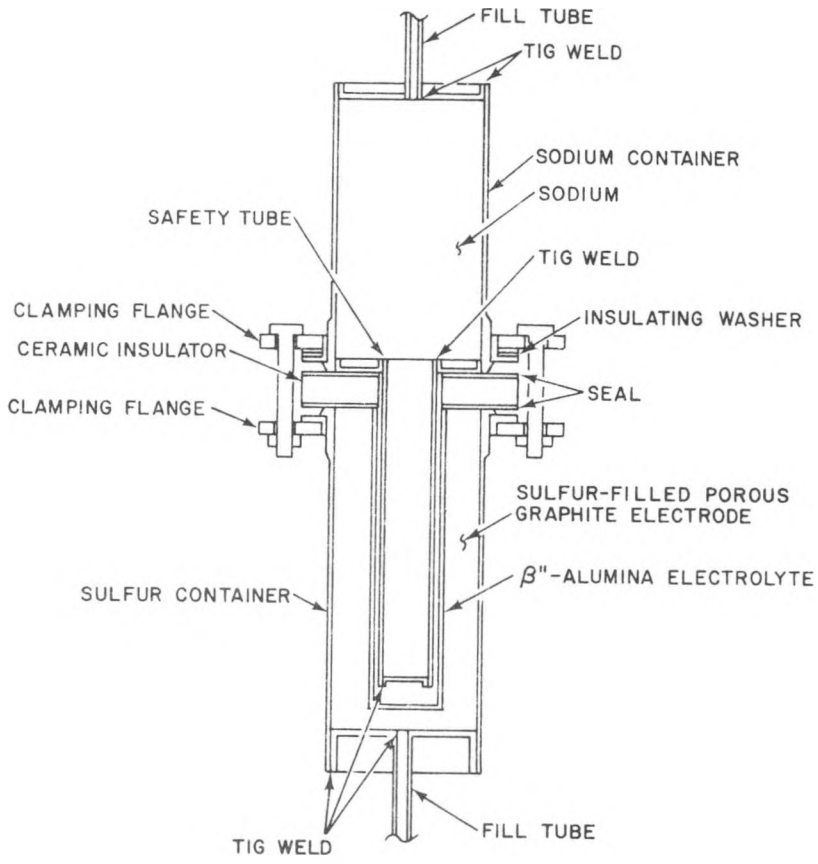

FIGURE V.4 - Mark-I Cell, Machined - Container Design

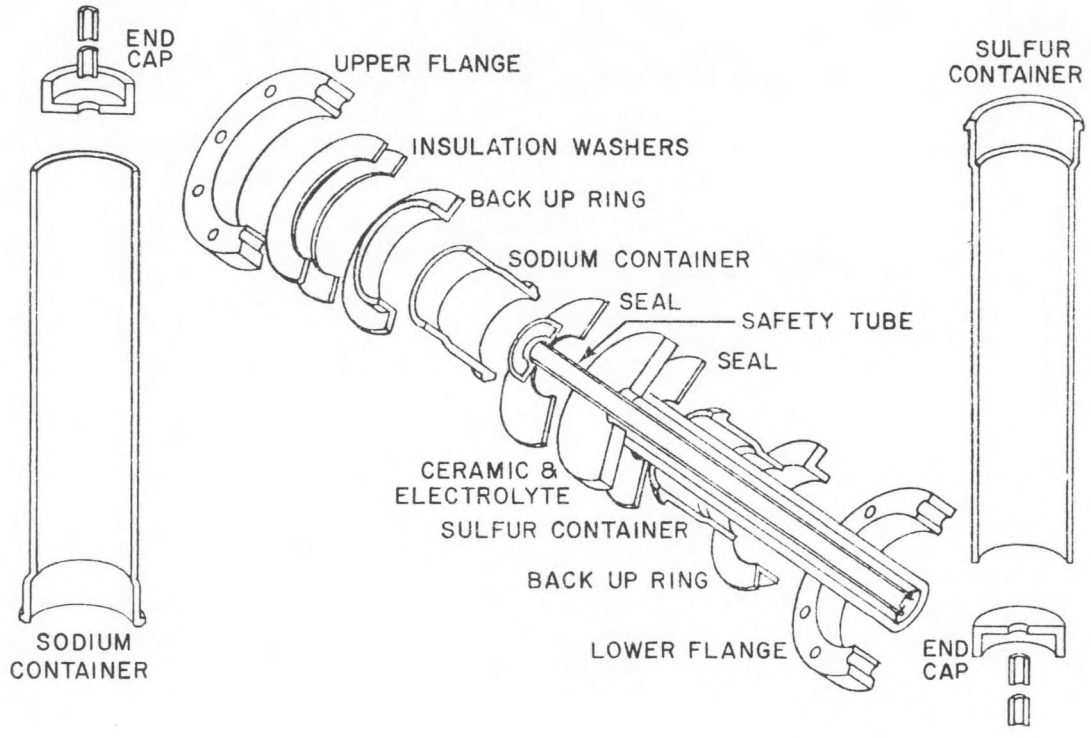

FIGURE V.5 - Schematic Showing Components of Mark-I Cell

CELL DESIGNS

Table V.1

Series/ Number of Cells	Sulfur Container		Sulfur Electrode		Theoretical Capacity Ah	Electrolyte Size DxL (cms)	Cell Weight (gms.)	Container Seals
	Substrate	Coating	Material	Treatment				
* A-10/5	446 Stainless	Graphite Filled Polyphenyl	WDF Felt	Shaped	75	1 x 15	640-660	Na-Brazed S-Glass
* A-20/5	446 Stainless	Oxidized & Graphite Filled Polyphenyl	WDF Felt Graphite Cloth	Shaped	75	1 x 15	640-660	"
* A-30/6	446 Stainless	Tiodize	WDF Felt Graphite Cloth	Shaped	64	1 x 15	750	Brazed
A-40/5	E-Brite	Cr/ Tiodize	WDF Felt	Additives Mixed	46	1.5 x 20	1100	Mechanical
A-50/4	E-Brite	Cr	WDF Felt	Alumina	101	"	940-960	"
A-50/3	347 Steel	Mo	WDF Felt	Alumina	"	"	"	"
A-50/5	E-Brite	Cr Oxidized	WDF Felt	Holes	"	"	"	"
A-60/3	Inconel	Oxidized	WDF Felt	"	202	"	1300	"
A-70/3	1010 Steel	Cr	WDF Felt	"	101	"	950-1000	"
A-70/3	E-Brite	Grafoil	WDF Felt	"	81	"	950	"
A-70/4	Kovar	Mo	WDF Felt	"	101	"	1020	"
A-100/14 A-120	E-Brite	Cr/ Tiodize	WDF Felt	"	101	"	910-980	"
A-120/5	E-Brite	Cr/ Tiodize	Chopped Graphite Fibers	-	101	"	960-1150	"
A-130/2	E-Brite	Tiodize	WDF Felt	-	35	"	750	"

*Cells tested under NSF Contract C805, AER-73-07199.

5.1 Testing

5.11 Safety Tests

Safety tests were carried out on two types of cells during Phase II. The first tests were performed on exploratory cells and later in the program when Mark-I cells became available the tests were repeated to demonstrate the safety of the larger cells. One objective of these tests was to characterize a worst-case failure in order to define the safety requirements for the test facility. An additional objective was to demonstrate the effectiveness of using a perforated liner (safety tube) inside of the ceramic tube to prevent a catastrophic reaction in case of internal cell failures.

Crush Tests on Laboratory Cells. Because of the unknown magnitude of the hazards involved in these tests, the first tests were carried out at Aeronutronic's San Juan Capistrano test site. This test site is in a remote area and is laid out so that test personnel can remain in a control room while commanding remote-controlled test apparatus.

The cells were slightly modified so that failures would represent the worst case. Only one strip of graphite was used so that the sodium and sulfur were free to mix. The cells were also modified so that application of a force to the outside of the sulfur container would cause the β"-alumina tube to break near its top. A chisel was incorporated into the sulfur container in a position such that slight inward movement of the container wall would cause the chisel to hit the β"-alumina tube near its top and cause it to break. This should represent the worst-case failure by allowing the maximum amounts of sodium and sulfur to mix. Approximately 193g of sulfur and 103g of sodium were present in each cell.

Tests were conducted on five cells, two of which had protective liners incorporated inside of the β"-alumina tubes. The cells were fabricated and assembled at Ford Motor Company. The sulfur containers were filled with sulfur

and the sodium containers were filled with argon prior to shipment. The sodium was cast into appropriate sized glass ampoules which were shipped separately. Filling of the sodium containers was done at the San Juan Capistrano test site just prior to testing.

To fill the sodium container, the cell and an ampoule of sodium were placed in an argon-purged glove bag. The cell was disassembled, the glass seal of the ampoule was broken, and the entire ampoule was placed in the sodium container. The cell was reassembled and checked for electrical isolation. The cell was removed from the glove bag, a vacuum system was connected to the filling tube of the sodium container and evacuation was begun immediately. After 30 minutes at a pressure less than 100 microns Hg, heating of the cell was begun. To ensure that the sodium would drop down into the electrolyte tube, the cell was vibrated when its temperature reached 150°C. When the cell reached the desired test temperature, the evacuation was stopped and the sodium container was backfilled with argon to 0 psig.

A remote controlled apparatus for breaking the β"-alumina tube is shown in the sketch in Figure V.6 and in the photograph in Figure V.7. In the photograph, a cell can be seen mounted on the test stand. After heating in the furnace shown at the bottom of the photograph, the cell could be raised to the position shown using remote control. The test plan called for heating the cells to ∿350°C, backfilling the sodium container with argon, lifting the cell out of the furnace, removing the furnace from the immediate area by means of a lanyard, and crushing the β"-alumina tube by activating a pneumatic cylinder which caused the cell to be struck.

Ten chromel-alumel thermocouples were welded to the cell at the positions shown in the Figure V.6 sketch. In tests No. 3 and No. 4, only 8 thermocouples were used with Nos. 6, 7 and 8 being equally spaced on the sodium container and with No. 4 at the same height as No. 3. Direct readout from these thermocouples was available in the control room and the thermal data were also recorded on magnetic tape and by an oscillographic recorder. The cell voltage was also monitored. A pressure transducer was connected to the filling tube of the sodium container to enable monitoring of the internal pressure, but

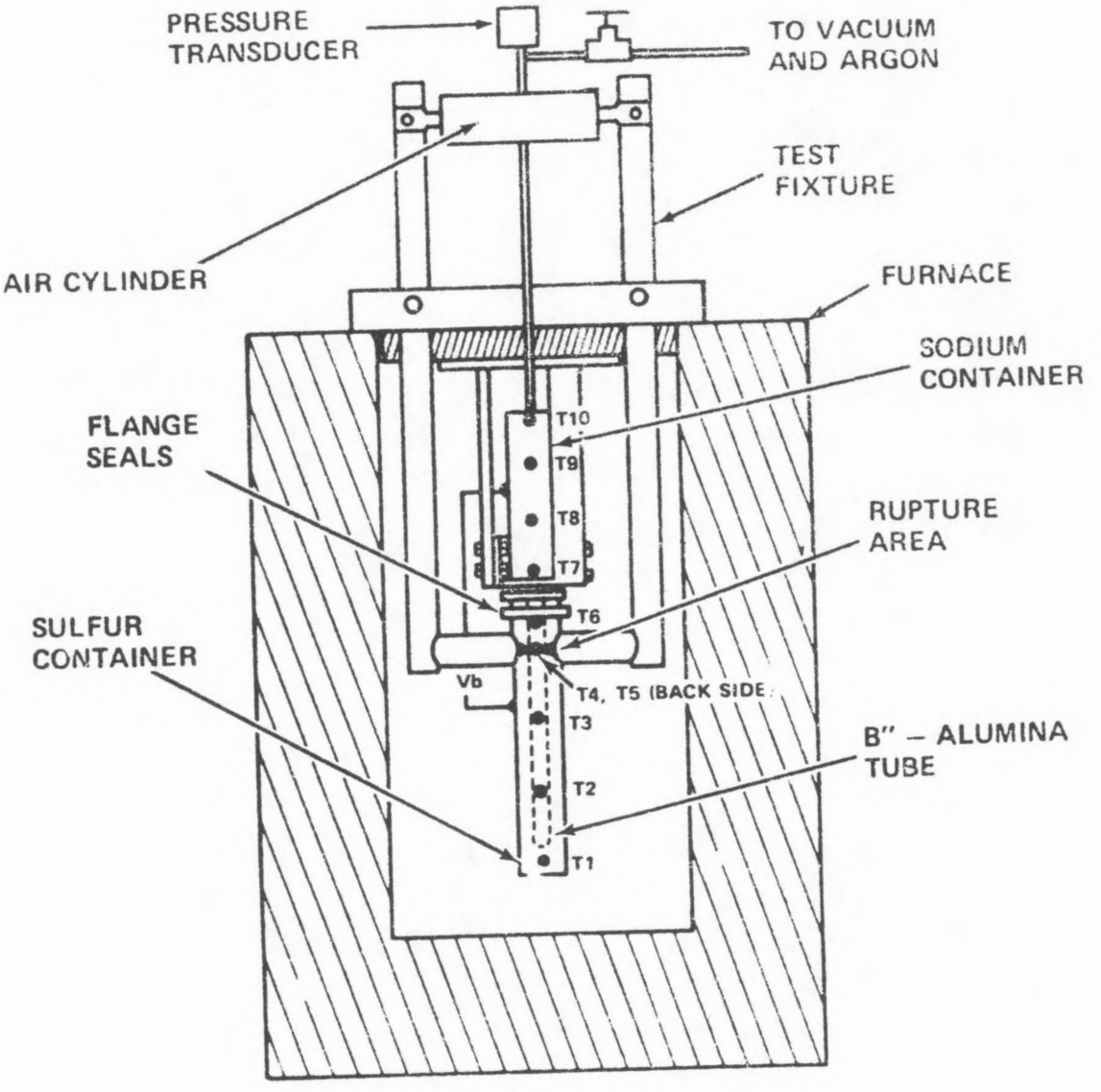

FIGURE V.6 - Sketch of Remote Controlled Apparatus for Breaking Electrolyte Tube

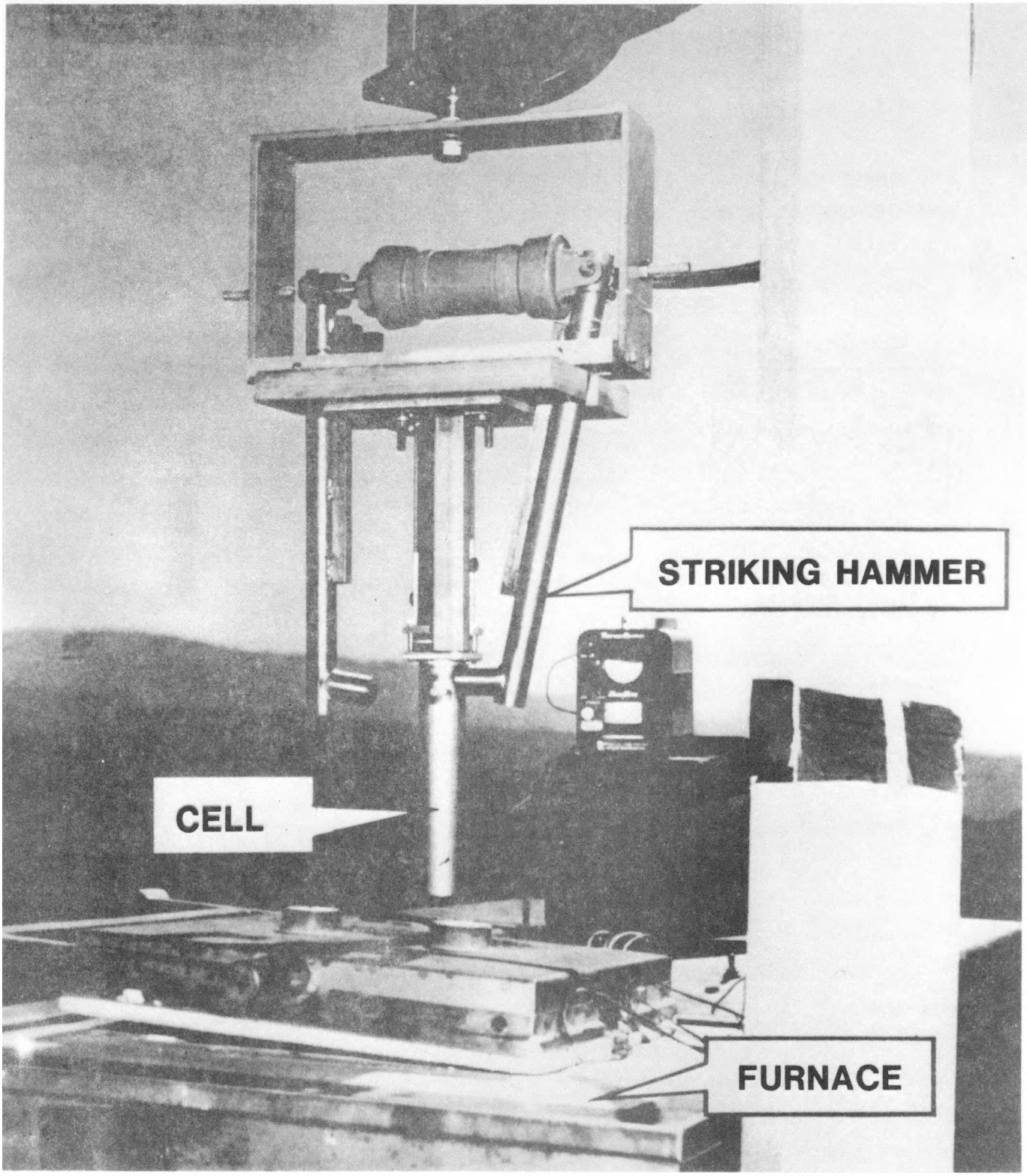

FIGURE V.7 - Photograph of Apparatus for Breaking Electrolyte Tube

plugging of the connecting tubing with sodium caused problems in obtaining valid pressure readings. Shock wave sensors were positioned at various intervals from the test setup to determine the magnitude of any pressure waves due to cell rupture.

All operations were monitored by closed circuit TV and video tapes. Real time and high-speed motion pictures and still photographs were also used to document the tests. A brief summary of the events and results of each test follows and a summary of the tests is presented in Table V.2.

Test No. 1 (Cell No. 2) The first test was carried out on a cell which did not have a safety tube. While heating the cell, a temperature excursion from 136 to 252°C in 7 minutes was observed at thermocouple No. 5. It was assumed that a small crack had occurred in the β"-alumina tube. The temperature indicated by thermocouple No. 5 began to drop slightly and heating of the cell was continued for ∿1 hour more. At that time, the temperature of the sodium container was 295°C (average of thermocouples attached to the sodium container) and the sulfur container temperature averaged 370°C with thermocouple No. 5 still being the hottest at 411°C. The vacuum pump connected to the sodium container was shut off and the sodium container was backfilled with argon to 0 psig. The cell was lifted from the furnace and was struck at the chisel point. When no changes indicative of failure were observed, the cell was struck again. This time a puff of white "smoke" was observed coming from the seal which had apparently been damaged by the second strike. No corresponding pressure variation was observed, but this was probably due to the tubing leading to the pressure transducer being plugged with solid sodium, a condition noted after the test. Approximately 10 minutes later a hot spot appeared on the sulfur container with thermocouple No. 5 reaching a temperature of 659°C. The cell began to cool, but several minutes later the temperatures increased again and a second hot spot (675°C at thermocouple No. 5) could be seen on the sulfur container. The cell remained intact. The long delay between striking the cell and observing a temperature rise might be explained by formation of small amounts of sodium polysulfides with high melting points during the low-temperature cracking of the β"-alumina tube. These polysulfides could have inhibited the mixing of reactants when the cell was struck.

TABLE V.2 - SUMMARY OF SAFETY TESTS ON LABORATORY CELLS

Test No.	Cell No.	Safety Tube	Description of Failure	POST-MORTEM EVALUATION			
				β″-alumina	Sulfur Container	Sulfur	Graphite
1	2	No	Thermal excursion from 136 to 252°C. Heated cell to ~350°C and struck it twice. Hot spot on sulfur container after 10 min. Another hot spot several min later. Max. temp. 675°C.	Cracked into many pieces	Intact, but discolored where hot spots had occurred	133g	No Change
2	3	No	Catastrophic failure when at 115-132°C. Rapid rise to 752°C. Sulfur container fell off. Sodium fire burned from sodium container for ~10 min.	Cracked into many pieces	Burnt through and broken in two places	17.5g	Crushed
3	1	Yes	Failed backfilling with argon at 337°C. Max. temp. 693°C. No further reaction upon striking cell.	Cracked into many pieces	No evidence of high temperatures on outside of container	89g	No Change
4	5	Yes	Five separate brief hot spots occurred ∿ 0.5 hr. after cell was struck. Max. temp. 844°C.	Cracked into many pieces	Top part of container corroded. Small hole near top.	0	No Change
5	4	No	Catastrophic failure at ~150°C. Max. temp. >1400°C. Fire.	Cracked into many pieces	Large hole	131g	No Change

During the post-mortem evaluation, the β"-alumina tube was found to be broken into many pieces. No changes in the graphite felt were observed. The sulfur container showed discoloration where the hot spots had occurred. Washing with carbon disulfide removed 133g of sulfur from the cell.

Even though some reaction had occurred prematurely as indicated by the temperature rise to 252°C early in the test, this test gives an indication of thermal behavior during a catastrophic failure at operating temperature.

Test No. 2 (Cell No. 3). The second test was also carried out on a cell without a safety tube. In this test, the β"-alumina tube failed catastrophically during the heatup. Just prior to failure, the temperature of the sodium container was 115°C, the sulfur container temperature averaged 132°C, and thermocouple No. 5 which was to become the hottest was indicating 119°C. A very rapid temperature rise to 752°C at thermocouple No. 5 was observed. The cell cooled slightly and when thermocouple No. 5 indicated 667°C, the sulfur container fell off from the rest of the cell which was held by the test fixture. Two minutes later the remaining part of the cell was raised from the furnace so that it could be observed. A sodium fire burning from the bottom of the container persisted for about 10 minutes.

The entire circumference of the sulfur container showed evidence of heat. The container was burnt through and broken into two sections in a zone from 1.0 to 3.25 inches from the top. Only 17.5g of sulfur remained in the container and the graphite felt was crushed.

Test No. 3 (Cell No. 1). This was the first test utilizing a cell with a safety tube in the β"-alumina tube. The cell was heated to 337°C without incident. Open circuit cell voltage was 2.1V. To avoid having a pressure differential inside the cell which would tend to force sulfur into the sodium container, the vacuum pump connected to the sodium container was shut off and the container was backfilled with argon. When an argon pressure of about 0.3 atm was reached, pressure and temperature increases indicative of internal failure in the cell were observed. A maximum temperature of 693°C was observed at thermocouple No. 6 and the cell voltage dropped to zero.

The cell was raised out of the furnace and struck, but no further temperature increases ensued. However, a puff of "smoke" was seen at the flange. The cell cooled without any further temperature excursions.

During post-mortem examination, the β"-alumina tube was found to be in many pieces with a 4.45-cm (1.75-in.) long piece at the bottom of the tube cracked but still sticking to the safety tube. There was no apparent damage to the graphite felt and 89g of sulfur remained. The interior of the sulfur container showed slight evidence of attack (discoloration) but there was no indication of high temperature being reached on the outside of the container. It appeared that the metering of the sodium through the safety tube had been effective in controlling the reaction rate between the sodium and the sulfur.

Test No. 4 (Cell No. 5). This was the second test using a cell which had a safety tube inside of the β"-alumina tube. The heatup period was uneventful. The cell was struck and one minute later a temperature of 786°C was observed at Thermocouple No. 4. In the next 32 minutes, four additional hot spots appeared, each lasting less than one minute. Temperatures as high as 844°C were observed briefly.

No sulfur was found in the cell during the post-mortem examination, indicating that complete reaction had occurred. The graphite felt showed no evidence of change near the seal area, but the top part of the sulfur container was corroded and darkened and a 3mm by 13mm (0.13 by 0.5 inch) hole was found 4.45cm (1.75 inch) from the seal. This test showed the effectiveness of the safety tube in allowing complete reaction of the sodium and sulfur at a slow enough rate to avoid a catastrophic cell failure.

Test No. 5 (Cell No. 4). No safety tube was incorporated in the β"-alumina tube of the cell used for this test. Wetting of the β"-alumina tube occurred at 150°C with an accompanying cell voltage rise. However, 17.5 seconds later, the β"-alumina tube broke and the voltage dropped abruptly. Concurrent with the voltage drop, temperatures as indicated by thermocouples Nos. 1, 2, 3, 5 and 6 rose abruptly. Thermocouples Nos. 4, 7 and 8 indicated a slower rise in temperature. Temperatures in excess of 1400°C were indicated and a fire was observed.

After the test, a 57mm (2.25 inch) hole was found in the sulfur container. The top of the hole was 57mm (2.25 inch) from the top of the container. The only part of the β"-alumina tube which was intact was a 13mm (1/2 inch) long piece at the bottom of the tube. The graphite felt appeared unchanged and 131g of sulfur remained in the container. This experiment represents another demonstration of the violent reaction which occurs when sodium and sulfur are allowed to react with no restriction.

On the basis of the five tests described above, it appeared that the safety tube inside of the β"-alumina tube was successful in preventing the type of catastrophic cell failure observed when no safety tube was used. With the safety tube present, high temperatures were still reached within the cells, but the duration of these high temperatures was short and explosions did not occur.

In general the failure mode for the container appeared to be rapid corrosion or burn-through. In Tests Nos. 2 and 5 (no safety tube) severe damage to the container resulted. In test No. 1 (no safety tube) the container remained intact but showed evidence that very high temperatures had been reached. This cell failed slowly, compared to the other cells tested, probably because of formation of some sodium polysulfide at lower temperatures during the heatup. This slower reaction and the damage to the seal area which provided pressure relief is probably what allowed the container to remain intact. The containers from cells tested with safety tubes showed much less damage. The container from test No. 3 showed no changes on the exterior and the container from test No. 4 had a small hole burnt through. In no case was there any evidence of container damage due to high pressure as might be evidenced by longitudinal splitting.

It is interesting to note that all three cells which had no safety tube showed evidence of failure of the β"-alumina tube during the heatup at about the time the tubes were wet with sodium. Both cells with the safety tube survived the heating without incident. While this is a small sample, it is some evidence of an additional safety feature of cells with safety tubes.

Safety Tests on Type A-110 (Mark-I) Cells. Type A-110 cells were also modified for the safety tests by inclusion of a chisel point in a manner similar to that

used in the laboratory cell crush tests. However, for these tests, the chisel point was located near the bottom of the solid electrolyte tube. Cells for these tests contained graphite in a configuration similar to that of the Mark-I cells. The clearance between the safety tube and the solid electrolyte was ∿2mm (0.079 inch).

This series of tests was performed in Building No. 12 of the ATC Laboratory. (This building is remote from the other ATC Laboratory buildings.) The cells for this test were shipped from Ford (Dearborn) containing sulfur, but no sodium. The operations of disassembling the cells, inserting a precast slug of sodium, and resealing the cells were carried out in a controlled-atmosphere glove box in the prepilot plant. Some difficulties were encountered in disassembly of the cells. The problems were related to "frozen" bolts and to the aluminum sealing gasket sticking to the container sealing face. "Aerokroil" was used to facilitate removal of the bolts, and the aluminum gaskets were replaced. The container sealing faces were electropolished in sodium hydroxide solution to remove small pieces of aluminum adhering to the sealing surface.

Test No. 1 (Cell A-110-2). A 186g slug of sodium was placed into the sodium container of this cell. The fill tube of the sodium container was attached to a vacuum line and the cavity was evacuated. A pressure of 70 microns was maintained for 30 minutes before sealing the container. The cell was placed into the test furnace and heated. A voltage of ∿2.2V developed at 279°C, indicating that sodium had wet the solid electrolyte. After the cell had been heated to ∿350°C and the voltage had stabilized at 2.04 V, it was removed from the furnace and the β"-alumina tube was crushed. A slight temperature increase was observed within minutes after striking the cell, but the temperature quickly subsided, and dropped to below 100°C within an hour. An X-ray evaluation showed that the solid electrolyte was cracked in many places. There was no external damage to the cell indicating the effectiveness of the safety tube.

Test No. 2 (Cell A-110-1). The sodium slug for this cell weighed 187g and the sodium container was sealed at a pressure of 200 microns. Upon heating to ∿370°C, the cell did not develop a voltage, indicating that sodium had not wet the β"-alumina tube. The cell was cooled and X-rayed to verify that sodium

had not filled the annulus between the safety tube and the ceramic. The cell was reinstalled in the test apparatus and the fill tube of the sodium container was connected to a gas line so that the container could be pressurized with argon. The container was pressurized to ~14 psig for a few minutes and was evacuated again without obtaining a voltage. As the cell was being cooled down in preparation for diagnostic procedures, there were indications that a voltage was developing. However, sodium was not apparent in the annulus in X-ray photographs. The cell was heated for a third time and with repressurization of the sodium container, a stable voltage was obtained. As a freeze-thaw test, the cell was cooled and reheated an additional time. X-ray photographs of the cooled cell verified the presence of sodium in the annulus. The cell survived the reheating without any apparent damage to the ceramic. The ceramic was then crushed. A small hole developed at the area where the chisel point was welded to the container. A small fire which appeared at this hole extinguished itself in about 30 seconds. No additional damage to the container was observed.

Test No. 3 (Cell A-110-3). This cell contained 187g of sodium. The test was essentially a repetition of test No. 1 with no exterior damage to the container and no sharp thermal excursions.

Test No. 4 (Cell A-110-4). The sodium slug for this cell weighed 186g. No safety tube was used in this test. A failure in the seal area occurred when the cell was struck. A sodium fire resulted which essentially demolished the sodium container, as shown in Figure V.8.

It was concluded on the basis of these tests, that the safety tube incorporated into the Mark-I cell design is effective in preventing hazardous cell failures in the event of breakage of the solid electrolyte. Subsequently, many cells have failed during electrical testing without incident or damage to equipment or personnel. Occasional leakage of reactants has occurred at the seal area, but has not resulted in any perforation of the containers.

5.12 Cell Evaluation

Exploratory Prototype Cells. The emphasis in the testing program during the current year has been to evaluate the effect on cell performance of various

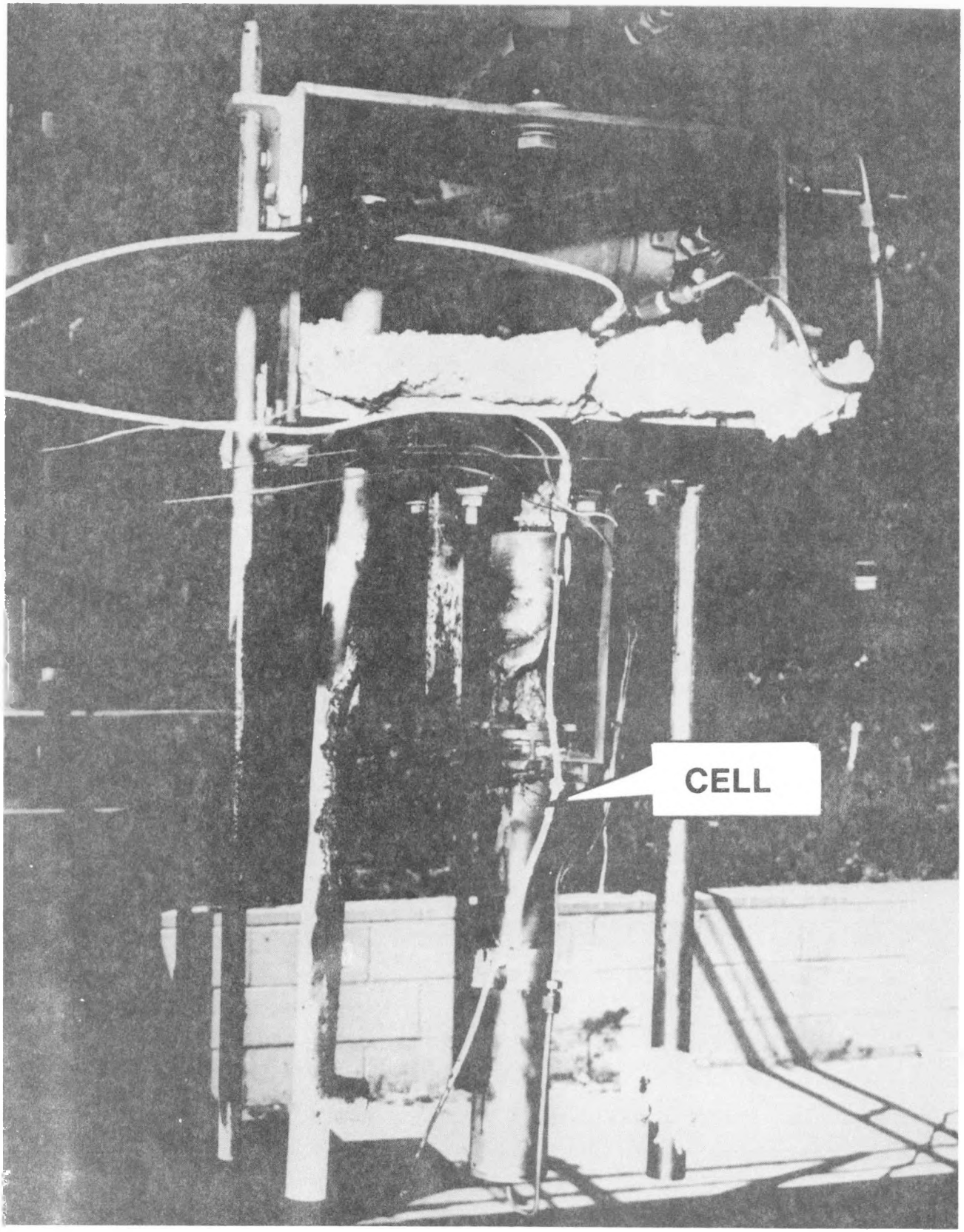

FIGURE V.8 - Safety Test Results - Mark I Cell Minus Safety Tube

sulfur container materials and coatings. All the cells have been operated at relatively low charge and discharge current densities of 64 mA/cm^2 at 350°C with voltage cutoff limits set at 1.5 and 2.5 volts. The low current densities were chosen in order to allow cell operation into the two phase region. The voltage limited cycle mode rather than a fixed time charge-discharge mode was used in order to study the cell performance as a function of lifetime, in order to see cycle to cycle variations in cell capacity.

The materials tested as substrates for sulfur containers were 446 stainless steel, E-Brite, Kovar, Inconel and 1010 steel. Protective coatings were applied to the inside surface of most containers. The coating materials included chrome, oxidized chrome, oxidized inconel, molybdenum, grafoil and graphite filled silicate over chrome. The electrode materials consisted of graphite felt, alumina coated graphite felt and chopped graphite fibers (see Table V.1).

The results for each of the series from A40 to A120 are summarized below. The data for A10, A20 and A30 series are discussed in the final NSF report (April 1978).

A40 Series: The sulfur containers used in this series were made from chrome plated E-Brite protected with a proprietary graphite filled silicate layer ("Tiodize"). This has been the most successful sulfur container to date. The A40 series cells is still operating after eight months (June 1977). All failures in this series have been due to corrosion of sulfur fill tube which had not been protected, and not due to ceramic failure. The decrease in capacity in A40/5 over the eight month period has been less than 13% and is shown in Figure V.9. The energy storage efficiency and reactant utilization are 83% and 58% respectively. The cycle capacity after seven months of operation (cycle #550) is a strong function of current density, as shown in Figure V.10, primarily because of current density dependence of two-phase rechargeability. At a current density of 96 mA/cm^2, the cell recharges approximately 30% into the two-phase region.

A50 Series: Three different types of sulfur containers were used in this series; bare and oxidized chrome plated E-Brite, and 347 steel with molybdenum coatings. Materials used for the sulfur electrode were untreated and aluminum-coated WDF felt cookies. The alumina-coated felt electrodes in cells with bare chrome

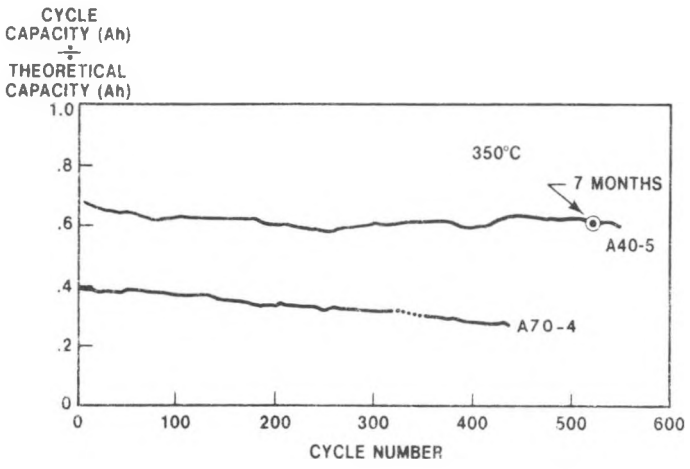

FIGURE V.9

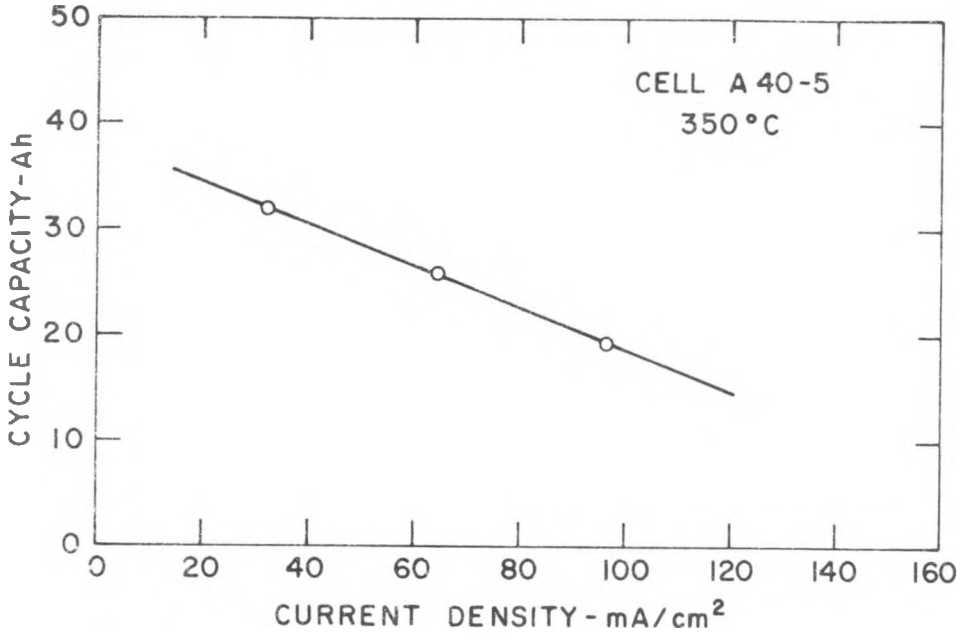

FIGURE V.10

plated sulfur containers (i.e., A50-2, Figure V.11) gave excellent initial performance with utilizations in the range of 80 to 90% and efficiencies in the order of 90%. The sharp decline in cycle capacity of these cells is attributed to the flaking off of the alumina coatings from the felt fibers. New methods of coating the felts are under active study.

Cells which had a "conducting" chrome oxide surface protecting the sulfur container (i.e., A51/10) had a very high initial cell impedance which gradually decreased and then increased again. The cycle capacity of A51/10 for the last few hundred cycles is shown in Figure V.11. These coatings were not sufficiently conductive and provided only marginal protection to the sulfur container.

The molybdenum coatings on 347 steel had poor adherence to the container. Post-mortem examination of cells showed that large areas of the coatings had peeled off the 347 steel.

A60 Series: This series of cells used oxidized inconel as the sulfur containers. The cells failed before sufficient time had elapsed to determine the effectiveness of the protective coatings.

A70 Series: Grafoil lined E-Brite, chrome plated 1010 steel and sputtered molybdenum coated Kovar were used as materials for the sulfur containers.

The grafoil lined cells operated only in the single phase region. For cell A70/4 the cycle capacity versus cycle number is shown in Figure V.9. The decline in capacity over a period of six months for this cell was from 31.8 Ah to 24 Ah before the cell failed. The molybdenum coated cells (i.e., A70/9, Figure V.11) showed an initial improvement in cycle capacity followed by a sharp decline. Post-mortem analyses of cells showed corrosion of the sulfur container both for the grafoil and molybdenum lined cells. The lifetime of cells with 1010 steel containers was too short to determine the effectiveness of the chrome plate.

A80 and A90 Series: These cells failed before any electrical testing could be done. The A80 series used a sulfur core design and the A90 series cells had a protective aluminum liner inside the sulfur container.

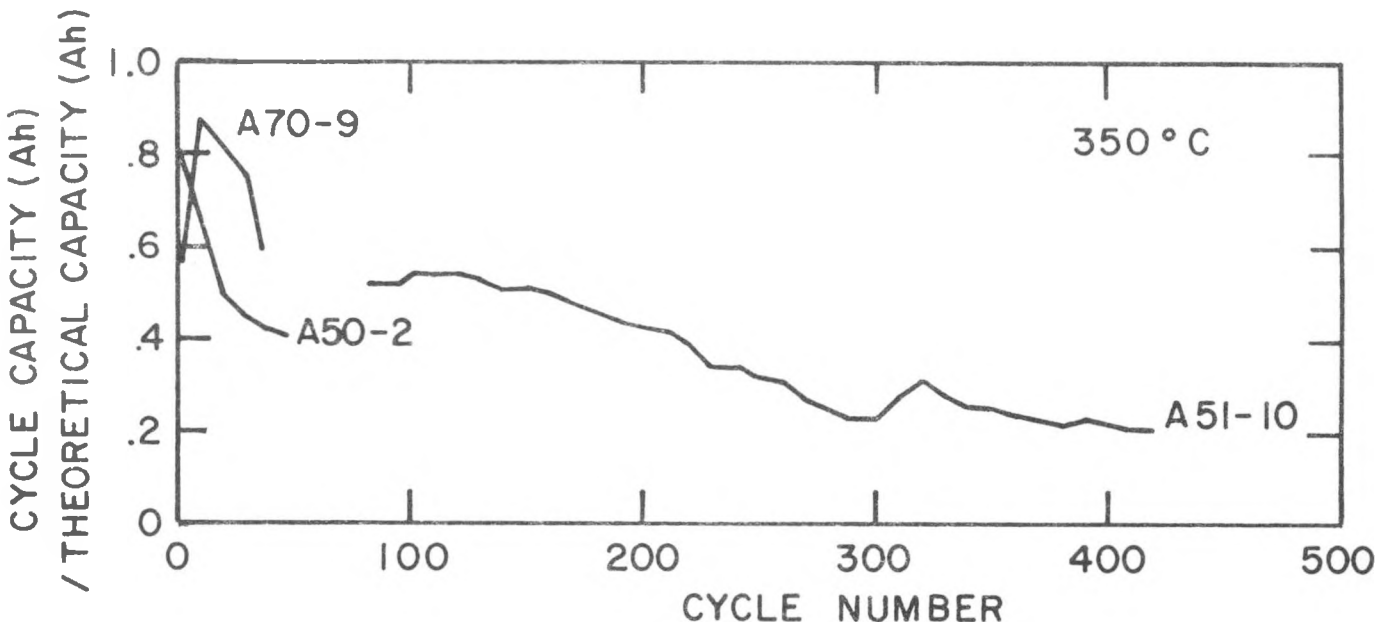
CYCLE CAPACITY (Ah)
/ THEORETICAL CAPACITY (Ah)
1.0
.8
.6
.4
.2
0
A70-9
350 °C
A50-2
A51-10
0
100
200
300
400
500
CYCLE NUMBER

FIGURE V.11

The A100 series cells are duplicates of the A40 series except that the size of the cells has been increased from 46 Ah to 101 Ah by increase in the diameter of the sulfur container. The initial performance characteristics of these cells show a wide variation in capacity (Figure V.12); some operate only in the single phase region, and others operate well into the two-phase region with utilizations of reactants greater than 80%. The lifetime of the A100 series cells has been limited due to the corrosion at the weld area of the sulfur fill tube, which had not been protected by the Tiodizing process. Energy densities greater than 160 Wh/kg at C/14 rate have been achieved in nonweight optimized cells of the A100 series.

A120 Series: This series used chrome plated, Tiodized, E-Brite sulfur containers. An alternate electrode material, chopped graphite fibers, which offers simplified cell assembly, was tested in this series. The utilization of reactants in these cells has varied from 30 to 65%. It has not been determined at this writing whether the lack of reproducibility from cell to cell is due to the fibers themselves or to other causes.

The results of the exploratory cells show that most of the materials used for the sulfur container have given inadequate performance and life. Some cells have given high utilization but many more have given poor performance. The reproducibility of cell performance and cell life (sulfur container protection) remain as areas for future development and work.

5.13 Cell Evaluation, Mark-I Prototype Cells

A few Mark-I prototype cells have recently been placed on to electrical testing. Only very limited data is available at this time. Because of the short duration of the tests and the fact that the cells under test were from the initial production runs, test results should be interpreted cautiously since they may not be indicative of Mark-I characteristics.

The first cell, Cell A, was heated to 350°C and cycled at constant currents up to 27.4 A (100 mA/cm^2) with the voltage cut-off limits set at 1.5 and 2.5 volts. The first seven cycles were carried out at a current density of 50 mA/cm^2. The cell impedance decreased with operation as reflected by the deeper discharges and higher cell voltages during discharge for successive cycles. At a current

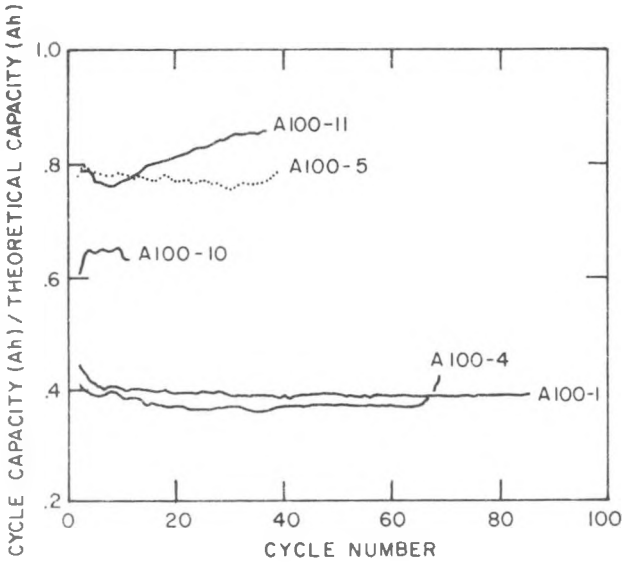
CYCLE CAPACITY (Ah) / THEORETICAL CAPACITY (Ah)
1.0
.8
.6
.4
.2
0
20
40
60
80
100
CYCLE NUMBER
A100-11
A100-5
A100-10
A100-4
A100-1

FIGURE V.12

density of 50 mA/cm^2, the cycle capacity increased from 82 to 95 A hr of which approximately 30 A hr was in the two-phase region. Based on conversion of all of the sulfur to Na_2S_3, the theoretical capacity of the cell was 143 A hr. At 50 mA/cm^2, the energy storage efficiency was 81 percent and the specific energy was 85 W hr/kg.

Performance data for this cell are shown in Table V.3,and Figure V.13 shows the cycle characteristics at various current densities. The effective cell resistivity was between 3 and 5 ohm cm^2. This relatively high value was reflected in a cycle efficiency which varied from 88 percent at a current density of 30 mA/cm^2 to 76 percent at a current density of 100 mA/cm^2. Cell operation was restricted to the single phase region at current densities greater than 50 mA/cm^2.

Table V.3

PERFORMANCE OF CELL A AT 350°C, CYCLING UNDER EQUAL CHARGE AND DISCHARGE CURRENTS

Cell Current, A	7.9	13.2	20.0	27.4
mA/cm^2	30	50	75	100
Cycle Capacity, A hr	94	86	64	55
Rate, hrs.	11.9	6.5	3.2	2.1
Turn Around Efficiency, %	88	81	79	76

The test results on the Mark-I prototype cells are too preliminary to draw any definite conclusions. The protection of the sulfur container and reproducibility of cell performance remain open issues at this time.

5.14 Facilities for Electrical Testing

The sodium-sulfur battery testing facility is located within the ATC Laboratory at Aeronutronic. At this writing, the facility is partially operational with some work on the submodule testing equipment still in progress. The remainder of this section describes the facility and test equipment.

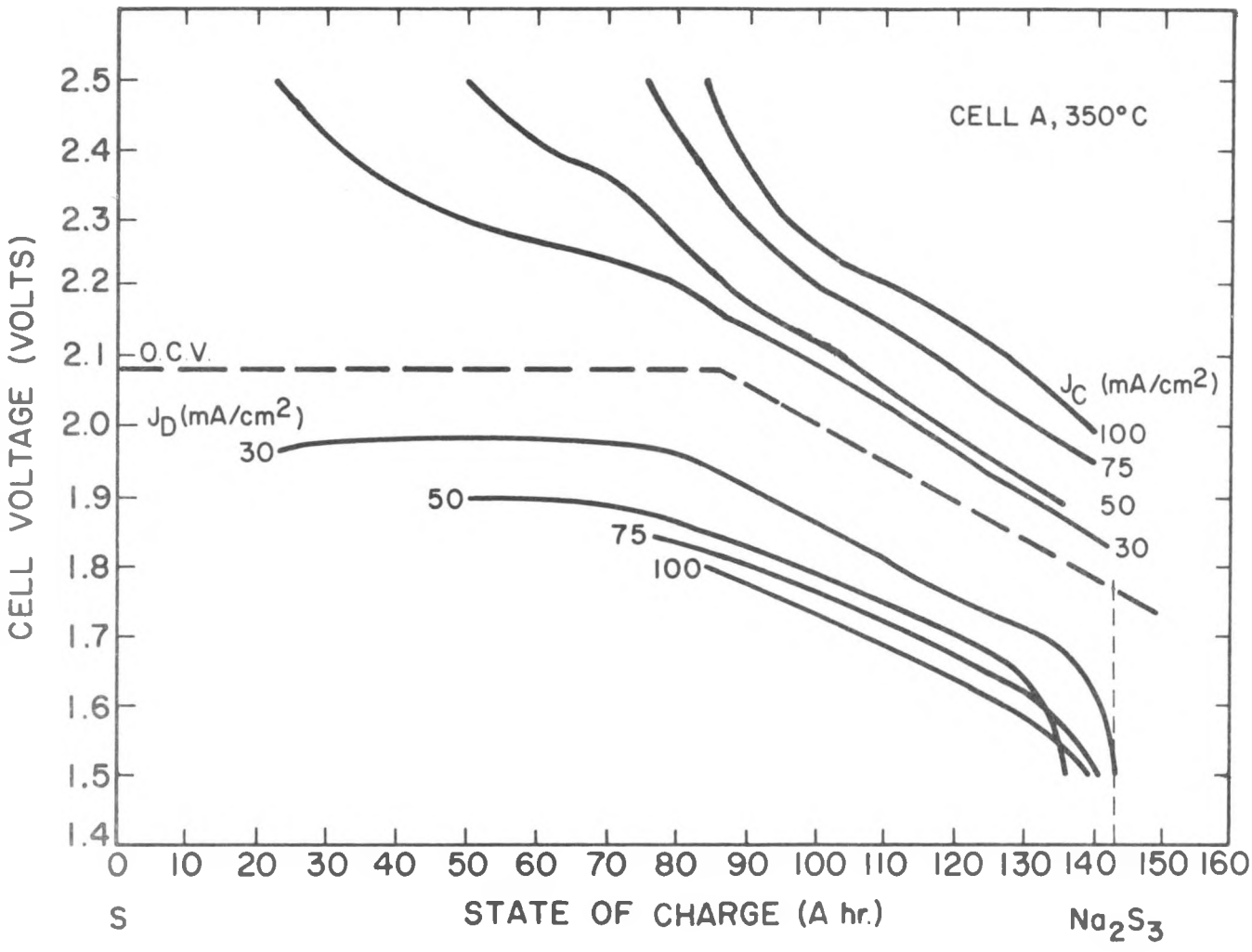

FIGURE V.13 - Cycle Characteristics of Cell A at Various Current Densities

Testing Facility Layout. A facility for testing sodium-sulfur cells individually and in groups was designed and is being built in Phase II. The layout of the facility is such that it can easily grow to accommodate the expanded needs of future phases of the program. Two buildings have been designated for testing. Most of the testing of single cells and submodules is being carried out in the battery test facility, the building in the foreground of Figure V.14. The exploratory test facility, which is somewhat remote from the other buildings in the ATC Laboratory, is used for tests which could be hazardous such as crush tests and tests of the first cells of new designs. The testing facility is described in more detail in the following paragraphs.

Battery Test Facility. This building is a concrete-walled structure encompassing 1740 ft^2. The existing building was modified to meet the needs of this program by installing room dividers to provide (1) a control room, (2) an assembly area for preparing cells and submodules for testing, and (3) a testing area. Other modifications included the installation of a 300 kVA power transformer and smoke control system.

The control room houses six microprocessor computer systems, a 5 kVA uninterruptible power supply (UPS) to provide power for the microprocessors in the event of a power failure, and a line printer for data recording and selected printout display. The printer/recorder is coupled directly to a NOVA computer via telephone lines. The NOVA computer is located within the main Aeronutronic facility. Through the NOVA, daily status reports of cells under test and selected cell life history reports are provided. During Phase III expanded software will result in computer plotting of cell performance data.

The assembly area is used to assemble manufactured cells into submodule groups as well as for instrumenting single cells prior to testing. Oven support racks as shown in Figure V.15 are used to configure submodule groups according to the test matrix.

Forty single cell tube furnaces and five Despatch ovens for groups of cells are located in the testing area. The tube furnaces are mounted in groups of ten on support tables. Single cells are placed directly into these furnaces and are supported by glass-tubing spacers resting on the furnace end plate. Four of the

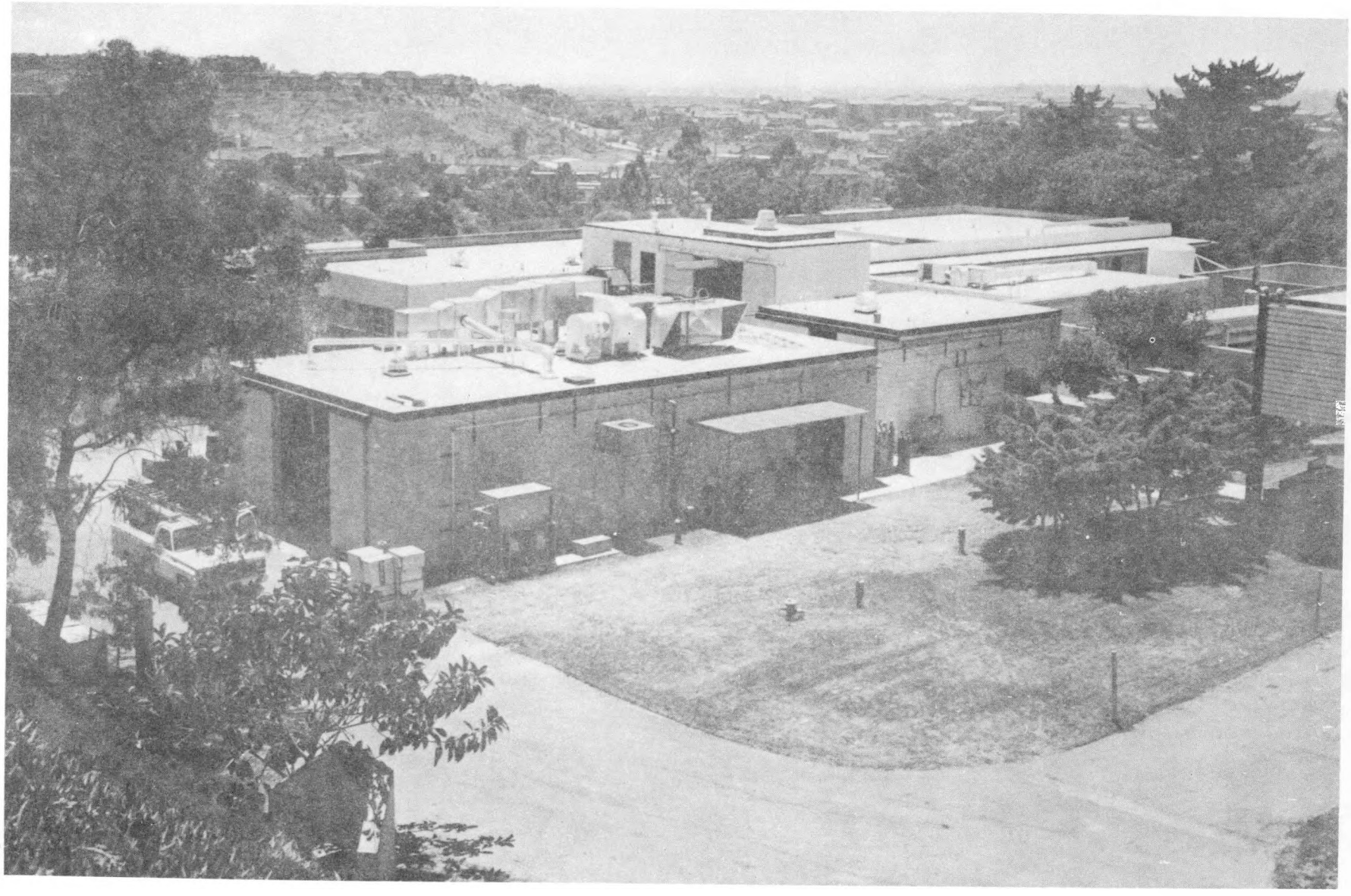

FIGURE V.14 - Test Facility Building

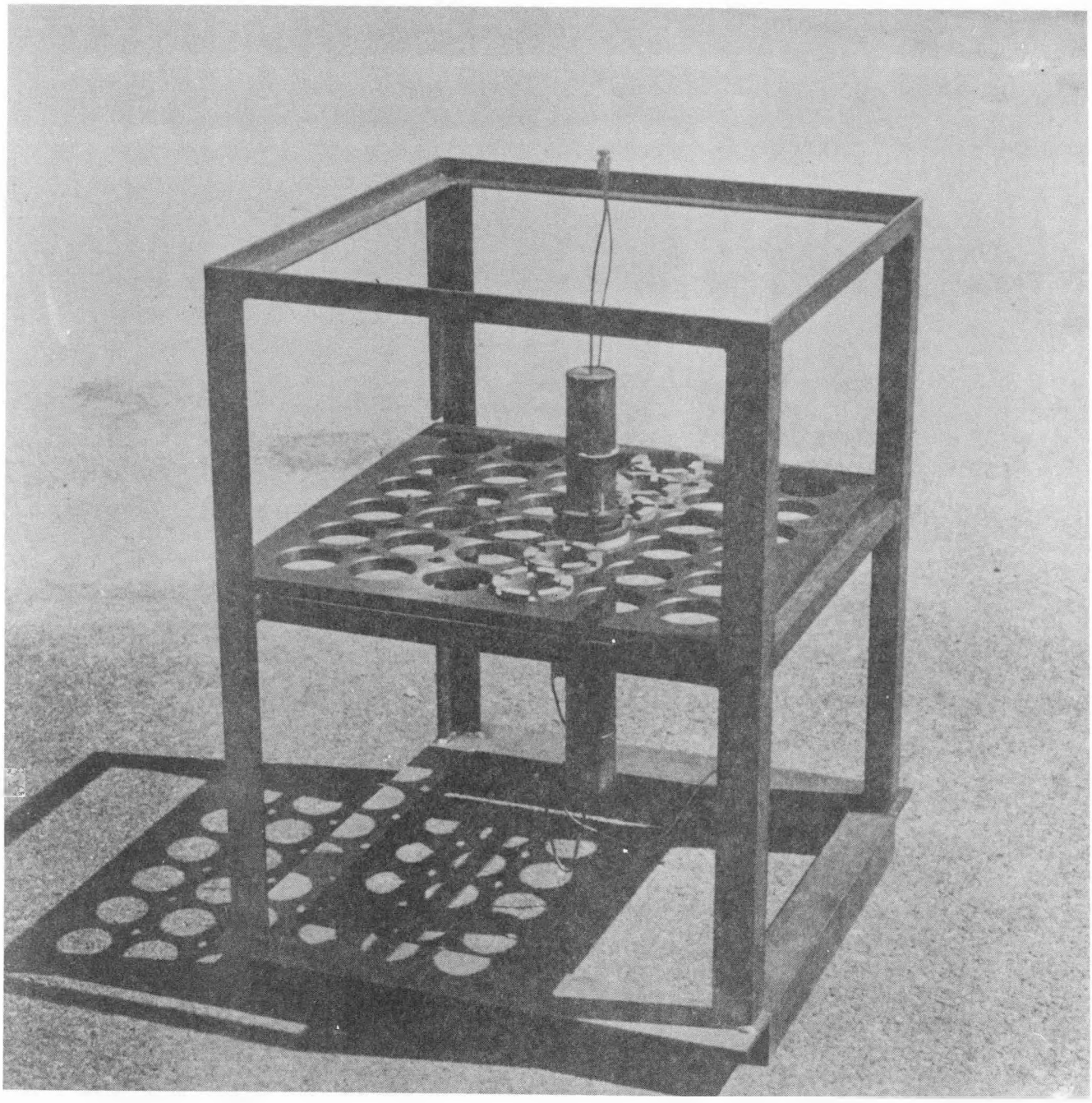

FIGURE V.15 - Oven Support Rack

large ovens are used for testing cell groups while one is allocated to the initial characterization of individual cells. Test stations utilizing these furnaces and ovens are discussed below. Figures V.16 and V.17 show some of the ovens and furnaces.

Each of the five Despatch ovens is connected directly to a common exhaust header. Hoods over the tube-furnace tables are also connected to this system. Approximately five percent of the recirculating gases from each oven and the required ventilation for each tube furnace table is vented through the common exhaust header. Redundant smoke sensors in the exhaust duct constantly sample the vented gases for smoke. In the event of a fire, the variable speed exhaust fan will go to maximum capacity, switch the exhausted gas to a high-purity filter bank, turn on a roof-mounted rotating beacon and notify a security guard via a direct signal line. Options are provided for automatic or manual flooding of each oven with nitrogen gas and shutdown of electrical power to the affected oven or cell table.

Exploratory Test Facility. The planned layout of this building is shown in Figure V.18 This building was used for tests which involved crushing cells and for the preliminary testing of single cells using a test setup as shown in Figure V.19. Because of its design and remote location of this building, tests of exploratory cells or tests which could be hazardous are carried out here rather than in the main testing area. This building is also designated for sodium disposal, parts degreasing, bulk sodium storage and post-test dissection of cells.

Test Stations. As shown in Figure V.17 the 40 single-cell tube furnaces are positioned on tables in four groups of ten each. An individual temperature controller with over-temperature protection is provided for each tube furnace. Skin temperatures of cells being tested can be monitored using a digital meter provided at each furnace table. Cells tested in 35 of these furnaces are series connected in groups of five. One 20-V, 115-A DC power supply is provided for testing each of these groups. Control of the series-connected strings of cells is by means of a Motorola 6800 microprocessor located in the control room. One microprocessor can handle up to four series strings (20 cells).

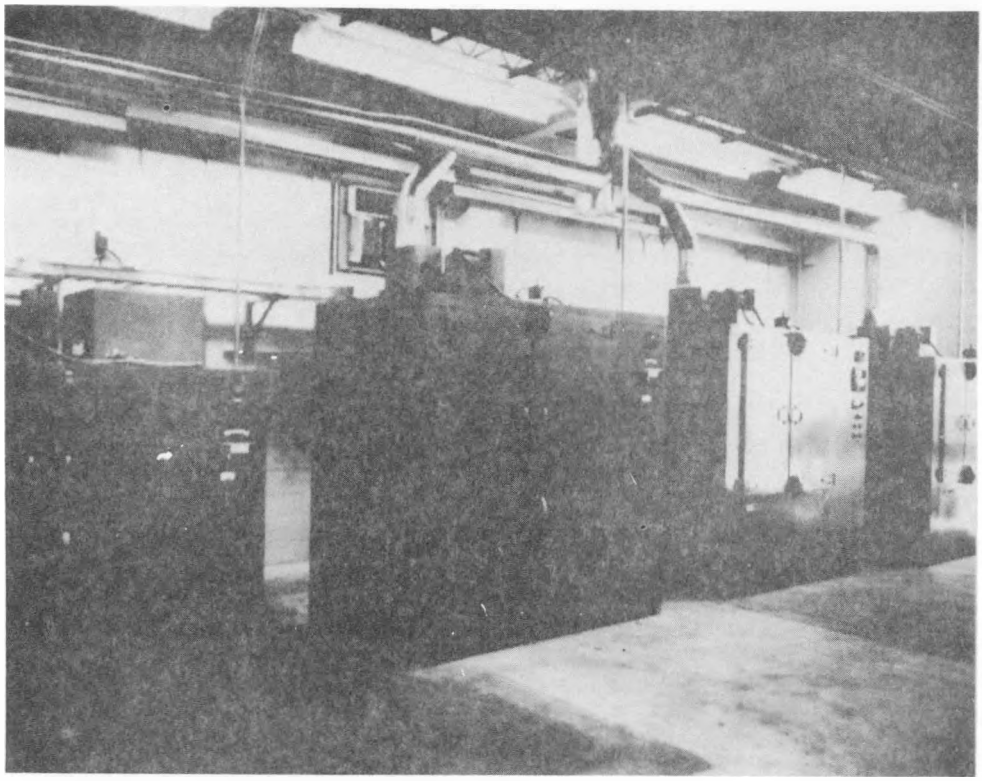

FIGURE V.16 - Ovens

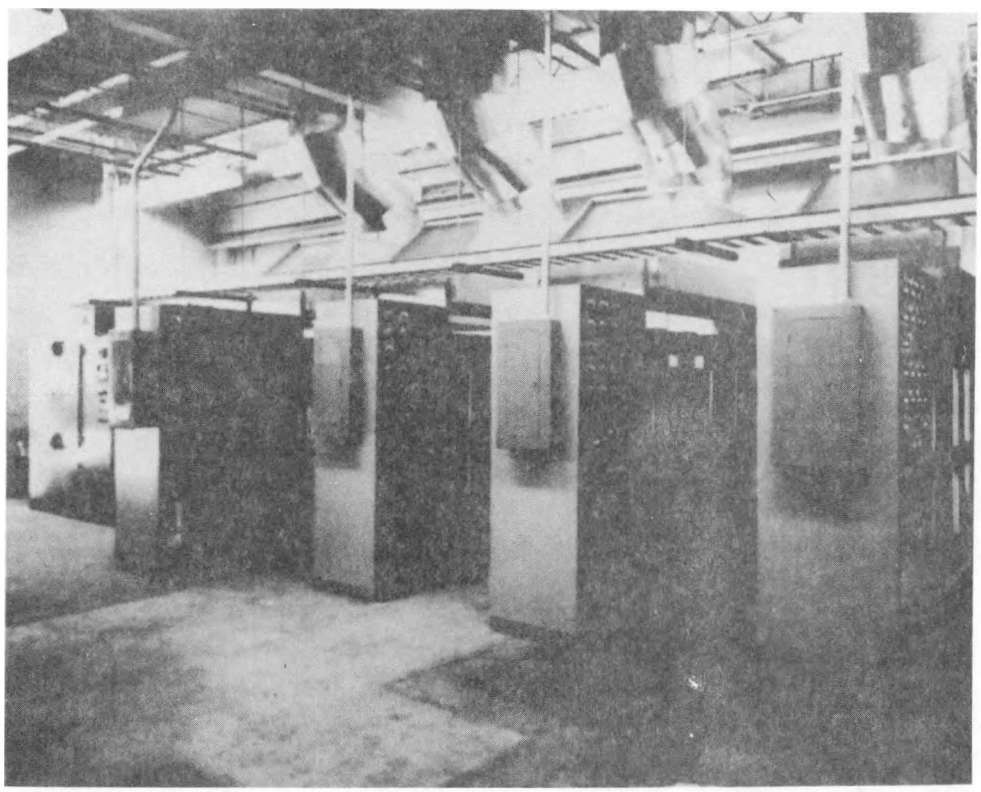

FIGURE V.17 - Furnaces

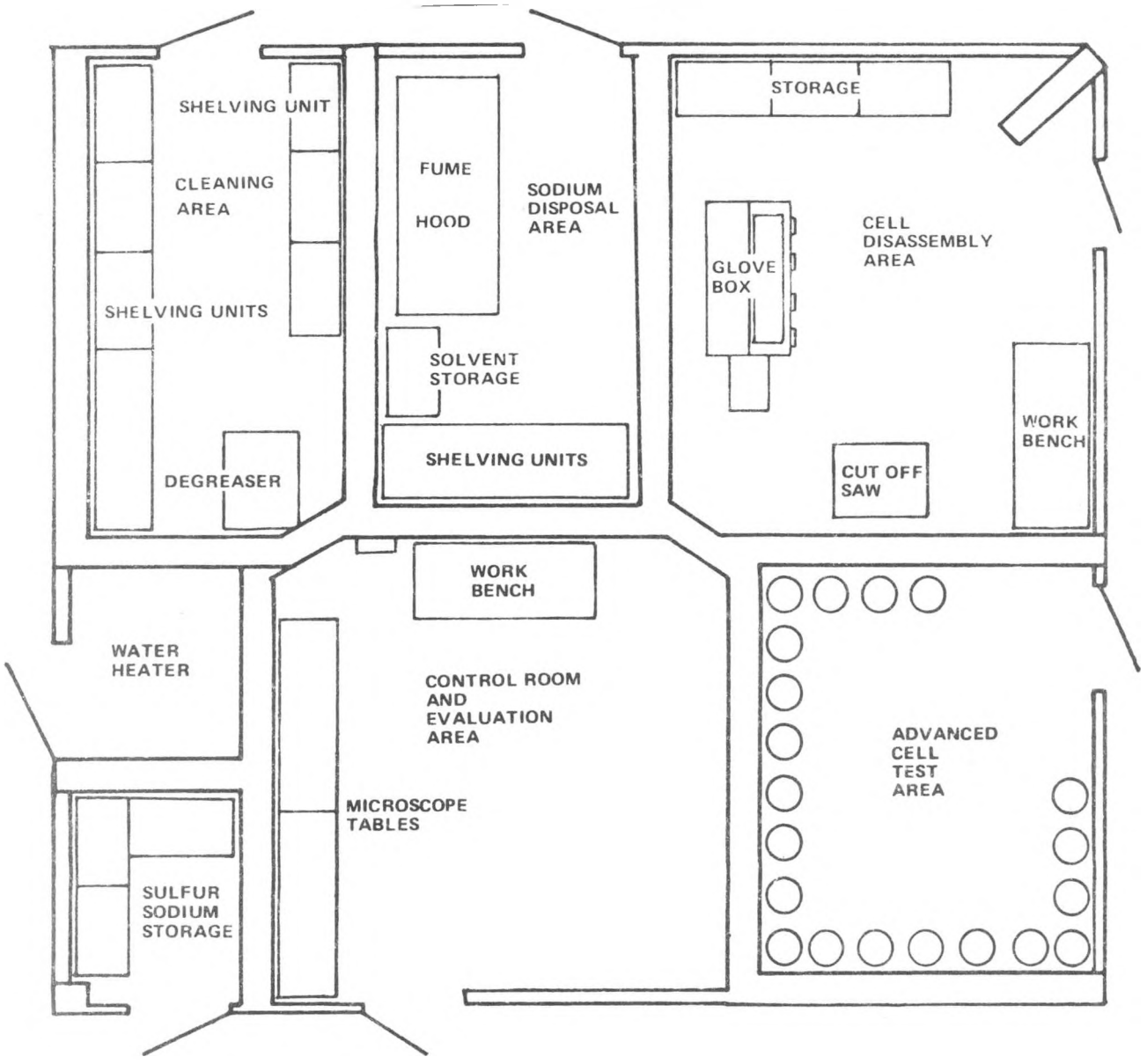

FIGURE V 18 - Building No. 12, Exploratory - Test Facility

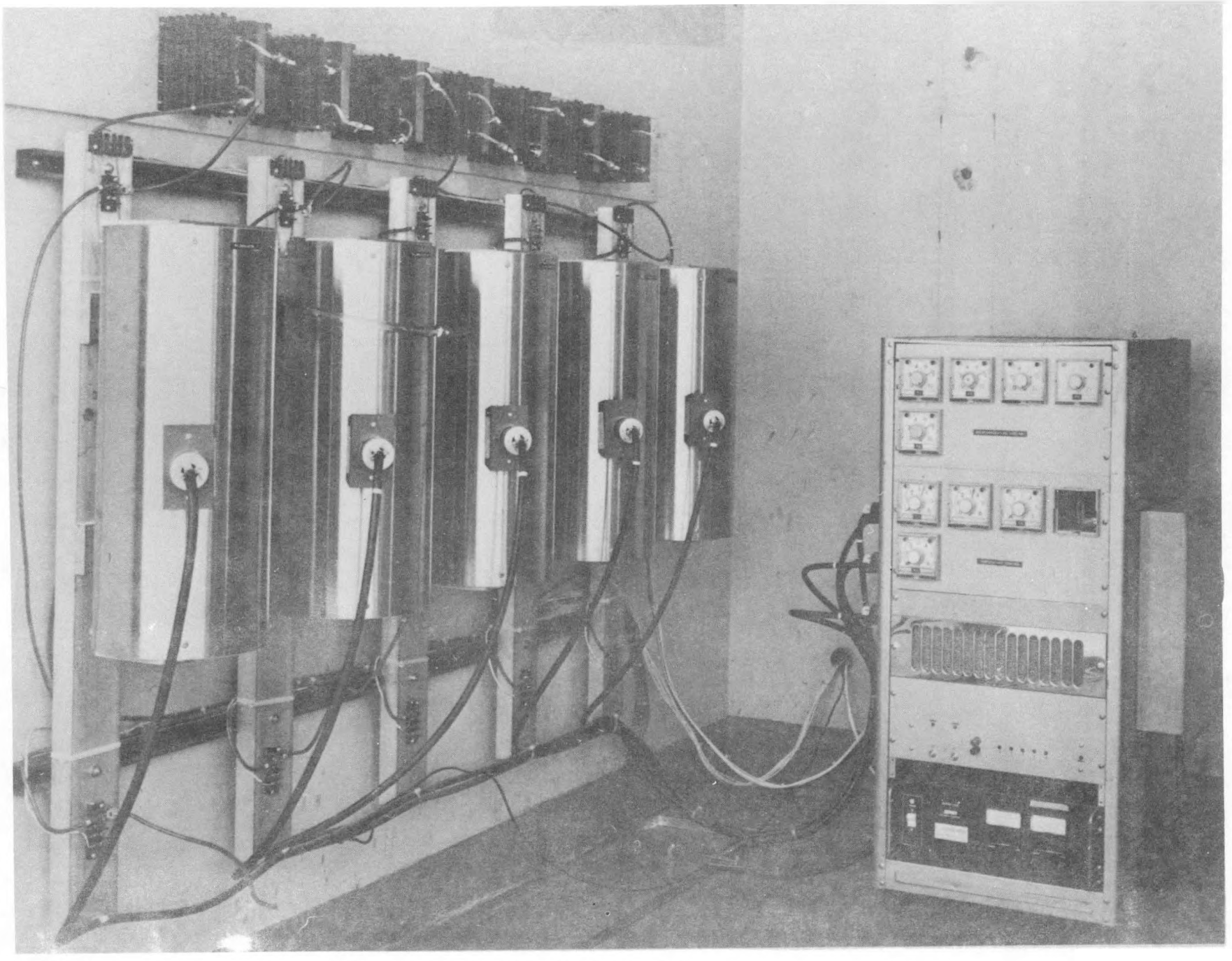

FIGURE V.19 - Single Cell Furnaces

The other five tube furnaces are utilized in test setups where a separate 10-V, 50-A power supply is provided for each cell. A set-point temperature programmer with five slave temperature controllers is provided for these test stations. Cell skin temperatures can be monitored using a digital meter and can be recorded along with charge and discharge currents and cell voltages through the microprocessor system.

Four large Despatch ovens are used for testing groups of cells in various series, parallel and series-parallel combinations. Each of these ovens has its own relay control box, DC power supply, and power resistor rack. The relay contacts and load resistors are sized to handle currents up to 400 A. A Motorola 6800 microprocessor also controls the testing of cell groups in these ovens. Data provided to the NOVA computer consist of selected temperatures, currents and voltages.

The fifth Despatch oven is configured for the testing of individual cells for quality control and characterization before selection for incorporation into submodules. The control hardware associated with these test stations is identical to that for the series-connected five-cell strings.

Equipment for Testing Cells in Series Strings. The system for testing series strings of cells uses Motorola 6800 microprocessors for charge/discharge control and data acquisition. Cell voltage readings and preset time intervals are used as a basis for determining charge or discharge mode. The processor program signals "charge/discharge reverse" or "idle" to relays which control cell currents from constant-current power supplies. Cell voltage data also may be used for current control on an emergency shut down basis.

The test system includes several control processors and one multiplexer processor. The series circuit equipment controls up to 20 cells (four strings of five cells each). The processor control equipment includes: analog input equipment for data acquisition, current-control relays for cell charge/discharge-idle functions, a data output channel to a multiplexer processor, and a control indicator panel. The multiplexer processor gathers control processor data and controls the output channels to a NOVA-2 computer or Texas Instruments (TI) terminal recorder for data storage. It also provides input-output control for

the transfer of data from the TI terminal to the NOVA computer. A system block diagram for the control processor is shown in Figure V.20. For testing of individual cells, a single-circuit system will be used.

Processor Operation. The processors control four separate circuits, each comprised of a power supply and five cells in series, through the use of one relay for each circuit. The four relay control units interface to the processor through peripheral interface adapter (PIA) cards and are optically isolated to prevent ground noise.

An analog-to-digital converter and multiplexer is interfaced to read all cell voltages and the current in each string (24 channels). The solid state multiplexers used have a differential input capability of up to 10 volts, common mode. To accommodate the voltage of a series string, the analog common is connected to the center of the cell string. A control panel on the processor is interfaced through PIA's with controls and indicators available for program operation.

The primary functions of the processor are control of cell current and data acquisition. The system has the following features:

1. Individual series circuits and control of individual cells may be activated or deactivated from the control panel.
2. Charge and discharge time may be set.
3. Initial mode (charge or discharge) may be set.
4. Voltage limits for determining end of charge and discharge may be set.
5. Charge/discharge reverse may be commanded from preset time or from occurrence of one cell in a string reaching preset voltage limit.
6. The run-time parameter values may be displayed.
7. Automatic string shutdown occurs when a cell voltage exceeds a "hazard value" of above 3 or below 1 volt.
8. Run-time parameters are printed out and a binary tape is prepared for subsequent reloading after a power failure.
9. Charging or discharging is carried out for the preset time; and when elapsed, the mode is reversed in the following manner:
   a. Power-supply current is set to zero.

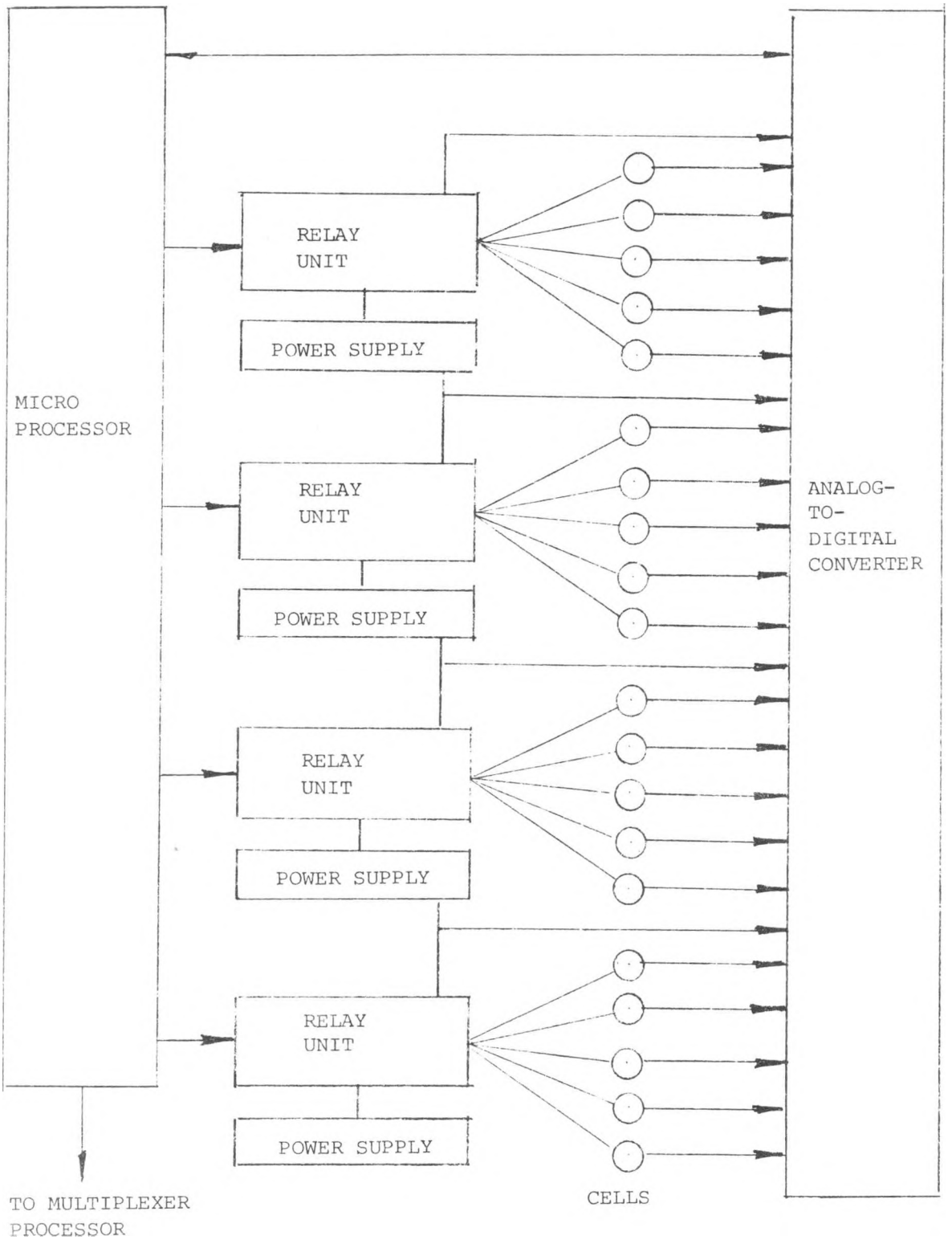

FIGURE V.20 - Block Diagram for Control Processor

b. After an 8-second delay, all idle/active relays are set to active.

c. Charge/discharge mode relay is reversed (appropriate current value is also selected).

d. Power-supply current is set to normal.

10. Error testing for failures is run continuously to test for the following conditions:

a. Power failure.

b. Processor failure.

c. Analog-to-digital converter failure.

d. Memory error.

e. Cell voltage higher than upper limit.

f. Cell voltage lower than lower limit.

g. Data transfer failure.

Data Acquisition. At the 11-second time signal, channel status is tested and the active channels are read through the multiplexer and analog-to-digital converter. The values are tested, and based on a comparison with present values for cell parameters, cell idle or shut down may be set. Data are summed to form an average value transmission each six minutes or 32 acquisitions (because of binary-division ease).

Charge/Discharge Relay Control Unit. Each relay control unit controls a string of five cells. Up to four units may be controlled by one processor. The relay control unit sets power supply currents, and switches cell circuits to idle/active, charge/discharge, and zero/normal current. Power-supply current passes through double power relay contacts to provide static current conduction of up to 50 amperes. Since switching current capability is much less, the power-supply current is set to zero before a power relay is operated. The relay control unit also switches current settings for charge and discharge modes when the current direction is reversed.

Each of the five-cell circuits uses an idle/active relay. When a cell is idle, the cell circuit is open and the power-supply current is bypassed. As each cell relay activates, the cells are connected in series. In the charge mode, five cells will require up to 15 volts from the power supply. As cells are idled, the power-supply voltage requirement is reduced. To avoid dumping a

higher power--supply filter voltage into remaining cells, prior to idling a cell, the power-supply current and voltage are set to zero and a delay is set to allow bleeder resistors to drop the filter voltage. When the voltage has dropped to a value below the remaining cell-string voltage, the idle relay is released and the power-supply current is set to normal. The power-supply voltage rises to the remaining cell voltage and current flow continues. When the charge/discharge mode is to reverse, a similar delayed operation is set; however, a longer time is required to allow the voltage to reach zero.

External series diodes drop the cell discharge voltage to prevent a negative voltage at the power supply. A 50-ampere current shunt provides a current monitor of one millivolt/ampere.

A manual relay control box is used to test the relay control unit. Operation of all the relays is possible for testing and setting the power supply currents.

Equipment for Testing Single Cells and Submodules. The single-circuit system used for testing submodules uses the same type processor as the system for testing cells in series strings, with the exception of the analog-to-digital converter interface. This processor controls a Computer Products wide-range analog input system through serial input/outputs (I/O) in place of the parallel I/O used for the analog-to-digital converter. All other processor hardware features are the same. The relay control units are different, however. Each relay unit controls three single circuits. They are controlled by the same PIA addresses and connector wiring configuration as used with the series circuit processor; however, the bit assignment is different. A block diagram of the single-circuit system is shown in Figure V.21.

The analog input data consists of cell voltage (for charge/discharge status control as well as performance information), cell currents, circuit currents, cell temperatures, and area temperatures. The system controls several different circuits all with different data requirements. These circuits consist of:

Single Cell Circuits	Series Circuits
Parallel Circuits	Series - Parallel Circuits

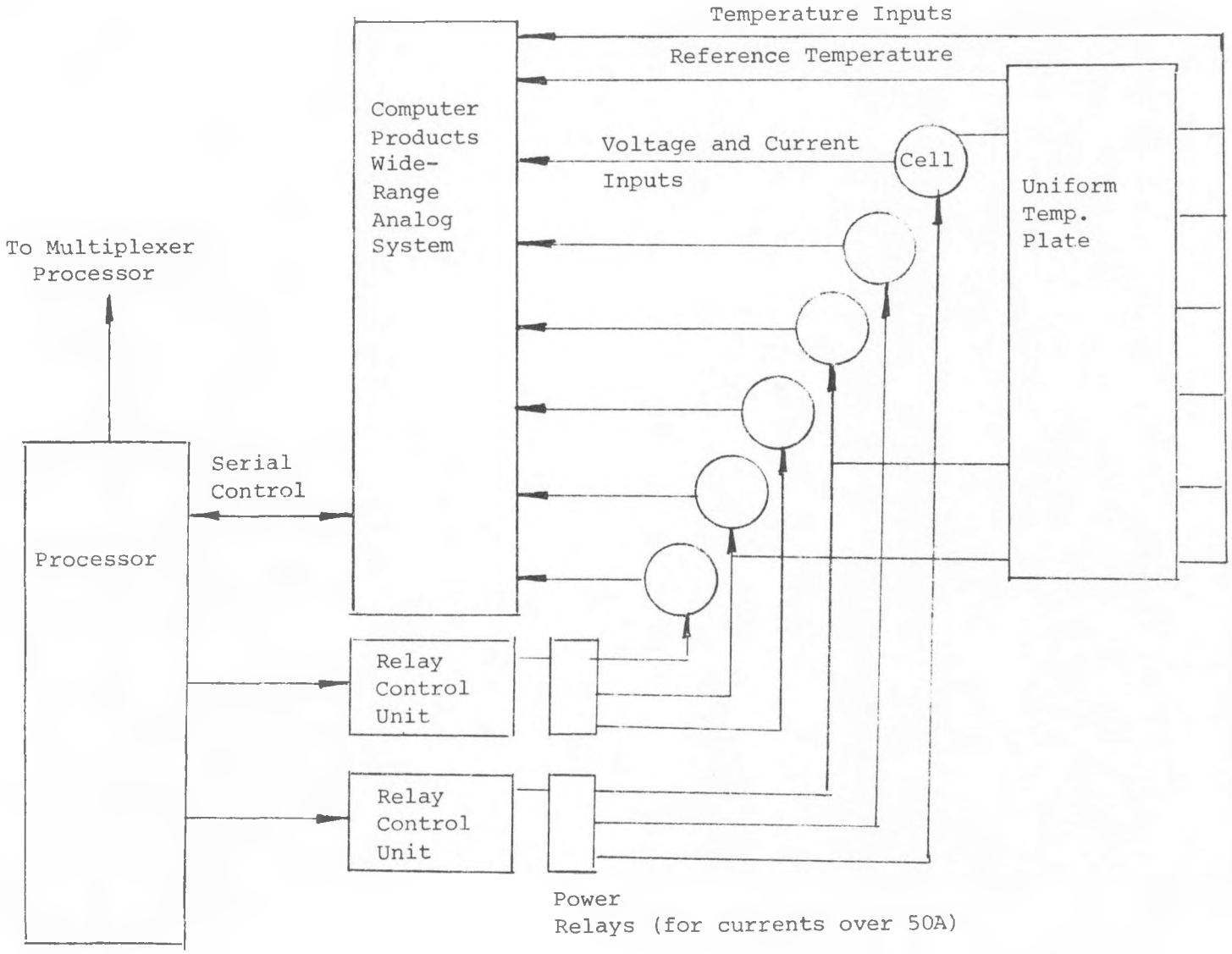

FIGURE V.21 - Block Diagram of Single-Circuit System

Circuits for Testing Single Cells. This circuit consists of one cell and one power supply. Figure V.22 shows the circuit. Up to five circuits can be controlled. From each circuit the following data are transmitted:

Cell Voltage
Cell Current
Cell Temperatures (two per cell)

Voltage and current data are handled as for the series strings. System control is the same as that described for series strings in that section. The system control is based on using voltage to determine charge/discharge or idle modes. Current reversal may be controlled by cell voltage or time. "Hazard" shutdown is also similar to that described for the series-circuit system.

Each thermocouple circuit transitions to copper at a uniform temperature plate (U.T.P.). A temperature sensor on the U.T.P. provides data necessary for converting the millivolt output to degrees.

Parallel Circuit. The system supports two parallel circuits of six cells. Figure V.23 shows the circuit configuration. From each circuit, the following data are read and transmitted:

Cell Voltage
Total Current and Individual Currents for Six Cells
Temperatures (two at each cell and two air temperatures at points of interest in the oven)

The voltage data handling and system control are the same as described for the single-cell circuit. Total current is read from a current shunt and individual cell currents are determined from voltage drops across connector straps. If the current exceeds a preset "hazard" value, shutdown will occur.

Temperature data collection is similar to that for the single-circuit data described above; however, shutdown will occur if any one temperature exceeds a preset limit.

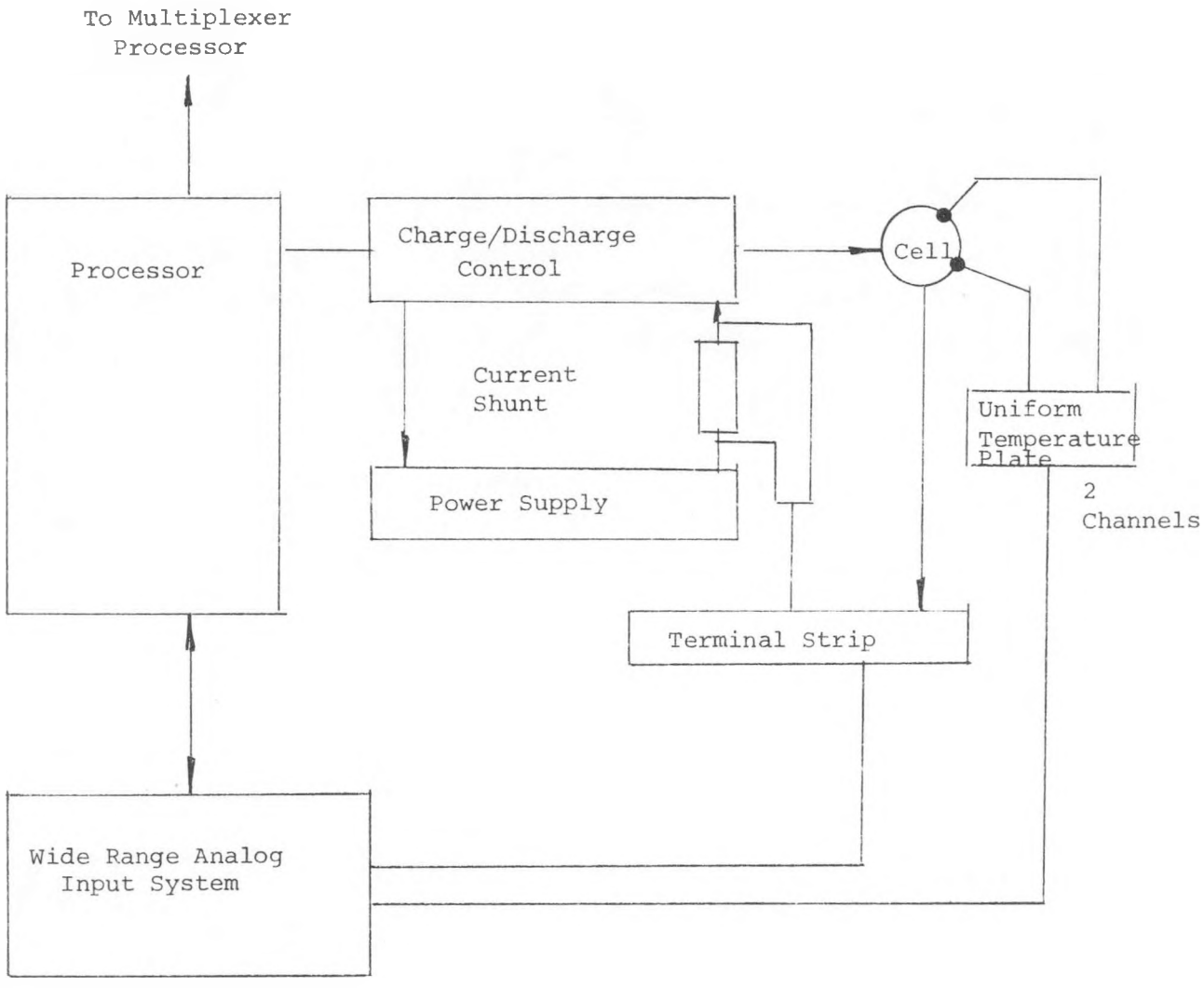

FIGURE V.22 - Circuit for Testing Single Cells

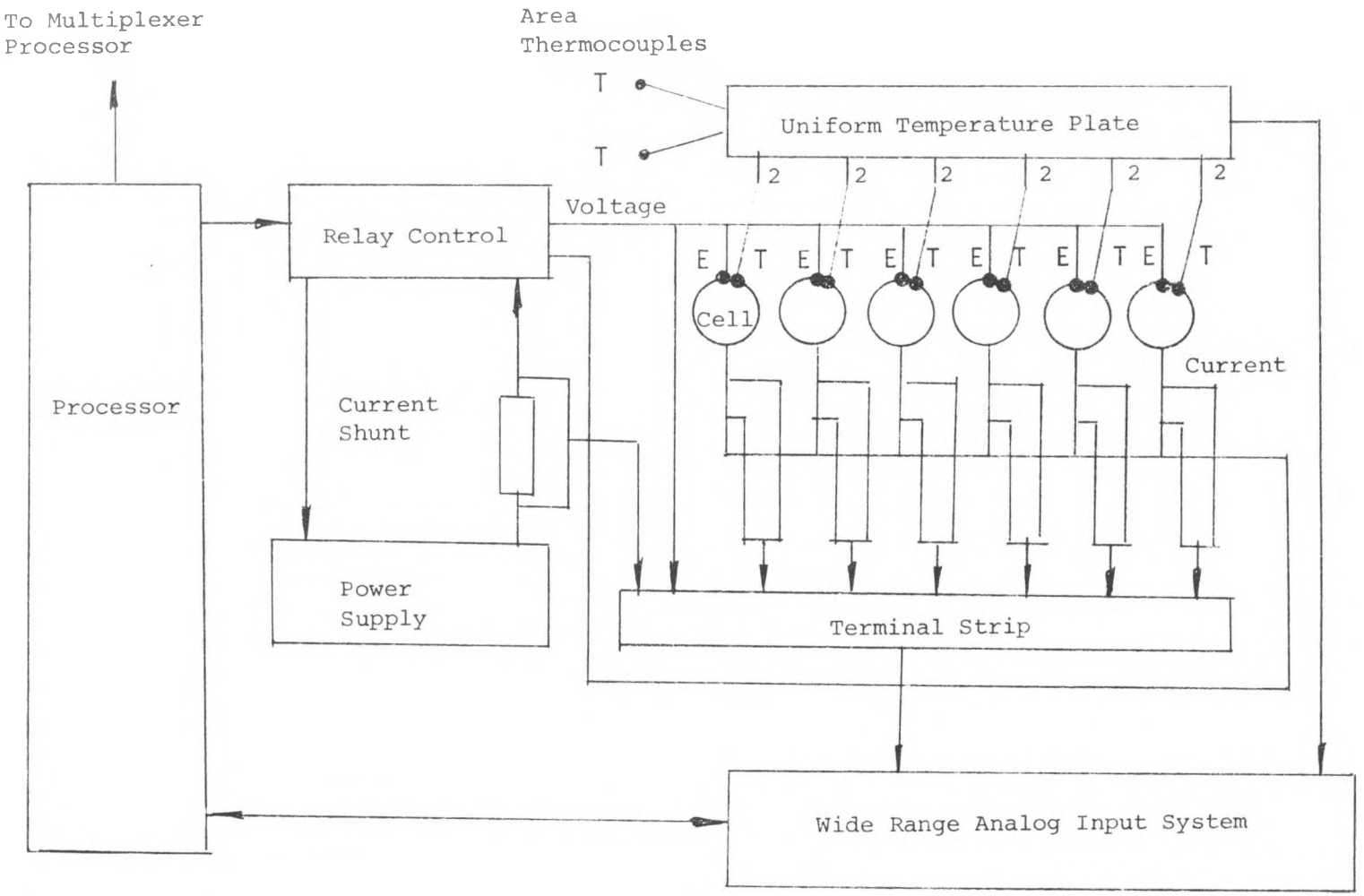

FIGURE V.23 - Circuit for Testing Cells in Parallel

Series Circuit. The system supports two series circuits of six cells each. Figure V.24 shows the circuit configuration. The charge/discharge circuit is treated as a single circuit. From each circuit, the following data are read and transmitted:

Cell Voltages
Total Currents
Temperature (6 cell temperatures and 2 air temperatures)

Each cell voltage is read. Charge/discharge reversal or idle is determined by the first cell voltage reaching a preset value. Circuit shutdown is also determined by any cell voltage exceeding the hazard limit. The current reading is taken from the current shunt connected in series with the power supply. A circuit shutdown will occur if the current exceeds a set limit. The temperature data is taken as described for the parallel circuit.

Series-Parallel Circuit. The system supports one series-parallel circuit. Figure V.25 shows the circuit configuration. The charge/discharge circuit is treated as one single circuit. The following data are read and transmitted:

Six Voltages
Thirty-seven Currents
Fifty-five Temperatures

The voltage data are treated as described for the series circuit, and the current data are treated as described for the parallel circuit. The temperature data are treated as described for the parallel circuit.

Parallel-Series Circuit. One circuit of 36 cells in a different configuration from the series - parallel circuit is also supported by the system. Figure V.26 shows this circuit. The following data are transmitted:

Thirty-six Voltages
Seven Currents
Forty Temperatures

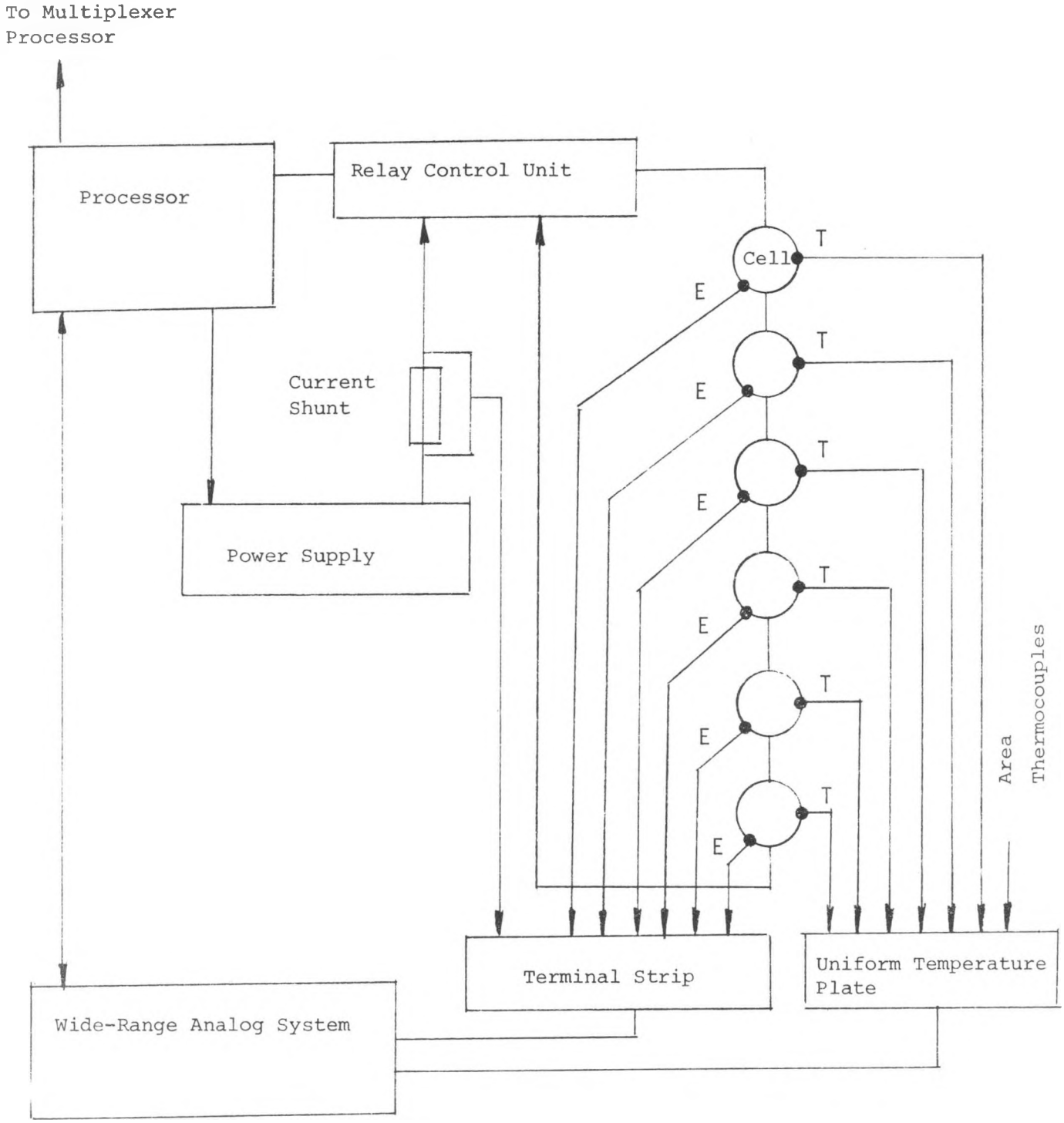

FIGURE V.24 - Circuit for Testing Cells in Series

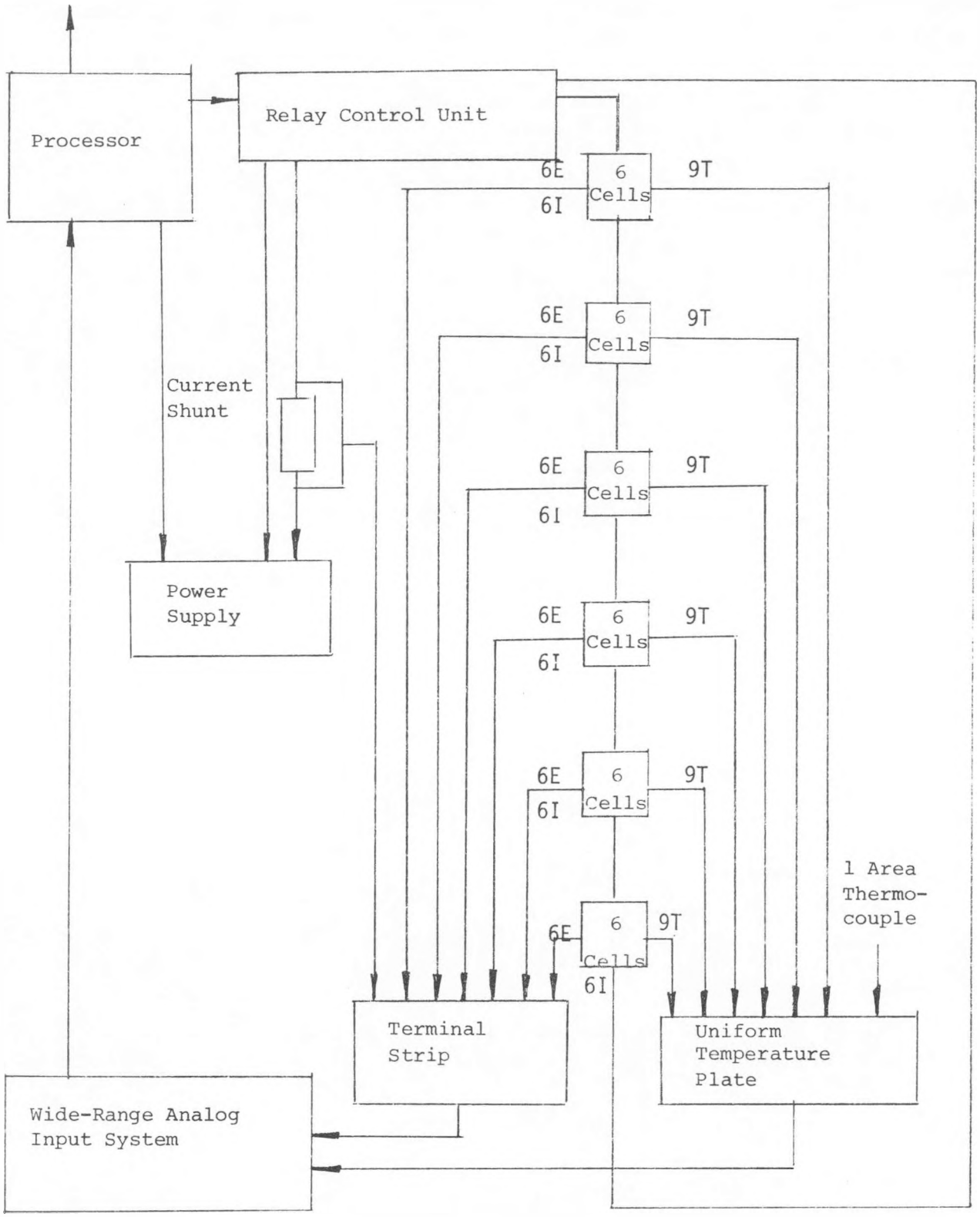

FIGURE V.25 - Circuit for Testing Cells in Series-Parallel Connections

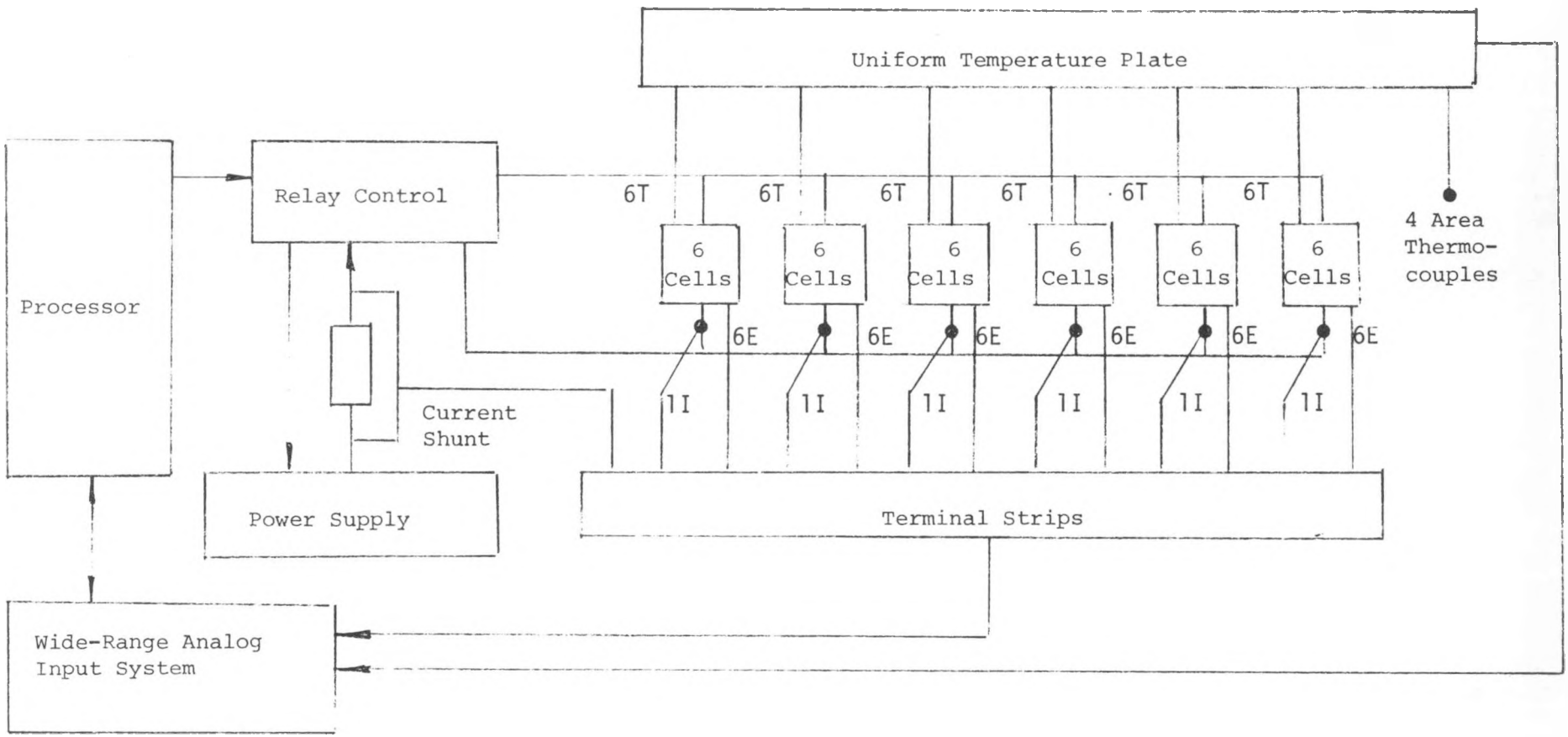

FIGURE V.26 - Circuit for Testing Cells in Parallel-Series Connections

The voltage data are treated the same as described for the series circuits. The current and temperature data are treated the same as described for the parallel circuit.

Data Processing. Each circuit type uses a different program module. Each circuit may be activated or idled at setup time. When a circuit is active, all associated data channels are read and transmitted. If some channels are not used, they must be ignored in the data.

When a circuit causes a voltage, current, or temperature hazard shutdown, the circuit is set to zero current and idle.

Before changing any relay state, the program must set the power supply current to zero and delay the relay operation until the output voltage drops to zero. This delay must be the longest for reversal from charge-to-discharge. The following delays are required for each circuit operation.

Circuit	Charge to Discharge	Discharge to Charge	Idle to Active	Active to Idle
Parallel	2 seconds	50 msec.	50 msec.	0.5 second
Series	10 seconds	50 msec.	50 msec.	0.1 second
Series-Parallel	10 seconds	50 msec.	50 msec.	0.5 second

Data output to the multiplexer processor is the same as for the series circuit control processor.

Each test circuit is setup through the control panel at run time with the following runtime parameters:

- Charge time
- Discharge time
- Starting mode (charge to discharge)
- Charging voltage
- Discharging voltage
- Preset channel values
- Active/idle

When the circuit is activated, data transmission is started. Transmission continues until the circuit is manually idled or an automatic circuit shutdown occurs because of an equipment error.

Equipment. As mentioned earlier, the single-circuit equipment is similar to the series-circuit equipment except for the analog equipment control and the relay control units. The processor control panel and circuits are interchangeable with the exception of the analog equipment I/O card.

The relay control unit controls up to three single circuits. Each circuit may be switched for zero/normal current, charge/discharge, and idle/active.

Two types of relay control units are available. One unit contains all the power relays. The other contains only control relays and a power source to operate high current external contactors. Both types operate from the processor in the same way. One unit will control two parallel circuits and one series-parallel circuit. Another will control two series circuits and one parallel-series circuit. Two control units are required for the five single-cell circuits.

Safety Considerations. The design of the test facility and the procedures for its operation were developed with regard for personnel safety. As mentioned previously, tests on cells of new designs are carried out in another building which is remote from the main testing facility. The more routine tests are carried out in the main facility where provisions have been made for automatic high speed exhausting of smoke and activation of warning systems in the event of failures which result in smoke and/or fire.

Procedures to be followed in the event of cell failure have been established. In general, the steps involve disconnecting the failed cell from the charge/discharge circuits and disconnecting the furnace power. If a fire should occur in the testing area, personnel will follow established procedures for fighting sodium fires. A wheeled pressurized Metal-X fire extinguisher (300 pound capacity) with a 50 foot long hose is available as are smaller hand-held Metal-X fire extinguishers. Fire-retardant clothing is provided for personnel working in the testing area.

APPENDIX A

PARAMETRIC ANALYSIS DEFINING RELATIVE CELL DIMENSIONS

The following analysis has proved helpful in gaining insight into the interrelationship between the size of the solid electrolyte (β''-alumina) and the other dimensions of a sodium-sulfur cell. These relationships have been used in other analyses. Early in the program they aided structural analysis by serving as a basis for predicting the size of future cells (during the period that the solid electrolyte was enlarged). They also form a basis for eventual mathematical modeling.

The discussion and derivations which follow pertain only to cells of the specific cylindrical configuration which is depicted in Figure A-1. A model is developed for a cell in which the bulk of the sodium is stored above a β''-alumina tube which also contains sodium and, in turn, is encompassed by the sulfur electrode. Dell (Proceedings of 11th Intersociety Energy Conversion Engineering Conference, Sahara Tahoe, Sept. 12-17, 1976, Vol. I, pp. 503-509) has referred to this configuration as the central sodium cell. Others call it the sodium core cell.

Note that in our model, as shown in Figure A-1, the sodium and sulfur containers have a common diameter. This greatly simplifies mathematics as well as manufacturability.

(a) Relative Lengths of Electrodes. If properly constructed to yield the optimum electricity, all of the sulfur within the cell is transformed into a polysulfide melt whose composition corresponds to the chemical compound, Na_2S_3. In terms of mass, 2.09 parts of sulfur combine with one part of sodium. Consequently, in practice cells generally are designed so that the mass of sulfur is about twice that of the sodium within the anode reservoir, i.e., the portion

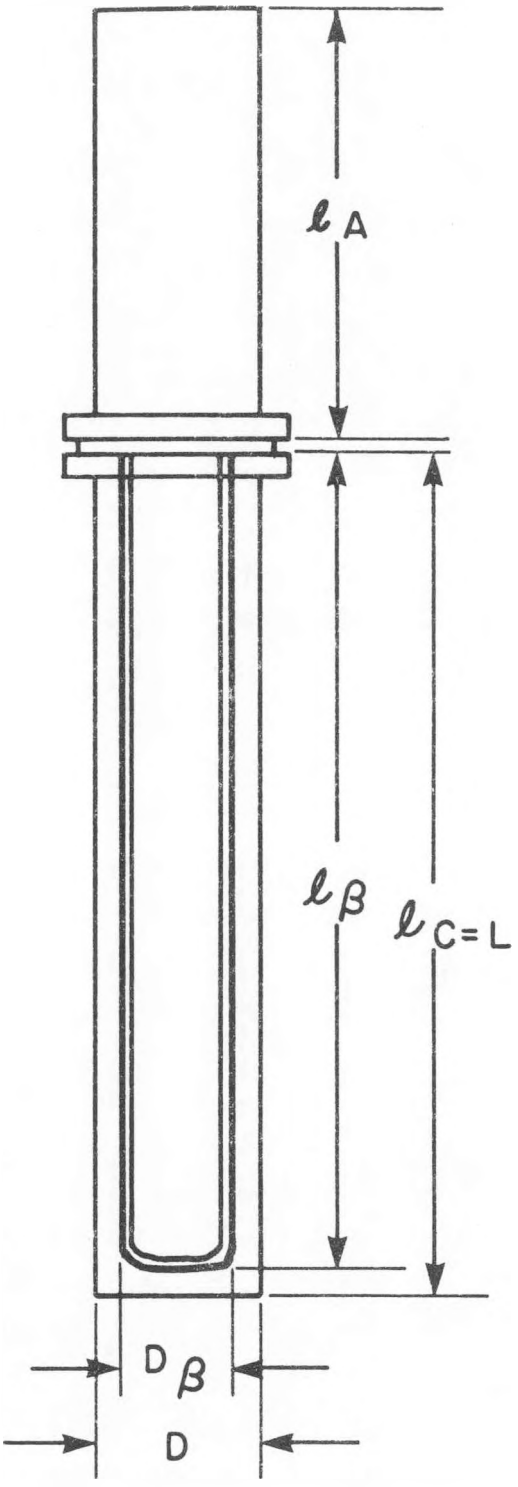

FIGURE A.1 - Basic Dimensions of Cell

of the sodium electrode above the β''-alumina tube. In other words, sufficient sodium is stored under a hydrostatic pressure head to form Na_2S_3 of all the sulfur in the cell. It follows then that in an ideal model the masses of the reactants are related one to the other by the relationships:

$$M_S/M_N = f_C V_C d_S / f_R V_R d_N = 3S/2Na \qquad \text{(A-1)}$$

In the equations above, the symbols have the following meanings:

Symbol	Meaning
f_C	fraction of the cathode or sulfur electrode which is filled with sulfur (at the operating temperature of the cell)
V_C	volume of the cathode
d_S	density of sulfur (at the operating temperature of the cell)
f_R	fraction of the reservoir portion of the anode which is filled with sodium (at the operating temperature of the cell)
V_R	volume of the reservoir
d_N	density of sodium (at the operating temperature of the cell)
S	the gram atomic weight of sulfur, 32 g
Na	the gram atomic weight of sodium, 23 g

Other symbols are defined by Figure A-1, which depicts the explicit geometry of our model. The following relationships are assumed:

$$D_R = D_C \equiv D; \text{ and} \qquad \text{(A-2)}$$

$$\ell_C = \ell_R/a = \ell_\beta/b \equiv L \qquad \text{(A-3)}$$

It follows then that the volumes of the active portions of the electrodes can be expressed by the equations:

$$V_C = (\pi/4)\left[D^2 L - D_\beta^2 \ell_\beta\right] \quad \text{(A-4a)}$$

$$= (\pi/4)\, L \left(D^2 - bD_\beta^2\right); \text{ and} \quad \text{(A-4b)}$$

$$V_R = (\pi/4)\, D^2\, \ell_R \quad \text{(A-5a)}$$

$$= (\pi/4)\, D^2\, aL \quad \text{(A-5b)}$$

Dividing Equation A-4b by Equation A-5b yields the expression:

$$V_C/V_R = (1/a)\left[1 - b\left(D_\beta^2/D^2\right)\right] \quad \text{(A-6)}$$

Rearranging Equation A-1 yields the identity:

$$V_C/V_R = (3S/2Na)\left(d_N/d_S\right)\left(f_R/f_C\right) = k \quad \text{(A-7)}$$

In other words, the relative volumes of the cathode and reservoir are constant for cells in which sulfur and sodium are stored in the same relative amounts (and same percentages of fill). In our model, we assume the reactants are stored in the ratio, 3S:2Na. The relationship would hold for any other ratio.

By combining Equations A-6 and A-7, one obtains the relationship:

$$a = (1/k) - \left(b\, D_\beta^2/k\right)\left(1/D^2\right) = \ell_R/L \quad \text{(A-8)}$$

(b) Hydrostatic Head for Transfer of Sodium. In Equation A-8, the parameter, a, is the relative length of the reservoir, that is to say, its height relative to that of the cathode. It also is directly proportional to the height (Δh) of the hydrostatic pressure head provided in the cell design for the transfer of sodium during cell discharge: for example,

if the orifices in the cell's safety tube are located near the bottom of the β″-alumina tube,

$$\Delta h \approx \left(\ell_R + \ell_\beta\right) - \ell_\beta = \ell_R = aL \qquad \text{(A-9)}$$

As there is little point in extending the length of the cathode much beyond the length of the β″-alumina tube, in practice the value of the parameter, b, does not differ greatly from unity. In other words,

$$\ell_c/\ell_\beta = b \simeq 1 \qquad \text{(A-10)}$$

Consequently, for a particular β″-alumina tube, the relative height of the reservoir (and hence the hydrostatic head) depends mainly on the diameter of the cell. For example, suppose that the parameter, b, has the value 0.95 then the parameter, a, ranges from 0.05 (1/k) to 1/k as the diameter of the cell is extended from that of the β″-alumina tube to infinity. In practice, however, D, the diameter of the cell seldom exceeds that of the β″-alumina by more than a few centimeters.

Figure A-2 is a plot of the parameter, a, versus the ratio, D/D_β, for a model cell which is nearly optimum, at least with respect to energy density. In this model cell, $f_R = 0.735$ and $f_C = 0.66$. These particular percentages of fill are chosen mainly for reasons which are discussed in Appendix C, which discusses the margin of safety in the cell design. Filled in this manner, the sodium reservoir has adequate capacity for liquid sodium, even if the temperature of a fully-charged cell should escalate inadevertently to the boiling point of sodium. Likewise, the sulfur container has capacity for all the polysulfide that generally will form (unless its temperature exceeds 635°C).

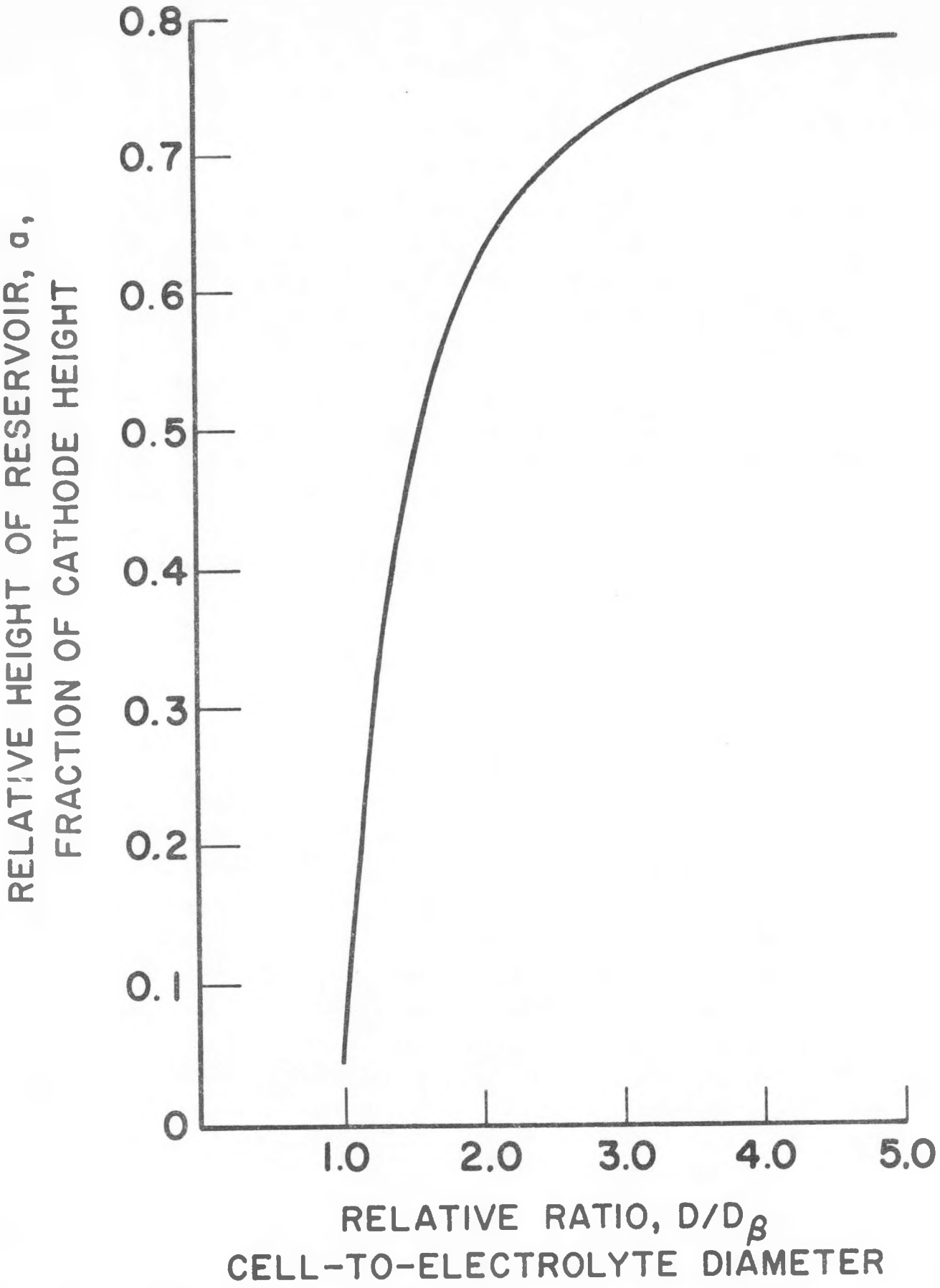

FIGURE A.2 - Interdependency of Cell Dimensions

(c) Electrical Capacity. The electrical capacity of a cell can be rated in terms of the transferable sodium. In our model, this is the mass of sodium stored in the anode reservoir (above the top of the β''-alumina tube). Consequently, expressed in ampere hours (A hr), the capacity of a cell is as follows:

$$C = (\pi/4)\, D^2\, (a/b)\, \ell_\beta f_R d_N\, (96{,}500/23)(1/3600) \qquad \text{(A-11a)}$$

$$= 0.92 \left(\ell_\beta f_R d_N / k\right) \left[\left(D^2/b\right) - D_\beta^2\right] \qquad \text{(A-11b)}$$

Note that theoretically C varies as the square of the cell diameter (for a fixed diameter of β''-alumina solid electrolyte, i.e., for a constant value of D). It is somewhat surprising, therefore, that the plot of C versus D depicted in Figure A-3 is essentially linear: A graph is shown in Figure A-3 for the capacity, C, of cells of various diameters (D); all cells contain a β'' -alumina tube, 3.35 cm in OD and 25 cm long. The cells are assumed to be filled to the same extent as the previously discussed model, i.e., $f_R = 0.735$ and $f_C = 0.66$. Linear regression analysis (LRA) of the data points of Figure A-2 results in a correlation whose coefficient of determination (r^2) is 0.9965. This means that less than 0.4 percent of the variance in the data is unaccounted for by the LRA -- a highly significant correlation.

(d) Internal Ohmic Resistance of Cells. Generally the internal resistance can be assumed to be mainly due to the cathode and to the β''-alumina. In other words, the resistance related to the passage of current through the sodium and its metal container is negligibly small compared to that due to the other components. Consequently,

$$R_i \simeq \frac{R_{M/F}}{S_o} + \frac{\rho_{gf}\,(D-D_\beta)}{2S_F} + \frac{R_{F/\beta}}{S_\beta} + \frac{\rho_\beta\, WD_\beta}{S_\beta} \qquad \text{(A-12)}$$

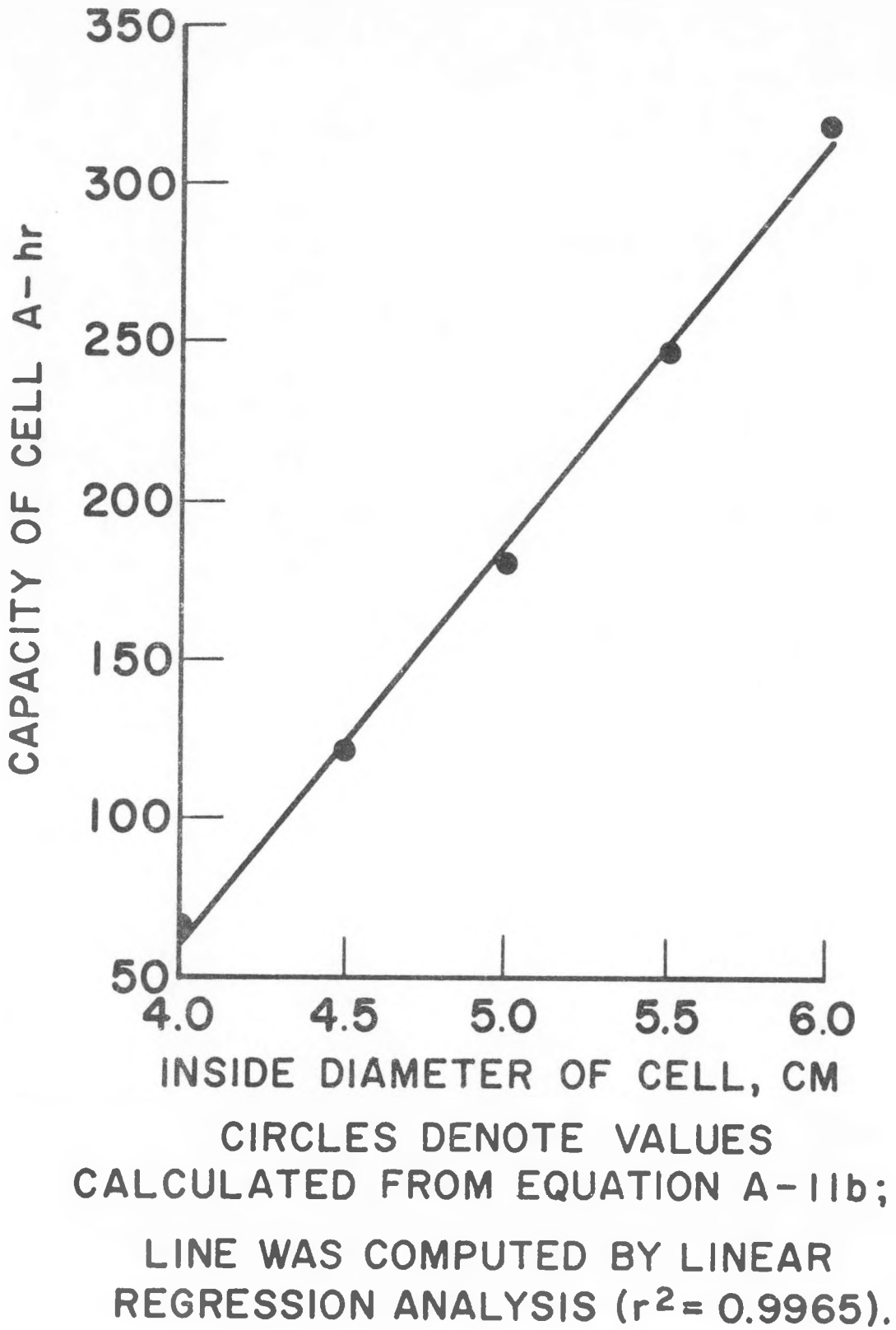

FIGURE A.3 - Capacity of Model Cells with 3.35-CM OD, 25-CM Long β"-Alumina Tubes

In Equation A-12, the symbols have the following meanings:

Symbol	Meaning
$R_{M/F}$	resistance due to contact between the graphite felt and metal container of the cathode
ρ_{gf}	resistivity of the graphite felt
$R_{F/\beta}$	resistance due to contact between the felt and β''-alumina
ρ_{β}	resistivity of β''-alumina
W	factor relating wall thickness of β''-alumina tube to its diameter, viz., $t = WD_{\beta}$
S_o	inner surface area of the metal container encapsulating the cathode
$\overline{S}_F$	the logarithmic mean surface area of the geometric envelopes encompassing the region of the cell occupied by the graphite felt; see Equation A-15 below.
S_{β}	the outer surface area of the β''-alumina tube

These symbols are defined further by the following equations:

$$S_o = \pi D \ell_{\beta}/b \qquad \text{(A-13)}$$

$$S_{\beta} = \pi D_{\beta} \ell_{\beta} \qquad \text{(A-14)}$$

$$S_F = (S_o - S_{\beta})/\ln (S_o/S_{\beta}) \qquad \text{(A-15a)}$$

$$= \pi \ell_{\beta} \left[(D/b) - D_{\beta}\right]/\ln \left(D/bD_{\beta}\right) \qquad \text{(A-15b)}$$

Substituting Equations A-13 through A-15 into Equation A-12 yields the expression:

$$R_i = \frac{1}{\pi \ell_{\beta}} \left\{ \rho_{\beta} W + \frac{R_{M/F}}{D/b} + \frac{R_{F/\beta}}{D_{\beta}} + \left(\rho_{gf}/2\right) \ln\left(D/bD_{\beta}\right) \frac{(D-D_{\beta})}{[(D/b) - D_{\beta}]} \right\} \qquad \text{(A-16)}$$

For a given cell, the IR drop in voltage, that is to say, the loss in potential due to internal ohmic resistance is

$$IR_i = iS_\beta R_i \qquad \text{(A-17a)}$$

$$= i\left\{R_{F/\beta} + D_\beta\left[(bR_{M/F}/D) + W\rho_\beta + \left(\rho_{gf}/2\right)\ln\left(D/bD_\beta\right)\frac{D-D_\beta}{[(D/b)-D_\beta]}\right]\right\} \qquad \text{(A-17b)}$$

Equations A-17a and A-17b indicate that the IR drop due to ohmic effects increases logarithmically with increasing cell diameter, D. Note also that it is independent of changes in the cell length.

APPENDIX B

ANALYSIS PERFORMED
TO SELECT PROPERTY DATA

Early in the program, a review was conducted to establish firm values for the physical properties and related parameters of cell reactants, products and components. These are required for analysis. Generally linear regression analysis (LRA) was performed to construct linear equations for the various parameters in the range of temperatures at which sodium-sulfur cells operate. These are particularly useful in mathematical modeling. Summaries of these analyses follow.

(a) Density of Cell Reactants and Products. Knowledge of the variation in density with temperature is essential for all reactants and products.

(1) Sodium. J. W. Mausteller, F. Tepper, and S. J. Rodgers, (Alkali Metal Handling and Systems Operating Techniques, Gordon and Breach, New York, Appendix 1, p. 218), recommend data of F. Tepper, J. Zelenak, F. Roehlich and V. May, ["Thermophysical and Transport Properties of Liquid Metals", Quarterly Progress Reports 1-3 of Contract AF33(615)-1273, MSA Research Corp., Callery, Pa. (1964)]: "The density of liquid sodium may be expressed by,

$$d\ (g/cm^3) = 0.9493 - 0.1245 \times 10^{-3}\ T\ (^oF)". \quad \text{(B-1)}$$

As $^oF = (9/5)\ (^oC) + 32$, it follows that

$$d\ (g/cm^3) = 0.9493 - (0.1245 \times 10^{-3})\ [(9/5)(^oC) + 32]$$

$$= 0.9453 - (2.241 \times 10^{-4})(T, ^oC) \quad \text{(B-2)}$$

Equation B-2 was adopted for determining the density of sodium in subsequent analysis reported herein. A comparison with other values from the literature is presented below:

Temperature, °C	Source	Density, d, g/cm³ Value Listed in Source	Value from Tepper's Equation
100	(1)	0.928	0.923
250		.891	.889
400		.854	.856
550		.817	.822
700		.780	.788
97.6	(2)	0.9287	.923
880		.7414	.748
200	(3)	0.903	.900
400		.854	.856
600		.805	.811

Sources: (1) R. N. Lyon, Liquid-Metals Handbook, 2nd Ed. (Revised), Jan. 1954, AEC-Navy NAVEXOS P-733 (Rev.). (2) R. E. Kirk and D. F. Othmer, Encyclopedia of Chemical Technology, Vol. 1, Interscience Encyclopedia, New York, p. 436; (3) C. F. Bonilla, Nuclear Engineering, McGraw-Hill, New York, 1957, App. B, p. 806.

(2) Sulfur. Data from two sources are presented below.

Temperature, °C	Density, d, g/cm³
120	1.805
140	1.793
160	1.773
180	1.768
200	1.755
250	1.727
300	1.697
350	1.667
400	1.637

Data at left from E. H. Conroy, "Sulfur," Article in Encyclopedia of the Chemical Elements," C. A. Hampel, Ed., Reinhold Book Corp., New York, 1968.

Linear Regression Analysis gives

$d\ (g/cm^3) = 1.8736-(5.9082 \times 10^{-4})T$

$r^2 = 0.9982$

Temperature, ^{o}F	Density, d, g/ml
314.4	1.7739
317.3	1.7729
321.8	1.7723
329.0	1.7714
340.3	1.7705
352.9	1.7671
363.2	1.7644
410.0	1.7509
463.1	1.7329
533.3	1.7096
674.6	1.6583
833.0	1.6060

Data at left are due to A. M. Kellas, J. Chem. Soc. 113, 903-922 (1918), cited by W. N. Tuller in The Sulphur Data Book, McGraw-Hill, New York, 1954, p. 17.

Linear regression analysis gives

$$d(g/ml) = 1.8806 - (3.2687 \times 10^{-4})(^{o}F)$$

$$r^2 = 0.9967$$

as $^{o}F = (9/5)(^{o}C) + 32$,

$$d(g/cm^3) = 1.8701 - (5.8836 \times 10^{-4})\ (^{o}C)$$

According to Conroy (op. cit.), the density in g/cm^3 at temperatures of the phase changes are as follows:

Liquid at freezing point (115.21°C)	1.808
Liquid at boiling point (444.6°C)	1.610

The expression $[1.87 - (5.9 \times 10^{-4})(^{o}C)]$ gives 1.802 and 1.608, respectively for these values.

For the purposes of subsequent analyses, the following equation was adopted:

$$d,\ g/cm^3 = 1.87 - (5.9 \times 10^{-4})\ (^{o}C) \qquad \text{(B-3)}$$

In reporting the results of linear regression analysis, in this report, the correlation coefficient is represented by r; and r^2 is the coefficient of determination. The latter coefficient is the fraction of the total variance accounted for by the linear regression analysis. In other words, there is less than one percent uncertainty

in the above correlations.

(3) Sodium Polysulfide. According to B. Cleaver and A. J. Davies, (Electrochimica Acta, 1973, Vol. 18, pp. 727-731), "plots of density against temperature were linear within experimental error. Values of D and E in the equation

$$\rho = D + E\,(T-600)$$

are presented (below):"

Melt	%S	Temperature Range - ^{o}K	Density, d, g/cm^3	10^4 E $g/cm^3/K$	Standard Deviation
Na_2S_3	67.6	590-683	1.887	-5.65	0.004
$Na_2S_{3.3}$	69.7	576-689	1.901	-7.96	.008
$Na_2S_{3.7}$	72.0	563-669	1.926	-5.47	.003
$Na_2S_{4.4}$	75.4	571-680	1.869	-6.66	.006
$Na_2S_{4.8}$	77.0	573-683	1.876	-7.16	.005

The value D above is the density at $327^{o}C$. Note that the variation in density with chemical composition is insignificant. If all of the data are treated as a group, the following linear equation can be obtained:

$$d,\ g/cm^3 = 2.1069 - \left(6.58 \times 10^{-4}\right)\left(^{o}C\right) \qquad \text{(B-4)}$$

Equation (B-4) was adopted for use in subsequent analysis.

Djong-Gie Oei also measured the density of Na_2S_4 and Na_2S_5. (See page 440, Inorg. Chem., Vol. 12 (No. 2), 1973.)

(b) Electrical Conductivity (Resistivity) of Cell Reactants, Products and Components. Values for conductivity or its reciprocal, resistivity, are needed for thermal analysis of the cell and its current collectors (and bus bars). The literature sources which were examined and the values selected for this program are summarized in following subsections.

(1) Sodium. The following data are from the Liquid-Metals Handbook, Second Edition (Revised); R. N. Lyon, editor-in-chief; AEC-Navy NAVEXOS-P-733, (Rev.), p. 43:

Temperature, °C	Electrical Resistivity, ρ, ohm cm
100	9.65×10^{-6}
200	13.18×10^{-6}
250	14.90×10^{-6}
300	16.70×10^{-6}
350	18.44×10^{-6}

LRA of the above data yields the following equation:

$\hat{\rho} = 6.13 + 0.035\ (°C)$, in $\mu\Omega$ cm; $\quad r^2 = 0.99998$

Kirk and Othmer (Ed., Encyclopedia of Chemical Technology, Vol. I, p. 436) cite the following data:

Temperature, °C	Electrical Conductivity, $ohm^{-1}/cm \times 10^4$	Electrical Resistivity, ohm cm
100	10.204	9.80×10^{-6}
250	6.7113	14.90×10^{-6}

C. C. Addison, G. K. Creffield, P. Hubberstey, and R. J. Pulham (J. Chem. Soc. (A) 1969, pp. 1482-1487) give the following equation:

$$\rho_L\ (\mu\Omega cm) = a + bT + CT^2 + dT^3 - eT^4$$

where T is in °C; $a = 6.87$; $b = 2.44 \times 10^{-2}$; $c = 2.67 \times 10^{-5}$; $d = 1.07 \times 10^{-7}$; and $e = 2.67 \times 10^{-10}$.

Temperature, °C	Resistivity, ρ, ohm cm according to Addison et al.
100	9.66×10^{-6}
200	13.25×10^{-6}
250	15.27×10^{-6}
300	17.32×10^{-6}
350	19.26×10^{-6}

J. W. Mausteller, F. Tepper and S. J. Rodgers (Alkali Metals Handling and Systems Operating Techniques, AEC Monograph, Gordon and Breach, New York, 1967, Appendix I, p 220) cite data of F. Roehlich:

$$\rho(\text{Na}) = 2.1729 + 7.6248 \times 10^{-3} T + 5.8313 \times 10^{-7} T^2 + 1.1260 \times 10^{-9} T^3$$

which is good from melting point to 2000°F; and T is in °F and ρ is in μ Ω in.

Temperature °F	Temperature °C	Resistivity, ρ, ohm in.	Resistivity, ρ, ohm cm
212	100	3.83×10^{-6}	9.72×10^{-6}
392	200	5.32×10^{-6}	13.51×10^{-6}
482	250	6.11×10^{-6}	15.52×10^{-6}
572	300	6.94×10^{-6}	17.62×10^{-6}
662	350	7.80×10^{-6}	19.82×10^{-6}

A comparison of data from the different sources follows.

Temperature, °C	Resistivity, ρ, (Ωcm)x10^6 Lyon	Addison et al.	Roehlich	$\hat{\rho}$
100	9.65	9.66	9.72	9.60
200	13.18	13.25	13.51	13.40
250	14.90	15.27	15.52	15.30
300	16.70	17.32	17.62	17.20
350	18.44	19.26	19.82	19.10

If all data are treated as a group, LRA yields

$$\rho = 5.7955 + 0.038\ T\ (^{o}C),\ \mu\Omega cm;\ r^2 = 0.989_3 \qquad (B\text{-}5)$$

Equation B-5 was selected for use in subsequent analysis. "Rho hat" ($\hat{\rho}$) indicates the value of ρ predicted by LRA.

(2) Sulfur. According to Conroy (op. cit.), the electrical conductivity of liquid sulfur is as follows:

Temperature, ^{o}C	Conductivity, σ, $(ohm\ cm)^{-1}$	Resistivity, ρ, ohm cm
231	2.2×10^{-12}	4.55×10^{11}
360	79×10^{-12}	1.27×10^{10}

Kirk & Othmer (op. cit.) give the values:

^{o}C	
440	8.3×10^{6} ohm (sq cm)/cm

Tuller (op. cit.) cites data from the International Critical Tables:

Temperature, ^{o}F	Temperature, ^{o}C	Resistivity, ρ, ohm cm
239	115	9.5×10^{11}
266	130	2.0×10^{10}
572	300	2.8×10^{8}
824	440	7.7×10^{6}

Plots of conductivity (or resistivity) vs. temperature (or reciprocal temperature) have been published by several investigators. For example, see G. C. Vezzoli, J. Am. Ceramic Soc., Vol. 55, No. 2, Feb. 1972, pp. 65-67; R. K. Steunenberg, C. Trapp, R. M. Yonco and E. J. Cairns, Advan. Chem. Ser., No. 110 (1972), pp. 190-200; and B. Cleaver et al., Electrochimica Acta 1973, Vol. 18, pp. 719-726.

Cleaver et al. (op. cit.) found that the electrical conductivity of liquid sulfur saturated with polysulfide (Na_2S_5) was about one million ($\sim 1 \times 10^{6}$) times

lower than that of polysulfide but somewhat greater than that of pure liquid sulfur. The electrical conductivity of polysulfide-saturated sulfur varied with temperature in a true Arrhenius manner whereas neither that of pure sulfur nor that of polysulfide did. From the data of Cleaver et al., the following equation can be constructed for σ, the electrical conductivity of polysulfide-saturated sulfur:

$$\hat{\sigma} = 3.13 \exp [-10,611.8/T], \qquad \text{(B-6)}$$

where $\hat{\sigma}$ is the predicted conductivity in reciprocal ohm cm; and T is the absolute temperature in ^{o}K.

A short table of values of the electrical resistivity of polysulfide-saturated liquid sulfur (as determined from Equation B-6 is presented below:

σ, $(\text{ohm cm})^{-1}$*	$10^3/T$ $^{o}K^{-1}$	T, ^{o}C	ρ, ohm cm	σ $(\text{ohm cm})^{-1}$
6.4×10^{-7}	1.45	416	1.56×10^{6}	6.5×10^{-7}
5.5×10^{-7}	1.475	405	1.82×10^{6}	5.0×10^{-7}
1.6×10^{-7}	1.562	367	6.25×10^{6}	2.0×10^{-7}
1.0×10^{-7}	1.6	352	1.0×10^{7}	1.3×10^{-7}
9×10^{-8}	1.62	344	1.11×10^{7}	1.1×10^{-7}
8.3×10^{-8}	1.635	338	1.20×10^{7}	9.1×10^{-8}
7×10^{-8}	1.66	329	1.43×10^{7}	7×10^{-8}
3.2×10^{-8}	1.735	303	3.13×10^{7}	3.2×10^{-8}

*Read from Cleaver's plot.

(3) Sodium Polysulfide. An extensive investigation has been conducted by B. Cleaver, A. J. Davies, and M. D. Hames. (See Electrochimica Acta 1973, Vol. 18, pp 719-726.) They found that the conductivity of a particular composition varied with temperature according to an equation of the type: $\sigma = A \exp [-E/R(T-T_o)]$. The electrical conductivity of Na_2S_3 was approximately twice that of Na_2S_5.

Multiple regression analysis of data from Cleaver et al for the temperature range, 300-400°C, and the composition range, 66.1 to 77.8% S ($Na_2S_{2.9}$ to $Na_2S_{5.1}$) yields the equation:

$$\hat{\sigma} = 1.1848 - 0.0311\ (\%S) + 0.0046\ (^{o}C); \qquad (B\text{-}7)$$

$\hat{\sigma}$ in $(ohm\text{-}cm)^{-1}$; $100\ R^2 = 98\%$

The coefficient of multiple determination, R^2, indicates that only two percent of the total variance in the data is unaccounted for by the analysis. The input data for the multiple regression analysis is tabulated in Table B-1.

TABLE B-1. ELECTRICAL CONDUCTIVITY OF SODIUM POLYSULFIDE MELTS*

Temperature, °C	Electrical Conductivity, $(ohm\ cm)^{-1}$					
	$Na_2S_{2.9}$	$Na_2S_{3.0}$	$Na_2S_{3.2}$	$Na_2S_{3.8}$	$Na_2S_{4.2}$	$Na_2S_{5.1}$
	Percent Sulfur					
	66.1	67.5	70.1	72.3	74.8	77.8
300	0.2873	0.4250	0.3887	0.3111	0.2572	0.2093
320	.4217	.5256	.4846	.3927	.3314	.2734
325	.4563	.5516	.5094	.4141	.3509	.2904
340	.5607	.6310	.5855	.4800	.4114	.3432
350	.6301	.6849	.6374	.5253	.4532	.3798
360	.6986	.7394	.6900	.5715	.4959	.4174
375	.7991	.8221	.7699	.6423	.5614	.4754
380	.8319	.8498	.7968	.6662	.5835	.4950
400	.9590	.9609	.9048	.7629	.6733	.5750

*From Cleaver et al., (op. cit.)

(4) β″-Alumina. A. V. Virkar, G. R. Miller and R. S. Gordon (Department of Materials Science and Engineering, University of Utah, Report UTEC-MSE 76-193, July 1976) provide a graph displaying the effect of temperature on the electrical resistivity of polycrystalline β″-alumina. (Specimens contained, in weight percent, 8.8 Na_2O, 0.75 Li_2O, and 90.45 Al_2O_3, and were sintered at 1600°C for 2 hours.) Table B-2 summarizes the linear regression analysis of the University of Utah data.

(5) Metallic Electrical Conductors. Data were compiled for three pure metals - - copper, aluminum and nickel - - and for ferritic stainless steel. Linear regression analysis (LRA) was performed to obtain a linear equation suitable for modeling. In addition to the referenced cited in the following paragraphs, the Handbook of Thermophysical Properties of Solid Materials (Rev. Ed., Vol. I: Elements, Macmillan Co., New York, 1961) contains graphical compilations of the electrical resistivity of pure copper, aluminum and nickel as determined by a number of investigators.

Pure Copper. The Handbook of Chemistry and Physics, 38th Edition (1956), page 236, lists the following values:

Resistivity of Pure Annealed Copper

Temperature, °C	ρ, ohm cm x 10^6	Source
20	1.692	Wolff, Dellinger, 1910
100	2.28	Northrup, 1914
200	2.96	"
500	5.08	"
1000	9.42	"
1500	24.62	"

Linear regression analysis of the first three data points

TABLE B-2

SUMMARY OF LINEAR REGRESSION ANALYSIS OF DATA

FOR ELECTRICAL RESISTIVITY OF β″-ALUMINA SOLID ELECTROLYTE

$\ln\left[\rho\left(10^3/T\right)\right]$	ρ	^oC	n=19		n=18	
			$\hat{\rho}$	Δ%	$\hat{\rho}$	Δ%
2.32	5.67	284	5.22	-7.9	--	
2.22	5.19	290	5.07	-2.3	4.97	-4.2
2.16	4.93	295	4.95	0.4	4.86	-1.4
2.12	4.77	300	4.82	1.0	4.74	-0.6
2.08	4.63	305	4.70	1.5	4.62	-0.2
2.04	4.48	310	4.57	2.0	4.51	0.7
2.00	4.35	315	4.45	2.3	4.39	0.9
1.96	4.21	320	4.32	2.6	4.27	1.4
1.92	4.07	324	4.22	3.7	4.18	2.7
1.88	3.95	329	4.10	3.8	4.07	3.0
1.84	3.83	335	3.95	3.1	3.93	2.6
1.81	3.75	340	3.82	1.9	3.81	1.6
1.77	3.62	344	3.72	2.8	3.72	2.8
1.73	3.51	350	3.57	1.7	3.58	2.0
1.70	3.44	356	3.42	-0.6	3.44	0.0
1.68	3.40	360	3.32	-2.4	3.34	-1.8
1.64	3.28	364	3.22	-1.8	3.25	-0.9
1.61	3.22	370	3.07	-4.7	3.11	-3.4
1.59	3.17	374	2.97	-6.3	3.02	-4.7

LRA of all entries (n=19): $\hat{\rho} = 12.33 - (0.03)\ (^oC)$; $r^2 = 0.96$

LRA of all but the first entry (n=18): $\hat{\rho} = 11.71 - 0.0232(^oC)$; $r^2 = 0.98$

gives $r^2 = 0.9995$; extrapolation gives $\rho = 4.0224$ at $350^{o}C$.

LRA of first four data points gives $r^2 = 0.99994$; interpolation gives $\rho = 4.023_8$ at $350^{o}C$; the equation is

$$\hat{\rho} = 0.00704\ (^{\circ}C) + 1.5598 \qquad \text{(B-8)}$$

A comparison of the experimental resistivity values with the predicted values is shown below.

Temperature, ^{o}C	ρ	$\hat{\rho}$	$\Delta\% = \frac{\hat{\rho}-\rho}{\rho}$ (100%)
20	1.692	1.700_6	0.5
100	2.28	2.263_8	-0.7
200	2.96	2.967_8	0.3
500	5.08	5.079_8	-0.004
1000	9.42	8.599_7	-8.7

In subsequent analysis, Equation B-8 was used to estimate the electrical resistivity of copper bus bars.

Pure Aluminum. T. E. Pochapsky (Acta Metallurgia, Vol. 1, Nov. 1953, pp. 747-751) determined the ratio, R/R_o, for pure aluminum to be as shown below. He also offers a favorable comparison of his data with that of Holborn (from the Landolt-Bornstein Tables).

Temperature, ^{o}C	R/R_o	
	Pochapsky	Holborn
0	1.000	1.000
100	1.448	1.442
200	1.911	1.890
300	2.400	2.346

Linear regression analysis of Pochapsky's data yields the equation:

$$\left(R/R_o\right) = 0.00466_3\ (^oC) + 0.9903_o \qquad \text{(B-9)}$$

K. R. Van Horn (in his treatise, Aluminum, Vol. I, p. 9, Am. Soc. for Metals, Cleveland, Ohio, 1967, p. 9) cites three values for the electrical resistivity of aluminum at 20^oC: 2.6548, 2.6434 and 2.6484 x 10^{-6} ohm cm. The mean of the three is 2.6488_{67} x 10^{-6} ohm cm. From Equation B-9, $\left(R/R_o\right)_{20^oC} = 1.08356_0$. Consequently, $R_o = R_{20^oC} / 1.08356 = 2.444596 \times 10^{-6}$ ohm cm. Combining this value of R_o with the linear regression analysis (Equation B-9) yields the expression:

$$\hat{R} = \left(1.3992 \times 10^{-8}\right)\left(^oC\right) + \left(2.4209 \times 10^{-6}\right) \qquad \text{(B-10)}$$

According to Van Horn (op. cit.), Willey found that the temperature coefficient for the electrical conductivity of pure aluminum was 1.15 x 10^{-8}, which agrees with the value 1.14 x 10^{-8} of Equation B-10.

Values for the electrical resistivity as determined by Equation B-10 are compared below with other data from Van Horn (op. cit.) which also apparently are due to Willey.

Temperature, ^oC	Resistivity, ohm cm	
	Equation B-10 Values	Values cited by Horn
350	$6.410_6 \times 10^{-6}$	
300	$5.840_6 \times 10^{-6}$	5.81×10^{-6}
250	$5.270_7 \times 10^{-6}$	
200	$4.700_7 \times 10^{-6}$	4.62×10^{-6}
150	$4.130_8 \times 10^{-6}$	
100	$3.560_8 \times 10^{-6}$	3.50×10^{-6}
50	$2.990_8 \times 10^{-6}$	
0	$2.420_9 \times 10^{-6}$	2.42×10^{-6}

These values were used in subsequent analysis to size

aluminum bus bars for submodules.

Pure Nickel. The American Institute of Physics Handbook (Second Edition, McGraw-Hill Book Co., New York, 1963, pp. 4-13) lists the following data:

Temperature, ^{o}C	Resistivity ρ, ohm cm
0	6.38×10^{-6}
100	10.61×10^{-6}
200	15.96×10^{-6}
300	23.04×10^{-6}

LRA yields the equation:

$$\hat{\rho} = (0.05533)\ (^{o}C) + 5.6980; \qquad \text{(B-11)}$$

$$r^2 = 0.9868$$

Extrapolation of Equation B-11 to $350^{o}C$ gives $\hat{\rho} = 25.06_4 \times 10^{-6}$ ohm cm.

The Handbook of Thermophysical Properties of Solid Materials (Rev. Ed., Vol. I, Macmillan Co., New York, p. I-N-3) presents a graph of electrical resistivity versus temperature. The plot shows a value of $\rho \simeq 30 \times 10^{-6}$ ohm cm at about 625 ^{o}K ($352^{o}C$). It also indicates an abrupt change in the slope of the trend line just above $350^{o}C$ due to the magnetic transformation. (The Curie point for nickel is $353^{o}C$.)

Ferritic Stainless Steel (Type 446). A "blue sheet" issued by Allegheny Ludlum Steel Corporation cites the following data:

Temperature, ^{o}C	Resistivity, p, ohm cm
20	67×10^{-6}
100	74×10^{-6}
200	83×10^{-6}
400	98×10^{-6}

LRA yields the equation:

$$\hat{\rho} = (0.08144)\ (^{o}C) + 65.84158; \qquad \text{(B-12)}$$

$$r^2 = 0.9978$$

Equation B-12 yields $\hat{\rho} = 94.344 \times 10^{-6}$ ohm cm at 350°C.

(c) Thermal Conductivity.

(1) Sodium. The Liquid-Metals Handbook, Second Edition (Revised) (R. N. Lyon, editor-in-chief; AEC-Navy NAVEXOS-P-733 (Rev.), p. 43) lists the values:

Temperature, °C	Thermal Conductivity, cal/sec·cm·°C.
100	0.2055
200	.1947
300	.1809
400	.1701
500	.1596

LRA yields the equation:

$$\hat{K} = 0.2171 - 0.0001\ (^{o}C); \qquad \text{(B-13)}$$

$$r^2 = 0.9977$$

The Encyclopedia of Chemical Technology (Kirk & Othmer, Ed.; Vol. I, p. 436) gives the thermal conductivity of solid sodium:

Temperature, °C	Thermal Conductivity, $cal/sec \cdot cm^2/^{o}C \cdot cm$
-100	0.305
0	.335
75	.270

(2) Sulfur, Sodium Polysulfide and Sulfur-Graphite Composites. E. H. Conroy (Encyclopedia of the Chemical Elements, C. Hampel, Ed., Reinhold Book Co., New York, 1968, p. 673) gives the equation:

$K\ (cal/cm \cdot sec \cdot {}^{o}C) = 3.06 \times 10^{-4} + 0.69 \times 10^{-6}\ (t-119)$

where t is in ^{o}C and the equation holds over the range of temperature, 119 to 159^{o}C.

Tuller (in Sulphur Data Book) cites work of G.W.C. Kaye and W. F. Higgins [Proc. Roy. Soc. (London) A12 (1929), pp. 633-646] which is copied below:

Temperature		Thermal Conductivity, K, cal/cm·sec·^{o}C	
^{o}F	^{o}C	Kaye	Conroy
239	115	3.142×10^{-4}	3.032×10^{-4}
260	127	3.183	3.115
280	138	3.224	3.191
300	149	3.266	3.267
320	160	3.348	3.343
329	165	3.348	3.377
340	171	3.431	3.419
360	182	3.514	3.495
380	193	3.638	3.571

Note: These may well be from the same source and the apparent differences may actually be due to rounding errors in converting from degrees Fahrenheit to degrees Centigrade. (Conroy cites Tuller but not Kaye.)

Extrapolation of Conroy's equation yields the following values:

Temperature, ^{o}C	Thermal Conductivity cal/cm·sec·^{o}C
300	4.309×10^{-4}
350	4.654
400	5.000

J. W. Cooke [Proceedings of the 6th Conference on Thermal Conductivity, October 19-21, 1966, Dayton, Ohio

(sponsored by Air Force Naterials Laboratory), pp 15-27] recommends the method due to M. R. Rao [Indian J. Physics, 16 (1942), p. 20] for estimation of the thermal conductivity of molten salts. Applied to Na_2S_4, the method yields the value $K \geq 9 \times 10^{-4}$ cal/cm sec ^{o}C or 3.75×10^{-3} W/cm·^{o}K, which is nearly the same value Dynatech R/D Co. obtained for sulfur-and polysulfide-filled graphite composites supplied by GE. (See EPRI Report EM-266 Dec. 1976, pp. B-13 and B-15.)

(3) β''-Alumina. Measurements are in progress at the University of Utah. Preliminary measurements at Ford (Dearborn) yield the value, 0.02 W/cm.^{o}C.

(4) Copper. The following values are from Table 4g-8, p. 4-90, American Institute of Physics Handbook, Second Edition, McGraw-Hill Book Co., New York, 1963

^{o}K	^{o}C	K, w/cm.^{o}K
273	0	4.0
373	100	3.8
573	300	3.8
973	700	3.5

These values are from the Handbook of Chemistry and Physics, 38th Ed., 1956, p. 225.

Temperature ^{o}C	cal/sec/cm^2/cm	w/cm^{o}C	
18	0.918	3.84	Jaeger & Dieselhorst,
100	.908	3.80	1900
100 - 197	1.043	4.36	
100 - 268	0.969	4.06	Hering, 1910
100 - 370	.931	3.90	

These values are from Table 3-294, p. 3-220 Chemical Engineers Handbook, Fifth Edition, McGraw-Hill Book Co., 1973.

Temperature, ^{o}C	Btu/hr/ft^2/^{o}F/ft	w/cm ^{o}C
0	224	3.88
100	218	3.77
200	215	3.72
300	212	3.67
400	210	3.64
500	207	3.58
600	204	3.53

Linear Regression Analysis (LRA) of data from the Chemical Engineers' Handbook yields the following:

Temperature, ^{o}C	K	$\hat{K}$	$\% = \left(\frac{\hat{K} - K}{K}\right) 100\%$
100	3.77	3.76_8	-0.05
200	3.72	3.72_2	0.05
300	3.67	3.67_6	0.16
400	3.64	3.63_0	-0.28
500	3.58	3.58_4	0.11

$$\hat{K} = 3.814 - (4.6 \times 10^{-4})(^{o}C) \qquad \text{(B-14)}$$

$$r^2 = 0.992$$

Temperature, °C	$\hat{K}$, w/cm °C
350	3.65_3
300	3.67_6
250	3.699
200	3.72_2
150	3.74_5
100	3.76_8
50	3.79_1
0	3.81_4

(5) Aluminum. K. R. Van Horn (Aluminum, Vol. I, Am. Soc. Metals, Metals Park, Ohio, p. 9) lists four equations for determining variation in thermal conductivity of aluminum with temperature. The mean of the first three equations cited by Van Horn yields the formula:

$$K, \text{cal/cm}^2\text{/sec/cm/}^\circ\text{C} = \left[\frac{4.99 \times 10^{-9}}{\rho}\right](273 + {}^\circ\text{C}) + 0.035$$

where ρ is the corresponding electrical resistivity in ohm cm

Suppose we use equation B-10 for ρ then

$$K = \frac{4.99 \times 10^{-9}\ (273 + {}^\circ\text{C})}{(1.14 \times 10^{-8})({}^\circ\text{C}) + 2.42 \times 10^{-6}} + 0.035 \qquad \text{(B-15)}$$

	K, $cal/cm^2/sec/cm/^oC$	
^oC	Equ 72-1	Values cited by Van Horn*
350	0.52	
300	.52	
250	.53	
200	.54	0.54
150	.55	
100	.56	0.56
50	.57	
0	.60	

(6) Nickel. The following values are from M. Jakob and G. A. Hawkins, Elements of Heat Transfer, 3rd Ed., Table II-8, p. 20:

	B hr^{-1} ft^{-1} F^{-1}		
% Impurities	32°F	392°F	752°F
0.1		42	34
1.0	35	34	34

These values are from a Huntington Alloys' brochure:

Nickel 200

70°F	520 Btu/ft^2hr in. °F	0.75 w/cm °C
1500°F	440	.63

Nickel 201

70°F	550 Btu/ft^2hr in. °F	0.79 w/cm °C
1500°F	450	.65

---

* Computed from mean of the four equations cited by Van Horn. The mean over the range, 50 to 350°C, is 0.55 cal/sec·cm·°C. To convert cal/sec to watts multiply by 4.185; hence $\overline{K} = 2.289_4$ w/(cm)(°C)

The following value is from Alloy Digest, Oct 1962, N.-75, for nickel 200:

thermal conductivity (27-100°C),
0.145 cal/sec cm °C or 0.607 w/(cm)(°C)

These values are from INCO Tech. Bull. T-15 (July 1949)

Temperature	cal/cm^2/sec/°C/cm	w/(cm)(°C)
27° - 100°C	0.145	0.607 w/(cm)(°C)
100°C	0.155	.649
200°C	0.139	.582
300°C	0.122	.511
400°C	0.112	.469
500°C	0.122	.511
600°C	0.136	.569

LRA of 100°, 200° and 300°C data points yields

$r^2 = 0.9997$; $\hat{K} = 0.71867 - (0.00069)(^{\circ}C)$ (B-16)

$\hat{K} = 0.477_{17}$ w/(cm)(°C) @ 350°C

Predicted thermal conductivity (based on Linear Regression Analysis, LRA, of INCO data, Equation B-16)

Temperature °C	$\hat{K}$, w/(cm)(°C)
350	0.47717
300	.51167
250	.54617
200	.58067
150	.61517
100	.64967
50	.68417

(d) Other Property Data Pertinent for Metals and Alloys. Mechanical property values for ferritic stainless steel -- Type 446 and the related E-Brite 26-1 -- were taken from the previously cited brochure from Allegheny Ludlum for Type 446 stainless steel and from I. A. Franson's article, "Mechanical Properties of High Purity Fe-26 Cr-1 Mo Ferritic Stainless Steel", (Metallurgical Transactions, Vol. 5, Nov. 1974, pp. 2257-2264) and Alloy Digest, Dec. 1972, for E-Brite 26-1.

APPENDIX C

STRUCTURAL ANALYSIS
PERTAINING TO
INTERNAL CELL PRESSURE
AND METALLIC CONTAINERS

The Mark-I load-leveling cell is designed purposely to provide margins of safety in the event of inadvertent escalations in cell temperature. In this Appendix, analyses are presented to ascertain the magnitude of the internal cell pressures arising from plausible events. An estimate also is included for the service life of metallic containers.

(a) Estimated Internal Pressures within the Cells. Owing to the cyclic transfer of sodium through the β"-alumina solid electrolyte, extensive changes in volumes of reactants and products occur within the electrode compartments during normal operation of the cell. In the following paragraphs, the magnitude of these changes is determined for the Mark-I cell and translated into an estimate of the extent of the excursion in internal pressure a cell experiences.

(1) Capacity of the Sulfur Container. The following estimate is for the "sunk" container option of the Mark-I cell.

Interior of the E-Brite Container - -

Height	26.04 cm	
ID	4.70 cm	
Volume		451.78 cm^3
Volume displaced by the β"-alumina tube		220.35 cm^3
Capacity for electrode materials		231.43 cm^3

Prior to filling the container with sulfur, approximately 52 washer-shaped pads of Union Carbide WDF

graphite felt are inserted. Each pad is about 5 mm thick; the OD is 4.73 cm and the ID is 3.3 cm. There are 24 3-mm diameter holes in each pad; consequently, the volume of a felt pad is as follows:

Overall volume of a graphite felt washer - -

$$(\pi/4)\left[(4.73)^2 - (3.3)^2\right](0.5) = 4.51\ cm^3$$

Volume of 24 3-mm diameter holes - -

$$24\left[(\pi/4)\ (0.3)^2\ (0.5)\right] = \underline{0.85}$$

$$\text{Geometric volume of felt pad} = 3.66\ cm^3$$

The apparent density of the felt is $0.085 g/cm^3$, whereas the true density of graphite is $2.22 g/cm^3$. Consequently, the volume displaced by wetted graphite is as follows:

$$\frac{(52\ pads)(3.66 cm^3/pad)(0.085 g\ C/cm^3)}{2.22 g\ C/cm^3} = 7.29\ cm^3$$

The capacity of the electrode for polysulfide (and/or sulfur) therefore is

$$231.43 - 7.29 = 224.14\ cm^3$$

If a cell is discharged completely, it may form a polysulfide whose chemical composition corresponds to the chemical formula $Na_2S_{2.7}$. Generally it is the practice in assembling cells to fill the sulfur container with only enough elemental sulfur to result in a fully discharged cell whose sulfur compartment is 90 percent occupied by $Na_2S_{2.7}$ (and graphite). From Appendix B, Equation B-2, one can calculate that the density of $Na_2S_{2.7}$ is $1.877 g/cm^3$ at 350^oC; and from Appendix B, Equation B-3, that the density of sulfur is $1.664\ g/cm^3$ at 350^oC. It follows that a Mark-I load-leveling cell

with a "sunk" E-Brite container) should be filled with the following mass of sulfur:

$$\left(224.14\ cm^3\right)\left(1.877g\ Na_2S_{2.7}/cm^3\right)\left(0.9\right)\left(2.7S/Na_2S_{2.7}\right)$$

$$= 247.1g\ S$$

If a Mark-I load-leveling cell is filled with the above mass of sulfur, then at 350°C the sulfur container is

$$\left[\frac{247.1g\ S}{1.644gS/cm^3} \Big/ 224.14\ cm^3\right] \quad 100\%$$

$$= 66\% \text{ filled.}$$

If the sulfur compartment of a Mark-I cell were filled with more than 279 g sulfur (75% filled) and discharged to form $Na_2S_{2.7}$, more polysulfide is formed (>101%) than the container can hold (at 350°C). Early in Phase II, a Mark-I load-leveling cell inadvertently was filled with about 280 g sulfur. When it was discharged, the pressure exerted by the expanding mass of polysulfide caused the β″-alumina tube to crack and the hermetic seal to rupture.

Suppose that the temperature of a fully discharged cell inadvertently exceeded its normal operating temperature (possibly due to overheating caused by an adjacent failed cell). At 350°C, the sulfur compartment normally would be 90% filled (at complete discharge) and contain 378.64 g $Na_2S_{2.7}$. The volumetric capacity is 224.14 cm^3; consequently, from Equation B-2 (in Appendix B), one can calculate the bursting temperature, that is to say, the temperature at which the expanding polysulfide exceeds the capacity of the cell:

$$378.64\ g = 224.14\ cm^3 \left[2.1069 - \left(6.58 \times 10^{-4}\right)T\right]$$

$$T = \frac{472.24 - 378.64}{0.15} \approx 635°C$$

In other words, there is a margin of safety of nearly 300 centigrade degrees.

(2) Capacity of the Sodium Container. The following estimate is for the "sunk" E-Brite 26-1 container option of the Mark-I cell. The Mark-I load-leveling cell is constructed to contain sufficient sodium in the anode reservoir (the cylindrical sodium container located above the β"-alumina tube) to form $Na_2S_{2.6}$ of all sulfur in the cell. In other words, it deviates from our model in that the reactants are stored in the ratio 2.6 S : 2 Na, instead of the normal ratio 3 S:2 Na. There are practical reasons for this deviation: As the Mark-I load-leveling cell is a beginning prototype, it is intended to evaluate it over a wide range of temperatures and current densities. The cell is designed to operate at temperatures as great as 375°C and at current densities as great as 500 mA/cm^2. At these extreme conditions,extra sodium is needed. At extreme temperatures, it is needed because more sodium can react with the sulfur and form a polysulfide richer in sodium. (At lower temperatures, these polysulfides would be solids.) At extreme current densities (rapid rates of discharge), additional sodium is needed to assure an adequate hydrostatic head so that the flow of sodium from the safety tube (into the annular region) is sufficient to keep up with the electrochemical reaction. (See Appendix E.)

As discussed in the preceding section, the cell generally contains 247 g sulfur; consequently the sodium reservoir should contain (at 350°C):

$$\frac{2\ (23\text{g/g atom Na}\ (247\ \text{g S})}{2.6\ (32\text{g/g atom S})} = 136.56\ \text{g Na}$$

With its end cap in place the height of the sodium container is about 13.4 cm and its ID is 4.7 cm; therefore the volume is 232.48 cm^3. From Equation B-2 in Appendix B, one can calculate that the density of sodium at 350°C is 0.867 g/cm^3. It follows that when fully charged, the reservoir is

$$\frac{(136.56 \text{ g Na}) \ (100\%)}{(0.867 \text{ g Na/cm}^3) \ (232.48 \text{ cm}^3)} = 67.8\% \text{ filled}$$

The nominal dimensions of a Mark-I load-leveling cell are such that within the sulfur container the relative heights of the components forming the sodium electrode are as depicted in Figure C-1.

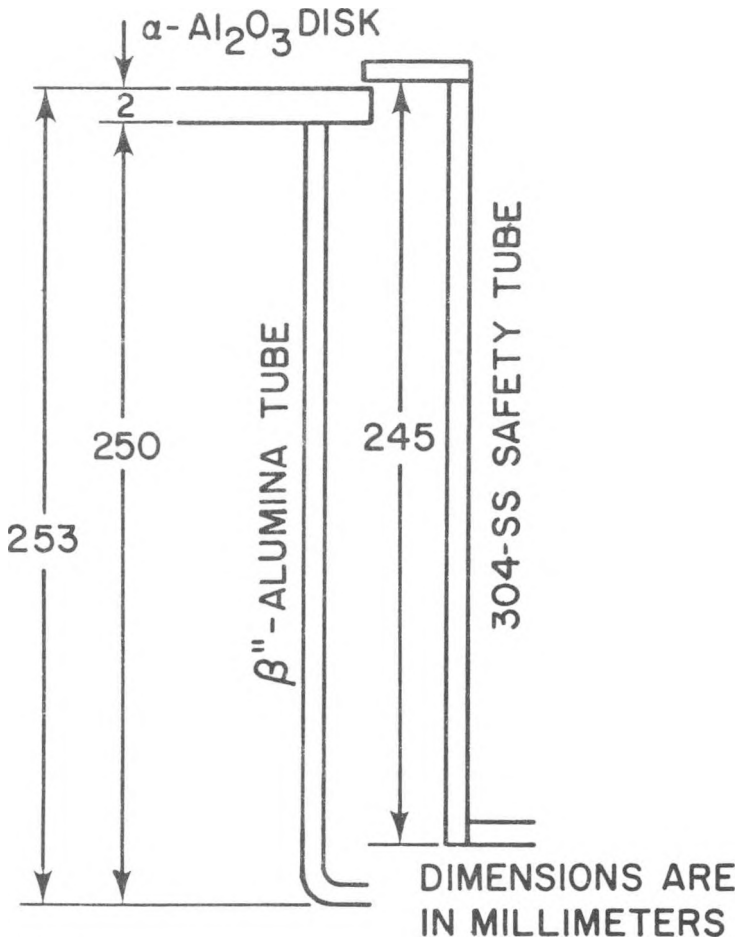

FIGURE C.1 - Sketch showing Relative Locations of Ceramic Components and Safety Tube

Let the length of the two ceramic components be $\ell_{\alpha\beta}$ (at 350°C); and the length of the safety tube (at 350°C) be ℓ_{ST}. Then

$$\ell_{\alpha\beta} = (253-2.5)\left[1 + \left(8 \times 10^{-6}\right)(350-20)\right]$$

$$= 250.5\ (1.0026)$$

$$= 251.16 \text{ mm}$$

and

$$\ell_{ST} = 245\left[1 + \left(17.8 \times 10^{-6}\right)(350-20)\right]$$

$$= 245\ (1.0059)$$

$$= 246.44 \text{ mm.}$$

The nominal clearance at the bottom of the safety tube is then 251.16 - 246.44 = 4.7 mm. Likewise, for the diameters,

$$D_{\beta} = [3.35 - 2\ (0.25)]\ [1 + (8 \times 10^{-6})\ (350-20)]$$

$$= 2.86 \text{ cm}$$

$$D_{ST} = 2.54\ [1 + (17.8 \times 10^{-6})\ (350-20)]$$

$$= 2.55 \text{ cm}$$

$$\Delta D = 3.026 \text{ mm}$$

Clearance: 1.5 mm

The University of Utah presently is required to bond the α-alumina disk to the β″-alumina tube so that the linear displacement from perpendicularity does not exceed 0.3 degree. As (250 mm)(sin 0.3) = 1.3 mm, this is a very tight tolerance (imposed for safety). The capacity of the annular region between the safety tube and the β″-alumina tube is as follows:

$$\text{Vol}_{350} = (\pi/4)\left[(2.8575)^2\ (25.116) - (2.5549)^2\ (24.644)\right]$$

$$= 34.7 \text{ cm}^3$$

$$\text{Mass}_{350} = \left(0.867 \text{g/cm}^3\right)\left(34.7_3 \text{cm}^3\right) = 30.1 \text{ gram}$$

Likewise, the capacity of the safety tube is the following:

$$V_{350} = \left[1 + 3\left(17.8\times10^{-6}\right)\left(325\right)\right](\pi/4)\left[2.54-2(0.028)(2.54)\right]^2$$
$$\left[24.5-(0.06)(2.54)\right]$$
$$= (1.017)(109.94) = 111.85 \text{ cm}^3$$
$$\text{Mass}_{350} = (0.867\text{g/cm}^3)(111.85 \text{ cm}^3) = 96.77 \text{ g Na}$$

It follows that in a fully charged cell (at 350°C) the distribution of sodium is as follows:

	Location	Mass, g Na	Percent of Total
1.	Anode Reservoir	136.56	51.80
2.	Safety Tube	96.97	36.78
3.	Annular Region	30.11	11.42
	Totals	263.64 g	100.00

The total volume of the sodium electrode (for sodium) is 379.1 cm^3. From Equation B-2 in Appendix B, it follows that at the boiling point of sodium (882.9°C), the sodium electrode of a fully charged cell is

$$\frac{(263.64 \text{ g Na})(100\%)}{(0.747 \text{ g Na/cm}^3)(379.1 \text{ cm}^3)} = 93.1\% \text{ filled}$$

If the sodium reservoir were filled to 73.5 percent of its capacity at 350°C, i.e., if $f_R = 0.735$, then the sodium reservoir of a fully charged cell would be 99 percent filled at the normal boiling point of sodium.

(3) Internal Pressure due to Confined Gases. If a Mark-I load-leveling cell is assembled and then hermetically sealed at some temperature T_o and pressure P_o, the anode contains n_A moles of residual gas (usually dry and inert). Expressed in mathematical symbols,

$$n_A = P_o V_o / RT_o = P_o (1/RT_o) (V_R + V_{\beta\alpha} - V_{ST}) [1-(f'_A d_T / d_o)],$$

where V_o is the void volume at T_o; and f'_A is the fraction of the total anode filled with sodium at T', which generally is taken as the operating temperature of the cell.

$f'_A = (f_A V_R + V_{\beta\alpha} - V_{ST}) / (V_R + V_{\beta\alpha} - V_{ST})$; and f_A is the fraction of the anode reservoir filled with sodium at T'.

Assuming the cell is sealed at room temperature, for Mark-I load-leveling cells, the various parameters (in the above equations) have the following values:

T	623 ^oK (350^oC); and
T_o	298 ^oK (25^oC)
V_R	232.5 cm^3
$V_{\beta\alpha}-V_{ST}$	146.6 cm^3
f_A	0.678

Consequently, $f'_A = 0.8025$; and

$$n_A = P_o \left[1/(82.05\ cm^3 \cdot atm/^oK)(298^oK)\right] \left[(232.5 + 146.6\ cm^3)\right] \left[1-(0.8025)(0.867) / (0.97)\right]$$

$$= P_o\ (4.09 \times 10^{-5}\ cm^3\ atm^{-1})(379.1\ cm^3)(0.28)$$

$$= 0.0044\ P_o$$

When fully charged and at some temperature, T, the pressure, P_{FCA}, exerted by the residual gases confined in the anode is obtainable from the equation:

$$P_{FCA} = n_A RT/V_{FCA} = n_A RT / (V_R + V_{\beta\alpha} - V_{ST}) - (m_A/d_T),$$

in which m_A is the mass of sodium in the anode; and

d_T is the density of sodium at T.

For a Mark-I load-leveling cell at 350°C, when fully charged, these values are 263.64 g and 0.867 g/cm^3, respectively. It follows that

$$P_{FCA} = (0.0044)\ P_o\ (82.05)(623)/[379.1-(234.64/0.867)]$$
$$= 3.0\ P_o$$

In other words, whatever residual pressure is encapsulated within a cell (sealed at 25°C) increases three fold at the operating cell temperature. As the cell is discharged, the pressure within the anode becomes steadily less because the level of sodium falls as sodium transfers into the cathode. When sufficient sodium has transferred to form Na_2S_3 of all sulfur in the cell, the pressure exerted by the residual gases confined in the anode, P_{CDA}, is:

$$P_{CDA} = (0.0051)P_o(82.05)(623)/[379.1-(127.08/0.867)]$$
$$= 1.12\ P_o$$

In the same manner that the pressures within the anode were estimated in the preceding paragraphs, one can estimate the pressures due to residual gases confined within the cathode. For a Mark-I load-leveling cell whose cathode is filled with sulfur and sealed at T_o and P_o, when the cell is heated to the operating temperature (and is fully charged), P_{FCC}, the pressure exerted by n_C moles of residual gasses confined in the cathode can be calculated as follows:

$$n_C = P_o\left(4.09 \times 10^{-5}\text{cm}^{-3}\text{atm}^{-1}\right)\left(224.14\ \text{cm}^3\right)\left[1-(0.66)(1.664)/(2.07)\right]$$
$$= 0.00043\ P_o$$

$$P_{FCC} = (0.0043)P_o(82.05)(623)\ [224.14-(247.1)/(1.664)]$$
$$= 2.91\ P_o$$

Less moles of residual gas are entrapped in the cathode but they are compressed to a slightly greater pressure than the residual gases within the anode. Moreover, the gases in the cathode are compressed to a greater pressure when the cell is discharged. At complete discharge (to Na_2S_3), P_{FDC}, the pressure exerted by the residual gases confined in the cathode of a Mark-I load-leveling cell is as follows:

$$P_{FDC} = (0.0043)P_o(82.05)(623)/[224.14)-(247.1 + 118.35)/(1.877)]$$
$$= 7.47\ P_o$$

In addition to the pressure exerted by confined residual gases (introduced in sealing) at the operating temperature of the cell, the vapor pressure of sulfur over the polysulfide melt must be considered.

A. Teder and J. Tiberg [Acta Chemica Scandinavica, Vol. 24 (1970), pp. 991-996] measured the vapor pressure of sulfur above Na_2S_4 at about 380°C and found it to be about 0.001 atmosphere. If cells are sealed at 1 atmosphere, the contribution to the total pressure due to sulfur vapor is insignificant. On the other hand, if cells are evacuated to 0.001 atm (~1 mm H_g), the contribution due to sulfur becomes significant.

In summary, the maximum pressure exerted by confined residual gases would occur in a fully discharged cell's cathode; and, if the cell were sealed at 1 atmosphere and 25°C, this pressure would be about 7.5 atmosphere or 110 psi.

(b) Bursting Point of Ferritic Stainless Steel Sodium Containers. According to M. G. Bassin et al. (Statics and Strength of Materials, Second Edition, McGraw-Hill Book Co., New York, 1969, p 203), the bursting point of a cylinder can be calculated from the formula:

$$S_t = \Delta P \cdot D/2t, \qquad \text{(C-1)}$$

in which S_t is the mean tensile stress on a longitudinal section in psi;

ΔP is the difference between the absolute internal pressure and the absolute external pressure;

D is the internal diameter of the cylinder in inches; and

t is the thickness of the cylinder's wall in inches.

An analogous expression is derived in most tests on strength of materials.

Suppose that the temperature of a fully charged (or newly assembled, unused) sodium-sulfur cell inadvertently escalates above its normal operating temperature. If its temperature reaches 446°C, the sulfur will begin to boil; i.e., the vapor pressure of sulfur will exceed 1 atmosphere. As the temperature of the container rises above the normal boiling point, the vapor pressure rises disproportionately. Table C-1 lists values for P_S, the vapor pressure of sulfur, and for the tensile strength of ferritic stainless steel (Type 446) and E-Brite 26-1 for various temperatures. As the temperature increases the ultimate tensile strength of these materials decreases and the internal pressure due to the boiling sulfur increases, until the container bursts.

If the pressure within a Mark-I load-leveling cell whose walls have been reduced in thickness (by the "machined-container" option) is expressed in atmospheres, then Equation C-1 becomes the following:

$$S_t = \Delta P \cdot D/2t = \frac{(1.9 \text{ in.})(14.7 \text{ psi/atm})}{2(0.03 \text{ in.})} \Delta P$$

$$= 465.5 \ (P_S - 1) \qquad \text{(C-2)}$$

Solutions to Equation C-2 are tabulated in Table C-1 for comparison with the tensile strength of the container. Although there is some disparity in the data from various sources, viewed overall, the bursting point of a 30-mil thick sulfur container probably is about 750°C. However, as depicted in Figure C-2, the bursting point of an E-Brite container might be 840°C if the data of I.A. Franson (source d, Table C-1) is taken as representative.

(c) Estimated Service Life of Ferritic Stainless Steel Sulfur Containers. For use as sulfur containers, ferritic stainless steels have the following advantages:

- Resistant to corrosion by polysulfides at 400°C
- Low thermal expansivity (important for coating and sealing)
- Good strength at elevated temperature
- Excellent resistance to corrosion by hot atmospheric gases

They also have the following disadvantages:

- Poor workability
- 475°C embrittlement

E-Brite 26-1 is a ferritic stainless steel with very low carbon and nitrogen contents; it has the following advantages over Type 446 stainless steel:

- Ductile as-welded
- Improved formability
- Good low-cycle fatigue properties

E-Brite 26-1 was chosen as the material for the Mark-I load-leveling cell; both the sulfur and sodium containers are

TABLE C-1. COMPARISON OF INTERNAL STRESS DUE TO SULFUR VAPOR AND ULTIMATE TENSILE STRENGTH OF SULFUR CONTAINER

Temperature		Ultimate Tensile Strength, psi				Vapor Pressure of Saturated Sulfur, atm		Longitudinal Stress Exerted by Sulfur Inside Sulfur Container, Calculated from Equ. C-2, psi
		Type 446 SS		E-Brite 26-1				
°F	°C	Source a	Source b	Source c	Source d	Source e	Source f	
RT		83,000	93,480	71,000				
200	93	78,000				4×10^{-5}		
300	149	75,000				6×10^{-4}		
400	204	73,500				5×10^{-3}		
500	260	72,500				0.026	0.023	
600	316	71,500	83,170	70,000		.100	.106	
700	371	70,500				.302		
800	427	68,500	82,380	72,000		.762		
900	482	66,000	80,630			1.68		316
1000	538	61,000	76,400	67,000		3.36	3.40	1,099
1100	593	43,500	63,660			6.03	6.44	2,342
1200	649	24,000	19,970	22,000	40,000	10.18	10.0	4,273
1300	704	17,000				16.18		7,066
1400	760	12,000	6,860	12,000	30,000	24.48		10,930
1500	816	8,000				35.50		16,060
1600	871	5,500	4,590	5,000	15,000	49.65		22,647

Sources:
a. 1948 Edition of Metals Handbook, p. 564
b. Allegheny Ludlum Blue Sheet on Type 446 Stainless Steel
c. Alloy Digest (Dec. 1972) (SS-285)
d. Taken from Fig. 2, p. 2264, Metallurgical Transactions (Vol. 5, Nov. 1974)
e. Calculated from the following equation:

$$\log_{10} P_{mm} = 7.43287 - 3268.2/[^{\circ}C + 273] \text{ (Recommended range: } 325\text{-}550^{\circ}C)$$

which is cited by E. H. Conroy in "Sulfur", an article in Encyclopedia of the Chemical Elements; C. A. Hampel, Ed., Reinhold Book Corp., New York, 1968, p. 673.
f. Sulphur Data Book, Ed. W. N. Tuller, McGraw-Hill, New York, 1954, p. 40

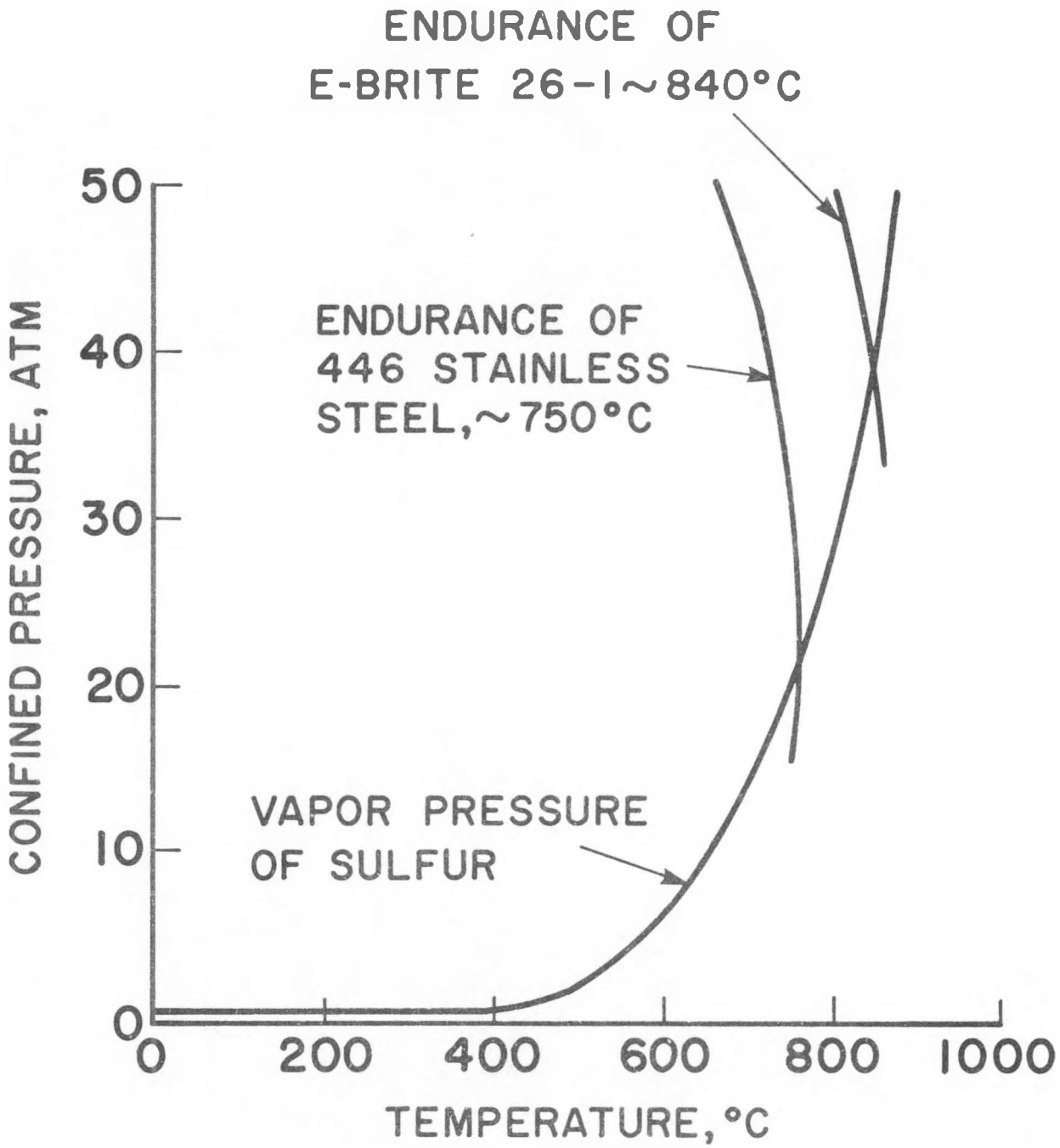

FIGURE C.2 - Bursting Points of 30-MIL Thick Sulfur Containers

constructed of 49-mil thick, 2-inch OD E-Brite tubing. In the following subsections, the service life of these containers is discussed.

(1) Resistance to Corrosion by Polysulfide. E-Brite 26-1 (and Type 446 stainless steel) exhibit moderate resistance to corrosion by polysulfide. In the Mark-I load-leveling cells, however, the E-Brite container is first coated with chromium and then with a graphite-silicate coating to enhance its corrosion resistance. See Section 2.2 for further discussion of these coatings and the resulting life expectancy based on static corrosion tests. Actual sodium-sulfur cells have been fabricated in this manner and have been operating continuously since November 1976.

(2) 885°F (475°C) Embrittlement. Ferritic stainless steels (and irons) containing more than 15 percent chromium are susceptible to embrittlement upon long exposures much above 350°C. Embrittlement is especially rapid at 475°C; ductility is restored by annealing above 550°C.

See M. Szczepanski's treatise, The Brittleness of Steel, (J. Wiley & Sons, Inc., New York 1963, pp. 248-255) for a review of the subject. I.A. Franson (Metallurgical Transactions, Vol. 5, Nov. 1974, pp. 2257-2264) reports actual measurements on E-Brite 26-1. The alloy exhibited virtually no room-temperature impact resistance after exposure to 371°C (700°F) for 5000 hours (~208 days). Specimens exposed to 343°C (650°F), however, were still ductile after 10,000 hours (~417 days). Exposure to 400°C (750°F) for 500 hours (~21 days) embrittled some specimens. Note that these measurements of impact resistance were performed at room temperature. According to data cited by Szczepanski (op. cit.), the impact

resistance at elevated temperature might be greater than at room temperature but still impaired.

According to most investigators, 475°C embrittlement is due to the formation of a chromium-rich phase, α', which precipitates along the dislocation paths in the alloy and thus prevents stress relief by slippage. See, for example, I. N. Bogachev and N. V. Papina, (Metallovedenie i Termicheskaya Orabotka Metalov, No. 5, May 1971, pp. 59-60 [translated by Consultants Bureau in 1972 as Met. Sci. Heat Treat., 13 (5-6), pp 415-416]. Also see P. J. Grobner, Metallurgical Transactions, Vol. 4 Jan. 1973 , pp 251-260. Embrittlement occurs as the result of nucleation and growth. At 475°C the process occurs nearly instantaneously; progressively longer periods are required at lower temperatures. Grobner (op. cit.) derived analytical expressions from classical nucleation theory which predicted that an alloy containing 18 percent Cr and 2 percent Mo would be brittle after exposure to 600°F (316°C) for 600,000 to 2,000,000 hours but some years later he performed additional measurements, the extrapolation of which predicted embrittlement at 600°F (316°C) after 10,000 to 20,000 hours (one to two years). (See P. J. Grobner and R. F. Steigerwald, J. Metals, July 1977, pp. 17-23.)

One concludes that the ductility of an E-Brite container will be substantially less after long-term exposure in a sodium-sulfur battery environment. Modules removed for maintenance probably will have to be handled with care as not only the inner β''-alumina tubes will be fragile but also the outer metallic cases may have reduced

fracture toughness. Consequently, it is essential that the cells and supporting fixtures (comprising a module) be designed to operate at low stress levels in a stable vibration-free environment.

APPENDIX D

STRUCTURAL ANALYSIS PERTAINING TO CERAMIC COMPONENTS

Considerable effort was expended on residual stresses in ceramic seals. The structural integrity of the ceramic components -- the β"-alumina solid electrolyte and the α-Al_2O_3 electrical insulator (and sealing surface) -- since they are critical to a durable cell. Various cell designs and contemplated changes were analyzed iteratively throughout the year. To facilitate the preparation of this report, these structural analyses are reproduced in their original format, that of an internal report.

The allowable misalignment of the ceramic electrolyte was examined early in the year. The findings are summarized in Aeronutronic Data Release (D.R.) No. 5826, a copy of which is attached.

D.1 RESIDUAL STRESSES IN THE α-ALUMINA/β"-ALUMINA BOND

This study was performed to evaluate stresses in the joint region of the β"-alumina tube and α-alumina insulator. Finite element models were generated and response stresses computed using Aeronutronic's linear elastic analysis code FINE. The ASAAS (Asymmetric Structural Analysis of Axisymmetric Structures) code was employed to obtain responses in the joint for conditions of lateral loading of the β"-alumina tube.

D.1.1 Summary of Analysis. Figure D-1 presents the finite element structural mesh utilized in the analysis. The analysis was performed in two stages to accommodate modeling limitations of the codes. Figure D-1 presents the coarse structural mesh for the plate element and a substantial section of the attached tube. Figure D-2 presents a finer mesh permitting detail evaluation of stresses in the joint region. Element responses were first obtained with the coarse mesh and appropriate responses were then applied at the boundaries of the finer mesh model of Figure D-2 to complete the solution.

Figure D-1 illustrates the applied moment loading permitted with the ASAAS code. The moment was introduced to the tube section of the model (along the J = 39 plane) as an axial loading varying as a cosine function circumferentially.

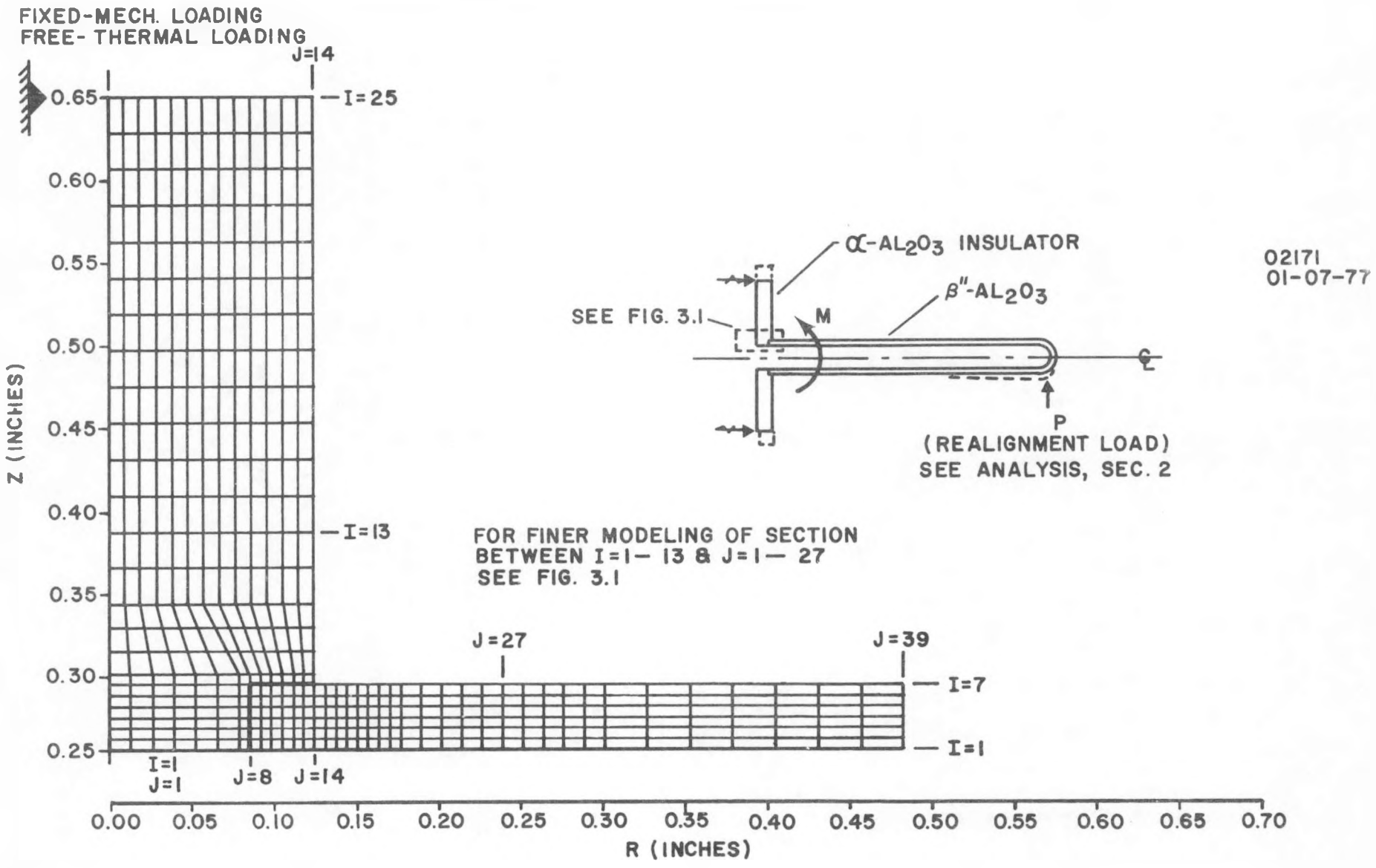
SODIUM BATTERY H=0+1 MESH PLOT
FIXED-MECH. LOADING
FREE- THERMAL LOADING
J=14
I=25
0.65
0.60
0.55
0.50
0.45
0.40
0.35
0.30
0.25
Z (INCHES)
I=13
I=7
I=1
J=27
J=39
I=1
J=1
J=8
J=14
0.00 0.05 0.10 0.15 0.20 0.25 0.30 0.35 0.40 0.45 0.50 0.55 0.60 0.65 0.70
R (INCHES)
FOR FINER MODELING OF SECTION
BETWEEN I=1— 13 & J=1— 27
SEE FIG. 3.1
α-AL2O3 INSULATOR
β"-AL2O3
SEE FIG. 3.1
M
P
(REALIGNMENT LOAD)
SEE ANALYSIS, SEC. 2
02171
01-07-77

FIGURE D.1

SODIUM BATTERY—EXPANDED MESH PLOT

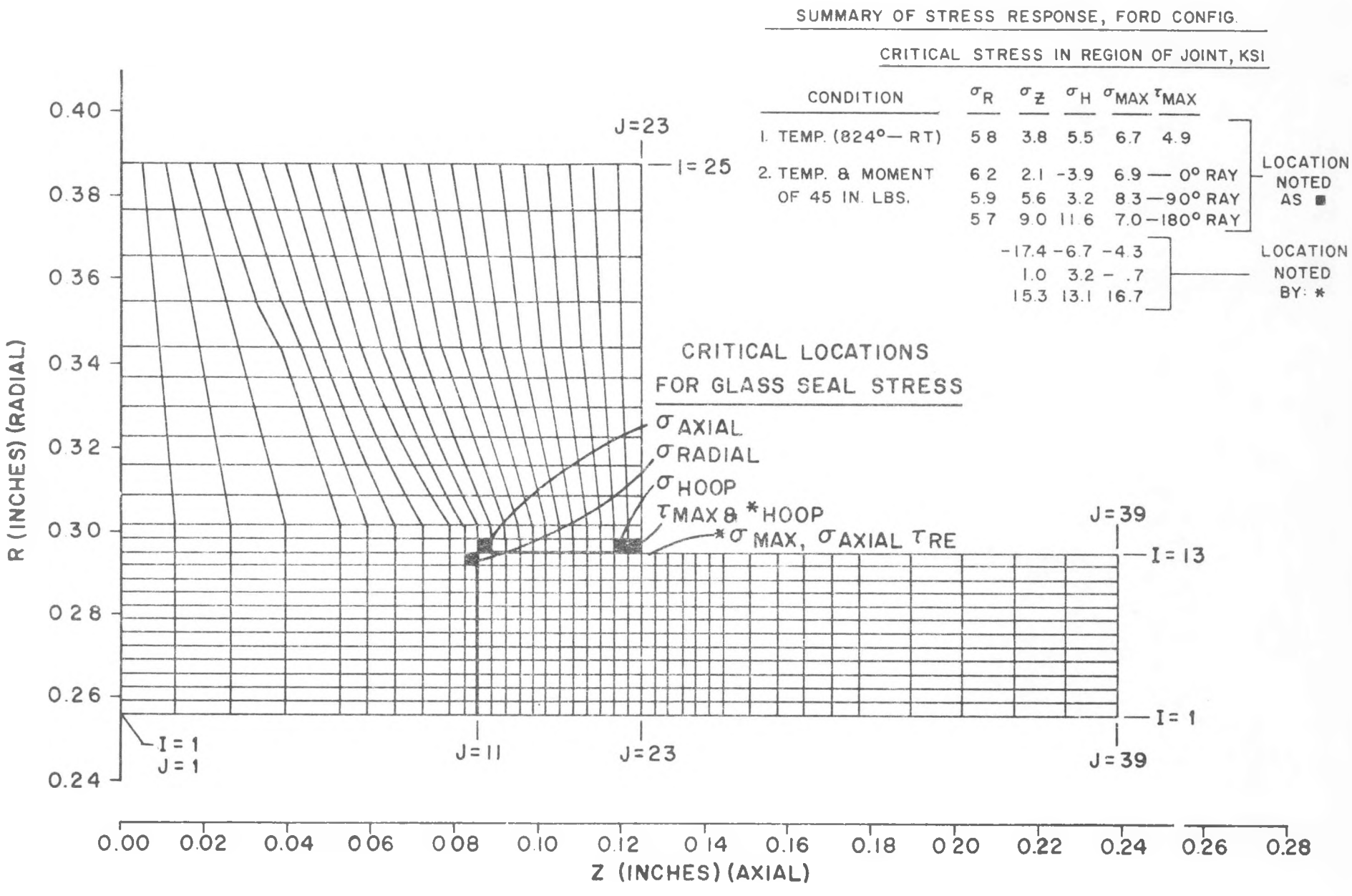

FIGURE D.2

The zero (0) degree meridian is the maximum compression ray, the 90 degree meridian is the meridian of zero axial loading and the 180 degree ray is the ray of maximum tensile loading. Stresses were applied to simulate a 45-in.-lb moment which is compatible with a realignment force, P, of 5.5 pounds necessary to correct for an initial tube run-out tolerance of 0.015 in.

The condition of cool down from the setting point of 824°F (440°C) was also considered and solved with the aid of the FINE code.

Figure D-2 presents a summary of the stresses in the joint region. The critical stress locations are noted for the condition of thermal stresses induced in the cool down from 824°F (440°C) and the condition of superposition of tube bending.

Thermal stresses induced from cool down are shown to be approximately 6000 psi. Superposition of tube bending results in substantial increase in stresses to a maximum of approximately 17,000 psi tension on the 180 degree meridian. Evaluation of stress contours shows concentration of critical stresses in the sharp structural discontinuity at the interface plane J = 23 of Figure D-2. Some reduction in these stresses could possibly be achieved with a configuration providing a more gradual change in geometry at this intersection.

The results of the analysis clearly illustrate the significance of stresses from mechanical loading and the need to minimize these stresses through change in geometry or close tolerance control and care during assembly.

D.1.2 Recommendations. Analyses have shown the insulator-to-tube joint stresses to be critical, particularly with respect to stresses from tube bending. The following recommendations are made to minimize stresses.

(a) Maintain close tolerance control on tube run-out.

(b) Exercise care during assembly to preclude objectionable lateral loading of the β-alumina tube.

(c) Modify the joint region to achieve a blend in the geometry between tube and insulator to soften the abrupt discontinuity.

D.2 EFFECT OF GEOMETRY OF THE β''-ALUMINA/α-ALUMINA JOINT ON RESIDUAL STRESSES FROM COOL DOWN FOLLOWING BONDING

This study was performed to evaluate stresses in the joint region of various configurations of the β''-alumina tube and α-alumina insulator for cool down from the setting point of 824°F (440°C). Aeronutronic's linear elastic analysis code FINE was used to generate finite element models and to compute element stresses.

Several joint models are evaluated which exhibit a range of flexibilities from imbedded tube (presented in Section D.1) to butt sealed tubes, curved plates and joints of two tubes of similar wall thickness to obtain maximum flexibility. The data show little difference in maximum residual principal tensile stress in the joint region.

The following joints were evaluated.

(a) Curved Insulator - Figure D-3
(b) Butt Joint to Cylindrical Section - Figure D-4
(c) Butt Joint to Thick Plate - Figure D-5
(d) Butt Joint to Thin Plate - Figure D-6

Configurations 1 and 2 were analyzed to evaluate stress levels associated with the simplest joint geometries. Table D-1 shows the maximum stresses obtained for each configuration in cooling down from the setting point.

Figure D-3 presents a sketch of the β''-alumina tube attached to a curved α-alumina element. Also shown is the structural mesh for the insulator and a section of the attached tube. This mesh was used in evaluating stresses in the joint region. Areas of critical stress for thermal stresses which resulted in cooling down from the glass setting temperature are indicated on the mesh plot. Thermal stresses induced from cool down are greatest in the area of the glass seal. Maximum principal stresses on the inside and outside of the β''-alumina tube in the area of the seal are shown in Figure D-7. Critical thermal stresses of 6500 psi and below occur along the entire length of the seal.

SODIUM SULFUR BATTERY CURVED ALPHA ELEMENT MESH PLOT

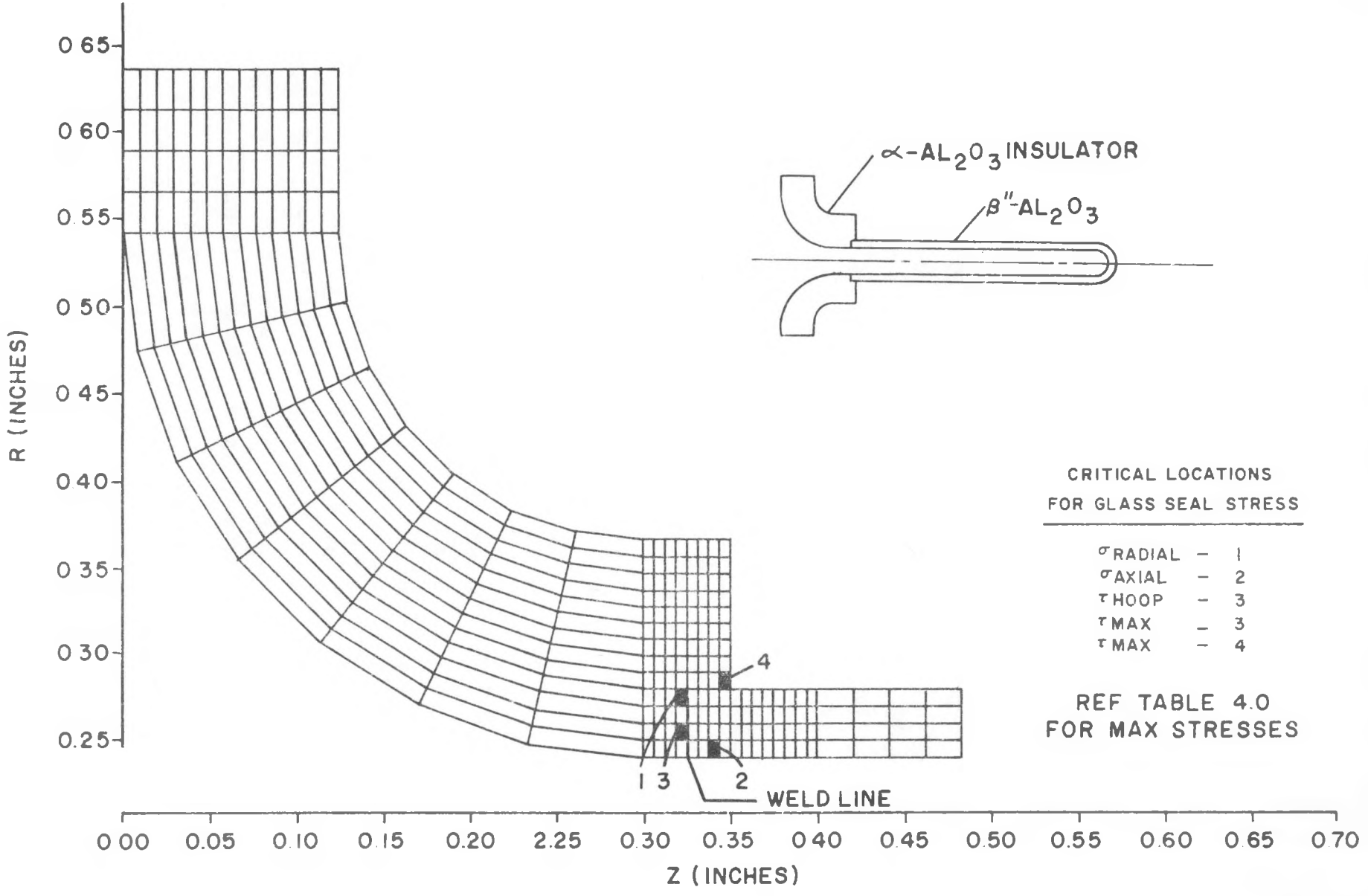

FIGURE D.3

SODIUM BATTERY, STRAIGHT WELD, CASE 2
MESH PLOT

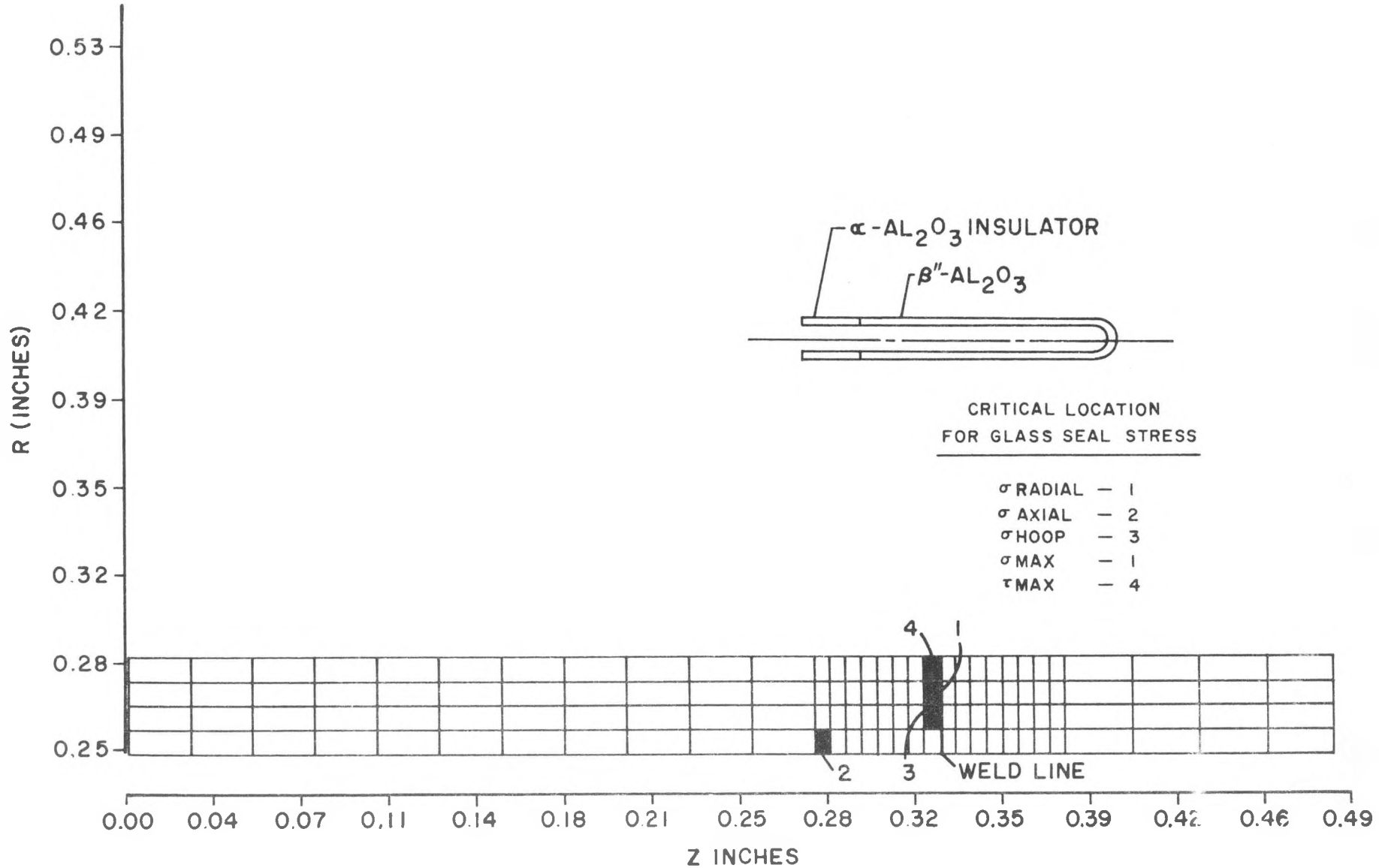

FIGURE D.4

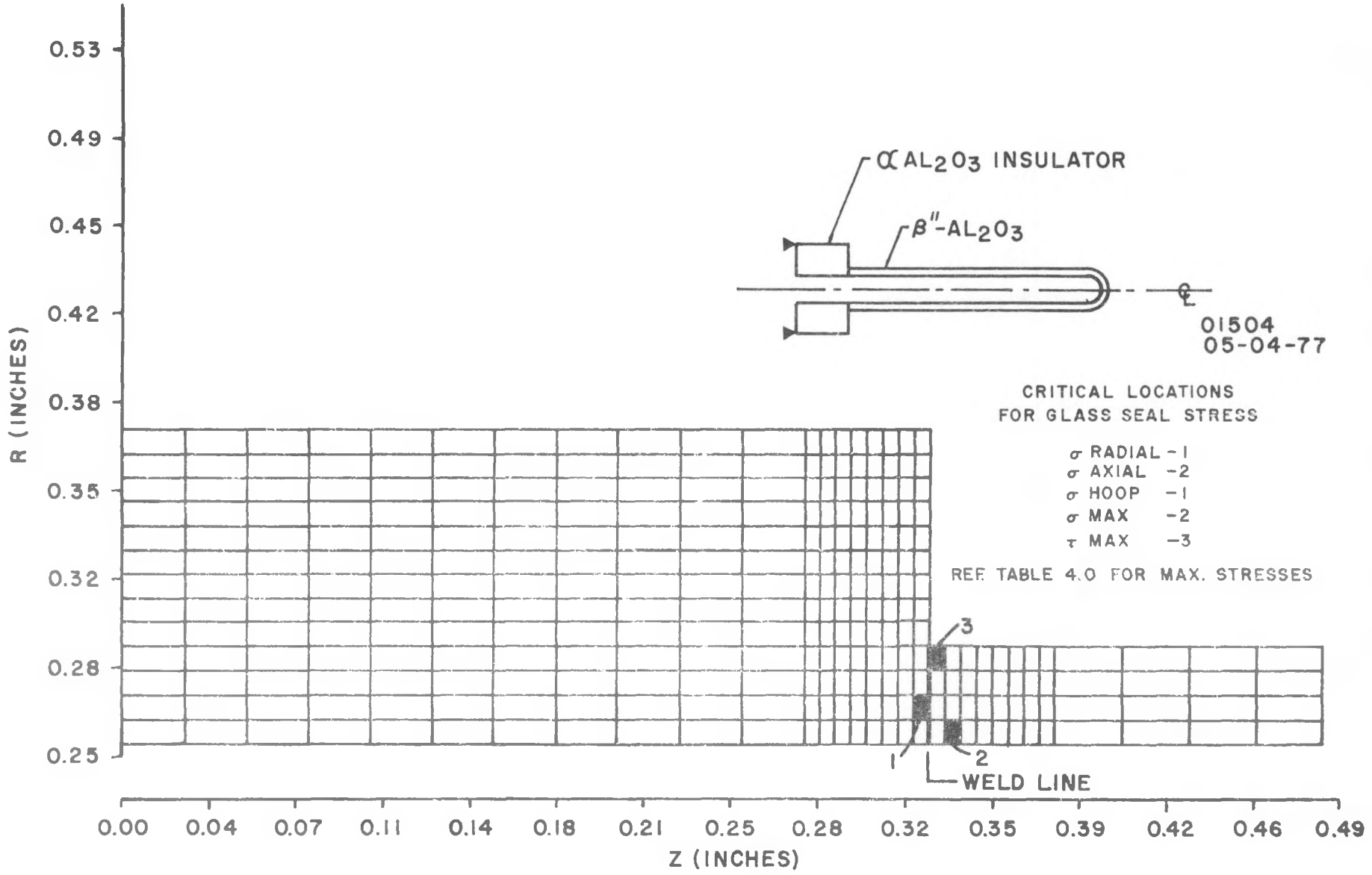
SODIUM BATTERY, STRAIGHT WELD, CASE 3 MESH PLOT
R (INCHES)
0.53
0.49
0.45
0.42
0.38
0.35
0.32
0.28
0.25
Z (INCHES)
0.00
0.04
0.07
0.11
0.14
0.18
0.21
0.25
0.28
0.32
0.35
0.39
0.42
0.46
0.49
α AL2O3 INSULATOR
β"-AL2O3
01504
05-04-77
CRITICAL LOCATIONS
FOR GLASS SEAL STRESS
σ RADIAL -1
σ AXIAL -2
σ HOOP -1
σ MAX -2
τ MAX -3
REF TABLE 4.0 FOR MAX. STRESSES
1
2
3
WELD LINE

FIGURE D.5

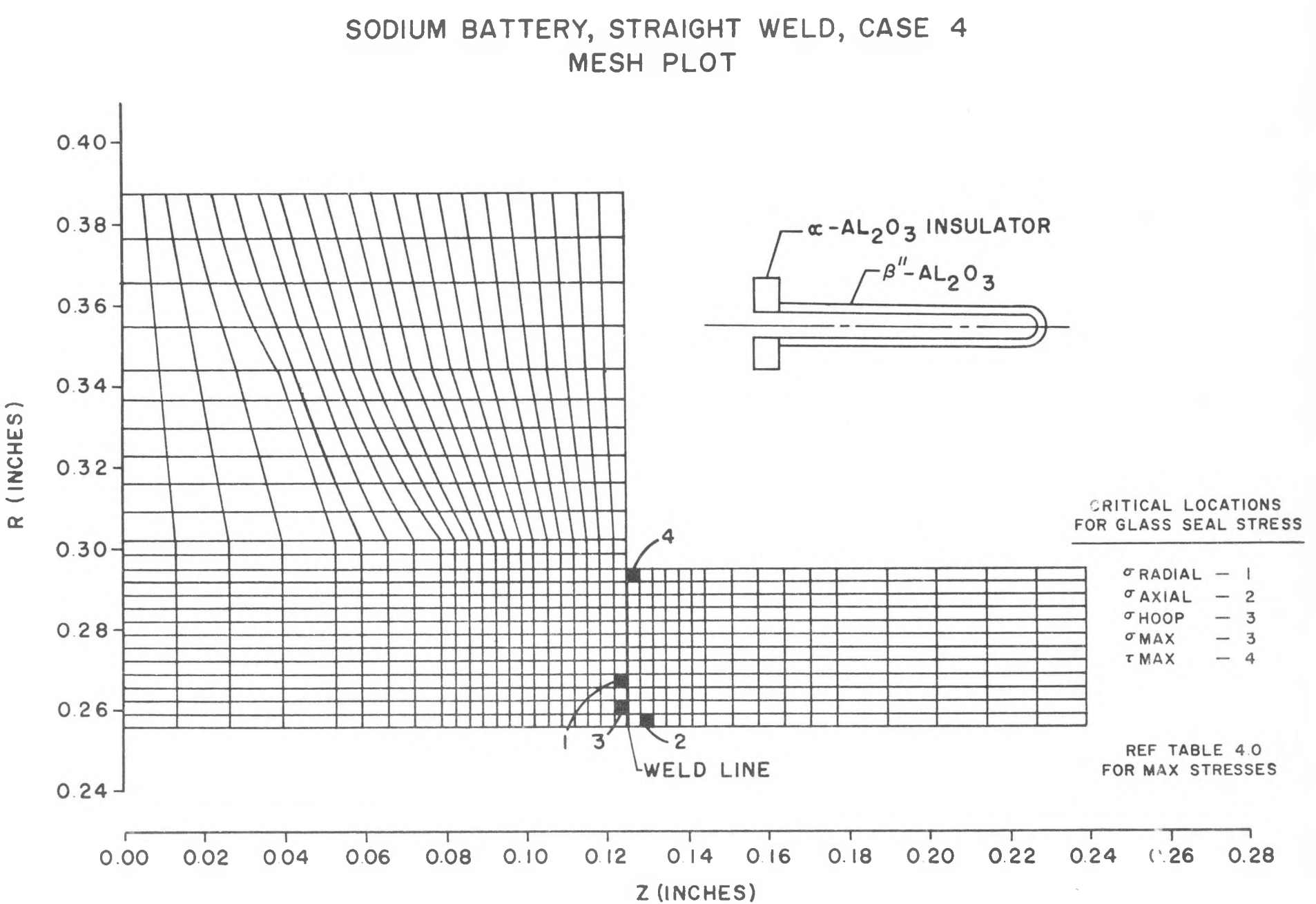
SODIUM BATTERY, STRAIGHT WELD, CASE 4
MESH PLOT
0.40
0.38
0.36
0.34
0.32
0.30
0.28
0.26
0.24
R (INCHES)
α-AL2O3 INSULATOR
β''-AL2O3
CRITICAL LOCATIONS
FOR GLASS SEAL STRESS
σ RADIAL — 1
σ AXIAL — 2
σ HOOP — 3
σ MAX — 3
τ MAX — 4
REF TABLE 4.0
FOR MAX STRESSES
1
2
3
4
WELD LINE
0.00
0.02
0.04
0.06
0.08
0.10
0.12
0.14
0.16
0.18
0.20
0.22
0.24
0.26
0.28
Z (INCHES)

FIGURE D.6

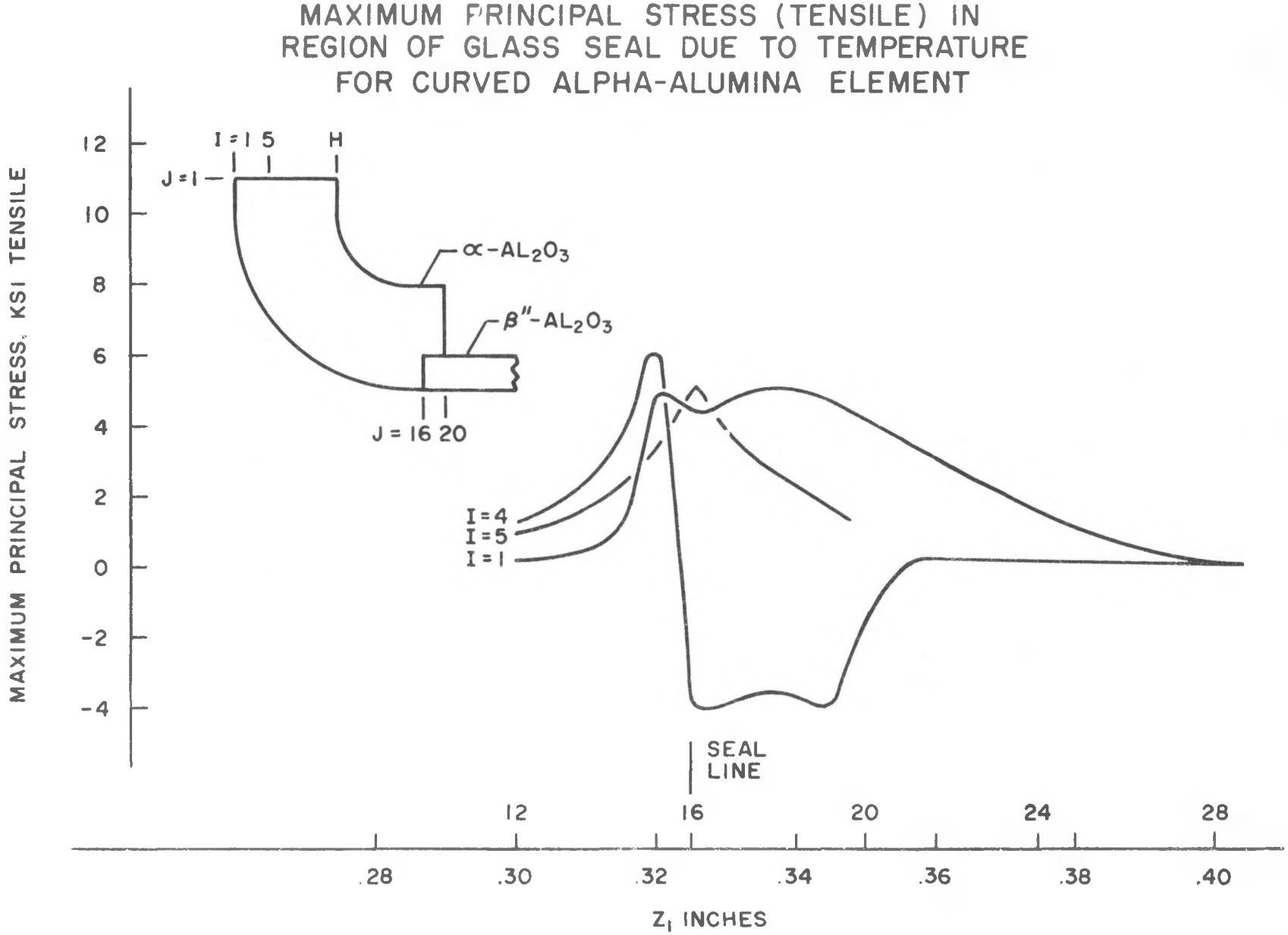
MAXIMUM PRINCIPAL STRESS (TENSILE) IN
REGION OF GLASS SEAL DUE TO TEMPERATURE
FOR CURVED ALPHA-ALUMINA ELEMENT
MAXIMUM PRINCIPAL STRESS, KSI TENSILE
12
10
8
6
4
2
0
-2
-4
I = 1 5
H
J = 1
α-AL2O3
β"-AL2O3
J = 16 20
I = 4
I = 5
I = 1
SEAL
LINE
12
16
20
24
28
.28
.30
.32
.34
.36
.38
.40
Z1 INCHES

FIGURE D.7

TABLE D.1. SUMMARY OF STRESS RESPONSE DUE TO COOL DOWN FROM 824°F TO 70°F

Configuration	Critical Stresses in Joint Region, ksi				
	σ_R	σ_Z	σ_H	σ_{max}	τ_{max}
1. Curved Alpha-Alumina Element (Figure D-3)	5.6	5.0	3.7	6.5	4.5
2. Straight Seal (Figure D-4)	5.5	3.4	7.5	6.1	3.8
3. Straight Seal (Figure D-5)	4.0	4.7	4.2	4.7	4.4
4. Straight Seal (Figure D-6)	5.1	6.3	6.4	6.7	5.4

The straight seal configuraton, Case 2, is shown on a sketch in Figure D-4. The finite element structural mesh used in analyzing this case as well as the critical stress locations for thermal stress are also presented. The greatest stresses were encountered in the area of the seal with the maximum stress being 6100 psi. Stresses elsewhere were 3500 psi and below. A plot of the maximum principal stresses in the region of the seal along both the inside and outside edges of the tube and insulator is shown in Figure D-8.

Figure D-5 shows the configuration of Configuration No. 3 and the mesh used to determine stresses in the model. The maximum stress of 4700 psi occurs at the inside edge of the seal. The stresses elsewhere in the ceramic elements are well below this amount. Figure D-9 is a plot of the principal stresses due to the cool down along I = 1, 4, and 5, or along the inside edge and on either side of a line extending along the outside edge of the tube.

The configuration of the element of Configuration No. 4 is slightly different from the element of Configuration No. 3. The insulator of Case 4 has a greater radius and a shorter length than that of the insulator of Case 3. The seal line remains flush with the side of the insulator. A sketch of the element along with the matrix used in obtaining the stresses is shown in Figure D-6. The region of greatest stress is the inside edge of the tube near the seal. The maximum stress in this region is 6700 psi. Stresses elsewhere do not exceed 3800 psi. Figure D-10 shows the maximum principal tensile stresses in the region of the glass seal along the inside and outside edge of the β''-alumina tube.

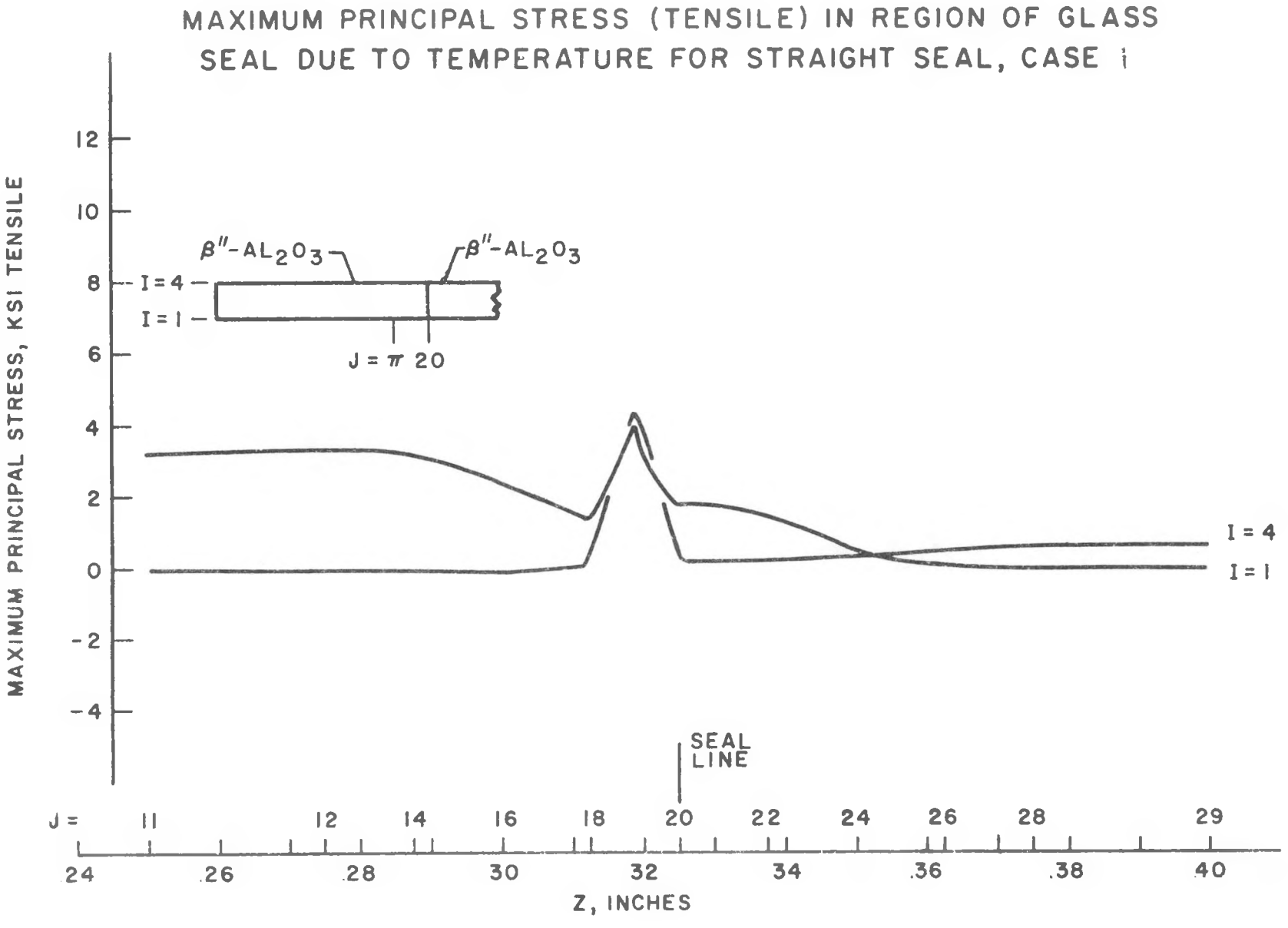
MAXIMUM PRINCIPAL STRESS (TENSILE) IN REGION OF GLASS SEAL DUE TO TEMPERATURE FOR STRAIGHT SEAL, CASE 1
MAXIMUM PRINCIPAL STRESS, KSI TENSILE
12
10
8
6
4
2
0
-2
-4
β''-AL2O3
β''-AL2O3
I = 4
I = 1
J = π 20
I = 4
I = 1
SEAL LINE
J = 11 12 14 16 18 20 22 24 26 28 29
24 .26 .28 30 32 34 .36 .38 40
Z, INCHES

FIGURE D.8

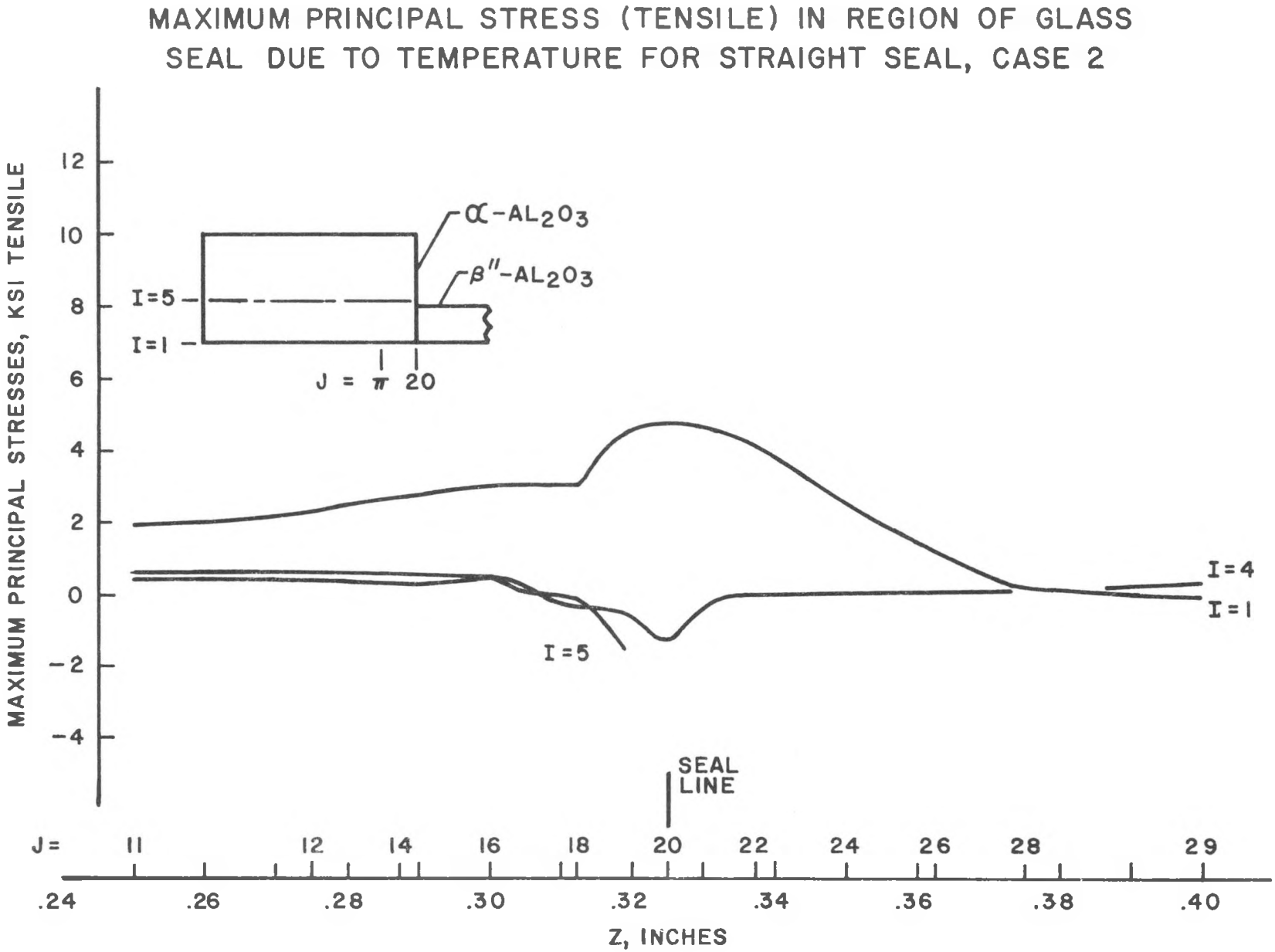
MAXIMUM PRINCIPAL STRESS (TENSILE) IN REGION OF GLASS SEAL DUE TO TEMPERATURE FOR STRAIGHT SEAL, CASE 2
MAXIMUM PRINCIPAL STRESSES, KSI TENSILE
12
10
8
6
4
2
0
-2
-4
α-AL2O3
β''-AL2O3
I=5
I=1
J = π 20
I=4
I=1
I=5
SEAL LINE
J= 11 12 14 16 18 20 22 24 26 28 29
.24 .26 .28 .30 .32 .34 .36 .38 .40
Z, INCHES

FIGURE D.2

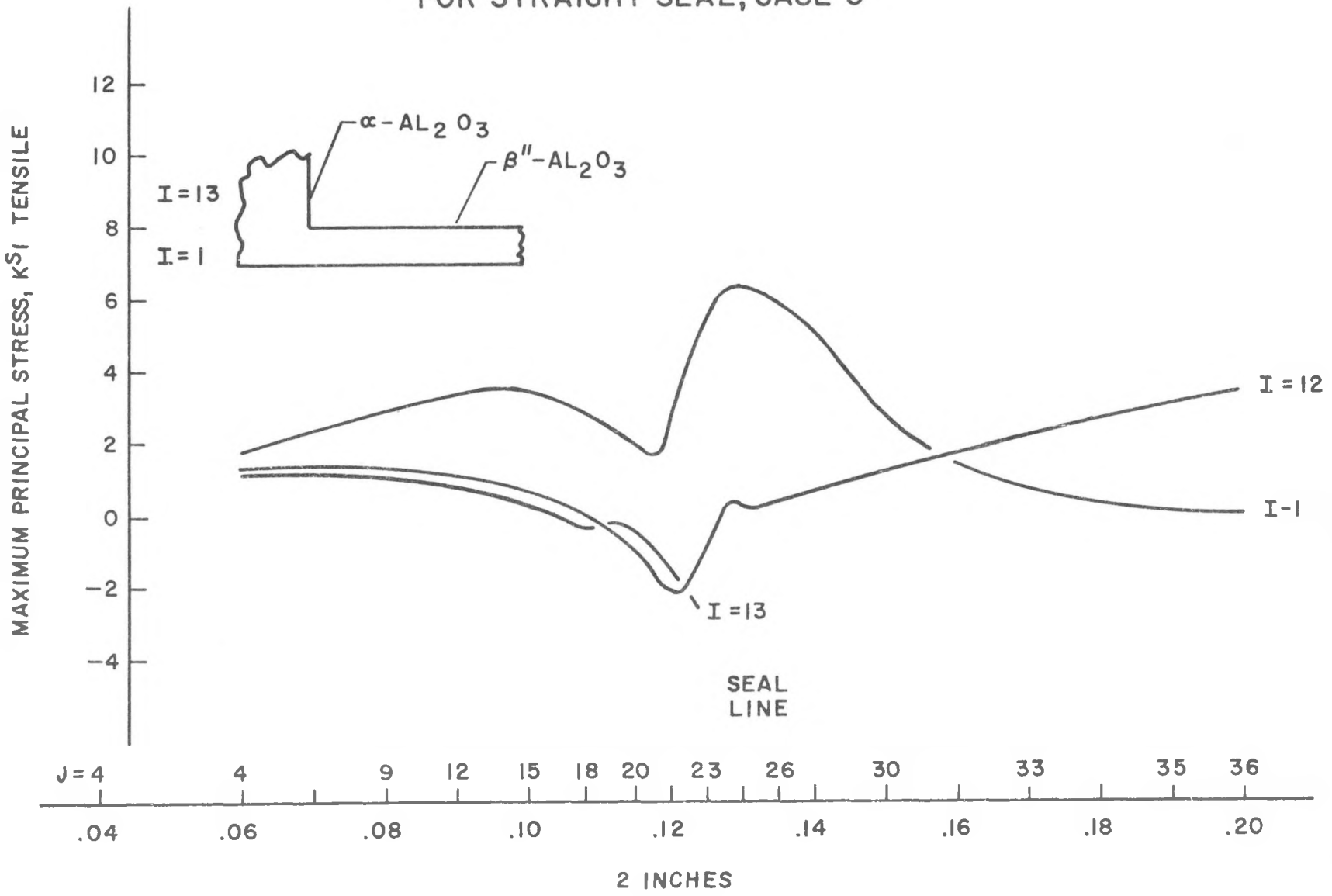
MAXIMUM PRINCIPAL STRESS (TENSILE) IN
REGION OF GLASS SEAL DUE TO TEMPERATURE
FOR STRAIGHT SEAL, CASE 3
MAXIMUM PRINCIPAL STRESS, KSI TENSILE
12
10
8
6
4
2
0
−2
−4
α-AL2O3
β''-AL2O3
I=13
I=1
I = 12
I-1
I =13
SEAL
LINE
J=4
4
9
12
15
18
20
23
26
30
33
35
36
.04
.06
.08
.10
.12
.14
.16
.18
.20
2 INCHES

FIGURE D.10

The straight seal configuration, Case 4, has a slightly greater maximum stress than the curved α-alumina element configuration, 6700 psi and 6500 psi respectively. Yet, points of critical stresses occurred all along the seal line in the curved α-alumina element configuration and only on the inside of the tube seal in Case 4, as can be noted from Figures D-7 and D-10. These data show that there is little improvement, as far as thermal stresses are concerned, by modifying the joint region to reduce the abrupt discontinuity. The butt-sealed joint stresses were comparable to those of the imbedded joint shown in Figure D-2 and should be given consideration as a production candidate due to its reduced complexity.

D.3 ALLOWABLE MISALIGNMENT OF THE CERAMIC ELECTROLYTE

Data Release (D.R.) No. 5826 "Computation of Cantilever Stresses in Sodium/Sulfur Cell Electrolyte for Misalignment Defects", is attached.

In summary, the data show that for an initial specified maximum misalignment of 0.039 inch, the residual β''-alumina tube stress would be 12,000 psi and require an alignment force of approximately 14 pounds for the tube geometry of: L = 8 inches, O.D. = 0.6 inch and wall t = 0.040 inch. to maintain stresses below 5000 psi would require a misalignment no greater than 0.015 inch.

FORD AEROSPACE & COMMUNICATIONS CORP.

Aeronutronic Division
Newport Beach, California

CLASSIFICATION Unclassified

CONTRACT NO. _____

ENGINEERING DATA REQUEST/RELEASE

PROGRAM NAME: Sodium/Sulphur Cell	DOCUMENT CONTROL NO.
WORK PACKAGE NO.: 2M55-2000	D.R. NO. 5826 REV
SUBJECT: Computation of Cantilever Stresses in Sodium/Sulfur Cell Electrolyte for Misalignment Defects	VEH. SYST. DESIG.

USE FOR REQUEST ONLY

FROM:

C.C. OF REQUEST

TO:

PROGRAM ENGINEER APPROVAL

DATE OF REQUEST

Distribution: C. Adams
G. Chase
D. Bridges
R. Harlow
H. Kato
J. Stanwood
M. Christensen (Mtr + 5)
E. Ritchie

DATE REQUIRED

PURPOSE OF DATA

IDENTIFIERS
(CHECK ONE OR MORE)

- [ ] SYSTEM
- [ ] ELECTRICAL
- [ ] EXPERIMENT
- [ ] GUIDANCE/CONTROL
- [ ] INSTRUMENTATION
- [ ] PROPULSION/ORDNANCE
- [ ] RF/TELEMETRY
- [ ] STRUCTURE
- [ ] THERMAL CONTROL
- [ ] AGE
- [ ] AERO/TRAJECTORY
- [ ] ANALYSIS
- [ ] DESIGN/DEVEL
- [ ] MASS PROPERTIES
- [ ] MATERIALS/PROCESS
- [ ] RANGE SAFETY
- [ ] REQUIREMENTS
- [ ] TEST PLANS
- [ ] TEST REPORTS
- [ ] VULNERABILITY AND HARDENING

USE FOR RELEASE ONLY

PREPARED BY	SUPERVISOR APPROVAL	DATE OF RELEASE
C. L. Adams CLA	J. W. Stanwood JWS	1/19/77

DETAILED RELEASE (SUPPLEMENT WITH ATTACHMENTS AS REQUIRED)

This Data Release documents a study of a mode of failure of the sodium/sulfur cell which results when the tip of the electrolyte is inserted off-center.

Stresses, moments, and lateral straightening forces are shown as a function of misalignment tolerance for geometry variations of the electrolyte.

ACTION REQUIRED

DISTRIBUTION LIST	APPROVED	PROGRAM ENGINEER APPROVAL
*	D. W. Bridges	

ARD 8265
MAY 71

CLASSIFICATION Unclassified

1.0 INTRODUCTION

One mode of failure of the sodium/sulfur cell which has been observed is the cracking of the beta-alumina tube where it is attached to the alpha-alumina collar when the tip of the tube is inserted off-center.

The electrolytes used in the sodium/sulfur cells are made of ceramics which conduct sodium ions. The beta-alumina electrolytes are tubular and normally have an O.D. of 0.4 - 1.2 inch, a wall thickness of .04 - .08 inch, and a length of 4 - 12 inches.

Maximum allowable loads and deflections were determined for several combinations of various lengths, diameters, and wall thicknesses of electrolytes. For each permutation of tube length, diameter, and wall thickness, cantilever stresses, moments, and lateral straightening forces were calculated for various misalignments of the beta-alumina electrolyte.

2.0 DISCUSSION

The geometry variations considered were:

Tube length, ℓ: 8, 12, and 16 in.
Tube diameter, b: 0.6, 0.9, and 1.2 in.
Tube wall thickness, c: .04, .06, and .08 in.

The following assumptions were made:

1. Beam is fixed at the top.
2. Force is applied at the tip.
3. For β-alumina (β-Al_2O_3);

   $E = 21 \times 10^6$ psi

   σ = 20,000 psi Tens.

The tube parameters were taken in all possible combinations. The maximum allowable load, bending moment, and deflection to which the tube may be subjected were calculated and are shown in Table 1.

Table II shows the lateral straightening forces, moments, and stresses for an off-center tube displacement of .039 in.

The moment of inertia for a tube is determined from:

$$I = \frac{\pi(d^4 - d_1^4)}{64}$$

$d = b$

$d_1 = b - 2c$

The maximum allowable loads and deflections for the fixed-end tube were determined from the following:

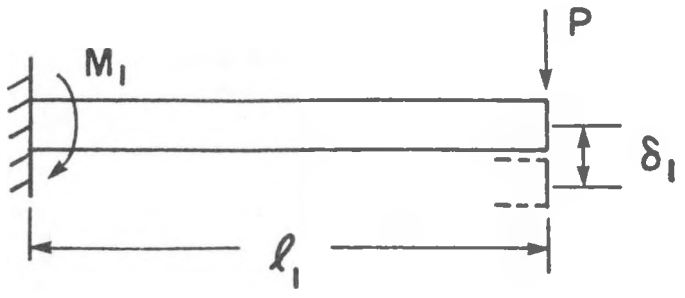

$$\sigma = \frac{M_r}{I} = \frac{P\ell_r}{I}, \quad \text{so}$$

$$P = \text{Allowable Load} = \frac{\sigma I}{\ell_r}$$

$$= \frac{40{,}000I}{\ell_b}$$

$$\delta_1 = \text{Deflection} = \frac{M_1 \ell_1^2}{3E_1 I_1} \qquad (1)$$

When a flexible plate is connected to the top of the beta-alumina tube, the following equations hold for the flexible end:

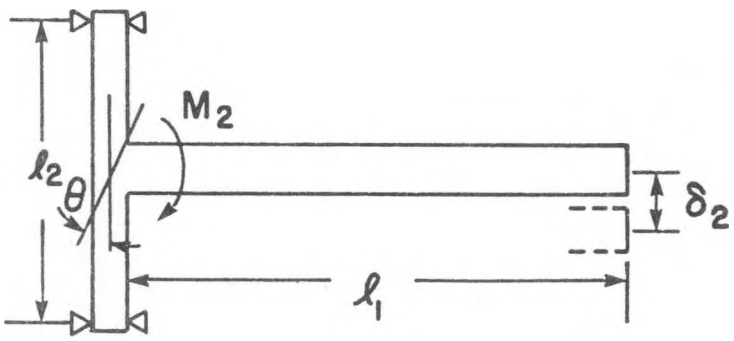

θ = Rotation of Flexible Plate (Rad.)

δ_2 = Tip Displacement

$= \theta \cdot \ell_1$

The situation under consideration is similar to case 5 on page 195 of Roark, which is a flat plate with edges supported and central coupling loading.

From page 216, Roark,

$$\text{Slope of Plate, } \theta = \frac{M_2}{\alpha E_2 t^3} \qquad (2)$$

where t = plate thickness

and α depends on ratio of r_o/a

r_o = 1/2 tube diameter

a = 1/2 ℓ_2

α can be found from the table on page 216, in Roark

For r_o = 1/2 b = 0.3 inch

a = 1/2 ℓ_2 = 0.7 inch

r_o/a = 0.428

From table on page 216, α = 4.7

since $\delta_2 = \theta \ell_1$, substituting into (2)

$$\frac{\delta_2}{\ell_1} = \frac{M_2}{\alpha E_2 t^3}$$

$$\text{and } \delta_2 = \frac{M_2 \ell_1}{\alpha E_2 t^3} \qquad (3)$$

For a tube with end flexibility, equations (1) and (3) are combined to determine the deflection, note that $M_1 = M_2$ for the combined case

$$\delta_1 + \delta_2 = \frac{M_2 \ell_1^2}{3E_1 I_1} + \frac{M_2 \ell_1}{\alpha E_2 t^3}$$

$$\delta = M_2 \ell_1 \left[\frac{\ell_1}{3E_1 I_1} + \frac{1}{\alpha E_2 t^3} \right] \qquad (4)$$

To determine the ratio of rigid support moment to flexible support moment for a specified tolerance misalignment,

For a flexible support,

$$\delta_1 + \delta_2 = M_2 \ell_1 \left[\frac{\ell_1}{3E_1 I_1} + \frac{1}{\alpha E_2 t^3} \right]$$

For a fixed support,

$$\delta_1 = \frac{M_1 \ell_1^2}{3E_1 I_1}$$

Ratio of flexible to fixed

$$\frac{\delta_1 + \delta_2}{\delta_1} + \frac{M_2}{M_1} \left[1 + \frac{3E_1 I_1}{\alpha E_2 t^3 \ell_1} \right] \qquad (5)$$

For the case of $\delta_1 = \delta_1 + \delta_2$,

$$\frac{M_1}{M_2} = \left[1 + \frac{3E_1 I_1}{\alpha E_2 t^3 \ell_1} \right] \qquad (6)$$

For a maximum off-center displacement of 0.039 inch, tube length of 8 inches, tube O.D. of 0.6 inch, and tube wall thickness of 0.04 inch, the flexible bending moment is

$$M_2 = \frac{M_1}{\left[1 + \frac{3E_1 I_1}{\alpha E_2 t^3 \ell_1}\right]}$$ from equation (6)

$M_1 = 107$ in-lb

$\ell_1 = 8$ in

$E_1 = E_2 = 21 \times 10^6$ psi

$I_1 = .0028$ in^4

$\alpha = 4.6$

$t = 1/8$ in

$M_2 = 96$ in-lb

$$\alpha = \frac{M(b/2)}{I} = 10{,}285 \text{ psi}$$

When tube end flexibility is considered, and the current tube dimensions are used (ℓ = 8 in, b = 0.6 in, c = .04 in), the flexible bending moment is found to be 96 inch-pounds. This refinement results in a reduction of only 10 percent in the calculated fixed base moment of 107 inch-pounds. The trade-off study has been performed using the conservative fixed base equations for the beta-alumina tube.

Figures D.11, 12 and 13 show alignment force as a function of tube deflection for tubes of 8, 12 and 16 inches and of varying diameters and wall thicknesses. Moment as a function of tube deflection for tubes of 8, 12 and 16 inches is shown in Figures D.14, 15 and 16. Figures D.17 and 18 are plots of stress as a function of tube deflection for each geometry variation. Figures D.17 and 18 differ in the scale used for tube deflection. Figure D.19 presents a three parameter (wall thickness, initial misalignment, and assembly alignment force) summary plot for the baseline beta-alumina

tube of 0.6 inch diameter and 8 inches length. Variation in required alignment force (and resulting in tube stress)is noted for variation in tube length and diameter. Lines of constant initial displacement are also lines of constant bending stress for a tube of given length and diameter as observed from the governing equations shown above and data of Figure D.17.

3.0 SUMMARY

The allowable tensile sustained tensile loading permitted to achieve cell life requirements has not been established. It is anticipated, however, that the sustained loading permitted will not exceed 5000 psi. From the data in Figure D.19, it can be noted that misalignment of the baseline beta-alumina tube must be held below .020 inch tip displacement with the alignment load induced during assembly being approximately 10 pounds. A substantial increase in alignment load requirement can be noted for tubes of increasing diameter. Significant reduction in both alignment force required and induced tube stresses result for extended length tubes, other parameters being held constant.

For a maximum tube misalignment of .039 inch, in order for the sustained loading not to exceed 5000 psi, the tube length must be greater than 12 inches for a tube diameter of 0.6 inch. When the tube length is increased to 16 inches, tube diameters of 0.6 and 0.9 inch are acceptable.

TABLE D-2

MAXIMUM ALLOWABLE LOADS AND DEFLECTIONS

CASE NO.	LENGTH, ℓ (IN)	TUBE O.D., b(IN)	THICKNESS, c(IN)	MOMENT OF INERTIA I,	MOMENT ABOUT BEAM TOP, M (IN-LB)	ALLOWABLE LOAD, P (LB)	MAX. ALLOWABLE DEFLECTION, δ_{MAX} (IN)
1	8	0.6	.04	.0028	187	23.3	.067
2	8	0.6	.06	.0038	253	31.6	.067
3	8	0.6	.08	.0045	300	37.5	.067
4	8	0.9	.04	.0100	444	55.5	.045
5	8	0.9	.06	.0140	622	77.7	.045
6	8	0.9	.08	.0175	778	97.2	.045
7	8	1.2	.04	.0245	817	102.1	.033
8	8	1.2	.06	.0350	1167	145.8	.033
9	8	1.2	.08	.0444	1480	185.0	.033
10	12	0.6	.04	.0028	187	15.5	.151
11	12	0.6	.06	.0038	253	21.0	.151
12	12	0.6	.08	.0045	300	25.0	.152
13	12	0.9	.04	.0100	444	37.0	.101
14	12	0.9	.06	.0140	622	51.8	.101
15	12	0.9	.08	.0175	778	64.8	.101
16	12	1.2	.04	.0245	817	68.0	.076
17	12	1.2	.06	.0350	1167	97.2	.076
18	12	1.2	.08	.0444	1480	123.3	.076
19	16	0.6	.04	.0028	187	11.6	.269
20	16	0.6	.06	.0038	253	15.8	.270
21	16	0.6	.08	.0045	300	18.7	.270
22	16	0.9	.04	.0100	444	27.7	.180
23	16	0.9	.06	.0140	622	38.8	.180
24	16	0.9	.08	.0175	778	48.6	.180
25	16	1.2	.04	.0245	817	51.0	.135
26	16	1.2	.06	.0350	1167	72.9	.135
27	16	1.2	.08	.0444	1480	92.5	.135

TABLE II.

LATERAL STRAIGHTENING FORCES, MOMENTS, AND STRESSES
FOR A TUBE DEFLECTION OF .039 INCH

CASE NO.	STRAIGHTENING FORCE, P (LBS)	STRESS (PSI)	MOMENT, M (IN-LB)
1	13.4	11,517	107
2	18.2	11,517	146
3	21.6	11,517	173
4	48.0	17,276	384
5	67.2	17,276	538
6	84.0	17,276	672
7	117.6	23,034	941
8	168.0	23,034	1,344
9	213.1	23,034	1,705
10	4.0	5,119	48
11	5.4	5,119	65
12	6.4	5,119	77
13	14.2	7,678	170
14	19.9	7,678	239
15	24.9	7,678	299
16	34.8	10,238	418
17	49.8	10,238	598
18	63.1	10,238	759
19	1.7	2,879	27
20	2.3	2,879	37
21	2.7	2,879	43
22	6.0	4,319	96
23	8.4	4,319	134
24	10.5	4,319	168
25	14.7	5,759	235
26	21.0	5,759	336
27	26.6	5,759	426

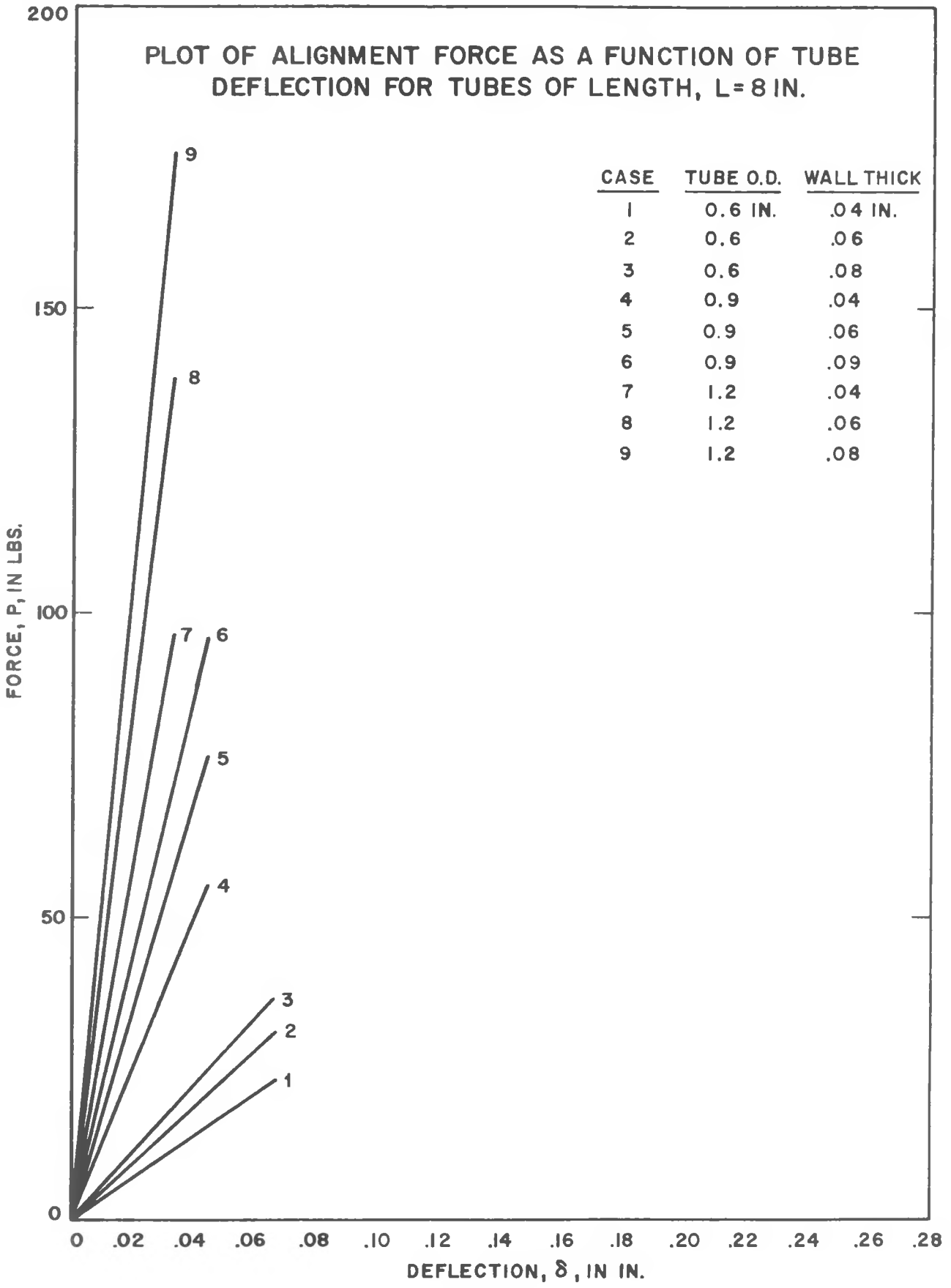
PLOT OF ALIGNMENT FORCE AS A FUNCTION OF TUBE DEFLECTION FOR TUBES OF LENGTH, L= 8 IN.
CASE TUBE O.D. WALL THICK
1 0.6 IN. .04 IN.
2 0.6 .06
3 0.6 .08
4 0.9 .04
5 0.9 .06
6 0.9 .09
7 1.2 .04
8 1.2 .06
9 1.2 .08
FORCE, P, IN LBS.
200
150
100
50
0
0 .02 .04 .06 .08 .10 .12 .14 .16 .18 .20 .22 .24 .26 .28
DEFLECTION, δ, IN IN.

FIGURE D.11

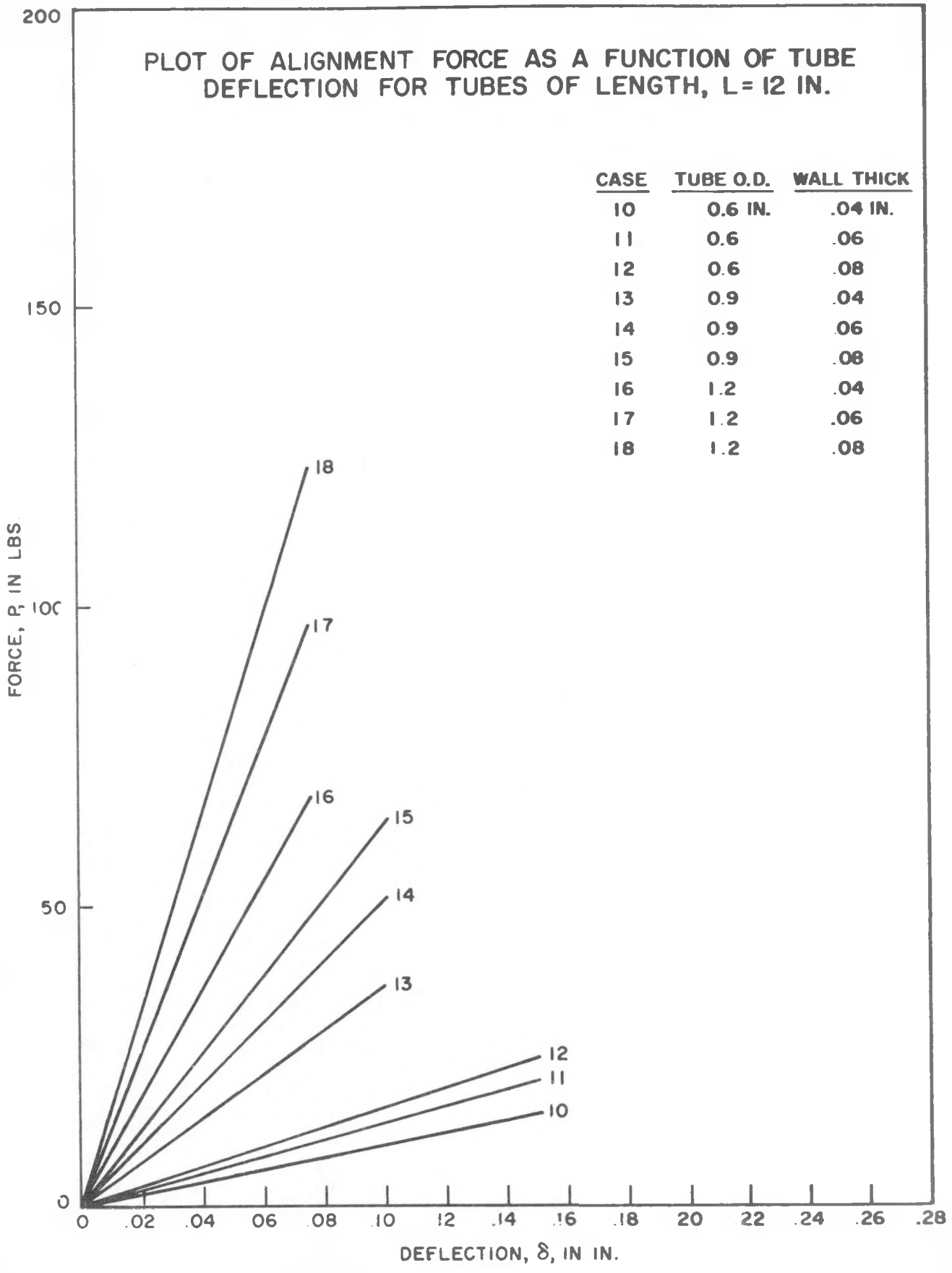
PLOT OF ALIGNMENT FORCE AS A FUNCTION OF TUBE DEFLECTION FOR TUBES OF LENGTH, L= 12 IN.
CASE TUBE O.D. WALL THICK
10 0.6 IN. .04 IN.
11 0.6 .06
12 0.6 .08
13 0.9 .04
14 0.9 .06
15 0.9 .08
16 1.2 .04
17 1.2 .06
18 1.2 .08
FORCE, P, IN LBS
200
150
100
50
0
18
17
16
15
14
13
12
11
10
0 .02 .04 .06 .08 .10 .12 .14 .16 .18 .20 .22 .24 .26 .28
DEFLECTION, δ, IN IN.

FIGURE D.12

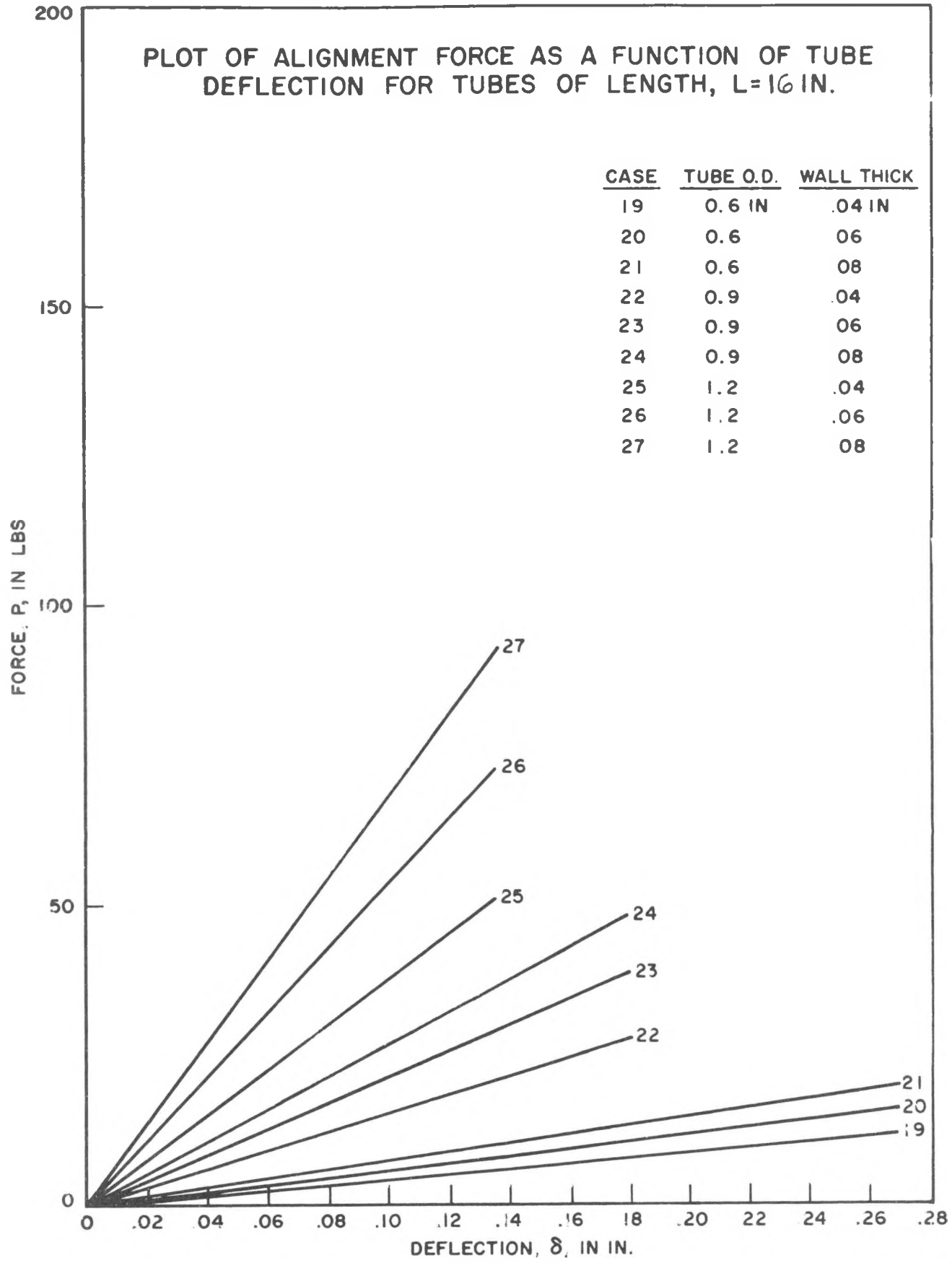
PLOT OF ALIGNMENT FORCE AS A FUNCTION OF TUBE DEFLECTION FOR TUBES OF LENGTH, L=16 IN.
CASE | TUBE O.D. | WALL THICK
19 | 0.6 IN | .04 IN
20 | 0.6 | 06
21 | 0.6 | 08
22 | 0.9 | .04
23 | 0.9 | 06
24 | 0.9 | 08
25 | 1.2 | .04
26 | 1.2 | .06
27 | 1.2 | 08
FORCE, P, IN LBS
200
150
100
50
0
0
.02
.04
.06
.08
.10
.12
.14
.16
18
.20
22
24
.26
.28
DEFLECTION, δ, IN IN.
27
26
25
24
23
22
21
20
19

FIGURE D.13

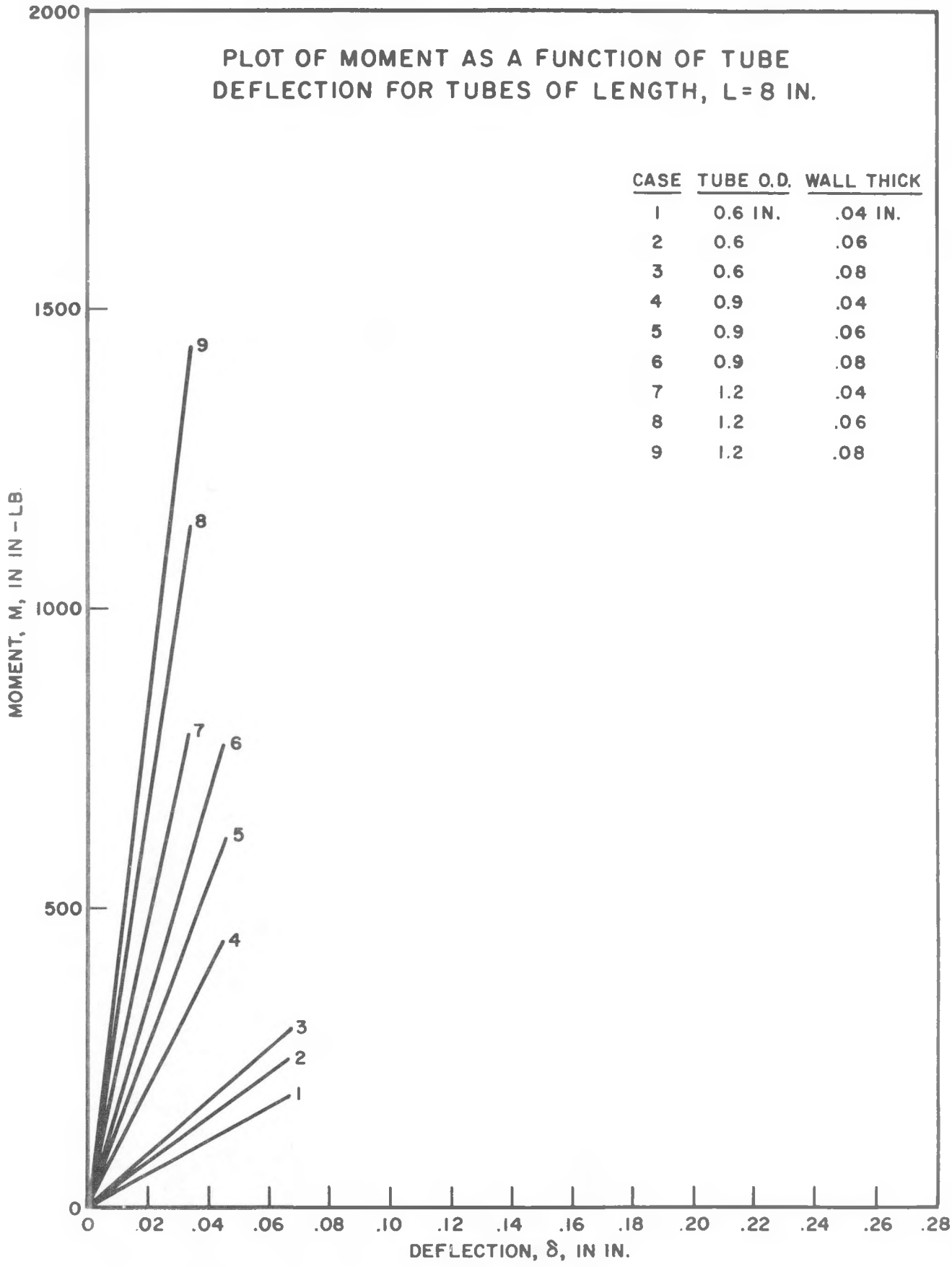
PLOT OF MOMENT AS A FUNCTION OF TUBE DEFLECTION FOR TUBES OF LENGTH, L = 8 IN.
CASE TUBE O.D. WALL THICK
1 0.6 IN. .04 IN.
2 0.6 .06
3 0.6 .08
4 0.9 .04
5 0.9 .06
6 0.9 .08
7 1.2 .04
8 1.2 .06
9 1.2 .08
MOMENT, M, IN IN-LB
2000
1500
1000
500
0
9
8
7
6
5
4
3
2
1
0 .02 .04 .06 .08 .10 .12 .14 .16 .18 .20 .22 .24 .26 .28
DEFLECTION, δ, IN IN.

FIGURE D.14

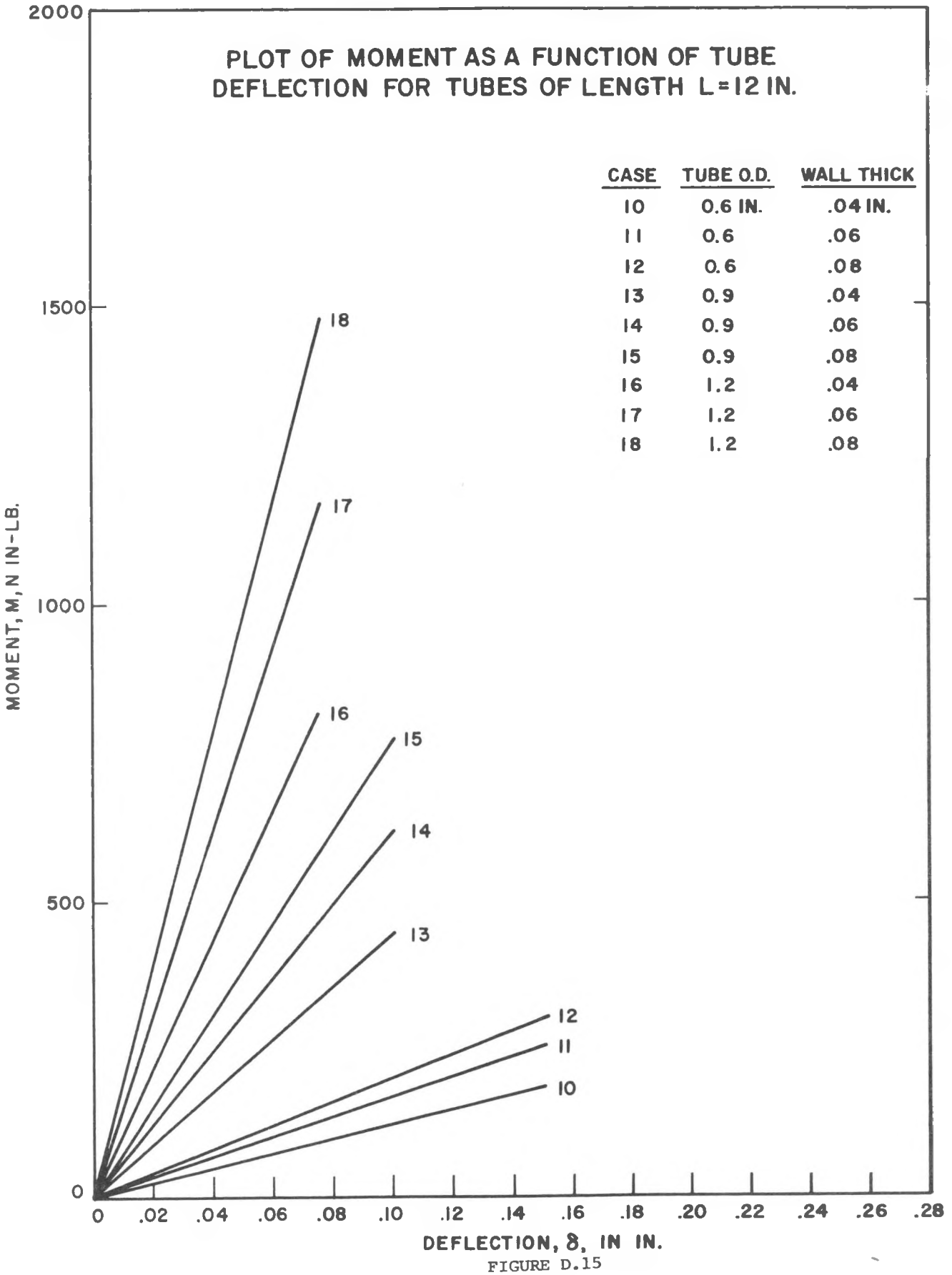
PLOT OF MOMENT AS A FUNCTION OF TUBE DEFLECTION FOR TUBES OF LENGTH L=12 IN.
CASE | TUBE O.D. | WALL THICK
10 | 0.6 IN. | .04 IN.
11 | 0.6 | .06
12 | 0.6 | .08
13 | 0.9 | .04
14 | 0.9 | .06
15 | 0.9 | .08
16 | 1.2 | .04
17 | 1.2 | .06
18 | 1.2 | .08
MOMENT, M, N IN-LB.
2000
1500
1000
500
0
18
17
16
15
14
13
12
11
10
0
.02
.04
.06
.08
.10
.12
.14
.16
.18
.20
.22
.24
.26
.28
DEFLECTION, δ, IN IN.

FIGURE D.15

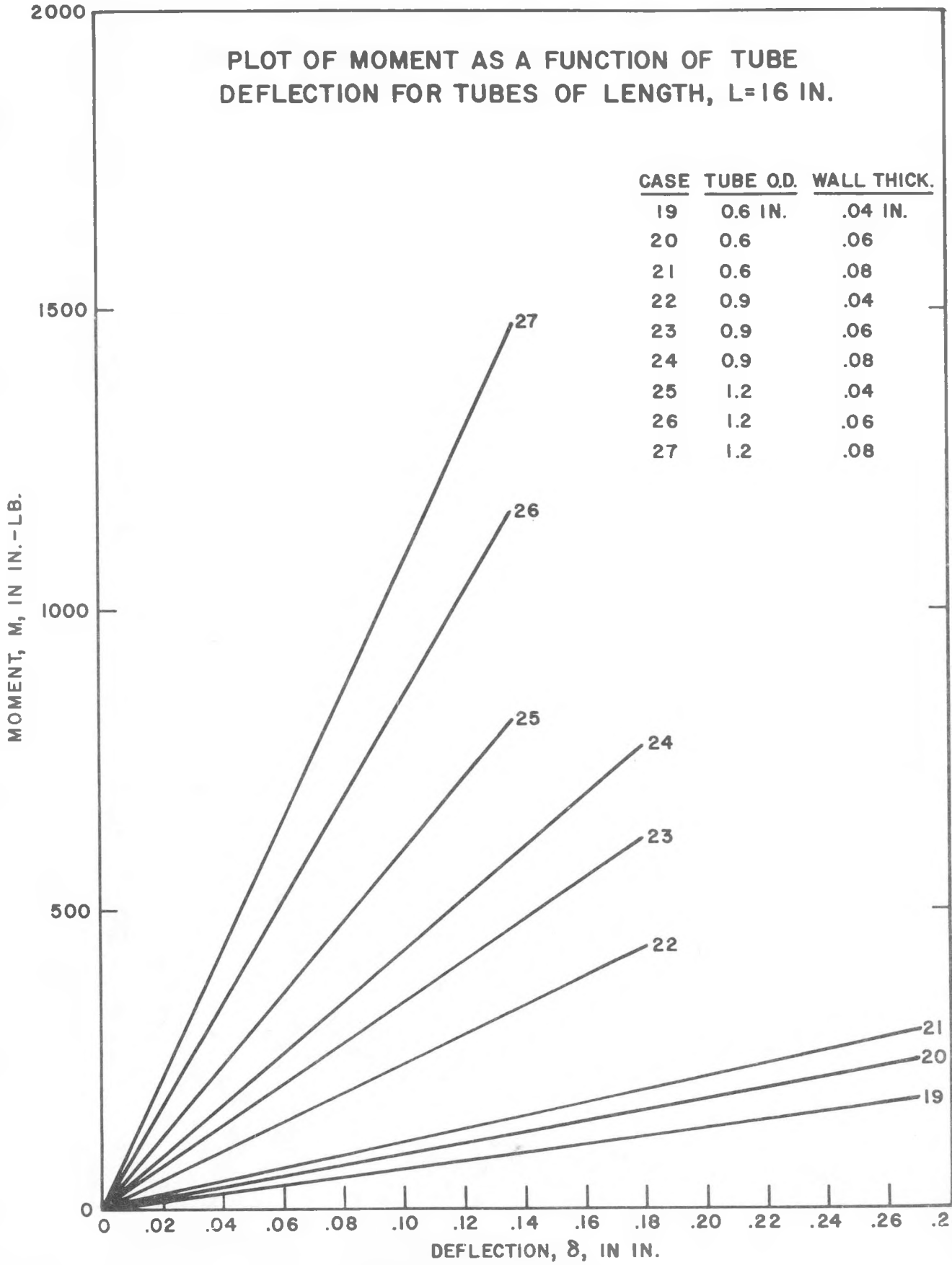
PLOT OF MOMENT AS A FUNCTION OF TUBE DEFLECTION FOR TUBES OF LENGTH, L=16 IN.
CASE TUBE O.D. WALL THICK.
19 0.6 IN. .04 IN.
20 0.6 .06
21 0.6 .08
22 0.9 .04
23 0.9 .06
24 0.9 .08
25 1.2 .04
26 1.2 .06
27 1.2 .08
MOMENT, M, IN IN.-LB.
2000
1500
1000
500
0
27
26
25
24
23
22
21
20
19
0 .02 .04 .06 .08 .10 .12 .14 .16 .18 .20 .22 .24 .26 .28
DEFLECTION, δ, IN IN.

FIGURE D.16

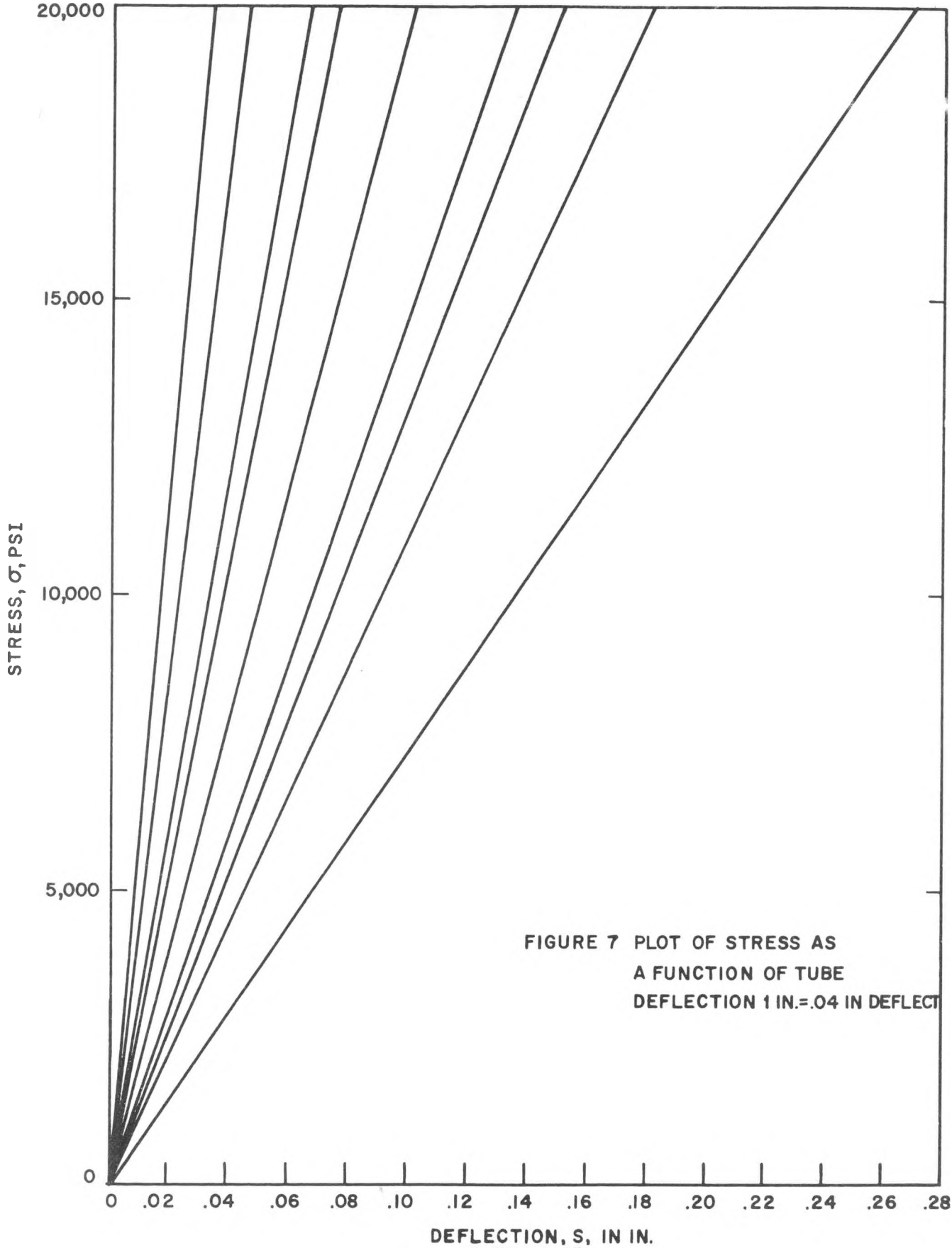

FIGURE 7 PLOT OF STRESS AS
A FUNCTION OF TUBE
DEFLECTION 1 IN.=.04 IN DEFLECT

FIGURE D.17

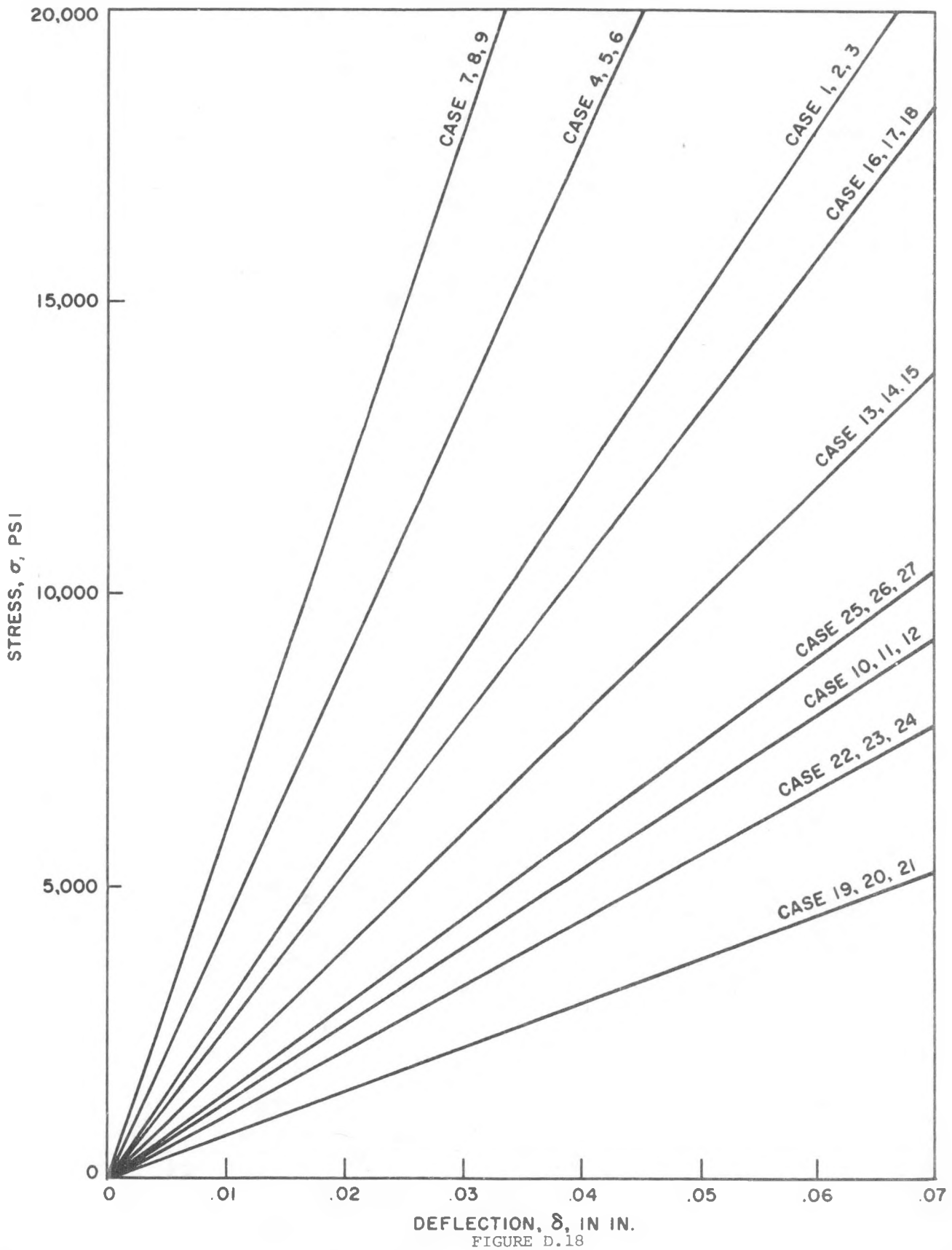
PLOT OF STRESS AS A FUNCTION OF TUBE DEFLECTION
1 IN. = .01 IN. DEFLECT.
20,000
15,000
10,000
5,000
0
STRESS, σ, PSI
CASE 7, 8, 9
CASE 4, 5, 6
CASE 1, 2, 3
CASE 16, 17, 18
CASE 13, 14, 15
CASE 25, 26, 27
CASE 10, 11, 12
CASE 22, 23, 24
CASE 19, 20, 21
0
.01
.02
.03
.04
.05
.06
.07
DEFLECTION, δ, IN IN.

FIGURE D.18

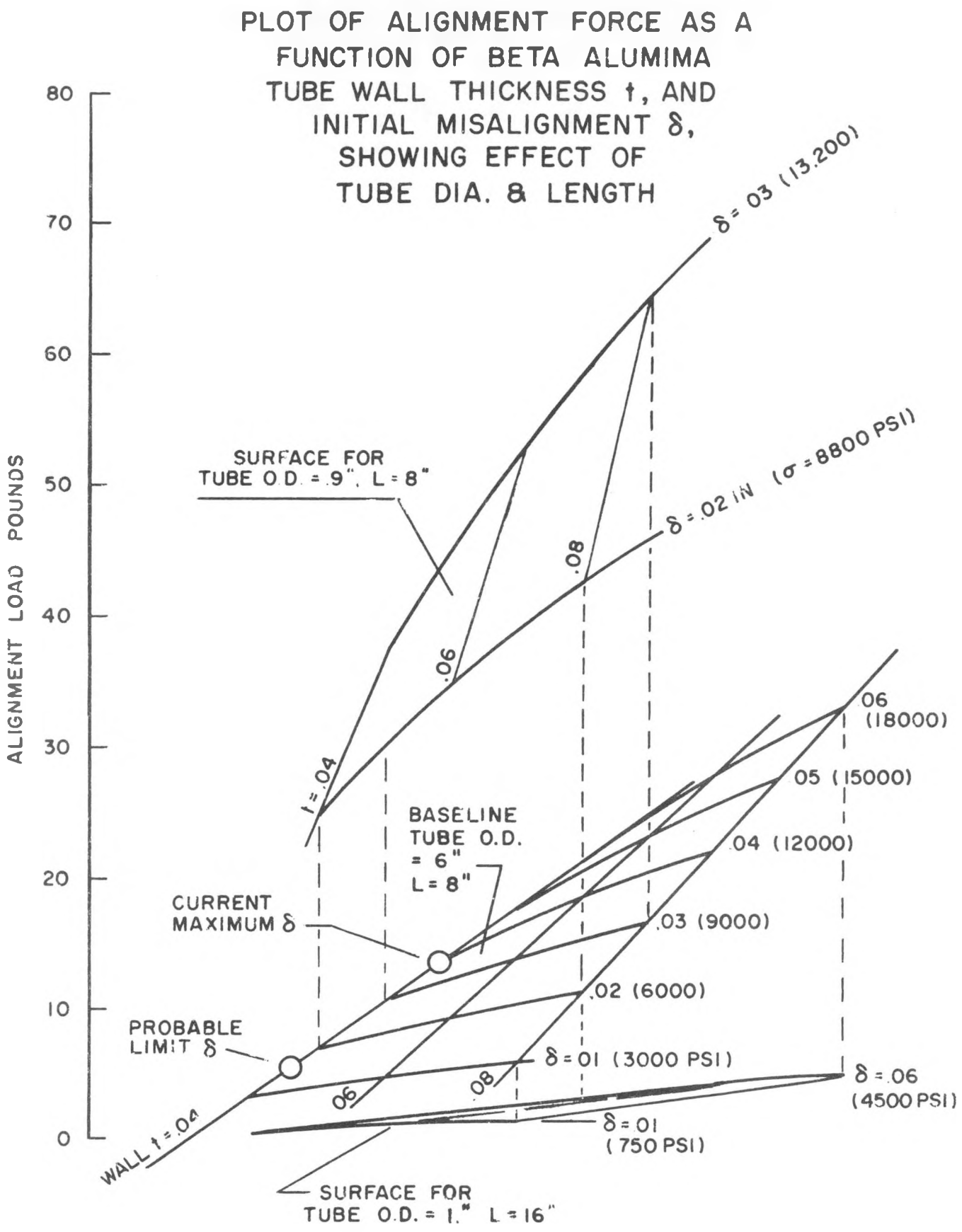
PLOT OF ALIGNMENT FORCE AS A FUNCTION OF BETA ALUMIMA TUBE WALL THICKNESS t, AND INITIAL MISALIGNMENT δ, SHOWING EFFECT OF TUBE DIA. & LENGTH
ALIGNMENT LOAD POUNDS
80
70
60
50
40
30
20
10
0
δ = 03 (13,200)
SURFACE FOR TUBE O.D. = .9", L = 8"
δ = .02 IN (σ = 8800 PSI)
.08
.06
t = .04
06 (18000)
05 (15000)
04 (12000)
BASELINE TUBE O.D. = 6" L = 8"
CURRENT MAXIMUM δ
.03 (9000)
.02 (6000)
PROBABLE LIMIT δ
δ = 01 (3000 PSI)
δ = .06 (4500 PSI)
06
08
WALL t = .04
δ = 01 (750 PSI)
SURFACE FOR TUBE O.D. = 1." L = 16"

FIGURE D.19

APPENDIX E

ANALYSIS PERTAINING TO THE SAFETY OF SODIUM-SULFUR CELLS

Developers and potential users of sodium-sulfur cells have expressed concern related to what might happen in the event of catastrophic failure of the solid electrolyte. Such a failure could lead to the failure of the hermetic seal or the container, possibly resulting in a hazardous situation for personnel or leading to further damage to the battery system.

Early in Phase II, the concept of using a "safety tube" to meter the flow of sodium and thereby control the maximum reaction rate in the event of electrolyte failure, was developed, tested, and shown to be effective. A safety tube was incorporated in the larger Mark-I cells and again, tests showed its effectiveness. Analysis pertaining to safety tube design is presented in this appendix. The safety tests are discussed in detail in the main text of this report (Sodium-Sulfur Battery Development-Phase II).

In the Mark-I load-leveling cell, a stainless-steel "safety tube" extends from the sodium reservoir into the β''-alumina tube. Its purpose is to restrict the flow of sodium from the reservoir if the β''-alumina tube fails. Sodium is metered into the β''-alumina tube through one or two extremely small holes in the sidewalls of the stainless-steel (safety) tube which fills most of the β''-alumina tube and protrudes from it into an overhead sodium reservoir. (See Appendix C for calculations showing the relative dimensions of the safety tube and β''-alumina tube.) Assembled in this manner, if the β''-alumina tube should break in a Mark-I load leveling cell, the rate of reaction between sodium and sulfur is restricted by the limited flow of sodium from the safety tube.

(a) The Rate of Flow from the Safety Tube. Most standard texts on fluid mechanics* contain a derivation of the following equation for dQ/dt, the rate of flow from a small opening in a relatively large vessel:

$$dQ/dt = d_N C_d A_o \sqrt{2 g h} \qquad \text{(E-1)}$$

In Equation E-1, the meanings and, in our case, values of the various symbols are as follows:

Symbol	Meaning	Value
d_N	density of liquid sodium	0.867 g/cm^3 @ 350°C
C_d	coefficient of discharge	0.82, for a "standard short tube"**
A_o	area of opening(s)	1.0×10^{-3} cm^2, for two 10-mil holes

*See, for example: R. W. Henke, Introduction to Fluid Mechanics, Addison-Wesley Pub. Co., Reading, Mass., 1961, pp. 75-98; B. S. Massey, Mechanics of Fluids, 2nd Edition, Van Nostrand Reinhold Co., London, 1970, pp. 83-88; and V. L. Streeter, Fluid Mechanics, 5th Edition, McGraw-Hill Book Co., New York, pp. 458-464.

**R. W. Henke (op. cit., p.86) defines a "standard short tube" as "a circular conduit 2½ times its diameter in length . . . (with) a square cornered entrance edge." According to Henke (loc. cit.) the discharge coefficient C_d is 0.82 for a standard short tube, whereas it is 0.6 for an orifice, i.e., a round hole in a material whose thickness is small relative to the diameter of the opening. In the Mark-I load-leveling cell, the ratio of the wall thickness to the diameter of the openings in the safety tube is 28 mils/10 mils = 2.8. W. Kaufmann (Fluid Mechanics, McGraw-Hill Book Co., Inc., N.Y. (1963), p. 110, states that a C_d of 0.85 is appropriate for a spout with the relative dimensions $L/D \simeq 2.5$ to 3.

g	universal constant (of gravitation)	980.7 cm/sec^2
h	hydrostatic head of sodium	9.1 cm, maximum, fully charged Mark-I load-leveling cell

It follows then that the maximum flow rate from the safety tube (in a fully charged Mark-I load-leveling cell) is

$$dQ/dt = 0.0319 \sqrt{h}$$
$$= 0.096 \text{ g/sec.}$$

The hydrostatic head (h), however, diminishes as sodium is dispersed from the reservoir. Consequently, the flow rate becomes less with time. Henke (op. cit., pp.102-3) and also Streeter (op. cit., pp.463-4) derive the following equation for t, the time to empty a reservoir to a desired level:

$$t = \frac{2A_R}{C_d A_o \sqrt{2g}} \left(\sqrt{h_o} - \sqrt{h_t} \right), \qquad \text{(E-2)}$$

in which the subscripts o and t denote time zero (initial state) and after t elapsed units (final state). For a Mark-I load-leveling cell, Equation E-2 reduces to the following:

$$t = \left(996.56 \text{ sec/cm}^{\frac{1}{2}} \right) \left(\sqrt{h_o} - \sqrt{h_t} \right) \qquad \text{(E-3)}$$

Suppose that we desire to compute the time required to empty the sodium container of a fully charged cell. Then, h_o = 9.1 cm and h_t = 0. It follows that t = 3006 sec or 50.1 min.

In Appendix C, an estimate was formulated of the capacity of the annular region (between the safety tube and β''-alumina tube) for sodium. At 350°C, in a Mark-I load-leveling cell, the annular region holds about 30 grams of sodium. If a crack occurred in the β''-alumina tube of a fully charged Mark-I load-leveling cell and if all the sodium in the annular region reacted to form sodium sulfide, from Equation E-3, it would take about 6 minutes to replace the expended mass (30 g) of sodium:

$$h_t = 9.1 - \left[(30\text{g Na}) / (0.867\text{g Na/cm}^3)(\pi/4)(4.83\text{cm})^2 \right]$$

$$= 7.21 \text{ cm}$$

$$t = (996.56)\left[\sqrt{9.1} - \sqrt{7.2} \right]$$

$$= 332.2 \text{ sec or } 5.5 \text{ minutes}$$

(b) Estimation of the Rate at Which Sodium Must be Supplied to Sustain the Electrochemical Reaction. The electrochemical equivalent for sodium is

$$(23\text{g/g atom Na}) / (96{,}500 \text{ A sec/g atom})$$
$$= 2.38_3 \times 10^{-4} \text{ g Na/A sec.}$$

In other words, the passage of an ampere-second (or coulomb) through the β''-alumina solid electrolyte is accomplished by the transfer of 0.238_3 milligrams of sodium.

In the Mark-I load-leveling cell, the surface area of the β''-alumina tube is about $\pi(3.35)(25) \simeq 263 \text{ cm}^2$. Suppose that a cell is discharged at a current density of 100 mA/cm^2. Then the total current drawn from the cell is

$$(0.1 \text{ A/cm}^2)\ (263 \text{ cm}^2) = 26.3 \text{ A}$$

In such an event, sodium must be supplied to the β''-alumina surface at the following rate:

$$(0.238_3 \text{ mg Na/A sec})\ (26.3 \text{ A})$$
$$= 6.27 \text{ mg Na/sec}$$

If we equate this critical rate to Equation E-1, the expression for the flow rate from the safety tube, and solve for h, we obtain the answer:

$$dQ/dt = 6.27 \times 10^{-3} \text{ g/sec} = 0.0319 \sqrt{h}$$
$$h = (6.27 \times 10^{-3})^2/(0.0319)^2 = 0.03_9 \text{ cm}$$

In other words, sodium can be supplied as fast as it is consumed (in a cell discharging at 0.1 A/cm^2). Since a cell normally is discharged in about 5 hours (at 0.1 A/cm^2) and, according to a previous calculation, the sodium reservoir can be emptied (through the safety tube) in about 50 minutes,

the last calculation probably was superfluous.

The hydrostatic head (h) at which the rate of flow from the safety tube just matches the electrochemical reaction rate can be calculated for any current density (i) from the following formula:

$$i^2 = \left[\frac{d_N C_d A_o \sqrt{2g}}{(23/96,500)A_e} \right]^2 h, \qquad \text{(E-4)}$$

in which A_e is the surface area of the solid electrolyte, 263 cm^2 for a Mark-I load-leveling cell. Equation E-4 reduces to the following:

$$h = 3.86\ i^2,$$

for Mark-I load-leveling cells. Some solutions are tabulated below:

h,cm	i, A/cm^2	h/h_o
0.04	0.1	0.004
.15	.2	.02
.35	.3	.04
.62	.4	.07
.97	.5	.11

In practice the depth of discharge seldom exceeds 85 percent of that to form Na_2S_3; consequently, the level of sodium seldom falls below a hydrostatic head of 2.725 cm. The minimum flow rate in practice, therefore, probably is about

$$dQ/dt = (0.0319)\sqrt{2.725}$$
$$= 0.053 \text{ g/sec or } 53 \text{ mg/sec},$$

which is more than eight times as fast as needed at 0.1 A/cm^2.

(c) Estimated Heat Generation from Direct Chemical Reaction (Following Failure of a β''-Alumina Tube). There is some variation among the standard references concerning the heats of formation for the various sulfides of sodium. The variance, however, is not important as the data listed in Table E.1

TABLE E.1. HEATS OF FORMATION FOR SODIUM SULFIDES

-ΔH, heat of formation			
Compound	kcal/mole	cal/g Na	Source
Na_2S	89.8	1952	1, 2
	89.2	1939	3
	93.0 ± 2.5	2022	4
Na_2S_4	99.8	2170	1
	101.4 ± 3.5	2204	4
	98.4	2139	3
Na_2S_2	99.0 ± 3.5	2152	4

Sources:
1. Bichowsky and Rossini, The Thermochemistry of the Chemical Substances, Reinhold, 1936
2. Chemical Engineers' Handbook, 5th Edition, McGraw-Hill Book Co., 1973
3. Handbook of Chemistry and Physics, 52nd Edition, 1971-1972
4. Kubashewski and Evans, Metallurgical Thermochemistry, 2nd Edition, Wiley, 1956

indicate: The mean of the values listed is 2083 cal/g Na; the coefficient of variation or relative standard deviation is about 5 percent of the mean. In other words, the amount of heat generated from the chemical reaction of sodium with sulfur is relatively insensitive to the relative proportion of sodium and of sulfur reacting. Gupta and Tischer (J. Electrochem. Soc., Vol. 119, No. 8, August 1972, pp. 1033-1037) found that a related electrochemically measured parameter also was insensitive. They reported that "the partial differential enthalpy ($\bar{H}_1$) of adding Na to the polysulfide melt is -47.6 kcal/mol (2070 cal/g Na) independent of melt composition and temperature." Consequently, one concludes that the reaction of one gram of sodium with any sulfurous substance present

in the cell will liberate a nearly constant quantity of heat, about 2075 calories.

It then follows that since heat can be generated only as rapidly as sodium can seep through the crack the maximum rate of heat generation is approximately

$$(dQ/dt)_i \Delta H = (0.1)(2075)$$
$$= 208 \text{ cal/sec } (870 \text{ W})$$

This estimate assumes that the crack is no larger in size than two 10-mil holes. Massive rupture of the entire β''-alumina tube conceivably might lead to rapid sulfidization of nearly all sodium in the annular region between the inner wall of the β''-alumina tube and the outer wall of the safety tube. In this event the maximum immediate release of heat would not exceed

(30 g Na)(2075 cal/g Na)
= 62,250 calories

This is equivalent to the energy derivable from the mass of sodium which otherwise would flow from the safety tube of a fully charged cell in about six minutes, according to a previous estimate.

One can envision that the reaction occurs along a narrow front bounded on the one side by molten sodium and on the other (behind a thin layer of polysulfide) by a sulfur-soaked felt of graphite fibers. The thermal conductivities of these substances are listed in Table E.2. The substances comprising the cell are ranked with more common materials according to the magnitude of the thermal conductivity. Note that the sulfur-impregnated felt is a better thermal insulator than many common ones and that liquid sodium is a relatively good thermal conductor, four times as good as stainless steel. Surprisingly alumina is nearly as good a thermal conductor at 300°C as stainless steel.

TABLE E.2. THERMAL CONDUCTIVITY OF CELL COMPONENTS COMPARED TO COMMON THERMAL CONDUCTORS AND INSULATORS

Substance	Thermal Conductivity watts/cm·°K @ 300°C
Copper	3.8
Aluminum	2.26
Liquid sodium	0.76
Stainless Steel	0.19
Alumina	.13 @ 400°C
Vermiculite refractory brick (0.47 g/cc)	.002
Diatomaceous refractory brick (0.4 g/cc)	.001
Glass wool (0.2 g/cc)	.0008
Sulfur- and sulfide-impregnated graphite felt	.00036

There is as great a difference between the thermal conductivities of the sulfur-impregnated felt and liquid sodium as there is between a lightweight refractory brick and copper metal. Heat dissipation from a reacting finger of sodium protruding from a crack into the sulfur-impregnated felt is analogous to that from the end of a small copper wire plunged into a refractory brick. In both cases most of the heat will be dissipated by conduction back through the metal.

The temperature within the cell probably will be greatest in those substances which are the poorest conductors. Because the heat is being dissipated predominantly through the sodium, the sulfur-impregnated felt (in the immediate vicinity of the reacting sodium) will be essentially as hot as the reaction zone.

There is no simple way to predict the temperature at which the reaction will take place. The heat from the combustion of a common liquid fuel such as gasoline, kerosene, or fuel oil is about 10,725 calories per gram. Sulfidization of one gram of liquid sodium liberates about 2075 calories, one fifth as much energy as combustion of a common liquid fuel. If only a small crack forms and sulfidization occurs as rapidly as leakage from the safety tube, then the rate of heating is about 208 calories per second or 870 watts. Hames and Tilley (in British Railways Board Technical Memorandum TM EC 10, Oct. 1975) describe an experiment in which a sodium-sulfur cell was discharged at a very high current density (1.5 A/cm^2). "The cell voltage and temperature stabilized at 0.8 volt and 630^oC, respectively." From other facts given in the report, one can calculate that the rate of heat dissipation dQ/dt was as follows:

$$dQ/dt = (E^o - E)\ I + 4.186\ (\Delta S/F)\ I\ T$$

where $E^o = 2.08$ volts

$E = 0.8$ volts

$I = 105$ amperes

$T = 630 + 273 = 903\ ^oK$

$\Delta S/F = 3.35$ e.u./96,500 $= 3.47_{15} \times 10^{-5}$

$dQ/dt = 134.4 + 13.78$

$= 148.18$ watts

In this high rate-of-discharge experiment the heat probably is generated over the entire surface of the beta-alumina tube, 70 cm^2. Heat is undoubtedly generated in a much more confined region, when sodium seeps into the cathode through a ruptured β''-alumina tube. Consequently, if the estimated 870 watts is at all realistic, the temperature of the reaction zone probably greatly exceeds 630^oC.

Some additional insight possibly can be gained by considering the stability of the substances taking part in sulfidization. In Table E.3 the energy needed to achieve the next major phase change, and the temperature at which the phase transformation occurs are listed for each substance. Comparing the relative stability of the reactants (and the product) indicates that extensive vaporization of sulfur almost certainly will occur. This will aid sulfidization, because the sulfur vapors will expand to fill any voids and thus promote contact with the liquid sodium. One can envision that incipient sulfidization occurs wherever the fluid sodium runs into islets of viscous sulfur. But when sufficient heat has been generated to raise the temperature along the reaction front above 445°C, enough sulfur vapor is present to cause sulfidization to occur all along the interface created by the expanding sodium.

TABLE E.3. COMPARISON OF STABILITY

Substance	Energy to Achieve Next Phase Change (Above 350°C), Calories/g Substance	Nature of Next Phase Change	Temperature of Phase Change, °C
Sulfur	85	Boiling Point	445
Sodium	1240	Boiling Point	883
Na_2S	250	Melting Point	1170

Sulfidization probably occurs initially between the two elements, sodium and sulfur. The advancing sodium contacts sulfur and reacts to form a molten (sulfur-rich) polysulfide. As more sodium reaches the reaction front it too reacts; it is assimilated into the polysulfide melt just as it is during the normal discharge of the battery. Soon, however, the relative proportion of sodium increases with respect to sulfur to a point that solidification occurs. Those familiar with the electrochemistry of the sodium-sulfur battery will recall that cell discharge is limited at 350°C to the formation of Na_2S_3 because a polysulfide more sodium rich than this is a solid at 350°C, and the battery will not function if a solid forms on the β″-alumina reaction surface between the electrodes. In the same manner the direct chemical reaction between sodium and sulfur will occur until a solid polysulfide forms. The highest melting substance comprised of sodium and sulfur is Na_2S. It melts at 1170°C. Consequently unless sulfidization occurs so rapidly that the temperature of the reaction zone exceeds 1170°C, eventually a solid polysulfide will form between the reactants, sodium and sulfur, thus impeding further reaction.

The formation of an impregnable barrier of solid sodium sulfide along the front of the advancing sodium is thwarted, however, by several other characteristics of the polysulfide. First, the polysulfide is a potent solvent for sulfur. Sodium-rich polysulfide reacts rapidly with elemental sulfur. Moreover, molten polysulfide is very fluid. Consequently it and the sodium probably tend to move through the sulfur-impregnated felt as a unit, oozing around any strongly resisting matter and channeling through the cathode by rapidly advancing from void to void in a progressively downward direction.

The reaction tends to follow a path directed toward the bottom of the cell because the polysulfide is a relatively dense

liquid; its specific gravity is about 1.9 whereas that of sodium is about 0.9. Consequently, the polysulfide tends to flow downwards buoying the sodium on its upper surface. As it "eats" its way through the sulfur-impregnated felt, the sodium follows. If rupture occurs in a fully charged cell, a dam of sodium can progressively grow in front of the crack inside the cathode; because as the polysulfide dissolves sulfur from the felt it coalesces the numerous small evenly dispersed voids into a single large cavity which immediately is filled by sodium from the anode.

Figure E-1 shows a cross section through a portion of a ruptured cell. The advancing sodium is shown as an expanding mass tending downward from the crack. A thin layer of solid sulfide surrounds the sodium. The layer is thicker on the topside of the sodium because the temperature is colder there than on the bottom where sulfidization is proceeding more rapidly. Liquid polysulfide is oozing through the felt and expanding toward the bottom of the cell.

Research conducted by Djong-Gie Oei indicates that "the reaction between Na_2S or Na_2S_2 and sulfur proceeds with the formation of Na_2S_5 as an intermediate step." (See Inorganic Chemistry, Vol. 12, No. 2, 1973, pp. 435-7.) Possibly the polysulfide opposite the sulfur interface would tend to be Na_2S_5; and the phases may be aligned at steady state in the following order:

$$Na_{(\ell)} \ / \ Na_2S_{(s)} \ / \ Na_2S_{5(\ell)} \ / \ S_{(\ell)}.$$

It is conceivable that the sulfidization process is oscillatory in nature: Sodium may unite with polysulfide until solid Na_2S forms. Further reaction may be so impeded by the presence of the solid that it practically stops. Meanwhile on the other side of the polysulfide, sulfur is assimilated into it until the composition is so sulfur rich that it in

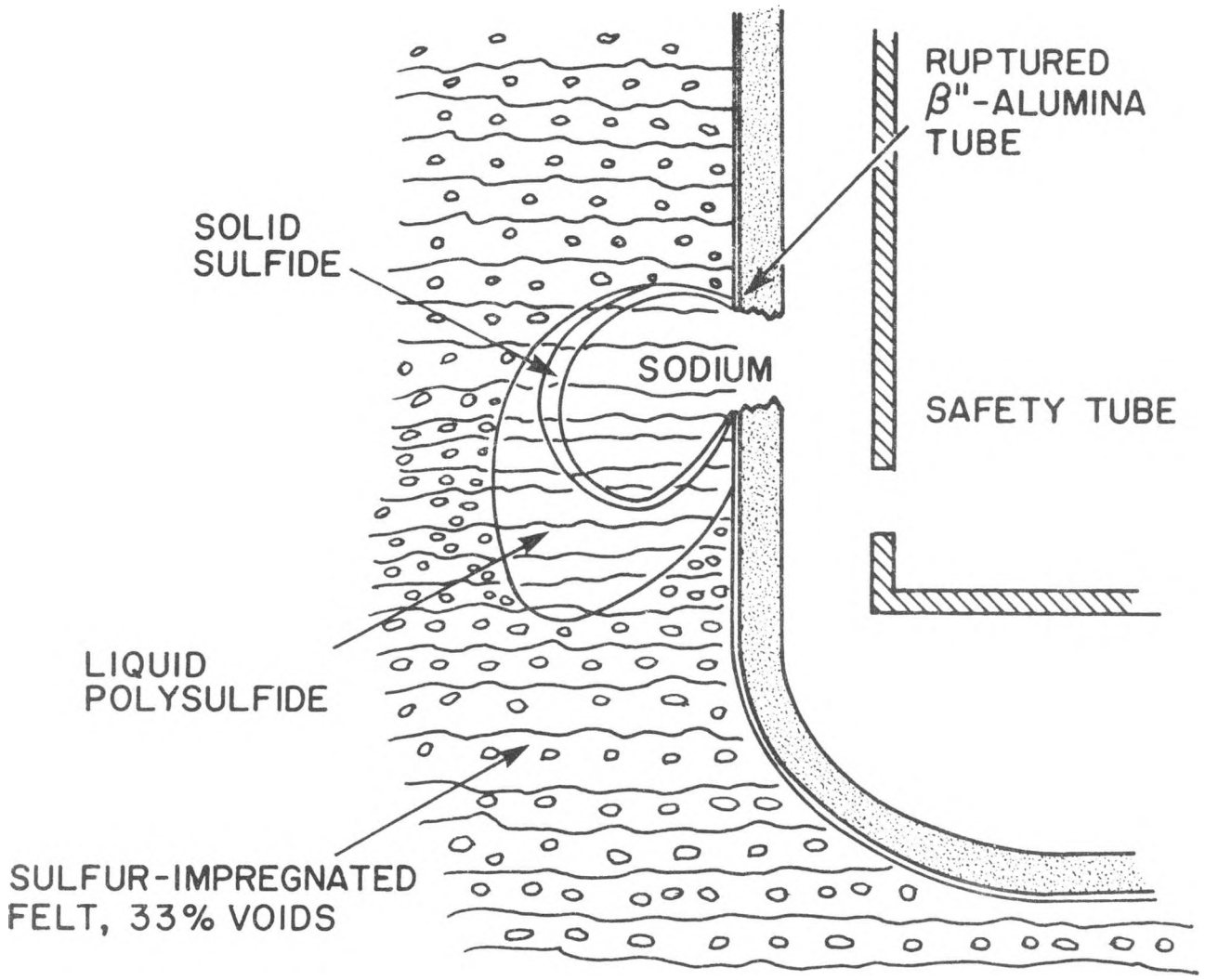

FIGURE E.1 - Probable Nature of Direct Chemical Reaction Between Sodium and Sulfur Following Fracture of Ceramic Electrolyte Tube

turn dissolves the Na_2S. Once the solid Na_2S is broken down, sodium again reacts with polysulfide and the cycle is repeated. Viewed in this manner, it is not surprising that the external surface of the cell experiences cyclic temperature excursions as internally sulfidization periodically is first accelerated and then retarded.

APPENDIX F

STATIC CORROSION TEST SAMPLE PREPARATION

Test samples were cut from commercially supplied sheet stock. The majority of the specimens were 2.54 to 3.81 cm long by 1.27 cm wide (1.0 to 1.5 in. long by 0.5 in. wide). The thickness varied from 1.0 to 3.8 cm (0.040 to 0.150 in.). The untreated metals and alloys were cleaned in detergent and tested. The edges and corners of the substrate alloys were machined round and ball milled to minimize edge effects on the coatings. Various surface treatments and coatings were then applied to these substrates. Most of the coatings and treatments were applied in commercial shops by established methods. The samples were carefully inspected, measured and weighed before testing.

Each sample was loaded into a separate 16-mm (0.63-in.) diameter by 120-mm (4.75-in.) long Pyrex tube which had been necked down on one end and joined to a 6-mm (0.24-in.) diameter evacuation tube. The large end of the tube was then sealed off, encapsulating the specimen. The capsules were evacuated to a pressure of less than 0.1-mm Hg and were passed into a glove box containing dry argon. Na_2S_4 (approximately 5 g) was introduced into the capsule through the 6-mm (0.24-in.) diameter tube. This was enough chemical to immerse approximately one half of the specimen in the melt, so that both liquid and vapor effects could be observed. The fill tube was swabbed clean, and a vacuum hose was attached. The capsule was evacuated to a pressure of less than 0.2-mm Hg and sealed off with a torch. A glass hook was formed on the sealed tube stub, and an Inconel wire ring was attached. The specimens were lowered into individual holes in an aluminum block which was maintained at 400 $\pm$ 5°C for the test period.

The Na_2S_4 was synthesized from high purity Na_2S and high purity sulfur. Throughout the filling and sealing procedure, and while in storage, the Na_2S_4 was not exposed to the open atmosphere.

The untreated metals and alloys were tested for 15 to 120 days and the surface-treated and coated samples were tested for 30 days. After the test period, the capsules were cooled to room temperature and broken open. The appearance of the sample and the melt were noted. The sample and melt were immersed in a beaker of warm water and the Na_2S_4 was dissolved. The solution was decanted, noting any precipitates. The specimen and any residue or spalled coating on the container bottom were examined with a stereo microscope. The thickness of any reaction products remaining on the sample was measured and the appearance noted. Any loose reaction product on the metal specimens was then mechanically removed. The cleaned specimen was weighed and measured and the corrosion rates were calculated. The results of the static corrosion tests are summarized in the following paragraphs.

Zirconium was used as a control material throughout the testing program. A specimen was put into test each time a different batch of Na_2S_4 was used. Nine 30-day test samples had an average corrosion depth of 15.6 microns with a relative standard deviation of 13.0 percent. The corrosion behavior of Type 446 stainless steel was observed to vary significantly more from batch to batch as shown in Table F-1, indicating that greater control could have been given to the purity of the Na_2S_4.

TABLE F.1 CORROSION TEST REPRODUCIBILITY

Spec. No.	Test Time (Days)	Weight (g)	Wt Loss (mg)	Wt. Loss (Adj. to 30 Days)	Sample Area (cm^2)	Na_2S_4 Batch No.	Corrosion Depth (Adj. to 30 Days) (Microns)
ZIRCONIUM							
21	31	3.2489	80.4	77.8	7.66	F-1	15.6
37	29	3.1284	60.2	62.3	7.42	F-3	12.9
70	33	3.2250	74.9	68.1	7.61	F-4	13.8
71	33	3.2560	75.4	68.5	7.67	F-3	13.7
75	35	3.1223	103	88.3	7.41	A-1	18.3
76	35	3.2498	102	87.1	7.66	A-1	17.5
104	31	3.2438	78	75.5	7.65	A-2	15.2
261	30	3.1325	72.3	72.3	7.42	A-7	15.0
262	30	3.2008	90.1	90.1	7.56	A-7	18.3
MEAN CORROSION DEPTH - 15.6 MICRONS STANDARD DEVIATION - 2.0 MICRONS							
TYPE-446 STAINLESS STEEL							
4	60	2.8144	139		7.4	F-1	25
79	30	3.0275	-			A-1	>600
80	30	3.1230	-			A-1	>600
260	30	2.9670	-			A-7	$\cong$ 10
GE*	15	0.5907	2			G.E.	5

Specimen Nos. 1 through 71 were tested in sodium tetrasulfide produced by Ford (Batches F-1 through F-4).

Specimen Nos. 72 through 268 were tested in sodium tetrasulfide produced by Aeronutronic (Batches A-1 through A-7).

(*) General Electric Co., Sodium-Sulfur Battery Development, EPRI Project RP 128, July 1974

APPENDIX G

Description of Current Standard Process for Fabricating β"-Alumina Electrolyte Tubing in the Pre-Pilot Batch Plant

The raw materials that are being used for tubing are (1) α-alumina (ERCHPS-DBM Reynolds low soda alumina), reagent grade sodium carbonate powder, and technical grade lithium oxalate powder. The current composition being used is 8.85% Na_2O, 0.75% Li_2O, and 90.4% Al_2O_3 by weight. Formulation is accomplished using the zeta process technique. The two components of the zeta process are blended separately in a twin shell blender in 8 kilogram batches. After calcining the two components in separate 1 kilogram batches at 1260°C for 2 hours, the appropriate amount of each component is added to one another. These batches are then milled by dry ball milling using one-gallon high purity alumina-drums and high purity α-alumina ball media. The powder is milled for 16 hours. After milling, the powder is mixed into an acetone-PVB binder slurry. The slurry is then dried overnight in a filtered air-stream. The powder is then milled again for 1 hour to break up soft agglomerates, after which it is screened through an 83 mesh nylon screen. The powder is then stored in plastic bags awaiting pressing.

The pressing tooling is filled to uniform pack density by placing the tooling on a mechanical tapper for time periods ranging from one to 4 minutes. The powder is then pressed to its tubular shape at 40 kpsi pressure. After removal from the pressing tooling the tube is cut to its proper dimensions. The green tubes are then subject to an overnight bisque cycle which reaches a maximum temperature of 750°C. The green tubes are then placed in platinum bags and sintered in a batch mode at 1570°C for 5 minutes. Annealing is performed immediately after sintering at 1475°C for time periods ranging from one to three hours.

After removal from the platinum bags the tubes are subjected to a visual inspection using transmitted and reflected light. This quality control check discloses surface and interior defects in the tube such as cracks, pressing defects, or dislocations. The tube is also checked for its dimensional uniformity. The dimensional quality control checks involve warpage, maximum and minimum outside diameters and wall thickness at the open end, and perpendicularity of the open end with respect to the tube axis. Warpage is measured by placing the tube horizontally on a flat surface and measuring directly the amount of bow in the tube using a taper gage. Outside diameter and wall thickness is measured using standard caliphers and micrometer gages. The perpendicularity of the tube is measured by placing the tube vertically on a flat surface with its open end down. The amount of deviation is then measured in degrees using a universal protractor.

A separate short section sintered along with each tube is subjected to density, resistivity and microstructural examination. Currently, approximately 90% of all tubing sintered have companion short sections. Of these, all are subjected to density and resistivity measurements. About 1/3 of the short sections are polished for microstructural examination. The tubes which pass the above quality control checks are then leak-checked using a Veeco helium leak detector.

Currently, the tubes are being sealed using a prototype sealing-alignment furnace designed here at Utah. The tubing is sealed to disk headers in a temperature interval which ranges from room temperature to 850°C and back to room temperature in a 3 hour cycle. After sealing, the tubes are again checked for their vertical perpendicularity when resting on a flat surface with the disk in contact with the surface. The sealed tubes are also leak checked a second time to determine if the alpha to beta seal is hermetic.

APPENDIX H

TECHNICAL PAPERS & PRESENTATIONS

Ford Motor Company

"Effect of Electrode Shape and Additives on Performance of the Na/S Cells", M. Mikkor, R. W. Minck, F. A. Ludwig, N. K. Gupta, Electrochem Soc. Meeting October 1976.

"The Sodium-Sulfur Battery - A Progress Report", S. A. Weiner, 27th Power Sources Conference June 1976.

"Chemistry of Sodium-Sulfur Battery", S. A. Weiner, Amer. Chem. Society August 1976.

"Review of the Ford Na-S Battery Program", S. A. Weiner, ERDA Battery Conference Coordination Meeting, January 1977, Germantown, Md., Also presented to BEST Facility - Work Shop II, February 1977, New Orleans, La.

"Application of Ford Na-S Battery in Electric Vehicles", L. E. Unnewehr, R. W. Minck, C. Owens, Paper 770382 SAE, February 1977, Detroit, Michigan.

"Status of Sodium-Sulfur Battery", R. W. Minck, S. A. Weiner, presented to SAE, February 1977, Detroit, Michigan.

"The Sulfur Electrode in Non-Aqueous Media", in Advanced in Electrochemistry and Electrochemical Engineering, Vol. 10, R. Tischer, F. Ludwig. Edited by H. Gerischer and C. Tobias. John Wiley and Sons (1977).

"Applications of Carbon in the Sodium-Sulfur Battery". F. Ludwig. 13th Biennial Conference on Carbon, July 1977, Irvine, Calif. Extended Abstracts pg. 39.

"NaS and Other Advanced Batteries", A. Topouzian, R. W. Minck, Forum on Energy Storage in Solar Applications and Transportation, October 23-28, 1977, St. Simons Island, GA.

"Mechanism of the Hydrogen Electrode Reaction on Platinum in Acid Solution", F. Ludwig, R. Sen, E. Yeager submitted to Elektrokhimaya, expected publication 1977.

"Performance and Design of Sodium-Sulfur Prototype Batteries", F. Ludwig, M. Mikkor, R. Minck, A. Topouzian. Fall Meeting, October, 1977, Atlanta, Georgia, Abstract #80. Also published as extended abstract in Load-Leveling Symposium Volume, The Electrochemical Society, October, 1977.

Presentation on "Corrosion of Materials in Molten Sodium Tetrasulfide", K. A. Kinsman, D. G. Oei, ECS Meeting, Oct. 1976.

Presentation on "Corrosion of Ni-base Superalloys in Sodium Tetrasulfide", K. A. Kinsman, D. G. Oei, ECS Meeting, October 1977.

Presentation on "Failure Analysis of Some β"-Alumina Membranes", G. Tennenhouse, American Ceramic Society, May 1966, Cincinnati.

University of Utah

"Application of Load-Relaxation Techniques to Study Subcritical Crack Growth in Brittle Materials:, Anil V. Virkar and Ronald S. Gordon, J. Amer. Ceram. Soc. 59 (1-2) 68-71 (1976).

"Fracture Properties of Polycrystallined Lithia-Stabilized β-Alumina", Anil V. Virkar and Ronald S. Gordon, J. Amer. Ceram. Soc. 60 (1-2) 58-61 (1977).

"Sintering Processes and Heat-Treatment Schedules for Conductive, Lithia-Stabilized β"-Al_2O_3", G. E. Youngblood, A. V. Virkar, W. R. Cannon and R. S. Gordon, Bull. Amer. Ceram. Soc. 56 (2) 206-210 (1977).

"Thermal Shock Behavior of Lithia-Stabilized β"-Al_2O_3", G. E. Youngblood, A. V. Virkar, W. R. Cannon and R. S. Gordon, Bull. Amer. Ceram. Soc. 56 (2) 206-210 (1977).

"Resistivity-Microstructure Relationships in Lithia-Stabilized Polycrystalline β"-Alumina", A. V. Virkar, G. R. Miller, and R. S. Gordon, J. Amer. Ceram. Soc. (in press).

"Evolution of Microstructures and Properties in Lithia-Stabilized Polycrystalline β"-Alumina", Anil V. Virkar and Ronald S. Gordon; and "Conversion Catalysis and Microstructure Control in the Sintering of Lithia-Stabilized β"-Alumina", Arun D. Jatkar, Ivan B. Culter, and Ronald S. Gordon. Proceedings of Sixth International Materials Symposium - Ceramic Microstructures, August 24-27, 1976, University of California, Berkeley, Edited by R. M. Fulrath and J. A. Pask. Ceramic Microstructures - 1976. Westview Press, Boulder, Colorado.

"Relative Effects of Phase Conversion and Grain Size on Sodium Ion Conduction in Polycrystalline, Lithia-Stabilized β"-Alumina", G. E. Youngblood and R. S. Gordon, Ceramurgia International (in press).

"A Metal-Clad Electronic Ceramic Container and Electrode System", O. W. Johnson and G. R. Miller, Bull. Amer. Ceram. Soc., Aug. 1977, p. 706.

"The Processing and Characterization of Beta-Alumina Ceramics for Use in the Sodium-Sulfur Battery", R. S. Gordon, Proceedings of the U.S. - Japan Seminar on Basic Science of Ceramics 1975 on Processing, Kinetics and Properties of Electronics and Magnetic Ceramics, Editors W. Komatsu, R. M. Fulrath, Y. Oishi, M. Koizumi, S. Somiya, Sponsored by Japan Society for the Promotion of Science and the U.S. National Science Foundation, pp. 117-124 (1976).

"The Preparation of Conductive Ta Doped Rutile: I. Sintering and Microstructure", O. W. Johnson, C. A. Venizelos, P. S. Beutler and G. R. Miller, J. Amer. Ceramic Soc. (to be published).

"The Preparation of Conductive Ta Doped Rutile: II. Defect Structure and Conductivity", O. W. Johnson and G. R. Miller, J. Amer. Ceramic. Soc., (to be published).

APPENDIX I

PHASE II - PATENTS ISSUED

Ford Motor Company

3,966,492 (6/76), F. A. Ludwig, Sodium Sulfur Battery or Cell with Improved Ampere-Hour Capacity.

3,976,503 (8-24-76), R. W. Minck, N. Weber, Y. C. Chang, Improved Process for Recharging Secondary Batteries.

3,980,496 (10-14-76), R. A. Ludwig, R. W. Minck, S. A. Weiner. Energy Conversion Devices with Improved Electrode Shapes.

3,985,576 (10-12-76), J. N. Lingscheit & T. H. Whalen Seal for Energy Conversion Devices.

3,985,575 (10-76), F. A. Ludwig Secondary Battery or Cell with Dual Electrode.

3,993,503 (11/76), F. A. Ludwig Secondary Battery or Cell with Composite Electrode.

3,994,745 (11/76), F. A. Ludwig Secondary Battery or Cell with Separate Charge and Discharge Zones.

4,002,806 (1/77), F. A. Ludwig with N. Gupta Secondary Battery or Cell.

4,002,807 (1/77) F. A. Ludwig Improved Alkali Metal/Sulfur Battery or Cell with Single Phase Sulfur Electrode.

4,020,134 (4-26-77) R. Gordon, W. Sutton, G. Tennenhouse Method for Preparing Shaped Green Ceramic Compacts.

4,038,465 (7/77) S. A. Weiner & F. A. Ludwig Sodium Sulfur Battery or Cell with External Storage

4,048,393 (7-13-77) W. K. Heintz & J. N. Lingscheit. Battery Structure

4,048,394 (9-77) F. A. Ludwig Graphite-Vitreous Carbon Sodium-Sulfur Battery Container and Current Collector.

4,049,889 (9-20-77) W. K. Heintz Hermetically Sealed Alkali Metal Battery.

APPENDIX J

Professional Staff*

Ford Motor Company

Mr. A. Topouzian
Dr. N. K. Gupta
Dr. K. R. Kinsman
Dr. J. N. Lingscheit
Dr. F. A. Ludwig
Dr. M. Mikkor
Dr. R. W. Minck
Mr. P. F. Nicholls
Dr. D. G. Oei
Mr. P. Pai
Dr. A. Sherman
Mr. A. G. Smith
Dr. R. P. Tischer
Dr. S. A. Weiner
Mr. W. J. Williams

Aeronutronic Division,
Ford Aerospace and Communications Corporation

Mr. R. A. Harlow
Dr. D. W. Bridges
Mr. G. Chase
Mr. J. K. Lewis
Mrs. M. L. McClanahan
Mr. B. B. Ritchie

University of Utah

Dr. R. S. Gordon
Dr. G. R. Miller
Mr. J. G. Azbill
Mr. B. J. McEntire
Dr. M. L. Miller
Dr. D. G. Paquette
Dr. A. V. Virkar

* Technicians and other departmental support not included.

☆U.S. GOVERNMENT PRINTING OFFICE: 1979-640-092/537